Assessing the contribution of solar-induced fluorescence (SIF) to the estimation of nutrient status in almond orchards

Yue Wang

ORCID: 0009-0005-8777-941X

Submitted in total fulfilment of the requirements for the degree of Doctor of Philosophy

Department of Infrastructure Engineering (IE)

Faculty of Engineering and Information Technology (FEIT)

The University of Melbourne

Australia

July 2023

Abstract

Macro- and micro-nutrients are essential for plants to function efficiently, resist disease, and produce high yields and quality fruits. These nutrients are involved in various aspects of almond growth and development throughout the phenological cycle. High levels of nitrogen, phosphorus, and potassium are the most important inputs for almond production. Micro-nutrients, although needed at much lower levels, also play an important role in supporting growth, especially in key tissues. The most important aspect of fertilizer management is balancing the fertilizer program in order to maximize yields while minimizing environmental impacts. In precision agricultural management, a precise assessment of nutrient status is crucial to determine the optimal application of fertilizers. The traditional method of assessing nutrients is tissue testing in biochemical laboratories, but this is not cost- or time-effective for continuous monitoring over a large area.

The use of remote sensing techniques has been explored in recent decades as a method of obtaining indicators for those nutrients, most notably nitrogen, in terms of their spatial orientation, efficiency, and rapidness. In remote sensing of leaf N assessment, empirical algorithms using chlorophyll $a+b$ sensitive vegetation indices, as well as radiative transfer model (RTM) inversion of plant pigments, are applied. In recent years, advances in leaf N estimation have relied on the assessment of leaf biochemistry and spectral characteristics linked to photosynthesis, such as solar-induced fluorescence (SIF), which has been demonstrated to be an indicator of stress caused by nutrient deficiencies in a wide range of crop species. As a result of the sensitive nature of SIF and the complexity of tree orchard canopy architecture, its performance and sensitivity to plant condition need to be evaluated in tree-structured almond orchards. In spite of this, there is still a lack of understanding of proxies for other macro- and micro-nutrients and their interactions, an area which requires further investigation.

This research investigates the response of spectral-based plant parameters to different nutrient elements in almond trees at both the leaf and canopy levels. It is intended that this study not only provides an improved assessment of N using a combination of robust proxies, but also it examines its evaluation at various spatial and spectral resolutions, from high-resolution airborne to coarser-resolution spaceborne platforms. The results from two years of data indicate that chlorophyll fluorescence can serve as a reliable proxy for the primary macro-nutrients (i.e., N, P, and K) across the two years, yielding r^2 = 0.74 (p-values < 0.005) for both leaf steady-state measurements and canopy SIF with leaf N. Moreover, the biochemical constituents derived from radiative transfer modeling exhibited strong correlations with the primary macro-nutrients for both years, whereas vegetation indices exhibited generally inferior relationships with nutrients. Taking leaf N as an example, SIF and C_{ab} derived from RTM inversion were found to be the most significant non-collinear indicators at both the airborne (0.4 m) and spaceborne (30 m) scales. An airborne-based model predicted field-measured leaf N with an r^2 of 0.95 and RMSE of 0.05% over the course of two years. The newly developed spectrometer DESIS onboard the International Space Station (ISS) provided a model with an r^2 of 0.83 and RMSE of 0.06% in 2021, while Sentinel-2 provided an inferior result (r^2 = 0.72, RMSE = 0.08%). An emphasis has been placed in this research on the importance of C_{ab}, SIF, and other plant pigments in determining the nutrient status of discontinuous tree-structured almond orchards. Moreover, this work provides a step forward towards achieving accurate and large-scale nutrient monitoring in precision agriculture.

Declaration

This is to certify that:

i. This thesis is an original work of the author except where due acknowledgement has been made.

ii. There has been no previous submission of this work, in whole or in part, for any other degree or qualification at any other university.

iii. This thesis represents the results of the research conducted during the official PhD candidature.

iv. The thesis consists of less than 100,000 words in length, exclusive of tables, maps, bibliographies, and supplementary materials.

Yue Wang

Melbourne, July 2023

Preface

This thesis is comprised of three core chapters (Chapters 2 to 4), which have been published or are in the process of being published in two journal papers, three conference proceedings, and one conference abstract, as follows:

Chapter 2 is planned for a journal publication.

Chapter 3 has been published in *Remote Sensing of Environment*:

- Wang, Y., Suarez, L., Poblete, T., Gonzalez-Dugo, V., Ryu, D., Zarco-Tejada, P.J., Evaluating the role of solar-induced fluorescence (SIF) and plant physiological traits for leaf nitrogen assessment in almond using airborne hyperspectral imagery**,** Remote Sensing of Environment, 279, 113141.

Chapter 4 is under review in *IEEE Transactions on Geoscience and Remote Sensing*:

- Wang, Y., Suarez, L., Hornero, A., Ryu, D., Moar, P., Zarco-Tejada, P.J., Quantification of leaf nitrogen in almond orchards from the spaceborne DESIS Hyperspectral Sensor: modeling and assessment with airborne hyperspectral and Sentinel-2 imagery, under review in IEEE Transactions on Geoscience and Remote Sensing.

The study has also been published in international conferences such as IGARSS and the 1st DESIS User Workshop attached in Appendix, as follows:

- Wang, Y**.**, Suarez, L., Qian, X., Poblete, T., Gonzalez-Dugo, V., Ryu, D., Zarco-Tejada, P.J., Assessing the Contribution of Airborne-retrieved Chlorophyll Fluorescence for Nitrogen

Assessment in Almond Orchards, IEEE International Geoscience and Remote Sensing Symposium IGARSS, 2021, pp. 5853-5856, doi: 10.1109/IGARSS47720.2021.9554648.

- Wang, Y., Suarez, L., Gonzalez-Dugo, V., Ryu, D., Moar, P., Zarco-Tejada, P.J., Leaf Nitrogen Assessment with ISS DESIS Imaging Spectrometer as Compared to High-Resolution Airborne Hyperspectral Imagery, IGARSS 2022 - 2022 IEEE International Geoscience and Remote Sensing Symposium, 2022, pp. 5444-5447, doi: 10.1109/IGARSS46834.2022.9884759.

- Wang, Y., Suarez, L., Ryu, D., Zarco-Tejada, P.J., Evaluating the Contribution of Cx to Leaf Nitrogen Quantification using Fluspect and Airborne Imaging Spectroscopy in Almond Orchards, accepted in IGARSS 2023 - 2023 IEEE International Geoscience and Remote Sensing Symposium.

- Wang, Y., Suarez, L., Ryu, D., Moar, P., Zarco-Tejada, P.J., Nitrogen Estimation in Almond Orchards from DESIS Imaging Spectrometer Onboard the International Space Station, ISPRS International Society for Photogrammetry and Remote Sensing, 1st DESIS User Workshop, 28th Sep-1st Oct, 2021.

Acknowledgements

In appreciation of the support that has been provided to me throughout my PhD journey towards the completion of my thesis, I wish to express my deepest and sincere gratitude to many people.

First and foremost, my thanks go to the most attentive, patient, and considerate supervisory team ever encountered – Prof. Pablo J. Zarco-Tejada, Dr Lola Suarez, and Prof. Dongryeol Ryu. Thank you for giving me the opportunity to learn from and work with you. Throughout this journey, you have taught me more about fishing rather than giving me a fish, encouraging me to think critically and supporting my ideas. The advice and constructive criticism you provided were always extremely helpful and motivating. Your guidance was always there for me whenever I needed it, you encouraged me to strive for the best and gave me opportunities that few others are fortunate enough to have. Your inspiring examples and your contributions to my personal and professional growth have been extremely valuable.

To the funding partners who made this research possible – the McPherson family and the Invergowrie Foundation, as well as the University of Melbourne scholarship. Your generosity, vision, and commitment to this important work are greatly appreciated.

To my advisory committee member, A/Prof. Glenn Fitzgerald, and committee chairs, A/Prof. Kourosh Khoshelham and Prof. Michael Stewardson, thank you for your professional and constructive feedback during my progress review meetings. My progress has been kept on track due to your valuable contributions and my tasks have been completed efficiently.

To my co-authors – Dr Tomas Poblete, Dr Victoria Gonzalez-Dugo, Dr Alberto Hornero, Prof. Peter Moar, and Dr Xiaojin Qian – thank you for the opportunity to collaborate. Thank you for sharing your considerable expertise, insight, and perspectives with me, which have enriched the quality of my work.

To the partners in the Mallee and Rebecca Wells from the Mallee Regional Innovation Centre (MRIC), thank you for your assistance with arranging possible collaborations with growers. Thank you to the owner of Aroona Farms, Brian Slater, for permission to conduct this research.

To the lab staff at QuantaLab IAS-CSIC (Spain), thank you for the laboratory support, particularly Rafael Romero and David Notario. To my fellow PhD students, thank you for your scientific discussions and company throughout these years, particularly Anirudh Belwalkar, Jie Jian, Dr Shuci Liu, Huazhen Li, Zitian Gao, Manish Kumar Patel, Dr Chih-chung Chou, Shirui Hao, Lilangi Wijesinghe, Peiye Li, Jia Xu, Zhiyuan Yang, and many others at the HyperSens Remote Sensing Laboratory and the MESM lab. It was a pleasure to have such informative conversations with you and I appreciate you sharing experience and including me in your research journeys.

To my parents, my family, and my other friends (e.g., Dr Yan Li, Jessie Xie, Vivian Shen, and Sarah Huang), who supported me throughout this journey, thank you for your unwavering love and for helping me to enjoy life. In particular, I am grateful to my parents and my parents-in-law for their unconditional love and for instilling the importance of education in me. Your sacrifices, love, encouragement, and support have enabled me to pursue my PhD studies.

And, last but not least, the most special mention goes to my husband, Evan Liu, who has been by my side all along my PhD journey, providing love, support, encouragement, and understanding as always. You have been a tremendous support to me throughout the past ten years of our marriage. My life is brightened by your presence and filled with love. Your support has been a constant source of my motivation.

Acknowledgements also go to all those who have contributed to this PhD project whom I may not have mentioned above, and to my own perseverance despite challenges. Without all your support, I would not have been able to progress as far as I have and achieve what I have achieved.

Table of Contents

ABSTRACT I
DECLARATION III
PREFACE IV
ACKNOWLEDGEMENTS VI
TABLE OF CONTENTS VIII
LIST OF TABLES X
LIST OF FIGURES XI

CHAPTER 1 : GENERAL INTRODUCTION 1

1.1 Background 1
1.2 Roles of nutrients in plant growth 3
1.3 Traditional methods for leaf nutrient assessment 11
1.4 Airborne remote sensing platforms for assessing leaf nutrients 12
1.5 Standard remote sensing methods for monitoring nutrient status 14
1.6 Plant traits retrieval from radiative transfer models 18
1.7 Chlorophyll fluorescence 20
1.8 Spaceborne platforms for assessing leaf nutrients 24
1.9 Objectives and thesis structure 27
References 32

CHAPTER 2 : ASSESSING THE PERFORMANCE OF SOLAR-INDUCED FLUORESCENCE (SIF) AND VEGETATION PLANT TRAITS FOR LEAF MACRO- AND MICRO-NUTRIENT CONCENTRATIONS 45

Abstract 46
2.1 Introduction 47
2.2 Material and methods 50
2.3 Results 58
2.4. Discussions 75
2.5. Conclusions 77
References 79

CHAPTER 3 : EVALUATING THE ROLE OF SOLAR-INDUCED FLUORESCENCE (SIF) AND PLANT PHYSIOLOGICAL TRAITS FOR LEAF NITROGEN ASSESSMENT IN ALMOND USING AIRBORNE HYPERSPECTRAL IMAGERY 84

Abstract 85
3.1 Introduction 87
3.2 Material and methods 91
3.3 Results 104
3.4 Discussion 119
3.5 Conclusions 122
References 123

CHAPTER 4 : QUANTIFICATION OF LEAF NITROGEN IN ALMOND ORCHARDS FROM THE SPACEBORNE DESIS HYPERSPECTRAL SENSOR: MODELING AND ASSESSMENT WITH AIRBORNE HYPERSPECTRAL AND SENTINEL-2 IMAGERY 131

Abstract *132*
4.1 Introduction *134*
4.2 Material and methods *137*
4.3 Results *151*
4.4 Discussion *161*
4.5 Conclusions *165*
References *166*

CHAPTER 5 : CONCLUSIONS 171

5.1 Summary and main conclusions *171*
5.2 Implications and contributions *173*
5.3 Recommendations for further research *176*
APPENDIX 1 177
APPENDIX 2 196
APPENDIX 3 201
APPENDIX 4 206
APPENDIX 5 211

List of Tables

Table 1.1. Common symptoms associated with nutrient deficiencies. A bold orange **X** indicates the most likely elements corresponding to the symptoms of deficiency (modified based on an image source: https://www.agrowtronics.com/nutrients-for-hydroponics/)..... 11
Table 2.1. Spectral vegetation index equations used in this study..... 56
Table 2.2. Descriptive data from the biochemical laboratory analysis of macro- and micro-nutrient concentrations and their ratios in almond leaves from the 15 study plots in 2020 and 2021..... 59
Table 2.3. Correlations (r^2) between leaf measurements and nutrient concentrations and their ratios for the 15 study plots in 2020 and 2021. Field measurements include leaf chlorophyll a+b (C_{ab}), flavonoids (Flav), anthocyanins (Anth), nitrogen balance index (NBI) measured with Dualex, and steady-state chlorophyll fluorescence (Ft) measured with FluorPen. Background color represents the p-value – dark green for $p < 0.005$, medium green for $0.005 \leq p < 0.01$, light green for $0.01 \leq p < 0.05$, and white for $p \geq 0.05$ (not significant). 63
Table 2.4. Correlations (r^2) between vegetation indices at the leaf level and nutrient concentrations for the 15 study plots in 2020 and 2021. Background color represents the p-value – dark green for $p < 0.005$, medium green for $0.005 \leq p < 0.01$, light green for $0.01 \leq p < 0.05$, and white for $p \geq 0.05$ (not significant). 67
Table 2.5. Correlations (r^2) between vegetation indices calculated from airborne hyperspectral imagery and nutrient concentrations for the 15 study plots in 2020 and 2021. Background color represents the p-value – dark green for $p < 0.005$, medium green for $0.005 \leq p < 0.01$, light green for $0.01 \leq p < 0.05$, and white for $p \geq 0.05$ (not significant)..... 70
Table 2.6. Correlations (r^2) between RTM-inverted plant traits from airborne hyperspectral imagery and nutrient concentrations and ratios for the 15 study plots in 2020 and 2021. Traits derived from airborne data include leaf chlorophyll a+b (C_{ab}), carotenoids (C_{car}), anthocyanin (Anth), photochemical reflectance parameter (C_x), dry matter content (C_{dm}), leaf area index (LAI) by inversion algorithm, and solar-induced fluorescence (SIF). Background color represents the p-value: dark green for $p < 0.005$, medium green for $0.005 \leq p < 0.01$, light green for $0.01 \leq p < 0.05$, and white for $p \geq 0.05$ (not significant). 72
Table 3.1. Spectral vegetation index equations used in this study..... 101
Table 3.2. Ranges of input parameters for the LUT of FluSAIL model. 103
Table 3.3. Coefficients of determination (r^2) for the intercorrelations among standard indices at canopy level from the same 15 study plots in two consecutive years and leaf N concentration (%), Dualex-derived leaf chlorophyll content (C_{ab}), nitrogen balance index (NBI), and steady-state chlorophyll fluorescence (Ft) measured with FluorPen. 110
Table 3.4. Coefficients of determination (r^2) for correlations among model-derived estimates from the same 15 study plots in two consecutive years, including leaf chlorophyll a+b (C_{ab}), carotenoids (C_{car}), anthocyanin (Anth), dry matter content (C_{dm}), photochemical reflectance parameter (C_x), leaf area index (LAI), measured leaf N concentration (%), Dualex-measured chlorophyll content, canopy SIF, and canopy photochemical reflectance index (PRI_{515}). 114
Table 4.1. Specifications of the sensors used in this study. 140
Table 4.2. Ranges of input parameters for the LUT of the FluSAIL Model..... 145
Table 4.3. Vegetation indices calculated in this study from Sentinel-2 data. 148
Table 4.4. Correlations (r^2) between image-derived spectral traits and field measurements. Rows indicate modeled traits, and columns indicate pairing of field data source (top row), year (second row), and HSI source (third row)..... 153
Table 4.5. Correlations (r^2) between model-derived plant traits and vegetation indices from Sentinel-2 against field measurements. 156

List of Figures

Fig. 1.1. The use of nitrogen fertilizer in Australia and around the world from 1960 to 2020 (data source: FAOSTAT https://www.fao.org). 2
Fig. 1.2. Water quality risks of global river basins, based on 2000-2010 data from Damania *et al.* (2019). Red or yellow show areas where biological oxygen demand, nitrogen fertilizer runoff, and electrical conductivity have significant impacts on freshwater and present a high risk of water pollution. Gray areas have no data for one or more parameters. 3
Fig. 1.3. Visible symptoms of nutrient deficiency (image source: https://www.agrowtronics.com/nutrients-for-hydroponics/). 10
Fig. 1.4. Representation of xanthophyll cycles in photosynthetic microbes. Violaxanthin-antheraxanthin-zeaxanthin (VAZ) cycles are modulated by light conditions (modified based on Saini *et al.* (2019)). 17
Fig. 1.5. At the top of the canopy, the total upwelling radiance (orange) and solar-induced fluorescence (SIF) spectra (blue) were collected in the range of 650-800 nm, with two oxygen absorption features marked with grey rectangles. 22
Fig. 1.6. Spaceborne imaging spectrometers recently launched or planned/approved (Rast and Painter, 2019). 26
Fig. 1.7. Observations of solar-induced chlorophyll fluorescence (SIF) made by past missions (gray), current missions (pink), and future missions (light blue). The font colors distinguish geostationary (green) from low-earth orbit (black) missions. The dashed-line boxes indicate the spatial and temporal resolution of value-added SIF products (purple) (Sun *et al.*, 2023). 'p.' denotes present. 27
Fig. 1.8. The flow between the main chapters demonstrates how the research development of this doctoral thesis is motivated by the key connections. 31
Fig. 2.1. a) The area of the 1200-ha almond orchard where the study was conducted. b) The location of the study site (magenta pointer) in Victoria, Australia. c) The landscape and row structure of the almond trees in the study area. d)-e) Close-ups of almond trees and the gap between rows. 51
Fig. 2.2. In situ leaf measurements of: a) leaf chlorophyll (C_{ab}), anthocyanins (Anth), flavonoid (Flav) content, and nitrogen balance index (NBI) using a Dualex 4 Scientific sensor; b) leaf reflectance spectra in the visible and near-infrared regions with a PolyPen RP 410 instrument; c) leaf steady-state chlorophyll fluorescence (Ft) with a FluorPen FP 110 instrument; and d) leaf sample collection and leaf measurements of sunlit leaves from the top of the ladder. 53
Fig. 2.3. a) High-resolution airborne hyperspectral image (color-infrared overview) over the study area at 40-cm spatial resolution collected with 371 spectral bands on 31 January 2021. The yellow areas represent the locations of the 15 study plots. b) Segmentation of sunlit crown area, the yellow rectangle representing an 8-tree × 6-row study plot. c) The reflectance spectra for two tree crowns segmented from a study plot. d) The radiance (L, green colors) spectra for two tree crowns and the irradiance (E, orange color) spectra for SIF calculation. Crosses indicate the spectral positions of the sensor bands. 54
Fig. 2.4. Ranges of variation for biochemical laboratory-derived leaf macro-nutrients of: a) Nitrogen; b) Phosphorus; d) Calcium; e) Magnesium; f) Sulphur; g) Carbon concentration (%w/w); and leaf micro-nutrients of: h) Iron; i) Manganese; j) Zinc; k) Copper; l) Boron concentration (mg/kg); and nutrient ratios of m) N/(N+P+K), n) K/(Ca+Mg), o) Fe/Mn in almond leaves for the 15 study plots in 2020 (green) and 2021 (brown). The crossed line and the line through the box indicate the median and mean values, respectively. Q1, Q2, and Q3 represent the limits of the first, second, and third quartiles, with 15 samples collected each year. 60
Fig. 2.5. Ranges of variation of leaf: a) chlorophyll (C_{ab}); b) flavonoids (Flav); c) nitrogen balance index (NBI) measured using Dualex; and d) steady-state chlorophyll fluorescence (Ft) using FluorPen in almond leaves for the 15 study plots in 2020 (green) and 2021 (brown). The crossed line and the line through the

box indicate the median and mean values, respectively. Q1, Q2, and Q3 represent the limits of the first, second, and third quartiles, with 15 samples collected each year. 61
Fig. 2.6. Relationships between in situ Dualex-measured: a) leaf chlorophyll (C_{ab}); b) flavonoid (Flav) content; c) nitrogen balance index (NBI) and biochemically derived leaf Nitrogen concentration (%w/w) in 2020 (hollow gray circle) and 2021 (solid black circle). Relationships between leaf steady-state fluorescence (Ft) and biochemically derived leaf macro-nutrients of: d) Nitrogen; e) Phosphorus; f) Potassium concentration (%w/w) in 2020 (hollow gray circle) and 2021 (solid black circle). All p-values are less than 0.005, except for the one marked n.s. (not significant). 64
Fig. 2.7. Relationships between leaf CTRI1, BGI1, PRI_{m4}, PRI_n, and biochemically derived leaf nitrogen concentration (%w/w) in 2020 (hollow gray circle) and 2021 (solid black circle). All p-values<0.005. 68
Fig. 2.8. Relationships between canopy solar-induced fluorescence (SIF) and biochemically derived leaf macro-nutrient levels of: a) Nitrogen; b) Phosphorus; c) Potassium concentration (%w/w) in 2020 (hollow gray circle) and 2021 (solid black circle). The highlighted text represents the p-value – below 0.005 (white), 0.01 (light gray), up to 0.05 (medium gray). 74
Fig. 3.1. Color-infrared (CIR) overview of the hyperspectral mosaic acquired with the VNIR hyperspectral sensor over the 1,200-ha study site collected on January 31, 2021. Spectral bands at 860 (R), 650 (G), and 550 (B) nm are shown with a spatial resolution of 40 cm per pixel. 95
Fig. 3.2. (a) Study plot consisting of six rows by eight trees within the blue solid line. Leaves from four trees within the yellow dashed rectangle were measured in the field. (b) The reflectance spectra of different scene components extracted from the airborne hyperspectral imager, including sunlit (green solid line) and shaded (grey dashed line) tree crown, and sunlit (orange dashed line) and shaded soil (brown dashed line) pixels. 96
Fig. 3.3. Thermal mosaic collected over the entire study area captured on January 31, 2021 at a spatial resolution of 60 cm. Cooler colors (purple and blue) indicate plant canopies, and yellow/brown colors indicate soil. 97
Fig. 3.4. Overview of the tree-crown segmentation applied to the hyperspectral mosaic (a, upper image in color-infrared, crown in green outline) and the thermal mosaic (c, bottom image displaying cooler canopy in blue and hot soil in red color, crown in yellow outline). Right column contains zoomed-in views (b and d) of the scenes within the white rectangle on the left. 98
Fig. 3.5. Segmentation of the sunlit crown area for SIF quantification on two study plots (a) higher nutrient level and (b) lower nutrient level. The irradiance spectrum (orange color) was used along with the radiance spectra (example shown in (c) for two study plots (green and grey lines) to calculate SIF. Crosses denote the spectral position of the sensor bands (c). 99
Fig. 3.6. Ranges of variation based on leaf steady-state chlorophyll fluorescence (Ft) quartiles for leaf phenotypes measured at the pre-harvest stage in 2020 (green) and 2021 (orange): a) nitrogen concentration, b) chlorophyll a+b (C_{ab}), c) flavonoid (Flav), d) Nitrogen Balance Index (NBI), e) anthocyanins (Anth), f) CTRI1, g) PRI, h) PRI·CI, and i) NPQI. The line through the box and marker 'x' refer to the median and mean value, respectively. 106
Fig. 3.7. Relationships between leaf N concentration (%) and a) leaf chlorophyll content, b) Nitrogen Balance Index (NBI), c) photochemical reflectance index (PRI), and d) steady-state chlorophyll fluorescence (Ft). Green and orange represent data in 2020 and 2021, respectively. Grey is used to represent correlation when combining data of 2 years. *p-value < 0.05; **p-value < 0.01; ***p-value < 0.005; n.s. = not significant. 107
Fig. 3.8. Relationships between canopy SIF and a) leaf steady-state chlorophyll fluorescence (Ft) and b) leaf N concentration (%) in 2020 (green), 2021 (orange), and the combined years (grey). *p-value < 0.5; **p-value < 0.05; ***p-value < 0.005. 111

Fig. 3.9. Leaf N against a) NDVI, b) MCARI, c) CTRI1, and d) PRI_{515} calculated from hyperspectral imagery acquired in 2020 (green) and 2021 (orange). *p-value < 0.05; **p-value < 0.01; ***p-value < 0.005; n.s. = not significant. 112
Fig. 3.10. Comparison of the average hyperspectral image spectrum (orange dashed line) and the corresponding spectrum obtained from the FluSAIL model inversion (blue solid line) for one monitored plot. The simulated FluSAIL spectral range is shown in the shaded grey area. 113
Fig. 3.11. The relative contribution from OOB importance scores of each variable to the predicted N concentration from a) all plant traits estimated from hyperspectral and thermal imagery and b) a non-collinear subset of variables (VIF < 5) 116
Fig. 3.12. Correlations between leaf N concentration (%) and predicted N using models based on a) chlorophyll a+b content alone, b) chlorophyll a+b content with canopy SIF, c) chlorophyll a+b content with leaf area index (LAI), and d) LAI with canopy SIF. The grey diagonal line is the 1:1 line. All p-values < 0.001. 117
Fig. 3.13. Interpolated map of a) chlorophyll a+b content, c) solar-induced fluorescence, and e) predicted N concentration derived from C_{ab} and SIF in 2021. Right column contains zoomed-in views (b, d and f) of the scenes on the left in the northeast blocks. Block numbers are displayed in the centers. 118
Fig. 4.1. Two adjacent scenes from the spaceborne DESIS hyperspectral sensor (30-m spatial resolution). The radiance spectra from randomly chosen fields are shown in the inset. The study site is demarcated by the yellow dashed line. 138
Fig. 4.2. Colour-infrared (CIR-R: 860, G: 650, B: 550) overview of a) airborne VNIR hyperspectral image (HSI) acquired at 0.4-m pixel size on January 31, 2021 and b) spaceborne DESIS VNIR HSI collected at 30-m pixel size on January 23, 2021 over the 1200-ha study site. (c-f) The irradiance (E) spectrum at each data collection date and the radiance (L) spectra of vegetation and soil from c) airborne HSI and d) spaceborne DESIS HSI over the 700-800 nm spectral region and e-f) their spectra over the O_2-A feature around 760 nm. 141
Fig. 4.3. Comparison of colour-infrared a) airborne and b) DESIS hyperspectral image (HSI), and the reflectance spectra for c) vegetation and d) soil, from the original spaceborne DESIS HSI (solid orange line), post-calibrated spaceborne DESIS HSI (solid green line), and airborne HSI (grey dashed line). 143
Fig. 4.4. Colour-infrared image from the a) airborne VNIR hyperspectral image (HSI) acquired at 0.4 m per pixel on January 31, 2021, b) post-calibrated DESIS HSI acquired at 30 m per pixel on January 23, 2021, and c) Sentinel-2 multispectral image at 10 m per pixel collected on January 23, 2021, with the reflectance spectra of vegetation (in green) and soil (in brown) within the DESIS pixel in the VNIR region. 144
Fig. 4.5. Colour-infrared overview of a 5-by-5 DESIS pixel window of a) the tree-crown segmentation in yellow colour and the average tree-crown reflectance spectrum (in orange) from an airborne hyperspectral image (HSI) at 0.4-m resolution, b) airborne HSI resampled to 30-m per pixel, c) post-calibrated DESIS HSI at 30 m per pixel, and d) Sentinel-2 multispectral image at 10 m per pixel. VNIR reflectance spectra within each green box are shown below each image. The solid green line represents the reflectance spectrum within the central DESIS pixel (in green) from different images compared with the tree-crown reflectance spectrum (orange dashed line). 146
Fig. 4.6. Schematic representation of the leaf N assessment from airborne hyperspectral, spaceborne DESIS hyperspectral imagery, and Sentinel-2 multispectral image in a dense canopy almond orchard. Underlined parameters were retrieved and used in the Sentinel-2 model. 150
Fig. 4.7. Relationships between estimates of plant characteristics by measurement methodology. Top row: spatially resampled (aggregated to 30 m) airborne hyperspectral vs. tree crown-based estimates for a) C_{ab}, and b) SIF in 2020 (12 points in the hollow grey circle) and 2021 (24 points in solid black circle). The solid blue line represents correlation when combining data from 2 years. Middle row: DESIS hyperspectral vs.

tree crown-based estimates of c) C_{ab} and d) SIF in 2021. Bottom row: e) C_{ab} and f) SIF index between DESIS hyperspectral and the spatially resampled airborne hyperspectral at 30 m. The orange dashed diagonal line is the 1:1 line. 152
Fig. 4.8. Importance of FluSAIL RTM-inverted traits and SIF used as predictors for leaf N. Models used traits derived from either DESIS (in orange) or airborne (in green) hyperspectral imagery in 2021. The two most important variables (non-collinear) are marked in a grey dashed rectangle..... 154
Fig. 4.9. Relationships between a) RTM-derived C_{ab} content from Sentinel-2 and leaf C_{ab} measured by Dualex, and b) $CI_{red\text{-}edge}$ calculated from Sentinel-2 and leaf N concentration (%) in 2021 (24 points). The grey dashed diagonal line is the 1:1 line. 155
Fig. 4.10. Importance of model-derived plant traits and vegetation indices (non-collinear, VIF < 5) calculated from Sentinel-2 in 2020 and 2021. 157
Fig. 4.11. Relationships between leaf N concentration model predictions based on a) airborne hyperspectral-derived N (C_{ab}, SIF) from tree crowns, b) Sentinel-2-derived N (C_{ab}, C_w, C_{dm}), and c) spaceborne DESIS hyperspectral-derived N (C_{ab}, SIF). Data from 2020 (12 points) are shown as hollow grey circles, and data from 2021 (24 points) are shown as solid black circles. The solid blue line represents the linear fit when combining data from 2 years. The orange dashed diagonal line is the 1:1 line. 159
Fig. 4.12. Estimated leaf N maps for the 2021 pre-harvest season based on models using a) airborne hyperspectral-derived C_{ab} and SIF from tree crowns, b) spatially resampled airborne hyperspectral imagery-derived C_{ab} and SIF, c) spaceborne DESIS hyperspectral imagery-derived C_{ab} and SIF, and d) Sentinel-2-derived plant traits C_{ab}, C_w, and C_{dm}. 161

Chapter 1 : General introduction

1.1 Background

Agricultural fertilizers are used to provide plants with nutrients that they may not be able to obtain from the soil alone, thereby increasing crop yields and enhancing agricultural productivity (Chen, 2006). Over the past few decades, steady growth in fertilizer use has occurred in Australia and around the world (Fig. 1.1) due to increasing agricultural intensity and a growing emphasis on maximizing yields for economic and food-security reasons. Since the 1960s, fertilizer use in Australia has increased significantly, with nitrogen and phosphorus fertilizers the most commonly used (MacDonald *et al.*, 2011, Lambers *et al.*, 2008). This is mainly due to the country's focus on agricultural exports, which has led to a need for higher yields and more intensive farming practices for high-value crops like horticultural crops and sugar cane (Angus, 2001, Angus and Grace, 2016). Since the mid-1990s, a significant increase in fertilizer use has also been observed for wheat and other dryland crops (Angus and Grace, 2016). The use of fertilizers has increased globally, with developing countries, in particular, experiencing significant increases in fertilizer consumption over the past few decades (Heffer and Prud'homme, 2016). This trend is expected to continue in the coming years as global food demand increases and agricultural productivity becomes increasingly important (Schmidhuber and Tubiello, 2007).

In addition to the effects on plant growth, plant nutrition has a profound impact on most other living organisms because plants are the foundation of many food chains. Various minerals are involved in different processes of the human body, so their abundance and distribution in plants affect human diets. According to White and Broadley (2005), iron, zinc, calcium, magnesium, and copper deficiencies are very common, especially in developing regions, and this is a result of the lack of minerals in natural sources (i.e., crops, food, water). Agricultural production and food

security are thus concerns all over the world and are subject to national regulations (Roy *et al.*, 2006).

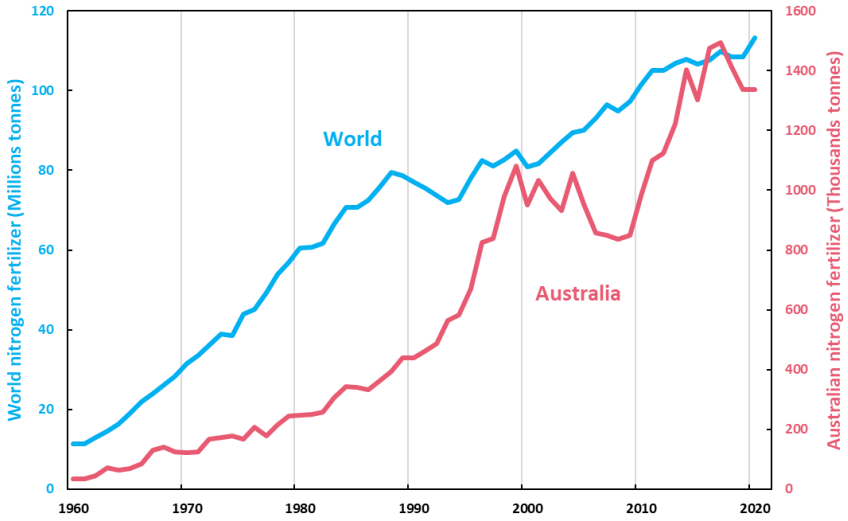

Fig. 1.1. The use of nitrogen fertilizer in Australia and around the world from 1960 to 2020 (data source: FAOSTAT https://www.fao.org).

The use of fertilizers has undoubtedly improved agricultural productivity and increased food production, but it appears that over-fertilization has become a common practice. Excess fertilization can sometimes damage plants, adversely impacting overall plant development and performance, and can lead to environmental problems like soil contamination, atmospheric pollution, algal blooms, biodiversity threats, and greenhouse gas emissions, thus prompting resource and economic concerns (Stewart *et al.*, 2005, Stevenson and Cole, 1999, Matson *et al.*, 1998, Sutton *et al.*, 2013, Skiba and Rees, 2014). Fig. 1.2 illustrates the global water pollution risks associated with fertilizer runoff, showing Australia among the high-risk countries. Therefore, it is imperative that fertilizers and other inputs are applied within the constraints and conditions of sustainable agricultural practices in order to effectively promote yields while minimizing

environmental impacts (Muhammad *et al.*, 2015). In fact, globally, about 47% of synthetic N fertilization fails to increase yield (Lassaletta *et al.*, 2014) due to various factors, including crop species and varieties, the form of N used, soil types, water availability, supply technology (e.g., timing, forms, placement), availability of other nutrients, and prevalent insect pests (El-Sharkawy *et al.*, 1998, Ospina *et al.*, 2014, Dobermann, 2005, Fageria and Baligar, 2005). In the context of precision agriculture management, nutrient status needs to be accurately assessed to enable optimal and sustainable application of fertilizers.

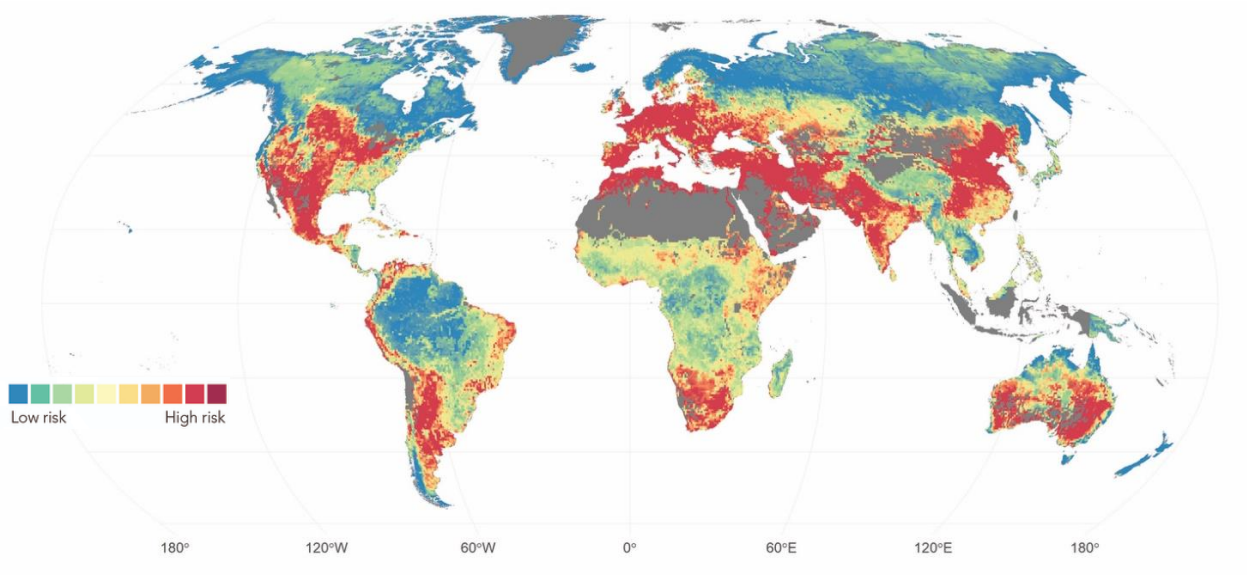

Fig. 1.2. Water quality risks of global river basins, based on 2000-2010 data from *Damania et al.* (2019). Red or yellow show areas where biological oxygen demand, nitrogen fertilizer runoff, and electrical conductivity have significant impacts on freshwater and present a high risk of water pollution. Gray areas have no data for one or more parameters.

1.2 Roles of nutrients in plant growth

To complete their life cycle, plants require numerous nutrients in varying amounts throughout the growing season. Carbon (C), hydrogen (H), and oxygen (O) are considered the three primary elements taken up through both air and water, whereas the other necessary elements are absorbed

462 from soil and fertilizers through plant roots (Marschner, 1986). Nutrients are usually classified into
463 macro-nutrients and micro-nutrients, based on their rate of absorption by plants (Stewart, 1988).
464 It is widely accepted that macro-nutrients are often essential for the structure of molecules, which
465 explains the need of plants for large quantities. Plant macro-nutrients are divided into two groups
466 based on their functions – primary macro-nutrients (i.e., nitrogen, phosphorus, potassium) and
467 secondary macro-nutrients (i.e., calcium, magnesium, sulfur). The role of plant micro-nutrients is
468 generally described as catalytic or regulatory (Carrow *et al.*, 2002, Ryan *et al.*, 2001). As the plant
469 moves through different stages of development, each nutrient plays a distinctive role in different
470 metabolic processes, such as constituting structural components or redox-sensitive components, as
471 well as protecting plants from various abiotic and biotic stresses (White and Brown, 2010, Morgan
472 and Connolly, 2013, Shanker and Venkateswarlu, 2011, Roy *et al.*, 2006, Tripathi *et al.*, 2014).

473 **Nitrogen (N)** is required by plants in large amounts throughout all phases of plant development
474 because it constitutes both structural (cell membranes) and nonstructural (amino acids, enzymes,
475 protein, nucleic acids, and chlorophyll) components (Chism, 2002, Mengel and Kirkby, 2012). For
476 example, N constitutes about 16% of total plant protein (Frink *et al.*, 1999) and approximately 1.5-
477 2.0% of plant dry matter (Lima *et al.*, 2007). Furthermore, N enhances fruit and seed production,
478 and produces rapid plant growth and high-quality forage crops (Mengel and Kirkby, 2012,
479 Marschner, 2011). Thus, N is regarded as the essential plant nutrient. In almonds, N is an extremely
480 important nutrient throughout the entire growth cycle. N is essential for building the tree canopy
481 and stimulating vegetation growth (e.g., promoting the growth of stems, full leaf expansion, and
482 hardening of nut shells), resulting in improved bud formation, higher yields, and higher protein
483 levels in nuts. Insufficient N stops leaf elongation (Marschner, 2011), inhibits photosynthesis
484 (Gregoriou *et al.*, 2007), reduces the size of chloroplasts (Li *et al.*, 2013), and produces plants

lacking vigor. It is common for plants that are deficient in N to show signs of chlorosis or yellowing leaves. On the other hand, the application of excessive N impairs hydraulics, limits photosynthesis, and alters the metabolic processes of almond trees (Sperling *et al.*, 2019).

Phosphorus (P) plays a vital role as the constituent of nucleic acids (i.e., DNA, RNA), adenosine triphosphate (ATP), and other plant components (e.g., teichoic acids and phospholipids), as well as being a central component of intermediary metabolism (Mills and WT, 1994, Hopkins and Hüner, 1995). The concentration of P in plants is approximately 0.05% to 0.5% of total dry weight. The presence of P contributes to the development of root and stem strength, flower initiation, seed formation, and fruit quality and production (He *et al.*, 1992, Malhotra *et al.*, 2018, Zhu and Smith, 2001). It is thus regarded as an essential nutrient for plant growth and development. There is much evidence that P aids in the photosynthetic process (Raaimakers *et al.*, 1995, Stitt, 1990), assists with plant maturation and stress resistance (Tripathi *et al.*, 2014), and increases crop yield (Hopkins and Hansen, 2019, Schlegel and Havlin, 2017, Hopkins *et al.*, 2010). When P is deficient, the growth of the plant is markedly restricted, resulting in retarded growth, tillering, root development, and delayed ripening. Conversely, excessive levels of P can cause toxic symptoms or the death of the plant in very severe cases (Roy *et al.*, 2006).

Potassium (K) is closely involved in many physiological processes (e.g., protein synthesis) and plays a major role as a cationic inorganic element in plants, helping to improve photosynthesis, enzyme activity, water balance, assimilation, and transportation (Barker and Pilbeam, 2015, Mengel and Kirkby, 2012, Pettigrew, 2008). More specifically, K is crucial in maintaining the water homeostasis of plants because it regulates stomatal opening and closing in plants and thus minimizes drought stress (Mahouachi *et al.*, 2006). K enhances fruit quality and yield, increases disease resistance, and reduces lodging in plants (Nursu'aidah *et al.*, 2014, Barker and Pilbeam,

2015, Pettigrew, 2008). Therefore, K is considered essential to all plant life. To be more specific, K is particularly important for nut-fill and is required in large quantities to achieve the highest yields. A sufficient supply of K leads to higher kernel weights, more split shells, and fewer blank nuts. There is evidence that K accounts for between 1% and 5% of plant dry matter. The fact that K, like N and P, is highly mobile in plant tissues explains why symptoms of primary macro-nutrient deficiency usually appear in the older leaves of a plant. Nevertheless, when K levels are low, the symptoms of deficiency are not as easily visually detectable as deficiencies of N or P are. At an advanced stage of K deficiency, chloroplasts and mitochondria collapse (Barker and Pilbeam, 2015).

Calcium (Ca) plays an essential role in plants as a structural component of cell walls and membranes and as a second intracellular messenger (Maathuis, 2009, Marschner, 2011). Critical for plant growth and development, it aids in activating enzymes, regulating water movement, and balancing salt levels in plant cells, and it also activates K to control the process of the opening and closing of stomata (Hepler, 2005). In this regard, Ca facilitates the response to biotic and abiotic stresses (e.g., salt stress, hyperosmotic stress), stomatal regulation, and physical damage (e.g., cold shock) (McAinsh and Pittman, 2009, Drøbak and Watkins, 2000, Kiegle *et al.*, 2000, Thor, 2019, Kudla *et al.*, 2010). In almond crops, Ca plays an important role in maintaining the integrity of cell membranes and building strong cell walls. Ca enables greater physiological stability of plant tissues, reducing the risk of physical damage and disorders. It also provides growth support for pollen tubes and aids in pollination. Ca constitutes between 0.1% and 5% of plant dry matter (White and Broadley, 2003). Deficiency of Ca is characterized by yellow coloration and black spots on leaves (Hepler, 2005), symptoms which first appear on growing tips and young leaves because Ca is immobile.

Magnesium (Mg) is known as one of the essential nutrient elements for plants because it is a central atom in chlorophyll and an important regulator of enzymes (Hopkins and Hüner, 1995, Wilkinson *et al.*, 1990). Additionally, it plays a significant role in plant photosynthesis, particularly in promoting light reactions in the stroma (Marschner, 2011, Maathuis, 2009). It has been found that Mg constitutes approximately 0.05-0.5% of total plant dry matter. Mg is a movable element in plants, which results in chlorophyll decreasing first in old leaves and the remaining Mg being transferred to younger leaves. It is commonly known that chlorosis (yellowing of the leaves) is a sign of Mg deficiency (Hermans *et al.*, 2010). Conversely, an adequate supply of Mg means that plants display resistance to diseases like root rot, bacterial spot, and early blight disease (Ishfaq *et al.*, 2022, Huber and Jones, 2013).

Sulfur (S) is an important constituent of proteins and coenzymes and is implicated in oil biosynthesis (Hopkins and Hüner, 1995, Fazili *et al.*, 2008), with a typical range of 0.1-0.4% in plant dry matter and a N/S ratio of approximately 15 (Roy *et al.*, 2006). Furthermore, S is a key component of legume N fixation and its application greatly enhances legume N fixation, plant growth, and yield (Jamal *et al.*, 2005, Jamal *et al.*, 2010, Zhao *et al.*, 1999). There is also evidence that S compounds are effective for the detoxification of heavy metals (Jones, 1985, Ernst *et al.*, 2008). S is mobile in plants. Nevertheless, the symptoms of S deficiency may not be recognized easily in the field, as they are only obvious in severely deficient plants, and they often resemble the symptoms of N deficiency, with yellowish leaves first observable on the younger leaves.

In comparison to macro-nutrients, micro-nutrients are required at much lower levels to promote plant growth and boost yield, all of which are crucial to the growth of key tissues, the biosynthesis of proteins, stress tolerance, and the formation of chlorophyll and secondary metabolites (Marschner and Rengel, 2007, Jatav *et al.*, 2020).

554 **Manganese (Mn)** serves as an enzyme cofactor as well as part of the oxygen-evolving complex
555 in chloroplast (Hopkins and Hüner, 1995). It is known that Mn is a primary component of the
556 water-splitting enzyme associated with photosystem II, with a typical concentration of 20-300
557 mg/kg (Aftab and Hakeem, 2020, Havlin *et al.*, 2016). It exhibits certain properties similar to Mg,
558 although Mn-deficiency symptoms appear first on the younger leaves, whereas Mg-deficiency
559 symptoms are evident first on the older leaves (Roy *et al.*, 2006).

560 **Iron (Fe)** is crucial for chlorophyll synthesis and electron transfer, as well as for N fixation (Aftab
561 and Hakeem, 2020, Hopkins and Hüner, 1995). Fe is generally the most abundant of the micro-
562 nutrients, with a dry matter concentration of 100-500 mg/kg (Havlin *et al.*, 2016). Similarly to Mn,
563 Fe is generally immobile in the phloem and the symptoms of Fe deficiency are comparable to those
564 of Mn deficiency because both deficiencies lead to a reduction in chlorophyll production. In cases
565 of severe deficiency, leaves become almost pale white due to loss of chlorophyll (Roy *et al.*, 2006).

566 **Zinc (Zn)** is an enzyme activator (Hopkins and Hüner, 1995) and is normally found in volumes
567 ranging from 27 to 150 mg/kg of dry matter (Havlin *et al.*, 2016). According to Cakmak (2008), a
568 deficiency of Zn impairs ribonucleic acid (RNA) and protein production due to its significant role
569 in photosynthesis and N metabolism. Further, Zn is essential for maintaining plant growth,
570 especially for new tissue development, with increased seed viability and seedling vigor, as well as
571 resistance to abiotic and biotic stresses. The mobility of Zn is low. Zn is commonly used as a
572 defoliant after harvesting to promote budding, pollination, and fruiting in the following season (Bi
573 *et al.*, 2005, Lin and Agehara, 2021).

574 **Boron (B)** contributes to cell division and elongation by maintaining the structural integrity and
575 thickness of the cell wall (Hopkins and Hüner, 1995). In addition, B promotes flower production
576 and retention, the elongation and germination of pollen tubes, and the development of seed and

577 fruit, and hence it promotes yield (Aftab and Hakeem, 2020, Roy *et al.*, 2006). Furthermore, it
578 improves the drought tolerance of crops. B is essential for flowering and pollination to ensure
579 successful fruit development. B constitutes about 10-20 mg/kg of plant dry matter (Havlin *et al.*,
580 2016). Any deficiency of B is usually observed on the growing points of roots, shoots, and young
581 leaves and may result in stunting, distortion, and brittle foliage, as well as yellowing of lower leaf
582 tips.

583 **Copper (Cu)** is a necessary cofactor of oxidative enzymes (Hopkins and Hüner, 1995) and is
584 involved in chlorophyll formation (Roy *et al.*, 2006). In addition to protecting plants from disease
585 and improving the fertility of male flowers, Cu also contributes to the oxidation of iron in plants
586 (Aftab and Hakeem, 2020). Cu constitutes approximately 5-30mg/kg of plant dry matter (Havlin
587 *et al.*, 2016). The first signs of a Cu deficiency include narrow, twisted leaves and pale white shoot
588 tips (Roy *et al.*, 2006).

589 In conclusion, it is evident that nutrients play significant roles in plant growth and development
590 and have an impact on every stage of plant life. When plants do not have access to enough nutrients,
591 they will show signs of deficiency, such as discolorations, spotting on leaves, wilting, or drooping
592 (see Fig. 1.3 and Table 1.1 for further details). When these symptoms are observed on younger
593 leaves, it indicates that the deficient elements are immobile, such as B, Ca, Cu, Fe, Mn, S, and Zn.
594 However, plant growth, yield, and fruit quality can be enhanced by the application of adequate
595 nutrients (Morgan and Connolly, 2013). Nevertheless, determining specific nutrient deficiencies
596 is often challenging due to the possibility of similar symptoms being caused by different nutrient
597 deficiencies (Table 1). The interrelationships between nutrients and their deficiencies which affect
598 plant growth are complex and difficult to define. Consequently, beyond examinations of a single
599 nutrient, interactions between nutrients are poorly understood and require further study.

Furthermore, visible symptoms of water deficiency and pathogenic infections may be similar. Consequently, visual observation alone may yield a flawed diagnosis, resulting in delayed remedial action for the affected plant. For this purpose, it is necessary to develop an effective, efficient, and robust method for assessing plant nutrient status over large agricultural areas.

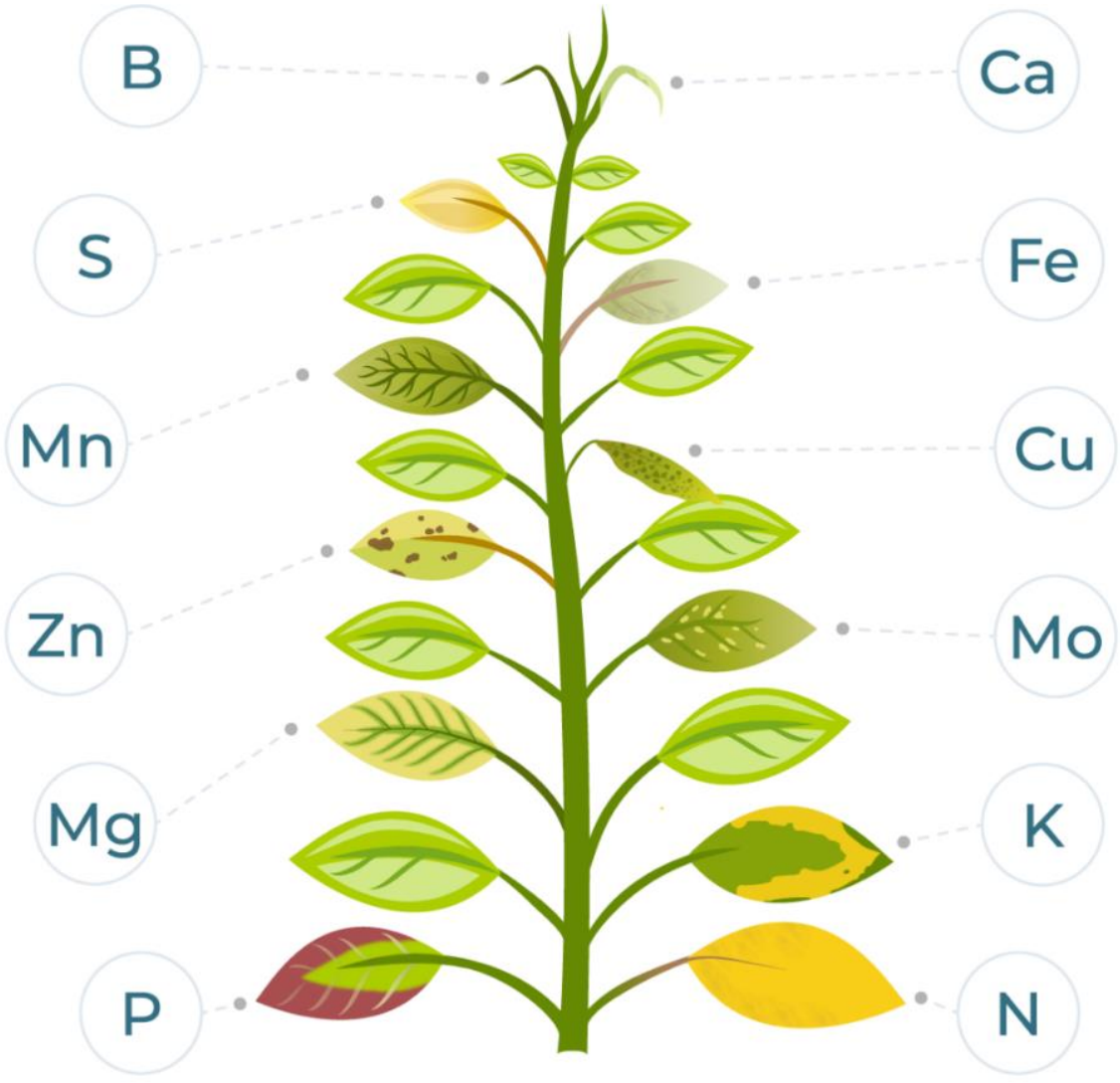

Fig. 1.3. Visible symptoms of nutrient deficiency (image source: https://www.agrowtronics.com/nutrients-for-hydroponics/).

Table 1.1. Common symptoms associated with nutrient deficiencies. A bold orange **X** indicates the most likely elements corresponding to the symptoms of deficiency (modified based on an image source: https://www.agrowtronics.com/nutrients-for-hydroponics/).

Symptoms	**Suspected nutrient element**										
	N	**P**	**K**	**Ca**	**Mg**	**S**	**Mn**	**Fe**	**Zn**	**B**	**Cu**
Necrosis (tissue death)			**X**		X		X	X	X		
Stunted growth	**X**	X	X						X	X	X
Wilting/drooping			X		X				X		
Thin stems	X	**X**	X			X					
Leaf drop	X										X
Deformed leaves			X	X						X	X
Chlorosis	**X**						X	X			
Tip burn		X	X								
Blossom end rot				**X**							
Brittle/weak stems		X	X			X					X
Chlorosis between veins					X		X	X	**X**		
Spotting/mottling							**X**				
Dark green or purple color		**X**									X

1.3 Traditional methods for leaf nutrient assessment

The analysis of leaf tissues has traditionally been regarded as an effective method of determining a plant's nutrient status and determining the best fertilization strategy (Smith, 1962, Ulrich, 1952, Embleton *et al.*, 1973, Jones and Janick, 1984). Destructive sampling techniques that use chemical analysis of leaf tissue have been widely used. There are two common laboratory methods, Kjeldahl digestion (Kjeldahl, 1883b, Kjeldahl, 1883a) and Dumas combustion (Dumas, 1831), which are accurate and reliable as reference methods for determining different macro- and micro-nutrient contents in leaf samples. Using the Kjeldahl digestion method, organic nitrogen is converted into ammonium by boiling in sulfuric acid and distilling with alkali to liberate ammonia, which is then determined by titration (Amin and Flowers, 2004). However, this method can only measure N which is bound to the organic components (proteins, amino acids, nucleic acids) and ammonium in the sample, while other N forms, such as nitrate and nitrite, are not amenable to measurement

and will thus produce a slightly lower value when using this procedure (Muñoz-Huerta *et al.*, 2013). The Dumas method overcomes this limitation and does not require toxic reagents, thus producing less pollution than the Kjeldahl method (Muñoz-Huerta *et al.*, 2013). Nevertheless, incomplete combustion results in the loss of nitrogen in the sample, and therefore a small sample weight is required for this method (Unkovich *et al.*, 2008).

However, this is not an efficient nor affordable approach to the continuous monitoring of nutrient status for large areas, especially when considering seasonal and within-field spatial variations. In contrast, non-destructive remote sensing (RS) techniques can determine spatial variability of photosynthesis-related proxies and plant physiological conditions over large areas in a rapid and cost-effective manner (Menesatti *et al.*, 2010, Prananto *et al.*, 2021, Wessman *et al.*, 1988, Martin and Aber, 1997, Smith *et al.*, 2002).

1.4 Airborne remote sensing platforms for assessing leaf nutrients

As most of the absorption features of green vegetation are located in the optical domain (400-2500 nm), optical sensing is generally used in remote sensing studies to analyze vegetation characteristics (Schaepman-Strub *et al.*, 2006). Hank *et al.* (2019a) outlined the spectral domain, in which reflectance is categorized into three major regions – visible (400-700 nm, VIS), near-infrared (700-1300 nm, NIR), and shortwave (1300-2500 nm, SWIR). VIS covers the spectral region of the absorption of foliar photosynthetic pigments, primarily chlorophylls, carotenoids, anthocyanins, and xanthophylls. In the NIR region, scattering occurs at both the leaf and the canopy scales, mainly determined by leaf structure, leaf area index (LAI), and plant density. Water,

641 lignin, cellulose, and proteins are the dominant absorption components in the SWIR range. For
642 nutrient assessment of extensive areas, optical sensors and cameras are usually mounted on aircraft.

643 Although drones are capable of capturing images with high spatial resolution, they are limited by
644 their flight altitude (normally less than 150 meters when keeping the platform within the line of
645 sight) and coverage capacity, consequently needing much more time to cover large areas than
646 aircraft-based platforms do. Due to the limited discrete spectral bands visible with multispectral
647 sensors (Landgrebe, 2003), these sensors typically make use of empirical methods based on
648 vegetation indices to assess nutrients (Maresma *et al.*, 2016, Tilling *et al.*, 2007, Boegh *et al.*,
649 2002). On the other hand, advances in hyperspectral sensors (Bioucas-Dias *et al.*, 2013) fitted to
650 manned/unmanned vehicles have enabled more accurate determination of pigment content (e.g.,
651 chlorophyll, carotenoids, anthocyanins, and xanthophyll cycle status) and other spectral traits (e.g.,
652 chlorophyll fluorescence, dry matter, and structural traits) as a result of their detailed contiguous
653 and narrow spectral information (Goetz, 2009), which is much better for determining the nutrient
654 status of large areas (Thenkabail and Lyon, 2016, Blackburn, 2007, Clevers and Kooistra, 2011).
655 In the past 20 years, the most widely used airborne imaging spectrometers include the NASA
656 Airborne Visible/Infrared Imaging Spectrometer (AVIRIS) (Vane *et al.*, 1993), the Australian
657 HyMAP (Cocks *et al.*, 1998), the Compact Airborne Spectrographic Imager (CASI) (Babey and
658 Anger, 1989), and the Airborne Prism Experiment (APEX) (Schaepman *et al.*, 2015). See the
659 review paper by Rast and Painter (2019).

660 **1.5 Standard remote sensing methods for monitoring nutrient status**

661 Typically, nutrient estimation, particularly for N, has been extensively investigated with optical
662 RS techniques which rely on proxy-based empirical methods. An early study by Evans (1989)
663 demonstrated a strong correlation between N and chlorophyll (Lee *et al.*, 2015) content. In practice,
664 handheld leaf-scanning instruments typically calculate C_{ab} *in situ* based on greenness readings
665 using two or more spectral bands, for instance, the SPAD-502 Chlorophyll Meter (Minolta Camera
666 Co. Ltd., Tokyo, Japan) and Dualex 4 Scientific (FORCE-A, Orsay, France). More specifically,
667 the SPAD-502 leaf chlorophyll meter is a non-destructive hand-held leaf-clip that measures
668 transmission through leaves with two light-emitting diodes in the red and infrared spectral regions
669 (650nm and 940nm) and a photodiode (Wood *et al.*, 1993, Markwell *et al.*, 1995). Other more
670 recently developed optical leaf-clip meters, like the Dualex 4 Scientific (FORCE-A, Orsay,
671 France), add flavonol (Flav) detection and the nitrogen balance index (NBI) (Goulas *et al.*, 2004).
672 These handheld leaf clips are widely used for rapid *in situ* leaf N status assessment of a wide range
673 of crops (e.g., rice, maize, wheat, cotton) (Cerovic *et al.*, 2012, Bullock and Anderson, 1998, Wood
674 *et al.*, 1992b, Wood *et al.*, 1992a) and also various different hardwood species (Netto *et al.*, 2005,
675 Chang and Robison, 2003, Cerovic *et al.*, 2012). Nevertheless, it has been demonstrated that
676 chlorophyll meter readings across species, varieties, cultivation practices, and growing stages vary
677 according to genetic and environmental factors and have limited sensitivity to high C_{ab} values,
678 thereby limiting the *in situ* assessment of leaf N (Houborg *et al.*, 2007, Xiong *et al.*, 2015, Cerovic
679 *et al.*, 2015).

680 Numerous studies have described different kinds of spectroscopic estimation of N using several
681 indices calculated from reflectance, particularly focusing on the visible and near-infrared (VNIR)
682 spectral domain. Close-range active spectral sensors are flexible in varying illumination conditions

683 because they are equipped with light-emitting components which provide radiation in specific
684 wavebands (Hatfield *et al.*, 2008). For example, Crop Circle (Holland Scientific Inc., Lincoln,
685 Nebraska) and GreenSeeker (NTech Industries Inc., Ukiah, California) can determine green
686 biomass and nitrogen uptake by detecting reflection in the VIS and NIR spectral regions. The N-
687 Sensor ALS® (YARA International, ASA, Dulmen, Germany) detects canopy reflectance by
688 flashing a xenon light source in the red-edge (730 nm) and NIR (760 nm) (Erdle *et al.*, 2011)
689 spectral regions. These field instruments provide simple canopy spectral ratios or indices from
690 specific spectral bands and can be installed on vehicles used for routine management. However,
691 the saturation occurs as a result of the biomass increase (Muñoz-Huerta *et al.*, 2013).

692 As an alternative to active sensors with spectral limitations, passive sensors (i.e., optical imagers
693 or spectral radiometers) have long been advocated as a useful means of characterizing spatial
694 variability in farm fields (Bhatti *et al.*, 1991). Due to strong chlorophyll absorption in the visible
695 and red-edge regions (Gitelson and Merzlyak, 1994), field spectrometers like the FieldSpec
696 (Analytical Spectral Devices, Boulder, CO, USA) and airborne imagers have made it possible to
697 estimate N content via canopy reflectance. The estimation of leaf N is typically based on empirical
698 relationships based on plant structure and C_{ab} content, which can be characterized using vegetation
699 indices derived from VNIR spectroscopy in a simple, speedy, and straightforward way. As
700 indicators of plant canopy structure, Normalized Difference Vegetation Index (NDVI) (Rouse *et*
701 *al.*, 1974) and its variants (e.g., RDVI, Green NDVI) (Roujean and Breon, 1995, Gitelson *et al.*,
702 1996) are most commonly used because chlorophyll strongly absorbs visible light while the cell
703 structure of leaves and the entire canopy scattering strongly reflects near-infrared radiation.
704 However, the indirect link between vegetation density and leaf N often results in an ineffective
705 response to leaf N variability, particularly when plants reach a certain height and density

706 (Thenkabail *et al.*, 2000, Scotford and Miller, 2003). Chlorophyll indices using the red-edge
707 spectral regions, which have much lower chlorophyll absorption, have thus been proposed and
708 successfully applied to determination of chlorophyll content (Gitelson and Merzlyak, 1994,
709 Haboudane *et al.*, 2002). An investigation by Schlemmer *et al.* (2013) revealed a strong linear
710 relationship between the red-edge chlorophyll index ((NIR/Red Edge)-1) and nitrogen content.
711 Chlorophyll *a*+*b* alone, however, is not sufficient to estimate nitrogen under nitrogen-rich
712 conditions because the chlorophyll-nitrogen relationship saturates at high nitrogen levels (Uddling
713 *et al.*, 2007, Padilla *et al.*, 2018) and shows a less robust correlation when other factors are taken
714 into account, such as leaf thickness, species, canopy shape, nutrient status, and water content
715 (Hatfield *et al.*, 2008). Moreover, the combination of chlorophyll and structural index is found to
716 perform better to assess leaf N, such as with TCARI/OSAVI (Haboudane *et al.*, 2002) and CCCI
717 (Fitzgerald *et al.*, 2010). Furthermore, indices calculated from the SWIR region add additional
718 capacity to determine crop water status and protein content, such as with $TCARI_{1510}/OSAVI_{1510}$
719 (Herrmann *et al.*, 2010). However, determining protein and nitrogen content independently of
720 water is difficult because protein absorptions are very shallow and are largely obscured by water
721 absorption features (Hank *et al.*, 2019b). Despite that, although spectral indices are functional and
722 widely accepted, they still encounter problems with transferability across different crop types and
723 are unstable across growth stages and varying environmental conditions (Li *et al.*, 2014, Basso *et*
724 *al.*, 2004, Li *et al.*, 2010).

725 Additionally, carotenoids play a role in the light-harvesting complex of the photosystem, which
726 plays a role in non-photochemical quenching. Xanthophylls, a specific group of carotenoids, are
727 known to be associated with these light-harvesting complexes (Siefermann-Harms, 1985). The
728 xanthophyll cycle refers to the process of interconversion of three specific xanthophylls –

violaxanthin (V), antheraxanthin (A), and zeaxanthin (Z) – in the chloroplast membrane of higher plants and algae (Yamamoto, 1979). During this cycle, excessive levels of light that cannot be used for photosynthesis induce the enzymatic de-epoxidation of V, resulting in the rapid conversion of this pool of energy into A and Z. In contrast, limiting light levels or adapting photosynthetic membranes to darkness reverses the process, resulting in the reformation of V via the epoxidation of Z and A (Fig. 1.4). In this context, certain vegetation indices based on the xanthophyll cycle and carotenoids are also used to assess nutrients, among them the PRI (photochemical reflectance index) families (Patel *et al.*, 2021, Strachan *et al.*, 2002, Peñuelas *et al.*, 1994, Wang *et al.*, 2017, Moran *et al.*, 2000), including PRI, (Gamon *et al.*, 1992), PRI_{m1} and PRI_{m4} (Hernández-Clemente *et al.*, 2011), PRI_{515} (Hernández-Clemente *et al.*, 2011), PRI_{n} (Zarco-Tejada *et al.*, 2013b), and PRI·CI (Garrity *et al.*, 2011). However, these indices are associated with light utilization efficiency but are only indirectly associated with nutrients.

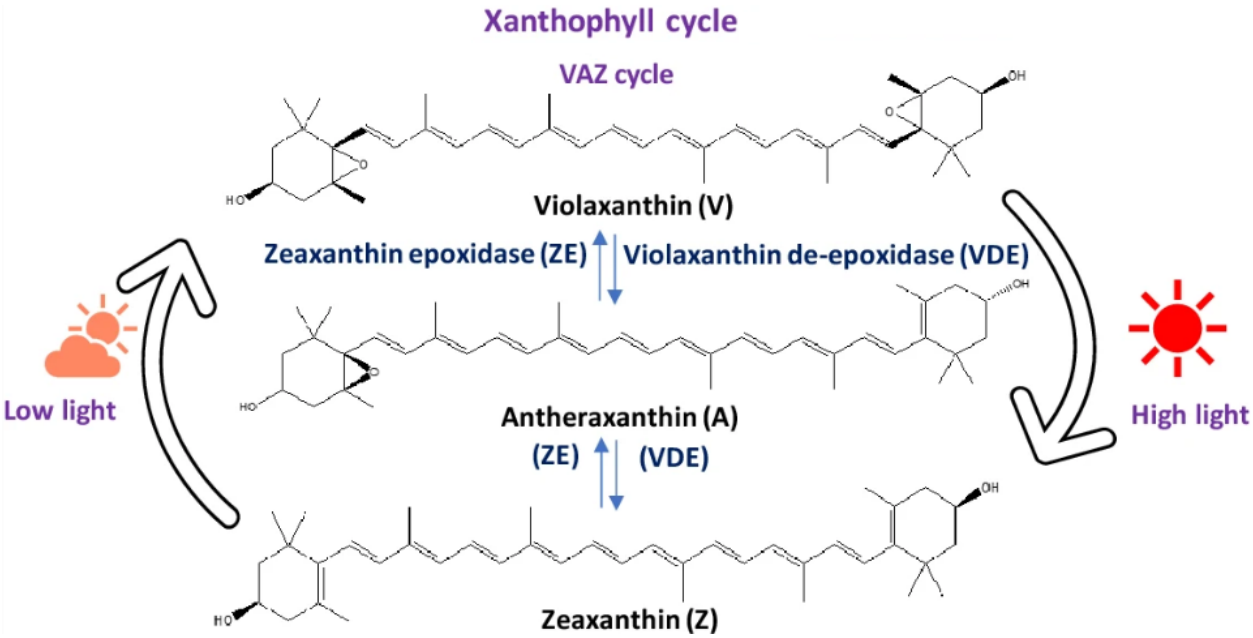

Fig. 1.4. Representation of xanthophyll cycles in photosynthetic microbes. Violaxanthin-antheraxanthin-zeaxanthin (VAZ) cycles are modulated by light conditions (modified based on Saini *et al.* (2019)).

1.6 Plant traits retrieval from radiative transfer models

In empirical approaches, the relationship between nutrients and indices can be greatly influenced by a number of leaf- and canopy-level factors. Because nutrients and leaf physiological traits are closely related in the context of plant photosynthesis, other studies using radiative transfer models (RTM) have explored the retrieval of C_{ab} contents, as well as other leaf and canopy traits (e.g., carotenoid (C_{car}), anthocyanins (Anth), dry matter (C_{dm}), water content (C_w), and leaf area index (LAI)) (Baret *et al.*, 2007, Jay *et al.*, 2017, Kimm *et al.*, 2020, Wang *et al.*, 2021, Zarco-Tejada *et al.*, 2004, Clevers and Kooistra, 2011). With RTMs, it is possible to simulate the absorption and scattering of light within vegetation canopies while also accounting for leaf biochemical constituents and canopy structural properties (Jacquemoud *et al.*, 2009), enabling a better understanding of how light interacts with plants at both leaf and canopy level. In this physical approach, leaf optical property models are combined with canopy bidirectional reflectance models like PROSAIL (Verhoef, 1984).

The simpler approximations of canopy RTMs have been developed from one-dimensional models, such as Scattering by Arbitrary Inclined Leaves (SAIL), which accounts for canopy scattering and extinction coefficients by using a 2-D turbid medium with horizontal and vertical leaf facets. Following this, several versions have been developed, including SAILH (Verhoef, 1998) with the foliage hotspot effects incorporated, and 4SAIL (Verhoef *et al.*, 2007), which provides numerically robust and speed-optimized simulations of thermal-infrared radiation scattering and emission in a geometrically homogeneous canopy with thermodynamic heterogeneity. This approach is more robust and transferable than index-based empirical models. Consequently, it is widely used for retrieving biochemical constituents with remote sensing data (Le Maire *et al.*, 2004). From local to regional spatial scales, these models have been extensively used to simulate homogeneous

canopies, such as wheat (Camino *et al.*, 2018b, Zhang *et al.*, 2016, Danner *et al.*, 2017), corn (Haboudane *et al.*, 2002), rice (Wan *et al.*, 2021, Darvishzadeh *et al.*, 2012), soybean (Verrelst *et al.*, 2016), potato (Clevers and Kooistra, 2011, Botha *et al.*, 2007), maize (Chakhvashvili *et al.*, 2022, Koetz *et al.*, 2005), sugar beet (Baret *et al.*, 1995, Jay *et al.*, 2017, Richter *et al.*, 2009), and even closed forest canopies (Zarco-Tejada *et al.*, 2001). Further, other studies have demonstrated that these models could also be inverted for discontinuous tree canopy/vineyard attribution with enough image spatial resolution for the extraction of pure canopy vegetation pixels (Suarez *et al.*, 2021b, Camino *et al.*, 2021, Suarez *et al.*, 2021a).

In contrast, more complex approximations focus on 3-D ray-tracing models incorporating three-dimensional structures simulating discontinuous and heterogeneous canopy structures (North, 1996, Gastellu-Etchegorry *et al.*, 1996, Li *et al.*, 1995). As an example, the Discrete Anisotropic Radiative Transfer (DART) model simulates radiative transfer in 3-D scenes that contain a variety of landscape features by dividing the scene into a rectangular cell matrix. In addition to topography and hot spots, leaf specularity and first-order polarization mechanisms are also modeled (Gastellu-Etchegorry *et al.*, 1996). The 3-D Forest Light Interaction Model (FLIGHT) is another example. Based on the Monte Carlo ray-tracing (MCRT) method, it simulates bidirectional reflectance in forest scenes using geometric envelopes that constrain the 3-D distribution of foliage elements (North, 1996). The use of these 3-D RTMs has been proven for heterogeneous canopies (Janoutová *et al.*, 2021, Banskota *et al.*, 2015, Hernández-Clemente *et al.*, 2017, Zarco-Tejada *et al.*, 2018), but they require complex input variables and heavy computational load (Gastellu-Etchegorry *et al.*, 2017, Miraglio *et al.*, 2019, Verrelst *et al.*, 2019). Hence, the feasibility and cost-effectiveness of complex 3-D RTMs with coarse spatial resolution imagery needs to be considered.

Inversion algorithms are often used to retrieve plant traits from reflectance spectra from RTM, and then regression models are developed using these traits to estimate nutrient content (Camino *et al.*, 2018a, Nevalainen *et al.*, 2013). Although this approach is promising, it has been validated mainly on relatively uniform and row-structured crops that grow into full canopy closure, such as wheat (Camino *et al.*, 2018a), potato (Clevers and Kooistra, 2011, Botha *et al.*, 2007), sugar beet (Jay *et al.*, 2017), and meadow (Clevers and Kooistra, 2011). As a result of extensive structural effects caused by clumping, crown shadows, and soil background, these model inversion methods present considerable challenges when applied to tree crowns (Camino *et al.*, 2018c), resulting in a lack of robust studies on orchard trees.

1.7 Chlorophyll fluorescence

Chlorophyll fluorescence is a re-emission of light by chlorophyll molecules during their transition from an excited state to a non-excited state (Rosenqvist and van Kooten, 2003). Chlorophyll fluorescence is generally considered to be a direct indicator of electron transport rates and thus of photosynthetic activity (Genty *et al.*, 1989). Plants under different types of stress require different amounts of light energy for photosynthetic quantum conversion, chlorophyll fluorescence, and heat production. In the absence of stress, the light energy is effectively used in plant photochemistry, thus reducing the fluorescence yield. Considering that the energy is dissipated in a short period of time, de-excitation is primarily accomplished through three competing processes – photochemistry, chlorophyll fluorescence (only 2-3%), and non-radiative thermal dissipation (Krause and Weis, 1991, Maxwell and Johnson, 2000). Due to the interdependence of these three pathways, any increase in the efficiency of one will result in a decrease in the efficiency of the other two. These competing processes change as a result of physiological and environmental

changes. Consequently, recent years have seen an increase in the use of chlorophyll fluorescence as a proxy for monitoring crop photosynthesis status. With the aid of remote sensing methods, we can determine changes in the efficiency of photochemistry and thermal dissipation by measuring chlorophyll fluorescence emissions (Maxwell and Johnson, 2000). Furthermore, the maximum carboxylation rate (V_{cmax}) has been shown to be highly correlated with SIF (Rascher *et al.*, 2015) via its strong connections to chlorophyll content and photosynthetic activity (Walker *et al.*, 2014, Camino *et al.*, 2019).

In the field, it has been proven that pulse amplitude modulation (PAM) fluorometers, along with saturation pulse methods, can be used for leaf-level measurement (Schreiber *et al.*, 1986, Schreiber, 2004). For example, the Li-Cor device (Li-Cor, Lincoln, NE, USA), PAM-2500 (Heinz Walz GmbH, Effeltrich, Germany), and FluorPen (Photon Systems Instruments, Brno, Czech Republic) are commonly used leaf-level measurement instruments that require active manipulation of the light environment. Scaling from leaf level to canopy level, however, presents many challenges. Rather than simply applying existing models to a large area, it is necessary to account for all photosynthetic processes, including light absorption, emission, scattering, and reabsorption by the canopy (Porcar-Castell *et al.*, 2014). In the past few decades, significant progress has been made since chlorophyll fluorescence was first demonstrated experimentally and analytically, with airborne hyperspectral data and model simulations as a signal superimposed upon apparent reflectance spectra in leaves and canopies (Zarco-Tejada *et al.*, 2000a, Zarco-Tejada *et al.*, 2000b). A number of advances have been made since then regarding sensor technology, retrieval algorithms, and modelling of leaf and canopy fluorescence. A full recent review on this topic can be found in Mohammed *et al.* (2019).

The typical method for retrieving SIF from passive sensors (i.e., hyperspectral imagery) is based on the Fraunhofer Line Depth (FLD) principle (Plascyk and Gabriel, 1975). In conceptual terms, FLD approaches use the different relative contributions of fluorescence to the upwelling radiance and the downwelling irradiance spectra, inside and outside of an absorption feature. As a result of the implementation of narrow-band hyperspectral sensors (generally with bandwidths less than 10 nm) on airborne platforms, SIF occurs in the 650-850 nm range with two peaks in the red (centered around 685 nm) and far-red regions (centered around 740nm), which can be quantified within the O_2 absorption features (Fig. 1.5). Due to the greater reabsorption of red fluorescence by chlorophyll during the transit of fluorescence to the leaf surface, the red peak typically appears lower than the far-red peak of healthy green leaves (Mohammed *et al.*, 2019). In addition, the O_2-B absorption features at 687 nm are much shallower and narrower than O_2-A absorption features at 760 nm, adding additional challenges for detecting chlorophyll fluorescence signal. In addition, SIF is dynamic and highly sensitive to a range of environmental factors, including atmospheric conditions, irradiance, structural characteristics, stress effects, and light absorption by chlorophyll (Buschmann, 2007). Due to the weak signal of SIF, all these factors contribute to the complexity of the retrieval and interpretation of SIF data.

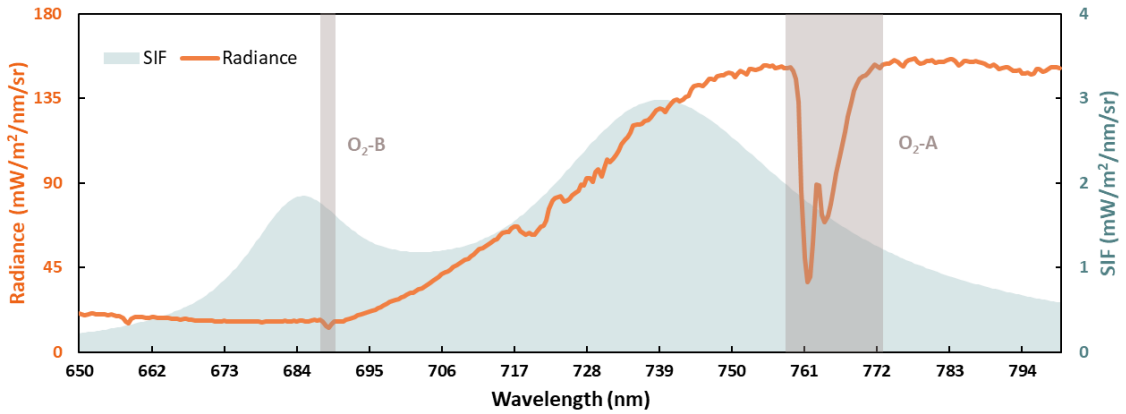

Fig. 1.5. At the top of the canopy, the total upwelling radiance (orange) and solar-induced fluorescence (SIF) spectra (blue) were collected in the range of 650-800 nm, with two oxygen absorption features marked with grey rectangles.

Since chlorophyll fluorescence emission is closely connected to photosynthetic status and is sensitive to plant stress (e.g., water, heat, biotic stresses) (Krause and Weis, 1991, Baker, 2008, Zarco-Tejada *et al.*, 2013a, Camino *et al.*, 2019, Mohammed *et al.*, 2019, Lang *et al.*, 1996), SIF has been used to detect nutrient deficiency in numerous studies (Tremblay *et al.*, 2012, Schächtl *et al.*, 2005). In a study conducted by Wei *et al.* (2016), it was shown that nitrogen has a significant impact on photosynthetic rate and thus on leaf fluorescence emission. The relationship is based on the fact that chlorophyll fluorescence emissions are dependent on chlorophyll concentration and PSI and PSII efficiency (Lichtenthaler *et al.*, 1996). Lu and Zhang (2000) demonstrated that nitrogen deficiency affects PSII photochemistry by reducing electron transport quantum yield and photochemical efficiency, thereby decreasing the net assimilation rate. Tremblay *et al.* (2012) investigated the use of SIF data to improve nitrogen quantification. Camino *et al.* (2018a) demonstrated the correlation between airborne-quantified chlorophyll fluorescence and nitrogen content in wheat. More importantly, the accuracy of nitrogen estimates for wheat improved significantly, yielding $r^2 = 0.93$ when SIF was added to the model based on the leaf biochemistry identified by RTM inversion. However, these results have only been demonstrated in homogeneous crops. It is therefore necessary to further investigate the contributions of SIF when explaining the variability of N and other nutrients in complex vegetation structures, such as fruit orchards. Besides N levels, Carstensen *et al.* (2019) demonstrated that chlorophyll fluorescence transients also allow the detection of latent P deficiency, crucial so that P deficiency can be speedily remediated to restore plant growth and development. This study was in agreement with those by Carstensen *et al.* (2018) and Goltsev *et al.* (2016) in demonstrating that chlorophyll fluorescence is a valuable proxy for P deficiency.

1.8 Spaceborne platforms for assessing leaf nutrients

On a regional or global scale, satellite remote sensing technologies are becoming increasingly significant tools supporting plant monitoring and management in a spatially, temporally, and cost-effective manner. A number of satellites equipped with multispectral imaging systems, such as Landsat, Sentinel, RapidEye, QuickBird, GeoEye, Worldview-2, and SPOT, have been used to assess chlorophyll and nutrient status based on reflectance indices and red-edge spectral band data (Ali *et al.*, 2016, Bausch *et al.*, 2008, Wong and He, 2013). In addition, two imaging spectrometers have been in orbit as demonstrations for nutrient status assessments – Hyperion (220 contiguous spectral bands in VIS-SWIR range with a 30-m spatial resolution) onboard NASA's Earth Observing-1 (EO-1) satellite (active between November 2000 and March 2017) (Datt *et al.*, 2003, Abdel-Rahman *et al.*, 2013, Sims *et al.*, 2013, Townsend *et al.*, 2003), and the Compact High Resolution Imaging Spectrometer (CHRIS, 19 spectral bands in VNIR range with an 18-m spatial resolution, operating between October 2001 and December 2022) onboard ESA's Proba-1 satellite (Castaldi *et al.*, 2016, Huber *et al.*, 2007, Vincini *et al.*, 2006, Huber *et al.*, 2010). A study conducted by Marshall and Thenkabail (2015) compared N uptake calculated from multispectral and crop biomass estimates with narrowband indices from EO-1 Hyperion. Crop biomass was derived using spectral indices from IKONOS, GeoEye-1, Landsat ETM+, MODIS, and WorldView-2. The performance of hyperspectral narrowband indices was found to explain a 5-31% greater variability of biomass than broadband indices from multispectral sensors could, emphasizing the need to use satellite data with higher spectral resolution. These studies demonstrate that imaging spectroscopy is a necessary tool for monitoring different plant traits throughout phenological stages.

The technology for spaceborne sensors is advancing rapidly and a number of narrow-band hyperspectral sensors are being developed for use on spaceborne systems (Fig. 1.6). For example, the PRecursore IperSpettrale della Missione Applicativa (PRISMA, with 250 spectral bands, launched in March 2019) (Labate *et al.*, 2009), and the Environmental Mapping and Analysis Program (EnMAP, with 228 spectral bands, launched in April 2022) (Guanter *et al.*, 2015), are two of the most recent spaceborne hyperspectral sensors launched in the VIS-SWIR range with a 30-m spatial resolution. In addition, the new-generation German Aerospace Center (DLR) Earth Sensing Imaging Spectrometer (DESIS), which has been operating onboard the International Space Station (ISS) since August 2018, collects hyperspectral imagery over 235 narrow spectral bands in the VNIR range at a spatial resolution of 30 m (Krutz *et al.*, 2019, Eckardt *et al.*, 2015). There are several more missions under development, including the Hyperspectral Infrared Imager (HysplRI, with a 150-km swath) (Team, 2018) onboard NASA's EO-1, now part of NASA's Surface Biology and Geology (SBG) mission, as well as the Copernicus Hyperspectral Imaging Mission for the Environment (CHIME, with 20-30 m spatial resolution) satellite (Rast *et al.*, 2021) of the European Space Agency (ESA). A satellite developed specifically for detecting chlorophyll fluorescence is the ESA's high-spectral-resolution (around 0.3 nm) Fluorescence Explorer FLEX (Drusch *et al.*, 2016), which covers the spectral range between 500 and 780 nm. Using HysplRI (SBG) mission and EnMAP within the VIS-SWIR spectral range, Pellissier *et al.* (2015) (Berger *et al.*, 2020) have successfully estimated N concentration in homogeneous crops. It should be noted, however, that spaceborne imagery often has limited spatial and/or spectral resolution. Consequently, it is necessary to validate the performance of these spaceborne sensors in assessing nutrients, especially in heterogeneous orchards, in terms of a spatial and spectral resolution trade-off.

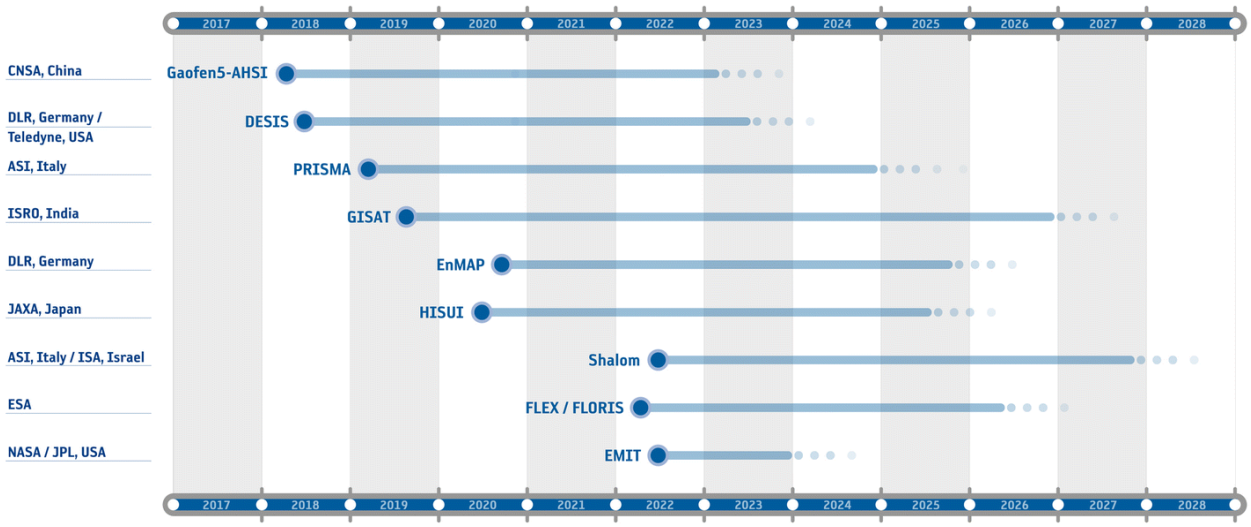

Fig. 1.6. Spaceborne imaging spectrometers recently launched or planned/approved (Rast and Painter, 2019).

It is noteworthy that breakthroughs in understanding the potential contribution of chlorophyll fluorescence, as well as in SIF retrieval methodologies, have enabled satellite-based SIF detection for global monitoring (Mohammed *et al.*, 2019). SIF was first identified globally in the far-red wavelengths with high spectral resolution spectrometers (i.e., 0.025 nm) by the Greenhouse gasses Observing SATellite (GOSAT) (Joiner *et al.* (2011)) at a 10.5-km spatial resolution with a revisit time of 3 days. Since then, retrievals have also been made possible by satellites with lower spectral resolution, such as the Global Ozone Experiment 2 (GOME-2, Joiner *et al.* (2013)) at a 0.5-nm FWHM and the SCanning Imaging Absorption spectroMeter for Atmospheric CartograpHY (SCIAMACHY, Joiner *et al.* (2012)) at the FWHM of 0.2-0.5 nm. In addition, there are more recent instruments with higher spatial resolution, such as the Orbiting Carbon Observatory 2 (OCO-2, Frankenberg *et al.* (2014)) and the Chinese Carbon Dioxide Observation Satellite Mission (TanSat) (Du *et al.* (2018)), which provide spatial resolution of approximately two kilometers and spectral resolution of 0.04 nm. With the increasing attraction of SIF and sensor capability development, a specific satellite mission designed for SIF measurement, FLEX, is

expected to be launched in 2025 with a single payload, the FluORescence Imaging Spectrometer (FLORIS), which has a 0.3 km × 0.3 km footprint, 0.3-2 nm FWHM, and 27-day repetition time (Drusch *et al.*, 2016). Nevertheless, the spatial resolution of these satellite sensors is not optimal for precision agriculture and nutrient assessment of crops. Fig. 1.7 illustrates past, present, and future missions based on spatial and temporal resolution (specifications from Mohammed *et al.* (2019)).

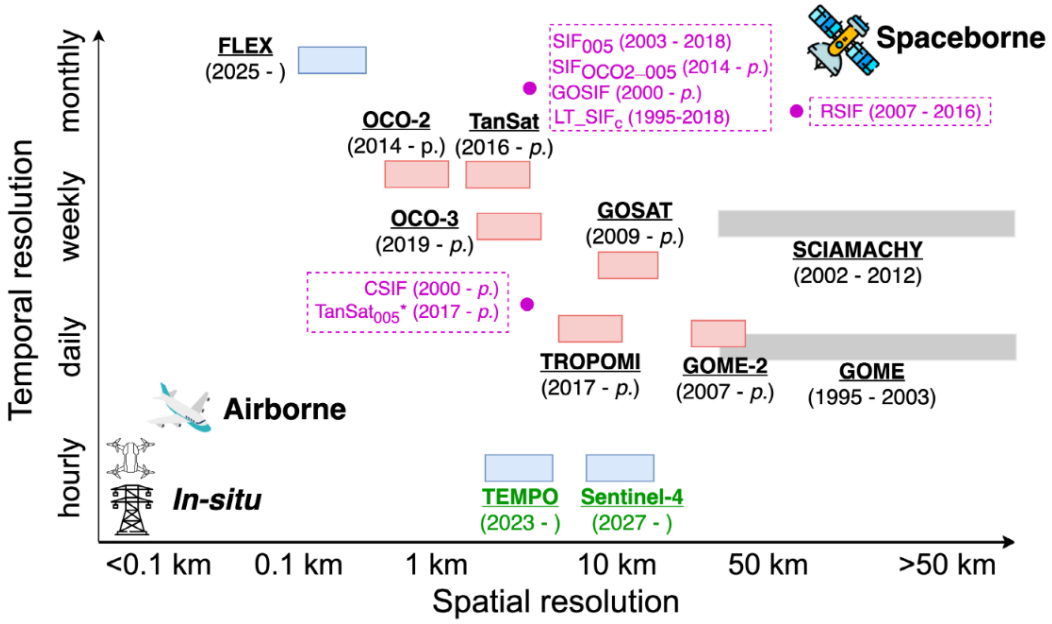

Fig. 1.7. Observations of solar-induced chlorophyll fluorescence (SIF) made by past missions (gray), current missions (pink), and future missions (light blue). The font colors distinguish geostationary (green) from low-earth orbit (black) missions. The dashed-line boxes indicate the spatial and temporal resolution of value-added SIF products (purple) (Sun *et al.*, 2023). 'p.' denotes present.

1.9 Objectives and thesis structure

1.9.1 Research objectives

According to the literature review, most studies have concentrated on homogenous and dense crops (e.g., wheat, maize) for nitrogen estimation, using vegetation indices, biochemistry quantification

from RTMs, and more recently SIF. It should be noted, however, that methods of estimating N using chlorophyll as a proxy for nitrogen content are strongly affected by the saturation of spectral indices at high N levels, as well as by canopy structure, varying leaf densities, and mixtures of sunlit and shaded canopy and soil background conditions (Camino *et al.*, 2018c). These effects are particularly evident in heterogeneous tree orchards, where the tree crowns' structural heterogeneity is a significant factor limiting the transferability of algorithms within and across tree species. In addition, there are large physiological differences between orchard trees and annual crops, and it is difficult to apply such methods across an extremely wide range of plant species. On the other hand, other macro- and micro-nutrients have been less thoroughly studied. Furthermore, at the outer space level, the global visibility of satellite images is negatively impacted by their spectral and spatial resolution, so it would be beneficial to assess the proposed methods for larger-scale application and determine the significance of spectral and spatial resolution for N assessment. In particular, the following objectives need to be addressed regarding discontinuous tree-structured orchards:

1. To investigate the links of chlorophyll fluorescence and plant pigments with the main macro- and micro-nutrients at the leaf and canopy levels in almond orchards;
2. To study biochemistry estimation using radiative transfer models (i.e., Fluspect-Cx and 4SAIL) by implementing inversion algorithms in almond orchards;
3. To assess the contribution of tree-level SIF quantification to explaining leaf N variability observed at the orchard level with airborne hyperspectral imagery;
4. To validate the accuracy and robustness of the proposed modeling methods for leaf N quantification in large almond orchards using the DESIS hyperspectral imager onboard the International Space Station (ISS);

5. To evaluate the effects of the spectral and spatial resolution of hyperspectral and multispectral sensors for the assessment of leaf N.

1.9.2 Research questions

The objectives of this research are to investigate robust methods for an assessment of nutrients and to develop algorithms for retrieving leaf nitrogen concentration from high-resolution airborne and spaceborne sensors in almond orchards by using SIF and leaf plant traits derived from physical models. The following questions will be addressed in accordance with the research objectives:

1. What are the robust proxies available for explaining nutrient (especially N, P, and K) variations in almond orchards?
2. What is the performance of the coupled Fluspect-Cx and 4SAIL models in retrieving biochemical constituents?
3. What is the performance of SIF quantification from high-resolution hyperspectral imagery, and how does it contribute to the assessment of leaf N in almond trees?
4. How effective is the DESIS imaging spectrometer onboard ISS for deriving plant traits and quantifying SIF for leaf N prediction?
5. How does DESIS compare to airborne hyperspectral and Sentinel-2 multispectral imagery in terms of spectral and spatial resolution for the assessment of leaf N?

1.9.3 Thesis structure

This doctoral thesis is presented in chapters that address the objectives previously described. Each of the main chapters (Chapters 2, 3, and 4) has been constructed as a stand-alone research article, and their connections are illustrated in Fig. 1.8.

Chapter 2 examines Objective 1 for different macro- and micro-nutrients and compares the performance of different spectral traits at the leaf level (field measurements) and the canopy level (estimation of traits based on RTM and SIF quantification from airborne hyperspectral imagery) over two growing seasons.

Chapter 3 addresses Objectives 2 and 3, focusing on the estimation of N based on tree crowns using RTM-derived plant traits and SIF quantified from high-resolution airborne hyperspectral imagery. In this chapter, we examine how different spectral traits (e.g., C_{ab}, C_{car}, Anth, C_x, C_{dm}, SIF, LAI) contributed to N assessment over the course of two years with different fertigation applications.

Chapter 4 addresses Objectives 4 and 5, applying methods for large-scale estimation, with the newly developed sensor DESIS onboard the International Space Station, which account for the mixed features of canopy, shadow, and soil background. In this chapter, space-based spectral traits are compared with those at airborne level. Furthermore, Sentinel-2, an open-source sensor with a medium spatial resolution and low spectral resolution, is also examined as a comparison for operational purposes.

Chapter 5 summarizes the key findings of each chapter and the overall conclusion of this doctoral thesis. Additionally, recommendations are made for future research.

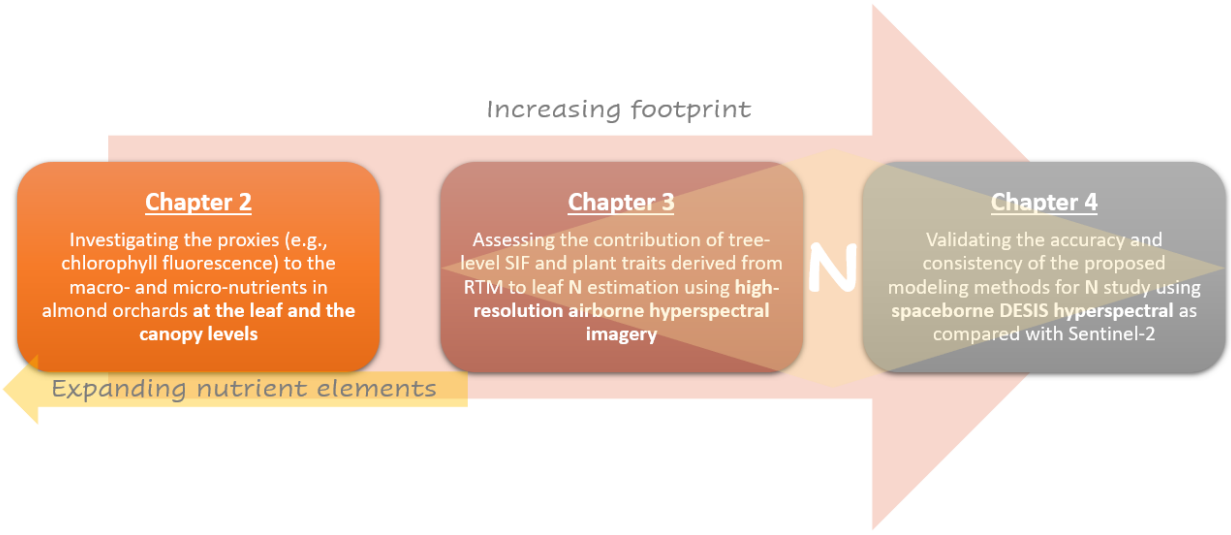

1011 Fig. 1.8. The flow between the main chapters demonstrates how the research development of this
1012 doctoral thesis is motivated by the key connections.

References

ABDEL-RAHMAN, E. M., AHMED, F. B. & ISMAIL, R. 2013. Random forest regression and spectral band selection for estimating sugarcane leaf nitrogen concentration using EO-1 Hyperion hyperspectral data. *International Journal of Remote Sensing,* 34**,** 712-728.

AFTAB, T. & HAKEEM, K. R. 2020. *Plant micronutrients: deficiency and toxicity management*, Springer Nature.

ALI, I., CAWKWELL, F., DWYER, E., BARRETT, B. & GREEN, S. 2016. Satellite remote sensing of grasslands: from observation to management. *Journal of Plant Ecology,* 9**,** 649-671.

AMIN, M. & FLOWERS, T. 2004. Evaluation of Kjeldahl digestion method. *J. Res. Science,* 15**,** 159-179.

ANGUS, J. 2001. Nitrogen supply and demand in Australian agriculture. *Australian Journal of Experimental Agriculture,* 41**,** 277-288.

ANGUS, J. & GRACE, P. Nitrogen use efficiency and nitrogen balance in Australian farmlands. International Nitrogen Initiative Conference," Solutions to improve nitrogen use efficiency for the world", Melbourne, Australia, 2016. 4-8.

BABEY, S. & ANGER, C. 1989. A compact airborne spectrographic imager (CASI). *Quantitative Remote Sensing: An Economic Tool for the Nineties, Volume 1,* 2**,** 1028-1031.

BAKER, N. R. 2008. Chlorophyll fluorescence: a probe of photosynthesis in vivo. *Annu. Rev. Plant Biol.,* 59**,** 89-113.

BANSKOTA, A., SERBIN, S. P., WYNNE, R. H., THOMAS, V. A., FALKOWSKI, M. J., KAYASTHA, N., GASTELLU-ETCHEGORRY, J.-P. & TOWNSEND, P. A. 2015. An LUT-based inversion of DART model to estimate forest LAI from hyperspectral data. *IEEE Journal of Selected Topics in Applied Earth Observations and Remote Sensing,* 8**,** 3147-3160.

BARET, F., CLEVERS, J. & STEVEN, M. 1995. The robustness of canopy gap fraction estimates from red and near-infrared reflectances: A comparison of approaches. *Remote Sensing of Environment,* 54**,** 141-151.

BARET, F., HOULÈS, V. & GUERIF, M. 2007. Quantification of plant stress using remote sensing observations and crop models: the case of nitrogen management. *Journal of experimental botany,* 58**,** 869-880.

BARKER, A. V. & PILBEAM, D. J. 2015. *Handbook of plant nutrition*, CRC press.

BASSO, B., CAMMARANO, D. & DE VITA, P. 2004. Remotely sensed vegetation indices: Theory and applications for crop management. *Rivista Italiana di Agrometeorologia,* 1**,** 36-53.

BAUSCH, W. C., HALVORSON, A. D. & CIPRA, J. 2008. Quickbird satellite and ground-based multispectral data correlations with agronomic parameters of irrigated maize grown in small plots. *biosystems engineering,* 101**,** 306-315.

BERGER, K., VERRELST, J., FÉRET, J.-B., HANK, T., WOCHER, M., MAUSER, W. & CAMPS-VALLS, G. 2020. Retrieval of aboveground crop nitrogen content with a hybrid machine learning method. *International Journal of Applied Earth Observation and Geoinformation,* 92**,** 102174.

BHATTI, A., MULLA, D. & FRAZIER, B. 1991. Estimation of soil properties and wheat yields on complex eroded hills using geostatistics and thematic mapper images. *Remote Sensing of Environment,* 37**,** 181-191.

BI, G., SCAGEL, C., CHENG, L. & FUCHIGAMI, L. 2005. Effects of copper, zinc and urea on defoliation and nitrogen reserves in nursery plants of almond. *The Journal of Horticultural Science and Biotechnology,* 80**,** 746-750.

BIOUCAS-DIAS, J. M., PLAZA, A., CAMPS-VALLS, G., SCHEUNDERS, P., NASRABADI, N. & CHANUSSOT, J. 2013. Hyperspectral remote sensing data analysis and future challenges. *IEEE Geoscience and remote sensing magazine,* 1**,** 6-36.

BLACKBURN, G. A. 2007. Hyperspectral remote sensing of plant pigments. *Journal of experimental botany,* 58**,** 855-867.

1061 BOEGH, E., SOEGAARD, H., BROGE, N., HASAGER, C., JENSEN, N., SCHELDE, K. & THOMSEN,
1062 A. 2002. Airborne multispectral data for quantifying leaf area index, nitrogen concentration, and
1063 photosynthetic efficiency in agriculture. *Remote sensing of Environment,* 81**,** 179-193.
1064 BOTHA, E. J., LEBLON, B., ZEBARTH, B. & WATMOUGH, J. 2007. Non-destructive estimation of
1065 potato leaf chlorophyll from canopy hyperspectral reflectance using the inverted PROSAIL model.
1066 *International Journal of Applied Earth Observation and Geoinformation,* 9**,** 360-374.
1067 BULLOCK, D. & ANDERSON, D. 1998. Evaluation of the Minolta SPAD-502 chlorophyll meter for
1068 nitrogen management in corn. *Journal of Plant Nutrition,* 21**,** 741-755.
1069 BUSCHMANN, C. 2007. Variability and application of the chlorophyll fluorescence emission ratio red/far-
1070 red of leaves. *Photosynthesis Research,* 92**,** 261-271.
1071 CAKMAK, I. 2008. Enrichment of cereal grains with zinc: agronomic or genetic biofortification? *Plant*
1072 *and soil,* 302**,** 1-17.
1073 CAMINO, C., CALDERÓN, R., PARNELL, S., DIERKES, H., CHEMIN, Y., ROMÁN-ÉCIJA, M.,
1074 MONTES-BORREGO, M., LANDA, B. B., NAVAS-CORTES, J. A. & ZARCO-TEJADA, P. J.
1075 2021. Detection of Xylella fastidiosa in almond orchards by synergic use of an epidemic spread
1076 model and remotely sensed plant traits. *Remote Sensing of Environment,* 260**,** 112420.
1077 CAMINO, C., GONZALEZ-DUGO, V., HERNANDEZ, P., SILLERO, J. & ZARCO-TEJADA, P. J.
1078 2018a. Improved nitrogen retrievals with airborne-derived fluorescence and plant traits quantified
1079 from VNIR-SWIR hyperspectral imagery in the context of precision agriculture. *International*
1080 *journal of applied earth observation and geoinformation,* 70**,** 105-117.
1081 CAMINO, C., GONZÁLEZ-DUGO, V., HERNÁNDEZ, P., SILLERO, J. & ZARCO-TEJADA, P. J.
1082 2018b. Improved nitrogen retrievals with airborne-derived fluorescence and plant traits quantified
1083 from VNIR-SWIR hyperspectral imagery in the context of precision agriculture. *International*
1084 *journal of applied earth observation and geoinformation,* 70**,** 105-117.
1085 CAMINO, C., GONZALEZ-DUGO, V., HERNANDEZ, P. & ZARCO-TEJADA, P. J. 2019. Radiative
1086 transfer Vcmax estimation from hyperspectral imagery and SIF retrievals to assess photosynthetic
1087 performance in rainfed and irrigated plant phenotyping trials. *Remote Sensing of Environment***,**
1088 111186.
1089 CAMINO, C., ZARCO-TEJADA, P. J. & GONZALEZ-DUGO, V. 2018c. Effects of heterogeneity within
1090 tree crowns on airborne-quantified SIF and the CWSI as indicators of water stress in the context of
1091 precision agriculture. *Remote Sensing,* 10**,** 604.
1092 CARROW, R. N., WADDINGTON, D. V. & RIEKE, P. E. 2002. *Turfgrass soil fertility & chemical*
1093 *problems: Assessment and management,* John Wiley & Sons.
1094 CARSTENSEN, A., HERDEAN, A., SCHMIDT, S. B., SHARMA, A., SPETEA, C., PRIBIL, M. &
1095 HUSTED, S. 2018. The impacts of phosphorus deficiency on the photosynthetic electron transport
1096 chain. *Plant physiology,* 177**,** 271-284.
1097 CARSTENSEN, A., SZAMEITAT, A. E., FRYDENVANG, J. & HUSTED, S. 2019. Chlorophyll a
1098 fluorescence analysis can detect phosphorus deficiency under field conditions and is an effective
1099 tool to prevent grain yield reductions in spring barley (Hordeum vulgare L.). *Plant and Soil,* 434**,**
1100 79-91.
1101 CASTALDI, F., CASTRIGNANÒ, A. & CASA, R. 2016. A data fusion and spatial data analysis approach
1102 for the estimation of wheat grain nitrogen uptake from satellite data. *International Journal of*
1103 *Remote Sensing,* 37**,** 4317-4336.
1104 CEROVIC, Z. G., GHOZLEN, N. B., MILHADE, C., OBERT, M. L., DEBUISSON, S. B. & MOIGNE,
1105 M. L. 2015. Nondestructive diagnostic test for nitrogen nutrition of grapevine (Vitis vinifera L.)
1106 based on dualex leaf-clip measurements in the field. *Journal of agricultural and food chemistry,*
1107 63**,** 3669-3680.
1108 CEROVIC, Z. G., MASDOUMIER, G., GHOZLEN, N. B. & LATOUCHE, G. 2012. A new optical leaf-
1109 clip meter for simultaneous non-destructive assessment of leaf chlorophyll and epidermal
1110 flavonoids. *Physiologia plantarum,* 146**,** 251-260.

1111 CHAKHVASHVILI, E., SIEGMANN, B., MULLER, O., VERRELST, J., BENDIG, J., KRASKA, T. &
1112 RASCHER, U. 2022. Retrieval of Crop Variables from Proximal Multispectral UAV Image Data
1113 Using PROSAIL in Maize Canopy. *Remote sensing,* 14**,** 1247.
1114 CHANG, S. X. & ROBISON, D. J. 2003. Nondestructive and rapid estimation of hardwood foliar nitrogen
1115 status using the SPAD-502 chlorophyll meter. *Forest Ecology and Management,* 181**,** 331-338.
1116 CHEN, J.-H. The combined use of chemical and organic fertilizers and/or biofertilizer for crop growth and
1117 soil fertility. International workshop on sustained management of the soil-rhizosphere system for
1118 efficient crop production and fertilizer use, 2006. Citeseer, 1-11.
1119 CHISM, C. J. C. 2002. *Nitrogen use efficiency of cotton following corn in rotation and foliar fertilization*
1120 *of cotton using leaf blade analysis*, Louisiana State University and Agricultural & Mechanical
1121 College.
1122 CLEVERS, J. G. & KOOISTRA, L. 2011. Using hyperspectral remote sensing data for retrieving canopy
1123 chlorophyll and nitrogen content. *IEEE Journal of selected topics in applied earth observations*
1124 *and remote sensing,* 5**,** 574-583.
1125 COCKS, T., JENSSEN, R., STEWART, A., WILSON, I. & SHIELDS, T. The HyMapTM airborne
1126 hyperspectral sensor: The system, calibration and performance. Proceedings of the 1st EARSeL
1127 workshop on Imaging Spectroscopy, 1998. 37-42.
1128 DAMANIA, R., DESBUREAUX, S., RODELLA, A.-S., RUSS, J. & ZAVERI, E. 2019. *Quality unknown:*
1129 *the invisible water crisis,* World Bank Publications.
1130 DANNER, M., BERGER, K., WOCHER, M., MAUSER, W. & HANK, T. 2017. Retrieval of biophysical
1131 crop variables from multi-angular canopy spectroscopy. *Remote Sensing,* 9**,** 726.
1132 DARVISHZADEH, R., MATKAN, A. A. & AHANGAR, A. D. 2012. Inversion of a radiative transfer
1133 model for estimation of rice canopy chlorophyll content using a lookup-table approach. *IEEE*
1134 *Journal of selected topics in applied earth observations and remote sensing,* 5**,** 1222-1230.
1135 DATT, B., MCVICAR, T. R., VAN NIEL, T. G., JUPP, D. L. & PEARLMAN, J. S. 2003. Preprocessing
1136 EO-1 Hyperion hyperspectral data to support the application of agricultural indexes. *IEEE*
1137 *Transactions on Geoscience and Remote Sensing,* 41**,** 1246-1259.
1138 DOBERMANN, A. R. 2005. Nitrogen use efficiency-state of the art. *Agronomy--Faculty Publications***,** 316.
1139 DRØBAK, B. K. & WATKINS, P. A. 2000. Inositol (1, 4, 5) trisphosphate production in plant cells: an
1140 early response to salinity and hyperosmotic stress. *FEBS letters,* 481**,** 240-244.
1141 DRUSCH, M., MORENO, J., DEL BELLO, U., FRANCO, R., GOULAS, Y., HUTH, A., KRAFT, S.,
1142 MIDDLETON, E. M., MIGLIETTA, F. & MOHAMMED, G. 2016. The fluorescence explorer
1143 mission concept—ESA's earth explorer 8. *IEEE Transactions on Geoscience and Remote Sensing,*
1144 55**,** 1273-1284.
1145 DU, S., LIU, L., LIU, X., ZHANG, X., ZHANG, X., BI, Y. & ZHANG, L. 2018. Retrieval of global
1146 terrestrial solar-induced chlorophyll fluorescence from TanSat satellite. *Science Bulletin,* 63**,** 1502-
1147 1512.
1148 DUMAS, J. B. A. 1831. Procedes de l'analyse Organic. *Annales de Chimie et de Physique (Annals of*
1149 *Chemistry and of Physics),* 247**,** 198-213.
1150 ECKARDT, A., HORACK, J., LEHMANN, F., KRUTZ, D., DRESCHER, J., WHORTON, M. &
1151 SOUTULLO, M. Desis (dlr earth sensing imaging spectrometer for the iss-muses platform). 2015
1152 IEEE international geoscience and remote sensing symposium (IGARSS), 2015. IEEE, 1457-1459.
1153 EL-SHARKAWY, M. A. S., LÓPEZ, L. F. C. & DE TAFUR, M. S. M. 1998. Nutrient use efficiency of
1154 cassava differs with genotype architecture. *Acta Agronomica,* 48**,** 23-32.
1155 EMBLETON, T. W., JONES, W. W., LABANAUSKAS, C. K. & REUTHER, W. 1973. Leaf analysis as
1156 a diagnostic tool and guide to fertilization. *The citrus industry,* 3**,** 183-210.
1157 ERDLE, K., MISTELE, B. & SCHMIDHALTER, U. 2011. Comparison of active and passive spectral
1158 sensors in discriminating biomass parameters and nitrogen status in wheat cultivars. *Field Crops*
1159 *Research,* 124**,** 74-84.

ERNST, W. H., KRAUSS, G. J., VERKLEIJ, J. A. & WESENBERG, D. 2008. Interaction of heavy metals with the sulphur metabolism in angiosperms from an ecological point of view. *Plant, Cell & Environment,* 31**,** 123-143.

EVANS, J. 1989. Photosynthesis and nitrogen relationships in leaves of C 3 plants. *Oecologia,* 78**,** 9-19.

FAGERIA, N. K. & BALIGAR, V. 2005. Enhancing nitrogen use efficiency in crop plants. *Advances in agronomy,* 88**,** 97-185.

FAZILI, I., JAMAL, A., AHMAD, S., MASOODI, M., KHAN, J. & ABDIN, M. 2008. Interactive effect of sulfur and nitrogen on nitrogen accumulation and harvest in oilseed crops differing in nitrogen assimilation potential. *Journal of plant nutrition,* 31**,** 1203-1220.

FITZGERALD, G., RODRIGUEZ, D. & O'LEARY, G. 2010. Measuring and predicting canopy nitrogen nutrition in wheat using a spectral index—The canopy chlorophyll content index (CCCI). *Field Crops Research,* 116**,** 318-324.

FRANKENBERG, C., O'DELL, C., BERRY, J., GUANTER, L., JOINER, J., KÖHLER, P., POLLOCK, R. & TAYLOR, T. E. 2014. Prospects for chlorophyll fluorescence remote sensing from the Orbiting Carbon Observatory-2. *Remote Sensing of Environment,* 147**,** 1-12.

FRINK, C. R., WAGGONER, P. E. & AUSUBEL, J. H. 1999. Nitrogen fertilizer: retrospect and prospect. *Proceedings of the National Academy of Sciences,* 96**,** 1175-1180.

GAMON, J., PENUELAS, J. & FIELD, C. 1992. A narrow-waveband spectral index that tracks diurnal changes in photosynthetic efficiency. *Remote Sensing of environment,* 41**,** 35-44.

GARRITY, S. R., EITEL, J. U. & VIERLING, L. A. 2011. Disentangling the relationships between plant pigments and the photochemical reflectance index reveals a new approach for remote estimation of carotenoid content. *Remote Sensing of Environment,* 115**,** 628-635.

GASTELLU-ETCHEGORRY, J.-P., DEMAREZ, V., PINEL, V. & ZAGOLSKI, F. 1996. Modeling radiative transfer in heterogeneous 3-D vegetation canopies. *Remote sensing of environment,* 58**,** 131-156.

GASTELLU-ETCHEGORRY, J.-P., LAURET, N., YIN, T., LANDIER, L., KALLEL, A., MALENOVSKÝ, Z., AL BITAR, A., AVAL, J., BENHMIDA, S. & QI, J. 2017. DART: recent advances in remote sensing data modeling with atmosphere, polarization, and chlorophyll fluorescence. *IEEE Journal of Selected Topics in Applied Earth Observations and Remote Sensing,* 10**,** 2640-2649.

GENTY, B., BRIANTAIS, J.-M. & BAKER, N. R. 1989. The relationship between the quantum yield of photosynthetic electron transport and quenching of chlorophyll fluorescence. *Biochimica et Biophysica Acta (BBA)-General Subjects,* 990**,** 87-92.

GITELSON, A. & MERZLYAK, M. N. 1994. Quantitative estimation of chlorophyll-a using reflectance spectra: Experiments with autumn chestnut and maple leaves. *Journal of Photochemistry and Photobiology B: Biology,* 22**,** 247-252.

GITELSON, A. A., KAUFMAN, Y. J. & MERZLYAK, M. N. 1996. Use of a green channel in remote sensing of global vegetation from EOS-MODIS. *Remote sensing of Environment,* 58**,** 289-298.

GOETZ, A. F. 2009. Three decades of hyperspectral remote sensing of the Earth: A personal view. *Remote sensing of environment,* 113**,** S5-S16.

GOLTSEV, V., KALAJI, H., PAUNOV, M., BĄBA, W., HORACZEK, T., MOJSKI, J., KOCIEL, H. & ALLAKHVERDIEV, S. 2016. Variable chlorophyll fluorescence and its use for assessing physiological condition of plant photosynthetic apparatus. *Russian journal of plant physiology,* 63**,** 869-893.

GOULAS, Y., CEROVIC, Z. G., CARTELAT, A. & MOYA, I. 2004. Dualex: a new instrument for field measurements of epidermal ultraviolet absorbance by chlorophyll fluorescence. *Applied Optics,* 43**,** 4488-4496.

GREGORIOU, K., PONTIKIS, K. & VEMMOS, S. 2007. Effects of reduced irradiance on leaf morphology, photosynthetic capacity, and fruit yield in olive (Olea europaea L.). *Photosynthetica,* 45**,** 172-181.

GUANTER, L., KAUFMANN, H., SEGL, K., FOERSTER, S., ROGASS, C., CHABRILLAT, S., KUESTER, T., HOLLSTEIN, A., ROSSNER, G. & CHLEBEK, C. 2015. The EnMAP spaceborne imaging spectroscopy mission for earth observation. *Remote Sensing,* 7**,** 8830-8857.

HABOUDANE, D., MILLER, J. R., TREMBLAY, N., ZARCO-TEJADA, P. J. & DEXTRAZE, L. 2002. Integrated narrow-band vegetation indices for prediction of crop chlorophyll content for application to precision agriculture. *Remote sensing of environment,* 81**,** 416-426.

HANK, T. B., BERGER, K., BACH, H., CLEVERS, J. G., GITELSON, A., ZARCO-TEJADA, P. & MAUSER, W. 2019a. Spaceborne imaging spectroscopy for sustainable agriculture: Contributions and challenges. *Surveys in Geophysics,* 40**,** 515-551.

HANK, T. B., BERGER, K., BACH, H., CLEVERS, J. G., GITELSON, A., ZARCO-TEJADA, P. & MAUSER, W. 2019b. Spaceborne imaging spectroscopy for sustainable agriculture: Contributions and challenges. *Surveys in Geophysics,* 40**,** 515-551.

HATFIELD, J., GITELSON, A. A., SCHEPERS, J. S. & WALTHALL, C. 2008. Application of spectral remote sensing for agronomic decisions. *Agronomy Journal,* 100**,** S-117-S-131.

HAVLIN, J. L., TISDALE, S. L., NELSON, W. L. & BEATON, J. D. 2016. *Soil fertility and fertilizers*, Pearson Education India.

HE, C.-J., MORGAN, P. W. & DREW, M. C. 1992. Enhanced sensitivity to ethylene in nitrogen-or phosphate-starved roots of Zea mays L. during aerenchyma formation. *Plant Physiology,* 98**,** 137-142.

HEFFER, P. & PRUD'HOMME, M. Global nitrogen fertilizer demand and supply: Trend, current level and outlook. International Nitrogen Initiative Conference. Melbourne, Australia, 2016.

HEPLER, P. K. 2005. Calcium: a central regulator of plant growth and development. *The Plant Cell,* 17**,** 2142-2155.

HERMANS, C., VUYLSTEKE, M., COPPENS, F., CRISTESCU, S. M., HARREN, F. J., INZÉ, D. & VERBRUGGEN, N. 2010. Systems analysis of the responses to long-term magnesium deficiency and restoration in Arabidopsis thaliana. *New Phytologist,* 187**,** 132-144.

HERNÁNDEZ-CLEMENTE, R., NAVARRO-CERRILLO, R. M., SUÁREZ, L., MORALES, F. & ZARCO-TEJADA, P. J. 2011. Assessing structural effects on PRI for stress detection in conifer forests. *Remote Sensing of Environment,* 115**,** 2360-2375.

HERNÁNDEZ-CLEMENTE, R., NORTH, P. R., HORNERO, A. & ZARCO-TEJADA, P. J. 2017. Assessing the effects of forest health on sun-induced chlorophyll fluorescence using the FluorFLIGHT 3-D radiative transfer model to account for forest structure. *Remote Sensing of Environment,* 193**,** 165-179.

HERRMANN, I., KARNIELI, A., BONFIL, D., COHEN, Y. & ALCHANATIS, V. 2010. SWIR-based spectral indices for assessing nitrogen content in potato fields. *International Journal of Remote Sensing,* 31**,** 5127-5143.

HOPKINS, B. G., ELLSWORTH, J. W., BOWEN, T. R., COOK, A. G., STEPHENS, S. C., JOLLEY, V. D., SHIFFLER, A. K. & EGGETT, D. 2010. Phosphorus fertilizer timing for Russet Burbank potato grown in calcareous soil. *Journal of Plant Nutrition,* 33**,** 529-540.

HOPKINS, B. G. & HANSEN, N. C. 2019. Phosphorus management in high-yield systems. *Journal of environmental quality,* 48**,** 1265-1280.

HOPKINS, W. G. & HÜNER, N. P. 1995. Introduction to plant physiology.

HOUBORG, R., SOEGAARD, H. & BOEGH, E. 2007. Combining vegetation index and model inversion methods for the extraction of key vegetation biophysical parameters using Terra and Aqua MODIS reflectance data. *Remote Sensing of Environment,* 106**,** 39-58.

HUBER, D. M. & JONES, J. B. 2013. The role of magnesium in plant disease. *Plant and soil,* 368**,** 73-85.

HUBER, S., KNEUBÜHLER, M., KOETZ, B., SCHOPFER, J. T., ZIMMERMANN, N., ITTEN, K., SCHAEPMAN, M. E., LIANG, S. & GROOT, N. E. Estimating Nitrogen Concentration from Directional CHRIS/PROBA Data. 2007. ISPRS.

HUBER, S., KOETZ, B., PSOMAS, A., KNEUBUEHLER, M., SCHOPFER, J. T., ITTEN, K. I. & ZIMMERMANN, N. 2010. Impact of multiangular information on empirical models to estimate canopy nitrogen concentration in mixed forest. *Journal of Applied Remote Sensing,* 4**,** 043530.

ISHFAQ, M., WANG, Y., YAN, M., WANG, Z., WU, L., LI, C. & LI, X. 2022. Physiological Essence of Magnesium in Plants and Its Widespread Deficiency in the Farming System of China. *Frontiers in plant science,* 13.

JACQUEMOUD, S., VERHOEF, W., BARET, F., BACOUR, C., ZARCO-TEJADA, P. J., ASNER, G. P., FRANÇOIS, C. & USTIN, S. L. 2009. PROSPECT+ SAIL models: A review of use for vegetation characterization. *Remote sensing of environment,* 113**,** S56-S66.

JAMAL, A., FAZLI, I. S., AHMAD, S., ABDIN, M. Z. & YUN, S. J. 2005. Effect of sulphur and nitrogen application on growth characteristics, seed and oil yields of soybean cultivars. *Korean Journal of Crop Science,* 50**,** 340-345.

JAMAL, A., MOON, Y.-S. & ZAINUL ABDIN, M. 2010. Sulphur-a general overview and interaction with nitrogen. *Australian Journal of Crop Science,* 4**,** 523-529.

JANOUTOVÁ, R., HOMOLOVÁ, L., NOVOTNÝ, J., NAVRÁTILOVÁ, B., PIKL, M. & MALENOVSKÝ, Z. 2021. Detailed reconstruction of trees from terrestrial laser scans for remote sensing and radiative transfer modelling applications. *in silico Plants,* 3**,** diab026.

JATAV, H. S., SHARMA, L. D., SADHUKHAN, R., SINGH, S. K., SINGH, S., RAJPUT, V. D., PARIHAR, M., JATAV, S. S., JINGER, D. & KUMAR, S. 2020. An overview of micronutrients: prospects and implication in crop production. *Plant Micronutrients***,** 1-30.

JAY, S., MAUPAS, F., BENDOULA, R. & GORRETTA, N. 2017. Retrieving LAI, chlorophyll and nitrogen contents in sugar beet crops from multi-angular optical remote sensing: Comparison of vegetation indices and PROSAIL inversion for field phenotyping. *Field Crops Research,* 210**,** 33-46.

JOINER, J., GUANTER, L., LINDSTROT, R., VOIGT, M., VASILKOV, A., MIDDLETON, E., HUEMMRICH, K., YOSHIDA, Y. & FRANKENBERG, C. 2013. Global monitoring of terrestrial chlorophyll fluorescence from moderate spectral resolution near-infrared satellite measurements: Methodology, simulations, and application to GOME-2. *Atmospheric Measurement Techniques Discussions,* 6**,** 3883-3930.

JOINER, J., YOSHIDA, Y., VASILKOV, A., MIDDLETON, E., CAMPBELL, P., YOSHIDA, Y. & HUZE, A. 2012. Filling-in of near-infrared solar lines by terrestrial fluorescence and other geophysical effects: simulations and space-based observations from SCIAMACHY and GOSAT. *Atmospheric Measurement Techniques,* 5.

JOINER, J., YOSHIDA, Y., VASILKOV, A., YOSHIDA, Y., CORP, L. & MIDDLETON, E. 2011. First observations of global and seasonal terrestrial chlorophyll fluorescence from space. *Biogeosciences,* 8**,** 637-651.

JONES, J. B. & JANICK, J. 1984. Soil testing and plant analysis: guides to the fertilization of horticultural crops. *Horticultural reviews. Vol. 7***,** 1-67.

JONES, M. M. 1985. Heavy-metal detoxification using sulfur compounds. *Sulfur reports,* 4**,** 119-150.

KIEGLE, E., MOORE, C. A., HASELOFF, J., TESTER, M. A. & KNIGHT, M. R. 2000. Cell-type-specific calcium responses to drought, salt and cold in the Arabidopsis root. *The Plant Journal,* 23**,** 267-278.

KIMM, H., GUAN, K., JIANG, C., PENG, B., GENTRY, L. F., WILKIN, S. C., WANG, S., CAI, Y., BERNACCHI, C. J. & PENG, J. 2020. Deriving high-spatiotemporal-resolution leaf area index for agroecosystems in the US Corn Belt using Planet Labs CubeSat and STAIR fusion data. *Remote Sensing of Environment,* 239**,** 111615.

KJELDAHL, J. 1883a. Neue methode zur bestimmung des stickstoffs in organischen körpern. *Fresenius' Journal of Analytical Chemistry,* 22**,** 366-382.

KJELDAHL, J. 1883b. A new method for the estimation of nitrogen in organic compounds. *Z. Anal. Chem,* 22**,** 366.

KOETZ, B., BARET, F., POILVÉ, H. & HILL, J. 2005. Use of coupled canopy structure dynamic and radiative transfer models to estimate biophysical canopy characteristics. *Remote Sensing of Environment,* 95**,** 115-124.

KRAUSE, G. & WEIS, E. 1991. Chlorophyll fluorescence and photosynthesis: the basics. *Annual review of plant biology,* 42**,** 313-349.

KRUTZ, D., MÜLLER, R., KNODT, U., GÜNTHER, B., WALTER, I., SEBASTIAN, I., SÄUBERLICH, T., REULKE, R., CARMONA, E. & ECKARDT, A. 2019. The instrument design of the DLR earth sensing imaging spectrometer (DESIS). *Sensors,* 19**,** 1622.

KUDLA, J., BATISTIČ, O. & HASHIMOTO, K. 2010. Calcium signals: the lead currency of plant information processing. *The Plant Cell,* 22**,** 541-563.

LABATE, D., CECCHERINI, M., CISBANI, A., DE COSMO, V., GALEAZZI, C., GIUNTI, L., MELOZZI, M., PIERACCINI, S. & STAGI, M. 2009. The PRISMA payload optomechanical design, a high performance instrument for a new hyperspectral mission. *Acta Astronautica,* 65**,** 1429-1436.

LAMBERS, H., RAVEN, J. A., SHAVER, G. R. & SMITH, S. E. 2008. Plant nutrient-acquisition strategies change with soil age. *Trends in ecology & evolution,* 23**,** 95-103.

LANDGREBE, D. A. 2003. *Signal theory methods in multispectral remote sensing*, John Wiley & Sons.

LANG, M., LICHTENTHALER, H. K., SOWINSKA, M., HEISEL, F. & MIEHÉ, J. A. 1996. Fluorescence imaging of water and temperature stress in plant leaves. *Journal of plant physiology,* 148**,** 613-621.

LASSALETTA, L., BILLEN, G., GRIZZETTI, B., ANGLADE, J. & GARNIER, J. 2014. 50 year trends in nitrogen use efficiency of world cropping systems: the relationship between yield and nitrogen input to cropland. *Environmental Research Letters,* 9**,** 105011.

LE MAIRE, G., FRANCOIS, C. & DUFRENE, E. 2004. Towards universal broad leaf chlorophyll indices using PROSPECT simulated database and hyperspectral reflectance measurements. *Remote sensing of environment,* 89**,** 1-28.

LEE, C. M., CABLE, M. L., HOOK, S. J., GREEN, R. O., USTIN, S. L., MANDL, D. J. & MIDDLETON, E. M. 2015. An introduction to the NASA Hyperspectral InfraRed Imager (HyspIRI) mission and preparatory activities. *Remote Sensing of Environment,* 167**,** 6-19.

LI, F., MIAO, Y., FENG, G., YUAN, F., YUE, S., GAO, X., LIU, Y., LIU, B., USTIN, S. L. & CHEN, X. 2014. Improving estimation of summer maize nitrogen status with red edge-based spectral vegetation indices. *Field Crops Research,* 157**,** 111-123.

LI, F., MIAO, Y., HENNIG, S. D., GNYP, M. L., CHEN, X., JIA, L. & BARETH, G. 2010. Evaluating hyperspectral vegetation indices for estimating nitrogen concentration of winter wheat at different growth stages. *Precision Agriculture,* 11**,** 335-357.

LI, X., STRAHLER, A. H. & WOODCOCK, C. E. 1995. A hybrid geometric optical-radiative transfer approach for modeling albedo and directional reflectance of discontinuous canopies. *IEEE Transactions on geoscience and remote sensing,* 33**,** 466-480.

LI, Y., REN, B., DING, L., SHEN, Q., PENG, S. & GUO, S. 2013. Does chloroplast size influence photosynthetic nitrogen use efficiency? *PloS one,* 8**,** e62036.

LICHTENTHALER, H., LANG, M., SOWINSKA, M., HEISEL, F. & MIEHE, J. 1996. Detection of vegetation stress via a new high resolution fluorescence imaging system. *Journal of plant physiology,* 148**,** 599-612.

LIMA, P. S., RODRIGUES, V. L. P., DE MEDEIROS, J. F., DE AQUINO, B. F. & DA SILVA, J. 2007. Yield and quality of melon fruits as a response to the application of nitrogen and potassium doses. *Revista caatinga,* 20.

LIN, S.-Y. & AGEHARA, S. 2021. Foliar application of defoliants before winter chill accumulation advances budbreak and improves fruit earliness of blackberry under subtropical climatic conditions. *HortScience,* 56**,** 210-216.

LU, C. & ZHANG, J. 2000. Photosynthetic CO2 assimilation, chlorophyll fluorescence and photoinhibition as affected by nitrogen deficiency in maize plants. *Plant Science,* 151**,** 135-143.

1358 MAATHUIS, F. J. 2009. Physiological functions of mineral macronutrients. *Current opinion in plant*
1359 *biology*, 12**,** 250-258.
1360 MACDONALD, G. K., BENNETT, E. M., POTTER, P. A. & RAMANKUTTY, N. 2011. Agronomic
1361 phosphorus imbalances across the world's croplands. *Proceedings of the National Academy of*
1362 *Sciences*, 108**,** 3086-3091.
1363 MAHOUACHI, J., SOCORRO, A. R. & TALON, M. 2006. Responses of papaya seedlings (Carica papaya
1364 L.) to water stress and re-hydration: growth, photosynthesis and mineral nutrient imbalance. *Plant*
1365 *and soil*, 281**,** 137-146.
1366 MALHOTRA, H., SHARMA, S. & PANDEY, R. 2018. Phosphorus nutrition: plant growth in response to
1367 deficiency and excess. *Plant nutrients and abiotic stress tolerance.* Springer.
1368 MARESMA, Á., ARIZA, M., MARTÍNEZ, E., LLOVERAS, J. & MARTÍNEZ-CASASNOVAS, J. A.
1369 2016. Analysis of vegetation indices to determine nitrogen application and yield prediction in maize
1370 (Zea mays L.) from a standard UAV service. *Remote Sensing*, 8**,** 973.
1371 MARKWELL, J., OSTERMAN, J. C. & MITCHELL, J. L. 1995. Calibration of the Minolta SPAD-502
1372 leaf chlorophyll meter. *Photosynthesis research*, 46**,** 467-472.
1373 MARSCHNER, H. 1986. Mineral nutrition of higher plants, Horst Marschner.
1374 MARSCHNER, H. 2011. *Marschner's mineral nutrition of higher plants*, Academic press.
1375 MARSCHNER, P. & RENGEL, Z. 2007. *Nutrient cycling in terrestrial ecosystems*, Springer Science &
1376 Business Media.
1377 MARSHALL, M. & THENKABAIL, P. 2015. Advantage of hyperspectral EO-1 Hyperion over
1378 multispectral IKONOS, GeoEye-1, WorldView-2, Landsat ETM+, and MODIS vegetation indices
1379 in crop biomass estimation. *ISPRS Journal of Photogrammetry and Remote Sensing*, 108**,** 205-218.
1380 MARTIN, M. E. & ABER, J. D. 1997. High spectral resolution remote sensing of forest canopy lignin,
1381 nitrogen, and ecosystem processes. *Ecological applications*, 7**,** 431-443.
1382 MATSON, P. A., NAYLOR, R. & ORTIZ-MONASTERIO, I. 1998. Integration of environmental,
1383 agronomic, and economic aspects of fertilizer management. *Science*, 280**,** 112-115.
1384 MAXWELL, K. & JOHNSON, G. N. 2000. Chlorophyll fluorescence—a practical guide. *Journal of*
1385 *experimental botany*, 51**,** 659-668.
1386 MCAINSH, M. R. & PITTMAN, J. K. 2009. Shaping the calcium signature. *New Phytologist*, 181**,** 275-
1387 294.
1388 MENESATTI, P., ANTONUCCI, F., PALLOTTINO, F., ROCCUZZO, G., ALLEGRA, M., STAGNO, F.
1389 & INTRIGLIOLO, F. 2010. Estimation of plant nutritional status by Vis–NIR spectrophotometric
1390 analysis on orange leaves [Citrus sinensis (L) Osbeck cv Tarocco]. *biosystems engineering*, 105**,**
1391 448-454.
1392 MENGEL, K. & KIRKBY, E. A. 2012. *Principles of plant nutrition*, Springer Science & Business Media.
1393 MILLS, S. & WT, F. J. 1994. Evaluation of phosphorus sources promoting bioremediation of diesel fuel in
1394 soil. *Bulletin of Environmental Contamination and Toxicology;(United States)*, 53.
1395 MIRAGLIO, T., ADELINE, K., HUESCA, M., USTIN, S. & BRIOTTET, X. 2019. Monitoring LAI,
1396 chlorophylls, and carotenoids content of a woodland savanna using hyperspectral imagery and 3D
1397 radiative transfer modeling. *Remote sensing*, 12**,** 28.
1398 MOHAMMED, G. H., COLOMBO, R., MIDDLETON, E. M., RASCHER, U., VAN DER TOL, C.,
1399 NEDBAL, L., GOULAS, Y., PÉREZ-PRIEGO, O., DAMM, A. & MERONI, M. 2019. Remote
1400 sensing of solar-induced chlorophyll fluorescence (SIF) in vegetation: 50 years of progress. *Remote*
1401 *Sensing of Environment*, 231**,** 111177.
1402 MORAN, J. A., MITCHELL, A. K., GOODMANSON, G. & STOCKBURGER, K. A. 2000.
1403 Differentiation among effects of nitrogen fertilization treatments on conifer seedlings by foliar
1404 reflectance: a comparison of methods. *Tree physiology*, 20**,** 1113-1120.
1405 MORGAN, J. Á. & CONNOLLY, E. Á. 2013. Plant-soil interactions: nutrient uptake. *Nature Education*
1406 *Knowledge*, 4**,** 2.
1407 MUHAMMAD, S., SANDEN, B. L., LAMPINEN, B. D., SAA, S., SIDDIQUI, M. I., SMART, D. R.,
1408 OLIVOS, A., SHACKEL, K. A., DEJONG, T. & BROWN, P. H. 2015. Seasonal changes in

nutrient content and concentrations in a mature deciduous tree species: Studies in almond (Prunus dulcis (Mill.) DA Webb). *European Journal of Agronomy,* 65**,** 52-68.

MUÑOZ-HUERTA, R. F., GUEVARA-GONZALEZ, R. G., CONTRERAS-MEDINA, L. M., TORRES-PACHECO, I., PRADO-OLIVAREZ, J. & OCAMPO-VELAZQUEZ, R. V. 2013. A review of methods for sensing the nitrogen status in plants: advantages, disadvantages and recent advances. *sensors,* 13**,** 10823-10843.

NETTO, A. T., CAMPOSTRINI, E., DE OLIVEIRA, J. G. & BRESSAN-SMITH, R. E. 2005. Photosynthetic pigments, nitrogen, chlorophyll a fluorescence and SPAD-502 readings in coffee leaves. *Scientia Horticulturae,* 104**,** 199-209.

NEVALAINEN, O., HAKALA, T., SUOMALAINEN, J. & KAASALAINEN, S. 2013. Nitrogen concentration estimation with hyperspectral LiDAR. *ISPRS Annals of Photogrammetry, Remote Sensing and Spatial Information Sciences,* 2**,** 205-210.

NORTH, P. R. 1996. Three-dimensional forest light interaction model using a Monte Carlo method. *IEEE Transactions on geoscience and remote sensing,* 34**,** 946-956.

NURSU'AIDAH, H., MOTIOR, M., NAZIA, A. & ISLAM, M. 2014. Growth and photosynthetic responses of long bean (Vigna unguiculata) and mung bean (Vigna radiata) response to fertilization. *J Anim Plant Sci,* 24**,** 573-578.

OSPINA, C., LAMMERTS VAN BUEREN, E., ALLEFS, J., ENGEL, B. V., VAN DER PUTTEN, P., VAN DER LINDEN, C. & STRUIK, P. 2014. Diversity of crop development traits and nitrogen use efficiency among potato cultivars grown under contrasting nitrogen regimes. *Euphytica,* 199**,** 13-29.

PADILLA, F. M., DE SOUZA, R., PEÑA, T., GALLARDO, M., GIMENEZ, C. & THOMPSON, R. 2018. Different responses of various chlorophyll meters to increasing nitrogen supply in sweet pepper. *Frontiers in plant science,* 9**,** 1752.

PATEL, M. K., RYU, D., WESTERN, A. W., SUTER, H. & YOUNG, I. M. 2021. Which multispectral indices robustly measure canopy nitrogen across seasons: Lessons from an irrigated pasture crop. *Computers and Electronics in Agriculture,* 182**,** 106000.

PELLISSIER, P. A., OLLINGER, S. V., LEPINE, L. C., PALACE, M. W. & MCDOWELL, W. H. 2015. Remote sensing of foliar nitrogen in cultivated grasslands of human dominated landscapes. *Remote Sensing of Environment,* 167**,** 88-97.

PEÑUELAS, J., GAMON, J., FREDEEN, A., MERINO, J. & FIELD, C. 1994. Reflectance indices associated with physiological changes in nitrogen-and water-limited sunflower leaves. *Remote sensing of Environment,* 48**,** 135-146.

PETTIGREW, W. T. 2008. Potassium influences on yield and quality production for maize, wheat, soybean and cotton. *Physiologia plantarum,* 133**,** 670-681.

PLASCYK, J. A. & GABRIEL, F. C. 1975. The Fraunhofer line discriminator MKII-an airborne instrument for precise and standardized ecological luminescence measurement. *IEEE Transactions on Instrumentation and measurement,* 24**,** 306-313.

PORCAR-CASTELL, A., TYYSTJÄRVI, E., ATHERTON, J., VAN DER TOL, C., FLEXAS, J., PFÜNDEL, E. E., MORENO, J., FRANKENBERG, C. & BERRY, J. A. 2014. Linking chlorophyll a fluorescence to photosynthesis for remote sensing applications: mechanisms and challenges. *Journal of experimental botany,* 65**,** 4065-4095.

PRANANTO, J. A., MINASNY, B. & WEAVER, T. 2021. Rapid and cost-effective nutrient content analysis of cotton leaves using near-infrared spectroscopy (NIRS). *PeerJ,* 9**,** e11042.

RAAIMAKERS, D., BOOT, R., DIJKSTRA, P. & POT, S. 1995. Photosynthetic rates in relation to leaf phosphorus content in pioneer versus climax tropical rainforest trees. *Oecologia,* 102**,** 120-125.

RASCHER, U., ALONSO, L., BURKART, A., CILIA, C., COGLIATI, S., COLOMBO, R., DAMM, A., DRUSCH, M., GUANTER, L. & HANUS, J. 2015. Sun-induced fluorescence–a new probe of photosynthesis: First maps from the imaging spectrometer HyPlant. *Global change biology,* 21**,** 4673-4684.

RAST, M., NIEKE, J., ADAMS, J., ISOLA, C. & GASCON, F. Copernicus Hyperspectral Imaging Mission for the Environment (Chime). 2021 IEEE International Geoscience and Remote Sensing Symposium IGARSS, 2021. IEEE, 108-111.

RAST, M. & PAINTER, T. H. 2019. Earth observation imaging spectroscopy for terrestrial systems: An overview of its history, techniques, and applications of its missions. *Surveys in Geophysics,* 40**,** 303-331.

RICHTER, K., ATZBERGER, C., VUOLO, F., WEIHS, P. & D'URSO, G. 2009. Experimental assessment of the Sentinel-2 band setting for RTM-based LAI retrieval of sugar beet and maize. *Canadian Journal of Remote Sensing,* 35**,** 230-247.

ROSENQVIST, E. & VAN KOOTEN, O. 2003. Chlorophyll fluorescence: a general description and nomenclature. *Practical applications of chlorophyll fluorescence in plant biology***,** 31-77.

ROUJEAN, J.-L. & BREON, F.-M. 1995. Estimating PAR absorbed by vegetation from bidirectional reflectance measurements. *Remote sensing of Environment,* 51**,** 375-384.

ROUSE, J. W., HAAS, R. H., SCHELL, J. A. & DEERING, D. W. 1974. Monitoring vegetation systems in the Great Plains with ERTS. *NASA special publication,* 351**,** 309.

ROY, R. N., FINCK, A., BLAIR, G. & TANDON, H. 2006. Plant nutrition for food security. *A guide for integrated nutrient management. FAO Fertilizer and Plant Nutrition Bulletin,* 16**,** 368.

RYAN, J., ESTEFAN, G. & RASHID, A. 2001. *Soil and plant analysis laboratory manual,* ICARDA.

SAINI, R. K., SIVANESAN, I. & KEUM, Y.-S. 2019. Emerging roles of carotenoids in the survival and adaptations of microbes. *Indian journal of microbiology,* 59**,** 125-127.

SCHÄCHTL, J., HUBER, G., MAIDL, F.-X., STICKSEL, E., SCHULZ, J. & HASCHBERGER, P. 2005. Laser-induced chlorophyll fluorescence measurements for detecting the nitrogen status of wheat (Triticum aestivum L.) canopies. *Precision Agriculture,* 6**,** 143-156.

SCHAEPMAN-STRUB, G., SCHAEPMAN, M. E., PAINTER, T. H., DANGEL, S. & MARTONCHIK, J. V. 2006. Reflectance quantities in optical remote sensing—Definitions and case studies. *Remote sensing of environment,* 103**,** 27-42.

SCHAEPMAN, M. E., JEHLE, M., HUENI, A., D'ODORICO, P., DAMM, A., WEYERMANN, J., SCHNEIDER, F. D., LAURENT, V., POPP, C. & SEIDEL, F. C. 2015. Advanced radiometry measurements and Earth science applications with the Airborne Prism Experiment (APEX). *Remote Sensing of Environment,* 158**,** 207-219.

SCHLEGEL, A. J. & HAVLIN, J. L. 2017. Corn yield and grain nutrient uptake from 50 years of nitrogen and phosphorus fertilization. *Agronomy Journal,* 109**,** 335-342.

SCHLEMMER, M., GITELSON, A., SCHEPERS, J., FERGUSON, R., PENG, Y., SHANAHAN, J. & RUNDQUIST, D. 2013. Remote estimation of nitrogen and chlorophyll contents in maize at leaf and canopy levels. *International Journal of Applied Earth Observation and Geoinformation,* 25**,** 47-54.

SCHMIDHUBER, J. & TUBIELLO, F. N. 2007. Global food security under climate change. *Proceedings of the National Academy of Sciences,* 104**,** 19703-19708.

SCHREIBER, U. 2004. Pulse-amplitude-modulation (PAM) fluorometry and saturation pulse method: an overview. *Chlorophyll a fluorescence.* Springer.

SCHREIBER, U., SCHLIWA, U. & BILGER, W. 1986. Continuous recording of photochemical and non-photochemical chlorophyll fluorescence quenching with a new type of modulation fluorometer. *Photosynthesis research,* 10**,** 51-62.

SCOTFORD, I. & MILLER, P. Monitoring the growth of winter wheat using measurements of normalised difference vegetation index (NDVI) and crop height. 4th European Conference on Precision Agriculture. Eds. J Stafford and A Werner, 2003. 627-632.

SHANKER, A. & VENKATESWARLU, B. 2011. *Abiotic stress in plants: mechanisms and adaptations*, BoD–Books on Demand.

SIEFERMANN-HARMS, D. 1985. Carotenoids in photosynthesis. I. Location in photosynthetic membranes and light-harvesting function. *Biochimica et Biophysica Acta (BBA)-Reviews on Bioenergetics,* 811**,** 325-355.

SIMS, N. C., CULVENOR, D., NEWNHAM, G., COOPS, N. C. & HOPMANS, P. 2013. Towards the operational use of satellite hyperspectral image data for mapping nutrient status and fertilizer requirements in Australian plantation forests. *IEEE Journal of Selected Topics in Applied Earth Observations and Remote Sensing,* 6**,** 320-328.

SKIBA, U. & REES, R. 2014. Nitrous oxide, climate change and agriculture. *CABI Reviews***,** 1-7.

SMITH, M.-L., OLLINGER, S. V., MARTIN, M. E., ABER, J. D., HALLETT, R. A. & GOODALE, C. L. 2002. Direct estimation of aboveground forest productivity through hyperspectral remote sensing of canopy nitrogen. *Ecological applications,* 12**,** 1286-1302.

SMITH, P. F. 1962. Mineral analysis of plant tissues. *Annual Review of Plant Physiology,* 13**,** 81-108.

SPERLING, O., KARUNAKARAN, R., EREL, R., YASUOR, H., KLIPCAN, L. & YERMIYAHU, U. 2019. Excessive nitrogen impairs hydraulics, limits photosynthesis, and alters the metabolic composition of almond trees. *Plant Physiology and Biochemistry,* 143**,** 265-274.

STEVENSON, F. J. & COLE, M. A. 1999. *Cycles of soils: carbon, nitrogen, phosphorus, sulfur, micronutrients*, John Wiley & Sons.

STEWART, G. 1988. Mineral nutrition in higher plants. JSTOR.

STEWART, W., DIBB, D., JOHNSTON, A. & SMYTH, T. 2005. The contribution of commercial fertilizer nutrients to food production. *Agronomy journal,* 97**,** 1-6.

STITT, M. 1990. The flux of carbon between the chloroplast and the cytosol. *Plant physiology, biochemistry and molecular biology***,** 319-339.

STRACHAN, I. B., PATTEY, E. & BOISVERT, J. B. 2002. Impact of nitrogen and environmental conditions on corn as detected by hyperspectral reflectance. *Remote Sensing of environment,* 80**,** 213-224.

SUAREZ, L., GONZÁLEZ-DUGO, V., CAMINO, C., HORNERO, A. & ZARCO-TEJADA, P. J. 2021a. Physical model inversion of the green spectral region to track assimilation rate in almond trees with an airborne nano-hyperspectral imager. *Remote Sensing of Environment,* 252**,** 112147.

SUAREZ, L., ZHANG, P., SUN, J., WANG, Y., POBLETE, T., HORNERO, A. & ZARCO-TEJADA, P. J. 2021b. Assessing wine grape quality parameters using plant traits derived from physical model inversion of hyperspectral imagery. *Agricultural and Forest Meteorology,* 306**,** 108445.

SUN, Y., WEN, J., GU, L., JOINER, J., CHANG, C. Y., VAN DER TOL, C., PORCAR-CASTELL, A., MAGNEY, T., WANG, L. & HU, L. 2023. From Remotely-Sensed SIF to Ecosystem Structure, Function, and Service: Part II-Harnessing Data. *Global change biology*.

SUTTON, M. A., BLEEKER, A., HOWARD, C., ERISMAN, J., ABROL, Y., BEKUNDA, M., DATTA, A., DAVIDSON, E., DE VRIES, W. & OENEMA, O. 2013. Our nutrient world. The challenge to produce more food & energy with less pollution. Centre for Ecology & Hydrology.

TEAM, H. M. C. 2018. HyspIRI Final Report. *Jet Propulsion Laboratory, California Institute of Technology, Pasadena, California***,** 1-87.

THENKABAIL, P. S. & LYON, J. G. 2016. *Hyperspectral remote sensing of vegetation*, CRC press.

THENKABAIL, P. S., SMITH, R. B. & DE PAUW, E. 2000. Hyperspectral vegetation indices and their relationships with agricultural crop characteristics. *Remote sensing of Environment,* 71**,** 158-182.

THOR, K. 2019. Calcium—nutrient and messenger. *Frontiers in plant science,* 10**,** 440.

TILLING, A. K., O'LEARY, G. J., FERWERDA, J. G., JONES, S. D., FITZGERALD, G. J., RODRIGUEZ, D. & BELFORD, R. 2007. Remote sensing of nitrogen and water stress in wheat. *Field Crops Research,* 104**,** 77-85.

TOWNSEND, P. A., FOSTER, J. R., CHASTAIN, R. A. & CURRIE, W. S. 2003. Application of imaging spectroscopy to mapping canopy nitrogen in the forests of the central Appalachian Mountains using Hyperion and AVIRIS. *IEEE Transactions on Geoscience and Remote Sensing,* 41**,** 1347-1354.

TREMBLAY, N., WANG, Z. & CEROVIC, Z. G. 2012. Sensing crop nitrogen status with fluorescence indicators. A review. *Agronomy for sustainable development,* 32**,** 451-464.

TRIPATHI, D. K., SINGH, V. P., CHAUHAN, D. K., PRASAD, S. M. & DUBEY, N. K. 2014. Role of macronutrients in plant growth and acclimation: recent advances and future prospective. *Improvement of crops in the era of climatic changes***,** 197-216.

UDDLING, J., GELANG-ALFREDSSON, J., PIIKKI, K. & PLEIJEL, H. 2007. Evaluating the relationship between leaf chlorophyll concentration and SPAD-502 chlorophyll meter readings. *Photosynthesis research,* 91**,** 37-46.

ULRICH, A. 1952. Physiological bases for assessing the nutritional requirements of plants. *Annual Review of Plant Physiology,* 3**,** 207-228.

UNKOVICH, M., HERRIDGE, D., PEOPLES, M., CADISCH, G., BODDEY, B., GILLER, K., ALVES, B. & CHALK, P. 2008. *Measuring plant-associated nitrogen fixation in agricultural systems*, Australian Centre for International Agricultural Research (ACIAR).

VANE, G., GREEN, R. O., CHRIEN, T. G., ENMARK, H. T., HANSEN, E. G. & PORTER, W. M. 1993. The airborne visible/infrared imaging spectrometer (AVIRIS). *Remote sensing of environment,* 44**,** 127-143.

VERHOEF, W. 1984. Light scattering by leaf layers with application to canopy reflectance modeling: The SAIL model. *Remote sensing of environment,* 16**,** 125-141.

VERHOEF, W. 1998. *Theory of radiative transfer models applied in optical remote sensing of vegetation canopies*, Wageningen University and Research.

VERHOEF, W., JIA, L., XIAO, Q. & SU, Z. 2007. Unified optical-thermal four-stream radiative transfer theory for homogeneous vegetation canopies. *IEEE Transactions on geoscience and remote sensing,* 45**,** 1808-1822.

VERRELST, J., MALENOVSKÝ, Z., VAN DER TOL, C., CAMPS-VALLS, G., GASTELLU-ETCHEGORRY, J.-P., LEWIS, P., NORTH, P. & MORENO, J. 2019. Quantifying vegetation biophysical variables from imaging spectroscopy data: a review on retrieval methods. *Surveys in Geophysics,* 40**,** 589-629.

VERRELST, J., RIVERA, J. P., GITELSON, A., DELEGIDO, J., MORENO, J. & CAMPS-VALLS, G. 2016. Spectral band selection for vegetation properties retrieval using Gaussian processes regression. *International journal of applied earth observation and geoinformation,* 52**,** 554-567.

VINCINI, M., FRAZZI, E. & D'ALESSIO, P. Angular dependence of maize and sugar beet VIs from directional CHRIS/Proba data. Proc. 4th ESA CHRIS PROBA Workshop, 2006. 19-21.

WALKER, A. P., BECKERMAN, A. P., GU, L., KATTGE, J., CERNUSAK, L. A., DOMINGUES, T. F., SCALES, J. C., WOHLFAHRT, G., WULLSCHLEGER, S. D. & WOODWARD, F. I. 2014. The relationship of leaf photosynthetic traits–Vcmax and Jmax–to leaf nitrogen, leaf phosphorus, and specific leaf area: a meta-analysis and modeling study. *Ecology and evolution,* 4**,** 3218-3235.

WAN, L., ZHANG, J., DONG, X., DU, X., ZHU, J., SUN, D., LIU, Y., HE, Y. & CEN, H. 2021. Unmanned aerial vehicle-based field phenotyping of crop biomass using growth traits retrieved from PROSAIL model. *Computers and Electronics in Agriculture,* 187**,** 106304.

WANG, S., GUAN, K., WANG, Z., AINSWORTH, E. A., ZHENG, T., TOWNSEND, P. A., LIU, N., NAFZIGER, E., MASTERS, M. D. & LI, K. 2021. Airborne hyperspectral imaging of nitrogen deficiency on crop traits and yield of maize by machine learning and radiative transfer modeling. *International Journal of Applied Earth Observation and Geoinformation,* 105**,** 102617.

WANG, Y., JANZ, B., ENGEDAL, T. & DE NEERGAARD, A. 2017. Effect of irrigation regimes and nitrogen rates on water use efficiency and nitrogen uptake in maize. *Agricultural Water Management,* 179**,** 271-276.

WEI, S., WANG, X., SHI, D., LI, Y., ZHANG, J., LIU, P., ZHAO, B. & DONG, S. 2016. The mechanisms of low nitrogen induced weakened photosynthesis in summer maize (Zea mays L.) under field conditions. *Plant physiology and biochemistry,* 105**,** 118-128.

WESSMAN, C. A., ABER, J. D., PETERSON, D. L. & MELILLO, J. M. 1988. Remote sensing of canopy chemistry and nitrogen cycling in temperate forest ecosystems. *Nature,* 335**,** 154.

WHITE, P. J. & BROADLEY, M. R. 2003. Calcium in plants. *Annals of botany,* 92**,** 487-511.

WHITE, P. J. & BROADLEY, M. R. 2005. Biofortifying crops with essential mineral elements. *Trends in plant science,* 10**,** 586-593.

WHITE, P. J. & BROWN, P. 2010. Plant nutrition for sustainable development and global health. *Annals of botany,* 105**,** 1073-1080.

1612 WILKINSON, S., WELCH, R. M., MAYLAND, H. & GRUNES, D. 1990. Magnesium in plants: uptake,
1613 distribution, function, and utilization by man and animals.
1614 WONG, K. K. & HE, Y. 2013. Estimating grassland chlorophyll content using remote sensing data at leaf,
1615 canopy, and landscape scales. *Canadian Journal of Remote Sensing,* 39**,** 155-166.
1616 WOOD, C., REEVES, D., DUFFIELD, R. & EDMISTEN, K. 1992a. Field chlorophyll measurements for
1617 evaluation of corn nitrogen status. *Journal of Plant Nutrition,* 15**,** 487-500.
1618 WOOD, C., REEVES, D. & HIMELRICK, D. Relationships between chlorophyll meter readings and leaf
1619 chlorophyll concentration, N status, and crop yield: a review. Proceedings of the Agronomy
1620 Society of New Zealand, 1993. 1-9.
1621 WOOD, C., TRACY, P., REEVES, D. & EDMISTEN, K. L. 1992b. Determination of cotton nitrogen status
1622 with a handheld chlorophyll meter. *Journal of Plant Nutrition,* 15**,** 1435-1448.
1623 XIONG, D., CHEN, J., YU, T., GAO, W., LING, X., LI, Y., PENG, S. & HUANG, J. 2015. SPAD-based
1624 leaf nitrogen estimation is impacted by environmental factors and crop leaf characteristics.
1625 *Scientific reports,* 5**,** 1-12.
1626 YAMAMOTO, H. Y. 1979. Biochemistry of the violaxanthin cycle in higher plants. *Carotenoids°C 5.*
1627 Elsevier.
1628 ZARCO-TEJADA, P., CAMINO, C., BECK, P., CALDERON, R., HORNERO, A., HERNÁNDEZ-
1629 CLEMENTE, R., KATTENBORN, T., MONTES-BORREGO, M., SUSCA, L. & MORELLI, M.
1630 2018. Previsual symptoms of Xylella fastidiosa infection revealed in spectral plant-trait alterations.
1631 *Nature Plants,* 4**,** 432-439.
1632 ZARCO-TEJADA, P. J., CATALINA, A., GONZÁLEZ, M. & MARTÍN, P. 2013a. Relationships between
1633 net photosynthesis and steady-state chlorophyll fluorescence retrieved from airborne hyperspectral
1634 imagery. *Remote Sensing of Environment,* 136**,** 247-258.
1635 ZARCO-TEJADA, P. J., MILLER, J. R., MOHAMMED, G. H. & NOLAND, T. L. 2000a. Chlorophyll
1636 fluorescence effects on vegetation apparent reflectance: I. Leaf-level measurements and model
1637 simulation. *Remote Sensing of Environment,* 74**,** 582-595.
1638 ZARCO-TEJADA, P. J., MILLER, J. R., MOHAMMED, G. H., NOLAND, T. L. & SAMPSON, P. H.
1639 2000b. Chlorophyll fluorescence effects on vegetation apparent reflectance: II. Laboratory and
1640 airborne canopy-level measurements with hyperspectral data. *Remote Sensing of Environment,* 74**,**
1641 596-608.
1642 ZARCO-TEJADA, P. J., MILLER, J. R., MORALES, A., BERJÓN, A. & AGÜERA, J. 2004.
1643 Hyperspectral indices and model simulation for chlorophyll estimation in open-canopy tree crops.
1644 *Remote sensing of environment,* 90**,** 463-476.
1645 ZARCO-TEJADA, P. J., MILLER, J. R., NOLAND, T. L., MOHAMMED, G. H. & SAMPSON, P. H.
1646 2001. Scaling-up and model inversion methods with narrowband optical indices for chlorophyll
1647 content estimation in closed forest canopies with hyperspectral data. *IEEE Transactions on*
1648 *Geoscience and Remote Sensing,* 39**,** 1491-1507.
1649 ZARCO-TEJADA, P. J., MORALES, A., TESTI, L. & VILLALOBOS, F. J. 2013b. Spatio-temporal
1650 patterns of chlorophyll fluorescence and physiological and structural indices acquired from
1651 hyperspectral imagery as compared with carbon fluxes measured with eddy covariance. *Remote*
1652 *Sensing of Environment,* 133**,** 102-115.
1653 ZHANG, L., GUO, C., ZHAO, L., ZHU, Y., CAO, W., TIAN, Y., CHENG, T. & WANG, X. 2016.
1654 Estimating wheat yield by integrating the WheatGrow and PROSAIL models. *Field Crops*
1655 *Research,* 192**,** 55-66.
1656 ZHAO, F., WOOD, A. & MCGRATH, S. 1999. Effects of sulphur nutrition on growth and nitrogen fixation
1657 of pea (Pisum sativum L.). *Plant and Soil,* 212**,** 207-217.
1658 ZHU, Y. & SMITH, S. 2001. Seed phosphorus (P) content affects growth, and P uptake of wheat plants
1659 and their association with arbuscular mycorrhizal (AM) fungi. *Plant and Soil,* 231**,** 105-112.

Chapter 2 : Assessing the performance of solar-induced fluorescence (SIF) and vegetation plant traits for leaf macro- and micro-nutrient concentrations

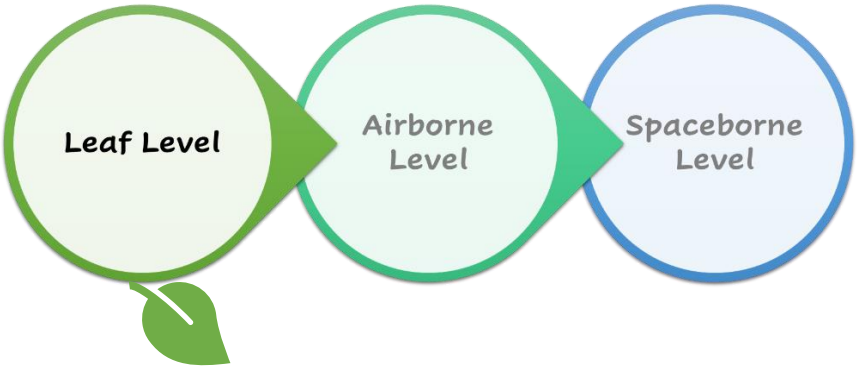

Abstract

Macro- and micro-nutrients are essential for plant functioning and to ensure crop growth, high yields, and quality fruit. Having a comprehensive understanding of nutrient status within the crop is essential for making effective fertilizer management decisions. Existing studies have demonstrated the feasibility of remote sensing techniques for nutrient assessment, although most of them have a particular focus on nitrogen status. The methods generally used are chlorophyll-sensitive indices, biochemical constituents, and fluorescence (SIF) derived from visible and near-infrared spectral domains. However, fewer studies have assessed other macro- and micro-nutrients which are critical for the growth and optimal management of crops. This study investigated the sensitivity of vegetation indices, plant traits, and fluorescence emission to explain the variability of 12 macro- and micro-nutrients, as well as 10 nutrient ratios at leaf and canopy levels, throughout two consecutive growing seasons. Results showed that chlorophyll fluorescence was a robust indicator of the three primary macro-nutrients, N, P, and K, at both leaf and canopy levels across both years, yielding $r^2 = 0.74$ (p-values < 0.005) for both leaf steady-state measurements and canopy SIF of leaf N for the two years of data. In addition, the biochemical constituents derived by radiative transfer modeling demonstrated strong correlations with the primary macro-nutrients for both years, whereas the vegetation indices exhibited generally weaker relationships with nutrients.

Keywords: Chlorophyll Fluorescence, SIF, Macro-nutrient, Micro-nutrient, Chlorophyll, Hyperspectral, Nitrogen (N), Phosphorus (P), Potassium (K), Almond

2.1 Introduction

Plant growth and development are heavily dependent on essential nutrients which contribute to different aspects of plant development and functioning at different phenological stages (Aftab and Hakeem, 2020, Roy *et al.*, 2006). Providing optimal and balanced nutrient inputs is becoming increasingly important to enhance the quality and yield of almonds in an environmentally friendly, sustainable, and productive manner (Roy *et al.*, 2006, Muhammad *et al.*, 2015). Thus fine-tuned, efficient, and sustainable fertilizer applications are critical to ensure optimum yields and quality while minimizing the impact on the environment.

According to plant uptake, nutrients are classified as: i) macro-nutrients, which are required in large quantities by plants and living organisms as substances essential for plant cell and tissue development, including carbon (C), hydrogen (H), oxygen (O), nitrogen (N), phosphorus (P), potassium (K), sulfur (S), calcium (Ca), and magnesium (Mg); and ii) micro-nutrients, which are required in lower quantities, like iron (Fe), zinc (Zn), manganese (Mn), copper (Cu), and boron (B) (Maathuis, 2009, George *et al.*, 2008). Among all nutrients, N, P, and K are the primary macro-nutrients and they are predominantly provided via fertilizer applications during active plant growth, aiming to achieve high photosynthetic rates. N is a crucial constituent of proteins and contributes to the formation of chlorophyll. P is essential for the growth of early roots, cell division, and the development of seed and fruit. K plays an important role in regulating stomatal opening and closing, which is crucial for the water balance of plants (Roy *et al.*, 2006). Micro-nutrients also play important roles in plant growth and functioning, even when they are less abundant (Sharma, 2006). For instance, Mn plays a role in splitting the water molecule during photosynthesis. In addition to controlling membrane integrity and cell-wall development, B is associated with pollen tube growth, which affects seed and fruit set and thus yield. More specifically to almonds, B application was

found to increase nut weight and number, and protein content. S, Cu, Fe, and Mn also assist in the formation of chlorophyll along with N (Roy *et al.*, 2006).

A number of studies have provided evidence of interactions between nutrient elements and stressed the importance of an optimal balance of internal reserves (Bloom *et al.*, 1985, Krouk and Kiba, 2020, Kumar *et al.*, 2021). Due to the large number of potential nutrient combinations, monitoring changes in nutrient status is crucial to maintain a balance between different elements regarding nutrient intake and usability under changing conditions throughout the phenological stages (Chapin *et al.*, 1987). For instance, many observations suggest that N affects P uptake positively (Grunes, 1959, Smith and Jackson, 1987) and that P starvation affects nitrate assimilation and uptake negatively (Gniazdowska and Rychter, 2000, De Magalhães *et al.*, 1998, Rufty Jr *et al.*, 1990). In the light of such interactions, the N/P ratio has been used to monitor the N-P balance in order to coordinate the application of N and P for growth optimization (Koerselman and Meuleman, 1996, McGroddy *et al.*, 2004, Güsewell, 2004, Tessier and Raynal, 2003). Consequently, an understanding of nutrient dynamics in almonds is essential, allowing growers to diagnose and prevent deficiencies throughout the growing season.

Traditionally, leaf analysis has been considered a practical approach to evaluating nutrient status and determining the best fertilization strategy (Smith, 1962, Ulrich, 1952, Embleton *et al.*, 1973, Jones and Janick, 1984). As a non-destructive, quicker, and cost-effective tool, remote sensing (RS) techniques employing spectrometers are capable of detecting photosynthesis-related proxies and stress indicators (Menesatti *et al.*, 2010, Prananto *et al.*, 2021). Current RS studies on leaf nutrient monitoring in almonds have focused primarily on leaf N estimation (Saa and Brown, 2014, Wang *et al.*, 2022, Wang *et al.*, 2021, Saa *et al.*, 2014, Zarate-Valdez *et al.*, 2015, O'Connell *et al.*, 2014, Morais *et al.*, 2020) due to it being needed in large quantities. Other macro- and micro-

nutrients seem to be difficult to assess and consequently only very few attempts have been made to characterize and monitor them together. Different macro-nutrients (e.g., N, P, K, Ca, Mg, and S) and micro-nutrients (e.g., Fe, Mn, Cu, and B) have been studied with handheld NIR spectrometers at the leaf level (Prananto *et al.*, 2021). At canopy level, RS approaches to macro-nutrient detection are typically based on chlorophyll-related indicators in the visible and near-infrared (VNIR) and the short-wave infrared (SWIR) spectral regions via vegetation indices derived from specific spectral bands. A few examples are: the Red Edge Chlorophyll Index (Gitelson *et al.*, 2005) proposed as a proxy for N; the ratio of reflectance difference index (Li *et al.*, 2018) for P; the three band vegetation index (Lu *et al.*, 2020) using both red-edge and SWIR for K; and the SWIR ratio index for Ca and Mg (Munyati *et al.*, 2020). In addition, there has been an increased interest in searching for other physiological traits and proxies, including a set of leaf biochemical constituents and biophysical traits derived by inverting the radiative transfer model (RTM), such as carotenoid (C_{car}), anthocyanin (Anth), dry matter (C_{dm}), the parameter of de-epoxidation state of the xanthophyll cycle (C_x), water content (C_w), and leaf area index (LAI). For instance, the leaf margins of plants with P deficiencies were found to have purple discolorations due to an increase in the production of Anth (Marschner, 2011). The link between N and C_{ab} and other pigments makes this physical method more practical for assessing N levels (Wang *et al.*, 2015, Camino *et al.*, 2018). Furthermore, solar-induced fluorescence (SIF) has attracted great attention due to its strong link with photosynthesis and its usefulness as an indicator of plant stress. Using simple image analysis, fluorescence changes can be interpreted by observing the pattern differences of leaves with N, P, or K deficiencies between their blue-green fluorescence (BGF), their chlorophyll-a fluorescence (ChlF) intensity induced by UV and blue excitations ($ChlF_{UV}/ChlF_{BLUE}$), and their ratio of red and far-red ChlF intensity (RF/FRF) (Cadet and Samson,

2011). The use of SIF for N assessment has already been reported in several studies (Cadet and Samson, 2011, Wang *et al.*, 2022, Camino *et al.*, 2018).

The present investigation aimed to analyze the relationships of leaf macro- and micro-nutrient concentrations and their ratios with different spectral traits and vegetation indices at the leaf and canopy levels across two years, and thus to identify the traits of robust almond trees with better predictive capacity.

2.2 Material and methods

2.2.1 Study area

This study was conducted in a commercial almond orchard located in Robinvale, situated on the south bank of the Murray River in Victoria, Australia, as illustrated in Fig. 2.1b. The orchard was monitored at the pre-harvest stage for two consecutive growing seasons in 2019/2020 and 2020/2021. There was a slight drop in the average maximum temperature for January 2021, 32.6°C, compared with that of January 2020, which was 33.2°C. As a result of its mediterranean climate, with annual precipitation of approximately 310 mm, this area is well known for high-volume production of almonds, olives, grapes etc. The industry statistics for 2019 indicate that 64,416 tonnes of almonds were produced in Victoria, out of a total of 104,437 tonnes in Australia.

This almond orchard (Fig. 2.1a), covering about 1240 hectares, is composed of northern and southern sites planted on sandy loam soils in 2006 and 2007, respectively. There are 67 blocks facing north-south on the northern site and 6 blocks facing east-west on the southern site. Nonpareil (1/2 of the rows), Carmel (1/3), and Price (1/6) were planted alternately in groups of six rows (Fig. 2.1c) at a spacing of 7 m (rows) by 4.4 m (trees). The diameters of the tree crowns typically range from 4 to 6.5 m, resulting in a dense cluster rather than a separated canopy between trees. Figs.

2.1d and 2.1e show more detail of the almond tree crowns and planting rows. A drip fertigation system was used to apply water and nutrients to Nonpareil and Carmel with Price varieties on an hourly basis. Macro-nutrients N, P, and K were applied throughout the growing season, while Ca and B nutrients were applied only during the bloom and nut growth stages, and S was applied after bloom. Fertigation rates were adjusted based on the data observed from the previous growing season. In 2019/2020, all varieties were fertigated at the same rate, while in 2020/2021, Carmel and Price varieties were fertigated about 10% more than Nonpareil was. Due to these factors, Nonpareil was fertigated at 325.6 kg N/ha, 44 kg P/ha, 241.5 kg K/ha, 125.6 kg S/ha, 35.3 kg Ca/ha, 3.5 kg B/ha, and 11,465 m^3 water/ha in 2019/2020, whereas in 2020/2021 it was applied at 318.7 kg N/ha, 42.2 kg P/ha, 270.8 kg K/ha, 128 kg S/ha, 35.3 kg Ca/ha, 3.5 kg B/ha, and 12,255 m^3 water/ha.

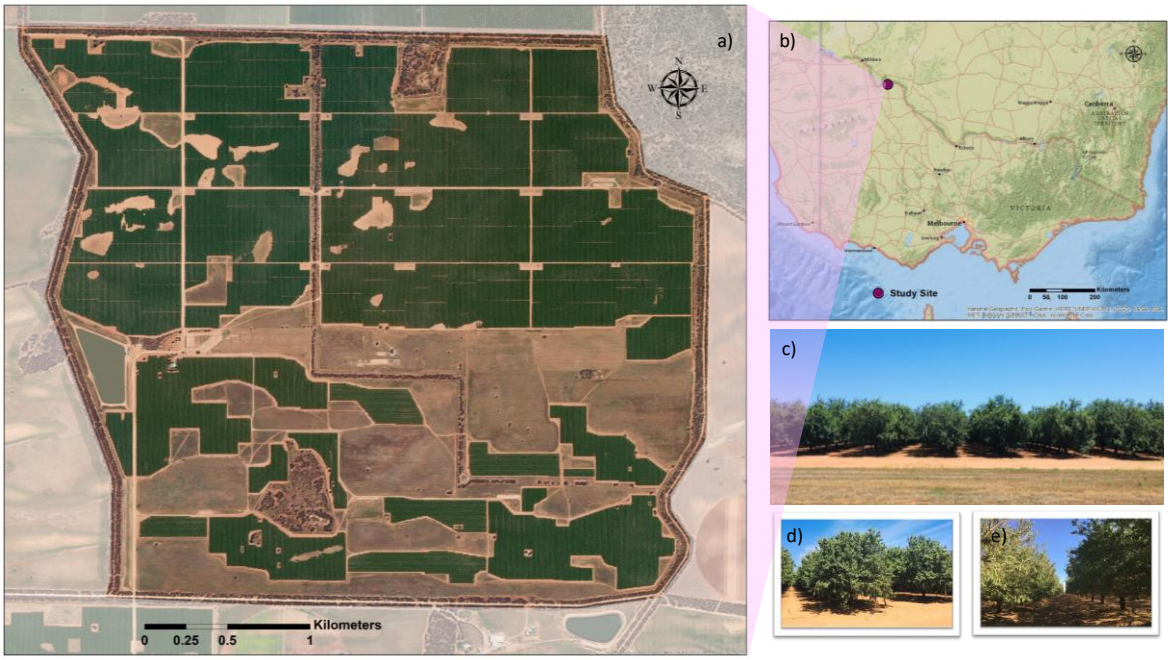

Fig. 2.1. a) The area of the 1200-ha almond orchard where the study was conducted. b) The location of the study site (magenta pointer) in Victoria, Australia. c) The landscape and row structure of the almond trees in the study area. d)-e) Close-ups of almond trees and the gap between rows.

2.2.2 Leaf-level data collection

In situ leaf measurements (Fig. 2.2) were conducted from the same study plots over 2 years. Monitoring was carried out on 15 homogeneous plots (presented in the yellow rectangle in Fig. 2.3) with different degrees of variability, planting ages, and orientations, each consisting of 6 rows with 7-8 trees. Four adjacent trees (two Nonpareil and two Carmel) were sampled in each study plot. Twenty representative mature sunlit leaves per tree were examined with various handheld instruments to assess leaf C_{ab}, anthocyanins (Anth), flavonoid (Flav) content, and nitrogen balance index (NBI) measured using a Dualex 4 Scientific sensor (FORCE-A, Orsay, France) (Fig. 2.2a). The FluorPen 110 (Fig. 2.2c) and PolyPen RP 410 (Fig. 2.2b) (PSI, Brno, Czech Republic) were used to measure leaf steady-state chlorophyll fluorescence (Ft) and leaf reflectance spectrum in the VNIR regions, respectively. Based on the average spectrum from each study plot, a number of vegetation indices were calculated, including chlorophyll *a+b* indices, xanthophyll indices, BGR indices, and fluorescence reflectance index, as listed in Table 2.1. An additional 20 leaves were collected along with the 80 leaves measured in order to increase the weight and size of the sample. The 100 leaves in each sample were used to analyze 12 macro- and micro-nutrient concentrations in a biochemical laboratory, using Dumas Combustion with a LECO TruMac CNS Macro Analyzer (LECO Corporation, MI, USA) and an inductively coupled plasma optical emission spectrometer (ICP-OES Optima 8300, Perkin Elmer, USA). The descriptive statistics for leaf nutrients and the measured indicators collected over two years were compared and their ranges of variation were calculated independently for three quartiles. In addition, the coefficients of determination were compared between *in situ* leaf measurements and 12 nutrient concentrations and 10 ratios, following the procedure of Horuz *et al.* (2013).

Fig. 2.2. In situ leaf measurements of: a) leaf chlorophyll (C_{ab}), anthocyanins (Anth), flavonoid (Flav) content, and nitrogen balance index (NBI) using a Dualex 4 Scientific sensor; b) leaf reflectance spectra in the visible and near-infrared regions with a PolyPen RP 410 instrument; c) leaf steady-state chlorophyll fluorescence (Ft) with a FluorPen FP 110 instrument; and d) leaf sample collection and leaf measurements of sunlit leaves from the top of the ladder.

2.2.3 Airborne hyperspectral datasets acquisition

In parallel with the collection of field data for image processing and calibration, airborne campaigns were conducted at solar noon under clear skies on 17 February 2020 and 31 January 2021 prior to harvest. A manned aircraft (Cessna 172R) carrying a hyperspectral line-scanning sensor (Micro-Hyperspec VNIR E-Series model, Headwall Photonics, Fitchburg, MA, USA) flew at 550 m above ground level (AGL) and collected data from north to east direction. The aircraft was operated by the HyperSens Remote Sensing Laboratory, the Airborne Remote Sensing Facility of the University of Melbourne. There are 371 spectral bands in the VNIR region covered by the hyperspectral imager with a full width at half maximum (FWHM) of 5.8 nm and a spectral sampling interval of 1.626 nm. For both years, the hyperspectral imager collected data at 40-cm spatial resolution with an angular field of view of 66^{o} and an 8-mm focal length. Each hyperspectral flight line was atmospherically corrected using the SMARTS model (Gueymard, 2001, Gueymard, 1995). At the time of each flight, aerosol optical measurements at 500 nm were taken using a Microtops II sunphotometer (Solar Light, PA, USA) connected to a GPS-12 navigator (Garmin, Olathe, KS, USA). The other input parameters (i.e., air temperature and

humidity) were calculated based on the averages of three nearby weather stations located between 4 and 15 km away. The orthorectification and mosaicking of images were performed using PARGE (ReSe Applications Schlapfe, Wil, Switzerland) and ENVI (Boulder, Colorado) software, respectively. To verify and correct the resulting image spectrum, reflectance data collected from *in situ* vegetation and soil targets with a FieldSpec Handheld Pro spectrometer (ASD Inc., CO, USA) was used. A false color composition of the airborne hyperspectral mosaic captured over the almond orchard in 2021 is shown in Fig. 2.3a.

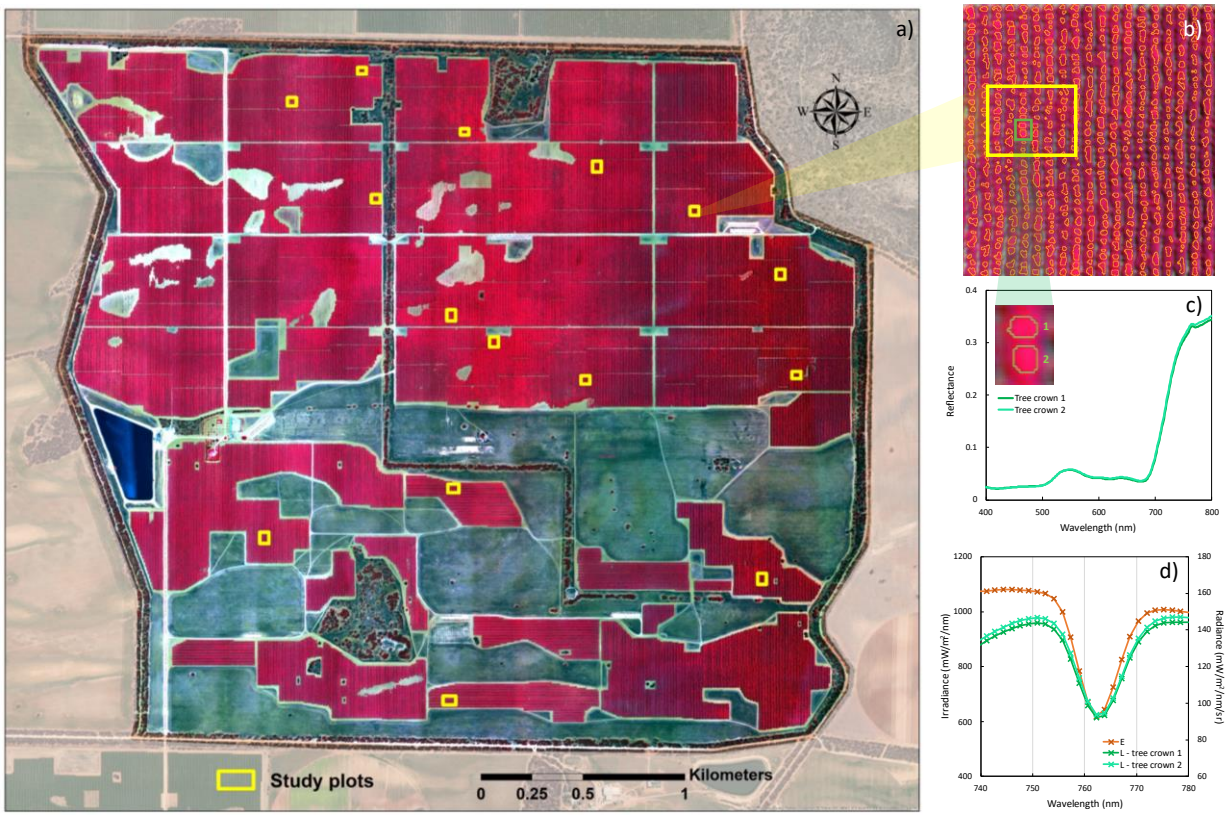

Fig. 2.3. a) High-resolution airborne hyperspectral image (color-infrared overview) over the study area at 40-cm spatial resolution collected with 371 spectral bands on 31 January 2021. The yellow areas represent the locations of the 15 study plots. b) Segmentation of sunlit crown area, the yellow rectangle representing an 8-tree × 6-row study plot. c) The reflectance spectra for two tree crowns segmented from a study plot. d) The radiance (L, green colors) spectra for two tree crowns and the irradiance (E, orange color) spectra for SIF calculation. Crosses indicate the spectral positions of the sensor bands.

2.2.4 Vegetation indices calculation

Due to the fine spatial resolution of the airborne hyperspectral imagery, it is possible to differentiate between sunlit and shaded canopies and soil background features. This feature differentiation was achieved by segmenting tree crowns using Fiji (Abràmoff *et al.*, 2004), combining Niblack's thresholding method (Niblack, 1985) on a NIR band (e.g., 800 nm) and Phansalkar's thresholding method (Phansalkar *et al.*, 2011) on a structural index (e.g., NDVI). The segmentation method was applied to each planting block with varying thresholds; an illustration of the segmented tree crowns is shown in Fig. 2.3b. The average spectrum of each tree-crown was calculated. Fig. 2.3 (c & d) shows an example of the reflectance and radiance spectra of two tree crowns and the irradiance spectra derived by the airborne sensors. Based on these spectra, a number of vegetation indices (full list in Table 2.1) were calculated and further analysis was carried out. The coefficients and the determination of these indices and leaf nutrients were then calculated.

Table 2.1. Spectral vegetation index equations used in this study.

Index	Equation	Reference
Structural indices		
NDVI	$(R_{800} - R_{670})/(R_{800} + R_{670})$	Rouse *et al.* (1974)
EVI	$2.5 \cdot (R_{800} - R_{670})/(R_{800} + 6 \cdot R_{670} - 7.5 \cdot R_{500} + 1)$	Liu and Huete (1995)
OSAVI	$(1 + 0.16) \cdot (R_{800} - R_{670})/(R_{800} + R_{670} + 0.16)$	Rondeaux *et al.* (1996)
Chlorophyll a+b indices		
CI	R_{750}/R_{710}	Zarco-Tejada *et al.* (2001)
CTRI1	R_{695}/R_{420}	Carter (1994)
SRPI	R_{430}/R_{680}	Penuelas *et al.* (1995)
NPQI	$(R_{415} - R_{435})/(R_{415} + R_{435})$	Barnes *et al.* (1992)
NPCI	$(R_{680} - R_{430})/(R_{680} + R_{430})$	Penuelas *et al.* (1995)
MCARI	$((R_{700} - R_{670}) - 0.2 \cdot (R_{700} - R_{550})) \cdot (R_{700}/R_{670})$	Daughtry *et al.* (2000)
TCARI	$3 \cdot ((R_{700} - R_{670}) - 0.2 \cdot (R_{700} - R_{550}) \cdot (R_{700}/R_{670}))$	Haboudane *et al.* (2002)
TCARI/OSAVI	$\frac{3 \cdot ((R_{700} - R_{670}) - 0.2 \cdot (R_{700} - R_{550}) \cdot (R_{700}/R_{670}))}{(1 + 0.16) \cdot (R_{800} - R_{670})/(R_{800} + R_{670} + 0.16)}$	Haboudane *et al.* (2002)
PSSRb	R_{800}/R_{650}	Blackburn (1998)
$DC_{ab}C_{xc}$	$R_{672}/(3 \cdot R_{550} \cdot R_{708})$	Datt (1998)
Xanthophyll indices		
PRI	$(R_{570} - R_{531})/(R_{570} + R_{531})$	Gamon *et al.* (1992)
PRI_{515}	$(R_{515} - R_{531})/(R_{515} + R_{531})$	Hernández-Clemente *et al.* (2011)
PRI_{m1}	$(R_{512} - R_{531})/(R_{512} + R_{531})$	Gamon *et al.* (1992)
PRI_{m4}	$(R_{570} - R_{531} - R_{670})/(R_{570} + R_{531} + R_{670})$	Gamon *et al.* (1992)
PRI_n	$PRI_{570}/(RDVI \cdot (R_{700}/R_{670}))$	Zarco-Tejada *et al.* (2013)
PRI·CI	$((R_{570} - R_{531})/(R_{570} + R_{531})) \cdot ((R_{760}/R_{700}) - 1)$	Garrity *et al.* (2011)
BGR indices		
B	R_{450}/R_{490}	Calderón *et al.* (2013)
BGI1	R_{400}/R_{550}	Zarco-Tejada *et al.* (2005)
BRI1	R_{400}/R_{690}	Zarco-Tejada *et al.* (2012)
Fluorescence reflectance index		
CUR	$(R_{675} \cdot R_{690})/R_{683}^2$	Zarco-Tejada *et al.* (2000)

2.2.5 Physiological traits retrieval from RTM and SIF quantification from airborne hyperspectral imagery

By inverting the average reflectance spectra in RTMs, plant physiological traits such as biochemical constituents and canopy biophysical traits were obtained for each tree-crown. For this study, the method was based on the leaf optical properties model Fluspect-Cx (Vilfan *et al.*, 2018) coupled with the canopy bidirectional reflectance model 4SAIL (Verhoef *et al.*, 2007), which is henceforth referred to as FluSAIL. Following the input parameter ranges provided by Wang *et al.* (2022), a look-up table (LUT) containing 500,000 FluSAIL model simulations was constructed using randomly assigned input parameters. With 70%, 15%, and 15% of the LUT samples, training,

testing, and validation were performed using the Statistics and Machine Learning Toolbox and the Deep Learning Toolbox in MATLAB version R2020a (MathWorks Inc., Natick, MA, USA). Using a 10-hidden-layer artificial neural network (ANN) (Hassoun, 1995, Combal *et al.*, 2003), the de-epoxidation state of the xanthophyll cycle (C_x) and other typical leaf biochemical constituents (i.e., C_{ab}, C_{car}, Anth, C_{dm}), along with canopy structural trait LAI, were identified simultaneously. Validation was performed with the forward mode of RTM, using the inverted parameters, and the minimum root mean square error (RMSE) between modeled and image spectra was used as a cost function for optimal selection.

SIF quantification was undertaken follow the Fraunhofer line depth (FLD) principle (Plascyk and Gabriel, 1975, Plascyk, 1975) based on three spectral bands (3FLD) (Maier *et al.*, 2004). The spectral windows for 'in' and 'out' of the peak irradiance (E) and radiance (L) using an oxygen A-band in-filling method around 760 nm were compared following Eq. 1. The E_{in}/L_{in} ratio corresponds to the minima of E/L in the 755-776 region, which was 762 nm in our observation. E_{out}/L_{out} is the average value of the maximum E/L from the two shoulder regions (i.e., 744-754 nm and 770-780 nm), which was the average from 750 nm and 778 nm in our observation. Moreover, a non-fluorescence offset was applied to SIF, based on the soil features identified by the airborne hyperspectral imagery, to reduce atmospheric and calibration effects (Belwalkar *et al.*, 2022). Following this, the inverted plant traits and SIF were assessed using field measurements and the coefficients of determination with leaf nutrients were also calculated:

$$SIF = (E_{out} \cdot L_{in} - E_{in} \cdot L_{out})/(E_{out} - E_{in}) \quad (1)$$

2.3 Results

2.3.1 Variability in nutrient concentrations from destructive sampling

Nutrient concentrations of 12 measured leaf macro- and micro-nutrient elements presented a wide range of variability within the study plots and across two growing seasons, as shown in Table 2.2. Total C featured the greatest concentration (mean values: 42.9% in 2020, 41.59% in 2021), followed by Ca (mean values: 2.37% in 2020, 3.09% in 2021), K (mean values: 2.13% in 2020, 2.65% in 2021), and N (mean values: 2.07% in 2020, 2.36% in 2021), which were substantially higher than Mg (mean values: 0.57% in 2020, 0.66% in 2021), S (mean values: 0.22% in 2020, 0.24% in 2021), and P (mean values: 0.15% both in 2020 and 2021). Among the micro-nutrients, Mn (mean values: 352.57 mg/kg in 2020, 452.25 mg/kg in 2021) and Fe (mean values: 223.37 mg/kg in 2020, 136.56 mg/kg in 2021) were the most abundant, while the mean values for the rest were around 100 mg/kg or less. Generally, the concentrations of nutrients were higher in 2021 than in 2020. For example, the median/mean value for 2021 is similar to the maximum value for 2020 for N, Ca, Zn, and N/P ratio. However, Fe concentrations were much lower in 2021 than in 2020, with the maximum concentration in 2021 being lower than the minimum value in 2020, which is also reflected in the Fe/Mn ratio.

Table 2.2. Descriptive data from the biochemical laboratory analysis of macro- and micro-nutrient concentrations and their ratios in almond leaves from the 15 study plots in 2020 and 2021.

		Minimum		Maximum		Median		Mean		Standard Deviation	
		2020	2021	2020	2021	2020	2021	2020	2021	2020	2021
Macro-nutrient concentration (%w/w)	Total Nitrogen (N)	1.80	2.15	2.36	2.69	2.04	2.33	2.07	2.36	0.17	0.16
	Phosphorus (P)	0.13	0.14	0.17	0.18	0.15	0.15	0.15	0.15	0.01	0.01
	Potassium (K)	1.53	1.97	3.05	3.61	1.91	2.52	2.13	2.65	0.50	0.60
	Calcium (Ca)	1.86	2.33	2.88	4.47	2.37	2.92	2.37	3.09	0.31	0.48
	Magnesium (Mg)	0.47	0.57	0.70	0.80	0.56	0.65	0.57	0.66	0.08	0.06
	Sulphur (S)	0.15	0.21	0.28	0.27	0.22	0.25	0.22	0.24	0.04	0.02
	Total Carbon (C)	40.50	40.22	44.50	42.52	43.00	41.65	42.90	41.59	1.02	0.63
Micro-nutrient concentration (10^{-6}%, mg/kg)	Iron (Fe)	176.50	114.87	314.00	157.60	213.50	136.17	223.37	136.56	39.19	15.18
	Manganese (Mn)	182.50	304.87	526.00	689.65	322.50	394.75	352.57	452.25	109.20	125.61
	Zinc (Zn)	64.05	88.55	120.00	170.83	86.65	114.11	89.23	125.56	17.56	26.42
	Copper (Cu)	40.25	45.39	118.80	205.56	67.80	90.14	67.35	90.99	20.83	38.89
	Boron (B)	28.90	32.38	40.25	45.91	32.15	37.47	33.59	38.58	3.45	4.60
Ratios	N/P	12.48	13.70	14.81	16.67	13.36	15.66	13.54	15.51	0.70	0.80
	N/K	0.74	0.70	1.27	1.19	1.07	0.93	1.01	0.92	0.21	0.15
	N/(N+P+K)	0.41	0.40	0.54	0.53	0.50	0.47	0.48	0.46	0.05	0.04
	K/Ca	0.53	0.53	1.46	1.55	0.91	0.90	0.93	0.89	0.29	0.30
	K/(Ca+Mg)	0.43	0.45	1.16	1.22	0.72	0.73	0.74	0.73	0.23	0.24
	Ca/Mg	3.62	3.62	5.28	5.62	3.89	4.78	4.19	4.69	0.58	0.53
	Fe/Mn	0.41	0.20	1.04	0.44	0.65	0.31	0.68	0.32	0.18	0.07
	Fe/N (10^{-6}%)	77.41	48.94	149.17	69.81	104.90	57.27	107.82	57.85	17.08	5.24
	Zn/N (10^{-6}%)	29.96	37.99	61.69	66.25	42.20	50.72	43.15	52.81	8.47	7.93
	B/N (10^{-6}%)	13.96	14.46	20.05	18.21	15.85	16.61	16.25	16.31	1.67	1.16

Fig. 2.4 illustrates the ranges of variation and the steady increase of the three quartiles for leaf macro- and micro-nutrients in the 15 study plots over two years. There was a significant increase in the mean concentrations of macro- and micro-nutrients (Figs. 2.4a-l) for each quartile in 2021 compared to 2020, except for total C (Fig. 2.4g) and Fe (Fig. 2.4h), whereas leaf P concentration (Fig. 2.4b) was quite consistent between the two years. Overall, the variation of each element among the three quartiles was reasonable, with a slightly larger variation in 2020 than in 2021. In 2021, the Q3 class, such as K, Ca, Fe, and Zn, appeared to have a greater range. In contrast to 2020, leaf Fe concentrations (mg/kg) decreased significantly with a gradual slope in 2021, leading to the same pattern for the Fe/Mn ratio. It is noteworthy that despite the increased N and K concentrations (%w/w) in 2021, the N/(N+P+K) ratio (Fig. 2.4m) was higher in 2020 than in 2021, indicating that the gain of N was lower than the K concentration in 2021. In contrast, the mean value for each quartile of the K/(Ca+Mg) ratio (Fig. 2.4n) remained stable for two years.

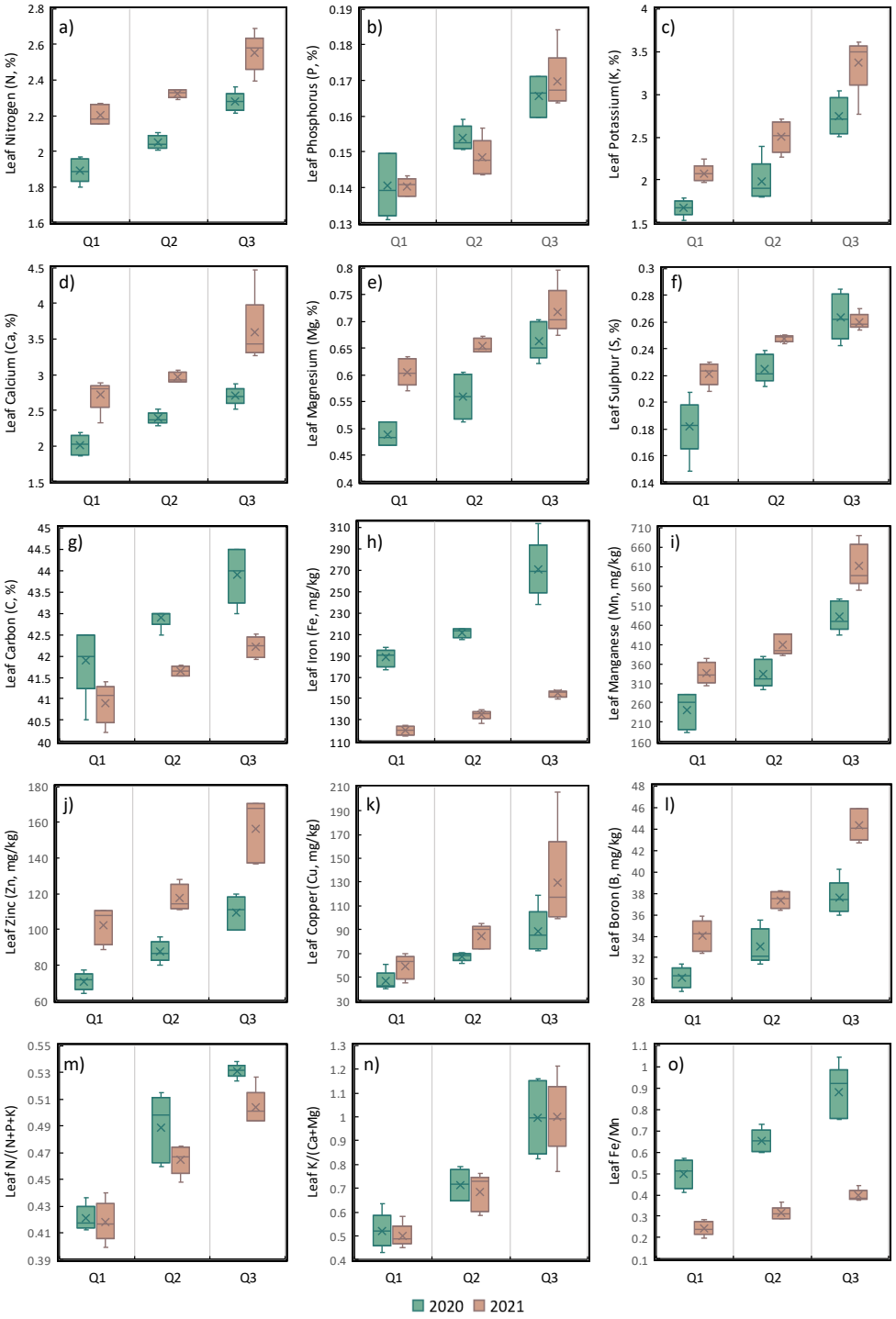

Fig. 2.4. Ranges of variation for biochemical laboratory-derived leaf macro-nutrients of: a) Nitrogen; b) Phosphorus; d) Calcium; e) Magnesium; f) Sulphur; g) Carbon concentration (%w/w); and leaf micro-nutrients of: h) Iron; i) Manganese; j) Zinc; k) Copper; l) Boron concentration (mg/kg); and nutrient ratios of m) N/(N+P+K), n) K/(Ca+Mg), o) Fe/Mn in almond leaves for the 15 study plots in 2020 (green) and 2021 (brown). The crossed line and the line through the box indicate the median and mean values, respectively. Q1, Q2, and Q3 represent the limits of the first, second, and third quartiles, with 15 samples collected each year.

2.3.2 Assessment of leaf spectral measurements

As shown in Fig. 2.5, the ranges of variation of leaf measurements using handheld instruments over two years were calculated using three quartiles independently. There was a greater range of variation observed in 2021 than in 2020, with the mean value of each quartile for C_{ab} (Fig. 2.5a) and Flav (Fig. 2.5b) content in 2020 being higher than in 2021. Furthermore, Anth (data not shown) increased from a mean value of 0.19 in 2020 to 0.24 in 2021, with a less steep upward slope among the three classes in 2021. However, the range of variation of NBI (Fig. 2.5c), defined as the ratio of C_{ab} to Flav, remained quite stable over the course of the two years. In contrast, Ft measured by FluorPen (Fig. 2.5d) increased steeply from 2020 to 2021 as a result of both inherent and environmental factors.

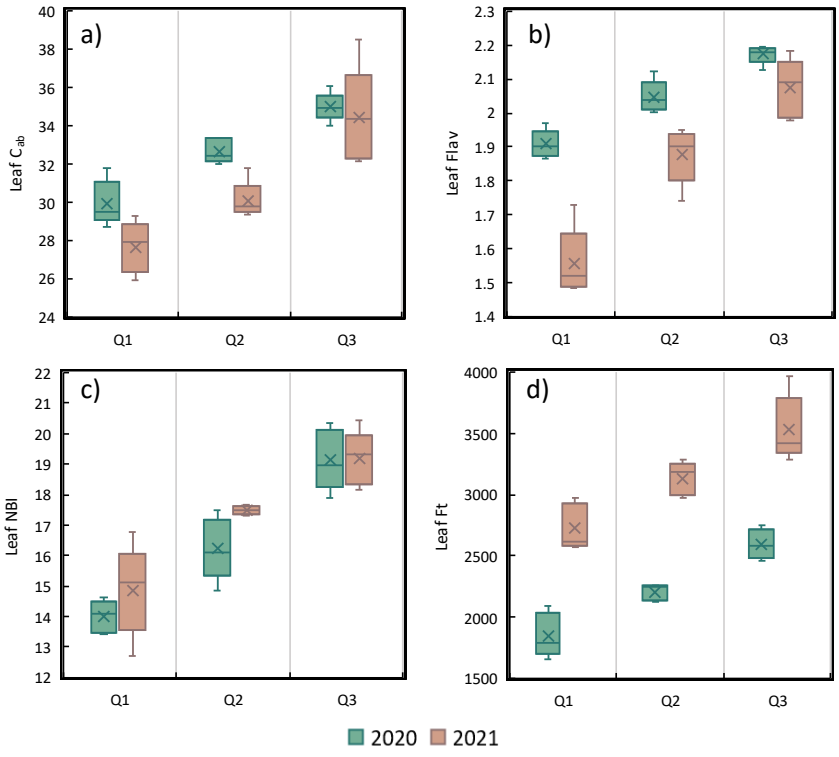

Fig. 2.5. Ranges of variation of leaf: a) chlorophyll (C_{ab}); b) flavonoids (Flav); c) nitrogen balance index (NBI) measured using Dualex; and d) steady-state chlorophyll fluorescence (Ft) using FluorPen in almond leaves for the 15 study plots in 2020 (green) and 2021 (brown). The crossed line and the line through the box indicate the median and mean values, respectively. Q1, Q2, and Q3 represent the limits of the first, second, and third quartiles, with 15 samples collected each year.

A summary of the correlations between *in situ* leaf measurements using handheld instruments and various nutrient elements and their ratios can be found in Table 2.3. What stands out in this table is the consistently significant correlations between Ft and the macro-nutrients of N, P, K ($r^2 \geq 0.48$, *p*-values < 0.005) and certain micro-nutrients (i.e., B with $r^2 \geq 0.47$, *p*-values < 0.005, and Zn with $r^2 \geq 0.39$, *p*-values < 0.05) and ratios (e.g., K/Ca with $r^2 \geq 0.48$, *p*-values < 0.005) across the two years, followed by Flav and NBI measured with Dualex. In 2020, Anth showed strong correlations with a number of nutrients, while none were observed in 2021. Despite this, C_{ab} was not sensitive to nutrient profile over the two years, except in the B/N ratio ($r^2 \geq 0.30$, *p*-values < 0.05). Upon closer inspection, C_{ab} showed positive and significant correlations with leaf N concentration in 2020 ($r^2 = 0.60$, *p*-value < 0.005), but was not sensitive in 2021 ($r^2 = 0.04$, not significant) (Fig. 2.6a). On the other hand, Flav ($r^2 \geq 0.52$, *p*-values < 0.005) and NBI ($r^2 \geq 0.64$, *p*-values < 0.005) displayed clearly strong relationships with leaf N across the two years, as shown in Figs. 2.6b and 6c, yielding $r^2 = 0.68$ and 0.50 (*p*-values < 0.005), respectively. In spite of this, the *in situ* leaf measurements were not statistically significantly correlated with other macro-nutrients, i.e., Ca, Mg, and S.

Table 2.3. Correlations (r^2) between leaf measurements and nutrient concentrations and their ratios for the 15 study plots in 2020 and 2021. Field measurements include leaf chlorophyll a+b (C_{ab}), flavonoids (Flav), anthocyanins (Anth), nitrogen balance index (NBI) measured with Dualex, and steady-state chlorophyll fluorescence (Ft) measured with FluorPen. Background color represents the *p*-value – dark green for $p < 0.005$, medium green for $0.005 \leq p < 0.01$, light green for $0.01 \leq p < 0.05$, and white for $p \geq 0.05$ (not significant).

Nutrients \ Field data		C_{ab}		Flav		Anth		NBI		Ft	
		2020	2021	2020	2021	2020	2021	2020	2021	2020	2021
Macro-nutrient concentration (%w/w)	Total Nitrogen (N)	0.60	0.04	0.52	0.73	0.59	0.01	0.68	0.64	0.54	0.52
	Phosphorus (P)	0.43	0.18	0.43	0.65	0.42	0.08	0.43	0.32	0.56	0.48
	Potassium (K)	0.01	0.22	0.44	0.90	0.39	0.01	0.32	0.46	0.49	0.68
	Calcium (Ca)	0.01	0.19	0.12	0.22	0.10	0.01	0.06	0.04	0.24	0.05
	Magnesium (Mg)	0.14	0.05	0.06	0.05	0.15	0.01	0.03	0.01	0.08	0.03
	Sulphur (S)	0.05	0.01	0.00	0.04	0.03	0.09	0.01	0.10	0.00	0.04
	Total Carbon (C)	0.02	0.05	0.49	0.12	0.43	0.20	0.53	0.30	0.27	0.10
Micro-nutrient concentration (10^{-6}%, mg/kg)	Iron (Fe)	0.04	0.00	0.51	0.30	0.33	0.08	0.48	0.34	0.16	0.41
	Manganese (Mn)	0.07	0.02	0.40	0.34	0.51	0.01	0.45	0.26	0.59	0.15
	Zinc (Zn)	0.02	0.13	0.35	0.68	0.36	0.03	0.30	0.39	0.39	0.50
	Copper (Cu)	0.00	0.07	0.20	0.37	0.18	0.05	0.13	0.22	0.38	0.18
	Boron (B)	0.00	0.20	0.46	0.89	0.30	0.00	0.36	0.49	0.47	0.60
Ratios	N/P	0.05	0.23	0.01	0.07	0.04	0.15	0.08	0.01	0.00	0.06
	N/K	0.18	0.30	0.17	0.81	0.13	0.02	0.07	0.31	0.22	0.69
	N/(N+P+K)	0.17	0.30	0.18	0.82	0.13	0.01	0.07	0.32	0.22	0.69
	K/Ca	0.00	0.26	0.41	0.77	0.35	0.01	0.28	0.34	0.48	0.49
	K/(Ca+Mg)	0.00	0.26	0.43	0.78	0.39	0.01	0.30	0.34	0.49	0.52
	Ca/Mg	0.10	0.19	0.01	0.24	0.01	0.03	0.00	0.05	0.04	0.05
	Fe/Mn	0.05	0.04	0.16	0.18	0.30	0.04	0.15	0.09	0.48	0.03
	Fe/N (10^{-6}%)	0.03	0.02	0.18	0.00	0.05	0.10	0.11	0.01	0.00	0.06
	Zn/N (10^{-6}%)	0.04	0.15	0.07	0.54	0.06	0.04	0.03	0.24	0.10	0.41
	B/N (10^{-6}%)	0.44	0.30	0.01	0.54	0.00	0.00	0.01	0.14	0.01	0.34

p-value < 0.005	*p*-value < 0.01	*p*-value < 0.05	not significant

Comparatively statistically significant correlations were clearly demonstrated between Ft and macro-nutrients N, P, and K, with a similar slope in both years (Figs. 2.6d-f). A consistent relationship between Ft and leaf N in both years ($r^2 = 0.54$ in 2020 and $r^2 = 0.52$ in 2021; *p*-values < 0.005) was observed (Fig. 2.6d). Upon combining two years of data, the trendline clustered and yielded $r^2 = 0.74$ (*p*-value < 0.005). Although Ft produced strong correlations with macro-nutrients P and K at the 0.005 level for the individual years, the relationship with leaf N was weaker when the data across the two years was aggregated.

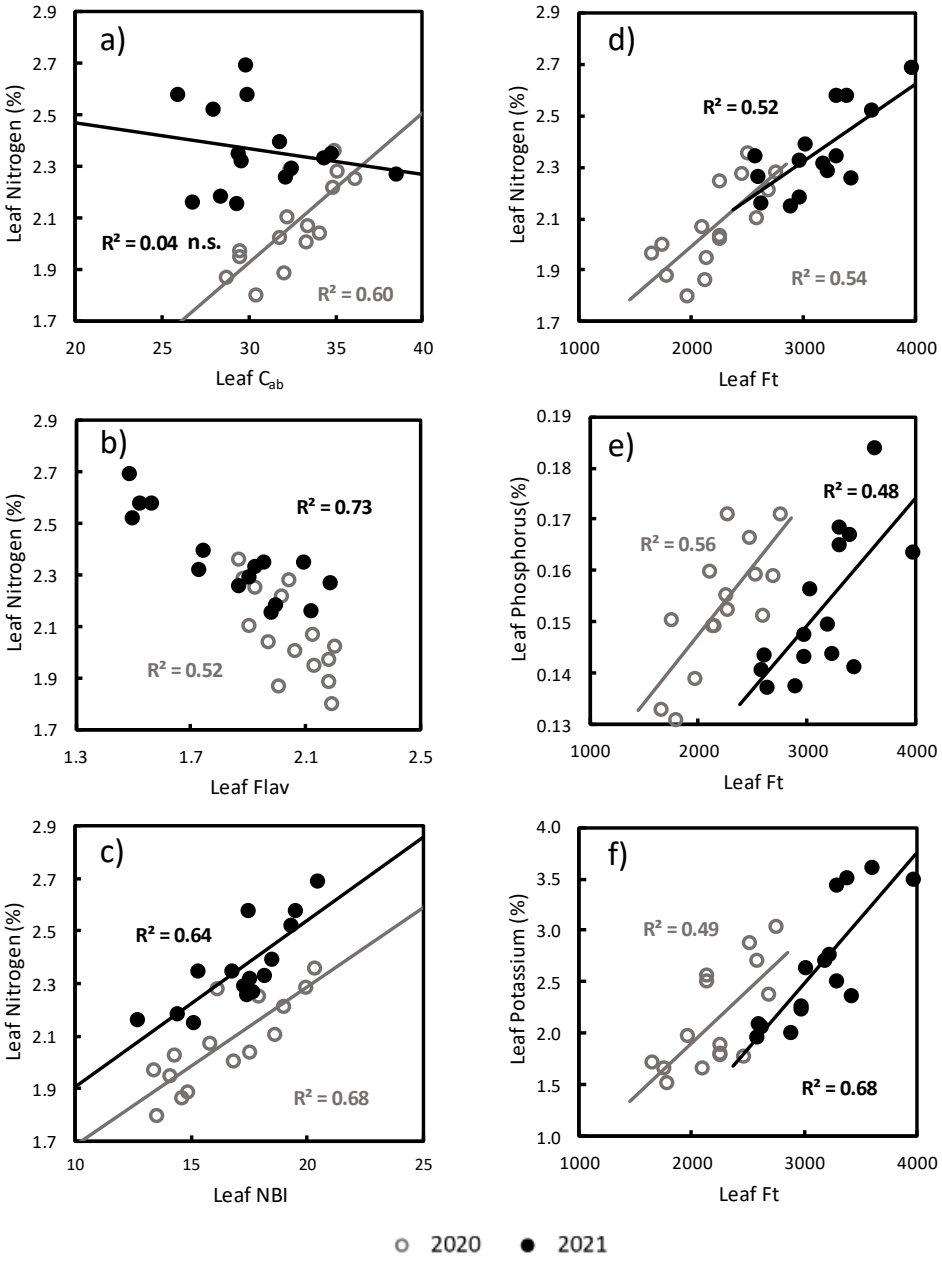

Fig. 2.6. Relationships between in situ Dualex-measured: a) leaf chlorophyll (C_{ab}); b) flavonoid (Flav) content; c) nitrogen balance index (NBI) and biochemically derived leaf Nitrogen concentration (%w/w) in 2020 (hollow gray circle) and 2021 (solid black circle). Relationships between leaf steady-state fluorescence (Ft) and biochemically derived leaf macro-nutrients of: d) Nitrogen; e) Phosphorus; f) Potassium concentration (%w/w) in 2020 (hollow gray circle) and 2021 (solid black circle). All p-values are less than 0.005, except for the one marked n.s. (not significant).

Table 2.4 presents the correlations between vegetation indices derived from the leaf reflectance spectra and leaf nutrient assessments for both years. Results indicate varying degrees of correlation and, in most cases, relationships were inconsistent between the two years. For both years, the xanthophyll indices, BGR indices, and fluorescence reflectance index calculated at leaf level demonstrated stronger relationships with primary macro-nutrient and micro-nutrient levels, but none of these indices had statistically significant relationships with the levels of macro-nutrients Ca, Mg, and S. More specifically, CTRI1, NPQI, PRI_n, PRI·CI, BGI1, and BRI1 had statistically significant relationships with the levels of N, P, K, and B for both years. Compared with other indices, chlorophyll *a*+*b* indices showed stronger correlations with N and P levels in 2020, whereas they were generally poorly correlated in 2021. For example, CI demonstrated significant correlation with N ($r^2 = 0.79$, *p*-values < 0.005) and P ($r^2 = 0.62$, *p*-values < 0.005) in 2020, but no significant correlation ($r^2 \leq 0.06$) was observed in 2021. Although BGI1 and PRI_{m4} demonstrated slightly higher correlations with leaf N for individual years, CTRI1 and PRI_n exhibited stable slopes across both years, leading to a more robust relationship when combined data over two years are considered (Fig. 2.7). Additionally, NPQI ($r^2 = 0.62$ and 0.72 in 2020 and 2021, respectively; *p*-values < 0.005) and some xanthophyll indices (i.e., PRI, PRI_n, and PRI·CI) were significantly and consistently correlated with leaf K ($r^2 \geq 0.48$, *p*-values < 0.005) in both years. At the 0.05 level, CTRI1 displayed reasonably strong relationships with leaf P and K levels over the two years. Regarding the micro-nutrient B, the NPQI ($r^2 = 0.65$ in 2020 and $r^2 = 0.68$ in 2021; *p*-values < 0.005) and PRI ($r^2 = 0.48$ in 2020 and $r^2 = 0.54$ in 2021; *p*-values < 0.005) deserve particular attention. Further, PRI_{m4} appears to be a reliable indicator of Fe ($r^2 = 0.67$ in 2020 and $r^2 = 0.61$ in 2021; *p*-values < 0.005) and Mn ($r^2 = 0.45$, *p*-values < 0.01 in 2020, and $r^2 = 0.54$, *p*-values < 0.005 in 2021) across years. In both years, the fluorescence reflectance index CUR displayed significant

relationships with N, P, and Mn at the 0.05 level, but these were weaker than those of Ft. On the other hand, structural indices, such as NDVI, did not present skills to estimate the concentrations and ratios of nutrients for both years.

Table 2.4. Correlations (r^2) between vegetation indices at the leaf level and nutrient concentrations for the 15 study plots in 2020 and 2021. Background color represents the *p*-value – dark green for $p < 0.005$, medium green for $0.005 \leq p < 0.01$, light green for $0.01 \leq p < 0.05$, and white for $p \geq 0.05$ (not significant).

Nutrients / Indices at leaf level	Macro-nutrient concentration (%w/w)														Micro-nutrient concentration (10^{-6}%, mg/kg)									
	N		P		K		Ca		Mg		S		C		Fe		Mn		Zn		Cu		B	
	2020	2021	2020	2021	2020	2021	2020	2021	2020	2021	2020	2021	2020	2021	2020	2021	2020	2021	2020	2021	2020	2021	2020	2021
Chlorophyll a+b indices																								
CI	0.79	0.06	0.62	0.00	0.13	0.00	0.00	0.13	0.13	0.30	0.10	0.03	0.23	0.00	0.14	0.10	0.39	0.09	0.07	0.00	0.11	0.01	0.16	0.02
CTRI1	0.55	0.53	0.34	0.33	0.33	0.43	0.02	0.04	0.13	0.02	0.03	0.16	0.21	0.04	0.15	0.25	0.52	0.24	0.05	0.53	0.15	0.18	0.34	0.39
SRPI	0.24	0.33	0.21	0.17	0.36	0.26	0.02	0.01	0.10	0.05	0.08	0.19	0.15	0.01	0.02	0.12	0.46	0.09	0.05	0.28	0.18	0.05	0.29	0.17
NPQI	0.45	0.61	0.31	0.67	0.62	0.72	0.05	0.29	0.06	0.09	0.00	0.20	0.47	0.00	0.40	0.23	0.71	0.33	0.18	0.63	0.22	0.36	0.65	0.68
NPCI	0.24	0.31	0.21	0.16	0.35	0.24	0.02	0.01	0.11	0.04	0.09	0.18	0.14	0.01	0.01	0.11	0.45	0.08	0.05	0.26	0.18	0.04	0.28	0.17
MCARI	0.70	0.18	0.42	0.03	0.07	0.02	0.02	0.00	0.09	0.03	0.00	0.00	0.14	0.09	0.27	0.13	0.22	0.20	0.05	0.20	0.07	0.23	0.14	0.04
TCARI	0.72	0.23	0.52	0.22	0.09	0.18	0.03	0.14	0.08	0.02	0.00	0.04	0.19	0.01	0.28	0.02	0.24	0.21	0.10	0.19	0.12	0.32	0.16	0.20
TCARI/OSAVI	0.64	0.06	0.52	0.07	0.19	0.08	0.02	0.23	0.03	0.42	0.00	0.11	0.46	0.08	0.43	0.09	0.37	0.02	0.23	0.01	0.10	0.00	0.25	0.08
PSSRb	0.01	0.23	0.03	0.33	0.11	0.35	0.01	0.33	0.02	0.29	0.01	0.18	0.25	0.03	0.03	0.00	0.11	0.11	0.10	0.15	0.01	0.11	0.08	0.30
$DC_{ab}C_{xc}$	0.45	0.12	0.42	0.17	0.16	0.14	0.00	0.26	0.01	0.19	0.00	0.09	0.43	0.02	0.25	0.02	0.27	0.10	0.21	0.05	0.09	0.14	0.18	0.14
Xanthophyll indices																								
PRI	0.42	0.57	0.30	0.44	0.51	0.64	0.02	0.08	0.03	0.09	0.01	0.17	0.36	0.06	0.10	0.28	0.57	0.26	0.12	0.53	0.17	0.19	0.48	0.54
PRI_{515}	0.43	0.00	0.13	0.10	0.16	0.05	0.05	0.18	0.07	0.16	0.02	0.08	0.22	0.18	0.44	0.12	0.30	0.03	0.15	0.02	0.01	0.00	0.16	0.02
PRI_{m1}	0.44	0.03	0.14	0.21	0.18	0.14	0.06	0.24	0.08	0.13	0.02	0.13	0.23	0.16	0.45	0.04	0.33	0.00	0.16	0.01	0.01	0.03	0.18	0.09
PRI_{m4}	0.52	0.76	0.21	0.43	0.33	0.68	0.04	0.05	0.01	0.00	0.04	0.04	0.50	0.23	0.67	0.61	0.45	0.54	0.23	0.86	0.03	0.44	0.37	0.71
PRI_n	0.59	0.60	0.40	0.43	0.48	0.64	0.05	0.06	0.08	0.06	0.02	0.14	0.29	0.09	0.12	0.33	0.56	0.28	0.11	0.58	0.23	0.21	0.46	0.55
PRI·CI	0.43	0.57	0.30	0.44	0.49	0.62	0.02	0.10	0.02	0.11	0.01	0.20	0.41	0.04	0.12	0.24	0.55	0.27	0.15	0.52	0.15	0.21	0.44	0.52
BGR indices																								
B	0.45	0.53	0.31	0.33	0.52	0.48	0.04	0.06	0.09	0.04	0.02	0.17	0.37	0.03	0.19	0.22	0.64	0.20	0.16	0.52	0.19	0.20	0.47	0.38
BGI1	0.62	0.72	0.35	0.47	0.33	0.61	0.07	0.08	0.17	0.01	0.01	0.15	0.19	0.06	0.24	0.42	0.49	0.32	0.10	0.76	0.17	0.33	0.34	0.55
BRI1	0.49	0.51	0.33	0.37	0.46	0.45	0.04	0.06	0.13	0.04	0.04	0.24	0.26	0.00	0.15	0.23	0.60	0.15	0.10	0.49	0.21	0.17	0.43	0.33
Fluorescence reflectance index																								
CUR	0.66	0.33	0.31	0.41	0.14	0.43	0.01	0.26	0.07	0.03	0.00	0.00	0.15	0.02	0.30	0.17	0.32	0.37	0.03	0.45	0.05	0.37	0.23	0.56

p-value < 0.005	*p*-value < 0.01	*p*-value < 0.05	not significant

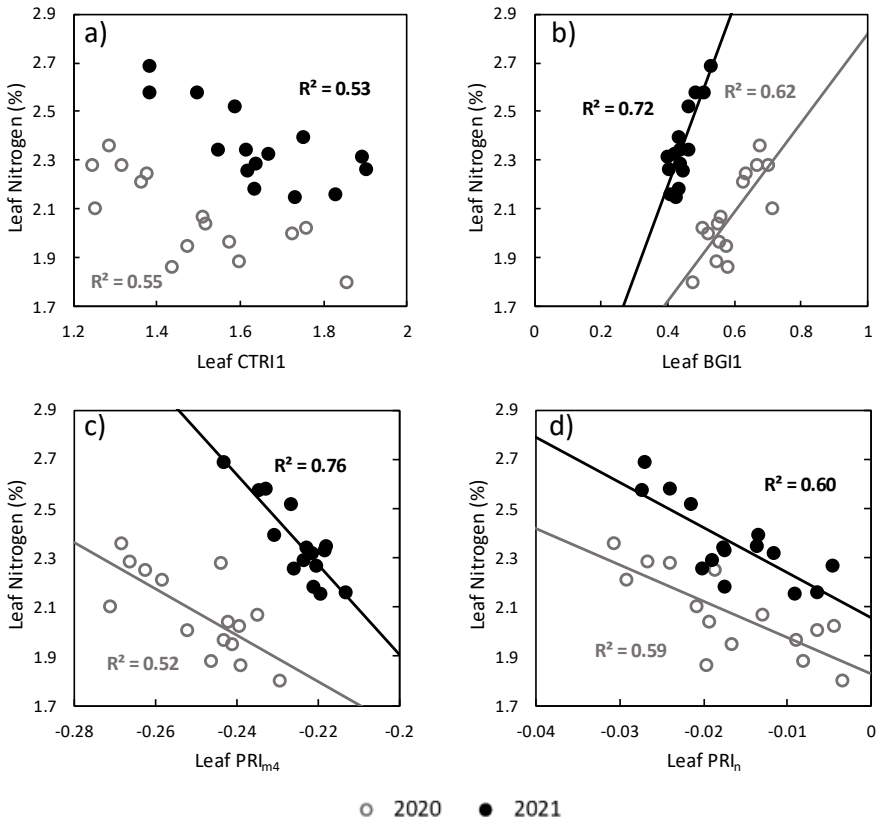

Fig. 2.7. Relationships between leaf CTRI1, BGI1, PRI_{m4}, PRI_n, and biochemically derived leaf nitrogen concentration (%w/w) in 2020 (hollow gray circle) and 2021 (solid black circle). All *p*-values<0.005.

2.3.3 Assessment of vegetation indices and trait retrievals from airborne hyperspectral datasets

When canopy structural and background effects were taken into account, vegetation indices calculated at canopy level (Table 2.5) typically showed weaker relationships with nutrients than those calculated at leaf level. In addition to the results at the leaf level, fluorescence reflectance index (*p*-values < 0.005) and xanthophyll indices (*p*-values < 0.05) derived at the canopy level also appear to have had significant correlations with macro-nutrients N and P over the two years. In addition, CTRI1 also demonstrated reasonably strong relationships with leaf N (r^2 = 0.61 in 2020 and r^2 = 0.52 in 2021; *p*-values < 0.005), P (*p*-values < 0.05), and K (*p*-values < 0.05) over the two

years. Additionally, the CUR fluorescence reflectance index presented surprisingly strong and consistently significant correlations with leaf N (r^2 = 0.75 in 2020 and r^2 = 0.58 in 2021) and P (r^2 = 0.53 in 2020 and r^2 = 0.58 in 2021) at the level of 0.005 over the two years, which is even stronger than the correlations observed at leaf level. In accordance with the leaf level results, CUR at canopy level also demonstrated a strong correlation with Mn (*p*-values < 0.05) for both years. Further, MCARI was able to provide a good estimate of leaf N (r^2 = 0.61 in 2020 and r^2 = 0.48 in 2021; *p*-values < 0.005), P (*p*-values < 0.05), and Zn (*p*-values < 0.05) at canopy level across both years. Besides this, the PRI family exhibited a generally stronger relationship with nutrient levels in 2021 than in 2020. Nevertheless, PRI_{m1} was statistically significantly correlated at the level of 0.05 with Mn for both years, and the same correlation was recorded for PRI·CI with S. Even though the structural indices at the canopy level were inferior to nutrients compared to pigment-related indices, their correlations still outperformed those at the leaf level. For example, EVI at the canopy level demonstrated strong relationships with leaf N (r^2 = 0.32 in 2020 and r^2 = 0.31 in 2021; *p*-values < 0.05) and the B/N ratio (r^2 = 0.46 in 2020 and r^2 = 0.44 in 2021; *p*-values < 0.01) for both years, while no significant relationships were found at the leaf level.

Table 2.5. Correlations (r^2) between vegetation indices calculated from airborne hyperspectral imagery and nutrient concentrations for the 15 study plots in 2020 and 2021. Background color represents the *p*-value – dark green for $p < 0.005$, medium green for $0.005 \leq p < 0.01$, light green for $0.01 \leq p < 0.05$, and white for $p \geq 0.05$ (not significant).

Nutrients / Indices at canopy level	Macro-nutrient concentration (%w/w)														Micro-nutrient concentration (10^{-6}%, mg/kg)									
	N		P		K		Ca		Mg		S		C		Fe		Mn		Zn		Cu		B	
	2020	2021	2020	2021	2020	2021	2020	2021	2020	2021	2020	2021	2020	2021	2020	2021	2020	2021	2020	2021	2020	2021	2020	2021
Structural indices																								
NDVI	0.05	0.13	0.01	0.15	0.04	0.21	0.01	0.16	0.24	0.00	0.19	0.03	0.00	0.03	0.02	0.04	0.01	0.19	0.03	0.21	0.13	0.24	0.08	0.37
EVI	0.32	0.31	0.17	0.31	0.02	0.38	0.07	0.20	0.49	0.01	0.30	0.01	0.01	0.06	0.01	0.15	0.02	0.27	0.04	0.28	0.01	0.29	0.05	0.53
OSAVI	0.21	0.22	0.09	0.23	0.04	0.29	0.03	0.18	0.38	0.00	0.25	0.00	0.00	0.05	0.01	0.10	0.01	0.24	0.04	0.26	0.05	0.28	0.08	0.46
Chlorophyll a+b indices																								
CI	0.04	0.01	0.05	0.02	0.50	0.03	0.00	0.07	0.22	0.00	0.29	0.14	0.40	0.04	0.17	0.00	0.13	0.11	0.08	0.05	0.25	0.08	0.55	0.15
CTRI1	0.61	0.52	0.45	0.35	0.35	0.35	0.00	0.05	0.00	0.00	0.00	0.29	0.55	0.02	0.30	0.24	0.58	0.06	0.11	0.31	0.07	0.22	0.41	0.21
SRPI	0.02	0.09	0.02	0.02	0.30	0.01	0.10	0.01	0.39	0.00	0.25	0.25	0.51	0.00	0.11	0.06	0.20	0.04	0.00	0.00	0.03	0.00	0.39	0.02
NPQI	0.38	0.00	0.50	0.03	0.16	0.04	0.32	0.04	0.33	0.00	0.19	0.07	0.04	0.03	0.12	0.00	0.22	0.04	0.27	0.01	0.20	0.01	0.10	0.05
NPCI	0.02	0.08	0.02	0.02	0.29	0.01	0.11	0.01	0.39	0.00	0.25	0.24	0.51	0.00	0.11	0.06	0.19	0.04	0.00	0.00	0.03	0.00	0.39	0.02
MCARI	0.61	0.48	0.38	0.46	0.18	0.50	0.10	0.09	0.17	0.02	0.04	0.32	0.25	0.01	0.31	0.21	0.31	0.12	0.29	0.34	0.02	0.25	0.13	0.33
TCARI	0.72	0.04	0.56	0.04	0.21	0.04	0.18	0.00	0.26	0.04	0.09	0.27	0.15	0.01	0.23	0.02	0.35	0.00	0.25	0.00	0.09	0.00	0.16	0.00
TCARI/OSAVI	0.64	0.00	0.56	0.00	0.41	0.00	0.18	0.04	0.10	0.02	0.02	0.16	0.23	0.01	0.27	0.00	0.42	0.04	0.25	0.02	0.20	0.04	0.36	0.06
PSSRb	0.14	0.12	0.07	0.12	0.21	0.15	0.02	0.13	0.44	0.00	0.32	0.07	0.12	0.08	0.00	0.04	0.00	0.22	0.00	0.19	0.07	0.18	0.20	0.35
$DC_{ab}C_{xc}$	0.69	0.20	0.48	0.20	0.08	0.23	0.12	0.02	0.42	0.06	0.23	0.32	0.04	0.01	0.09	0.07	0.21	0.01	0.13	0.10	0.05	0.05	0.04	0.10
Xanthophyll indices																								
PRI	0.48	0.27	0.26	0.18	0.11	0.16	0.00	0.00	0.03	0.03	0.14	0.18	0.36	0.03	0.19	0.35	0.18	0.01	0.06	0.15	0.06	0.16	0.16	0.03
PRI_{515}	0.39	0.53	0.28	0.53	0.17	0.65	0.05	0.24	0.07	0.00	0.02	0.03	0.30	0.04	0.37	0.19	0.43	0.26	0.23	0.55	0.00	0.50	0.15	0.69
PRI_{m1}	0.40	0.47	0.29	0.48	0.12	0.59	0.04	0.27	0.08	0.01	0.02	0.01	0.26	0.04	0.35	0.17	0.37	0.27	0.24	0.50	0.00	0.48	0.11	0.67
PRI_{m4}	0.34	0.50	0.27	0.56	0.16	0.71	0.13	0.29	0.19	0.02	0.11	0.04	0.12	0.01	0.22	0.14	0.34	0.23	0.22	0.53	0.00	0.46	0.09	0.71
PRI_n	0.31	0.35	0.22	0.24	0.05	0.23	0.07	0.01	0.65	0.04	0.47	0.12	0.06	0.07	0.00	0.41	0.02	0.03	0.02	0.24	0.00	0.23	0.07	0.09
PRI·CI	0.13	0.18	0.08	0.10	0.27	0.09	0.00	0.00	0.28	0.00	0.27	0.32	0.10	0.00	0.01	0.22	0.00	0.00	0.01	0.06	0.11	0.06	0.24	0.00
BGR indices																								
B	0.11	0.06	0.18	0.06	0.38	0.06	0.00	0.02	0.03	0.12	0.00	0.25	0.26	0.07	0.10	0.00	0.52	0.03	0.01	0.00	0.08	0.01	0.43	0.01
BGI1	0.70	0.28	0.66	0.24	0.19	0.31	0.09	0.10	0.23	0.04	0.16	0.23	0.14	0.03	0.19	0.06	0.48	0.02	0.14	0.21	0.10	0.17	0.18	0.19
BRI1	0.41	0.07	0.34	0.01	0.43	0.01	0.00	0.02	0.02	0.00	0.02	0.29	0.62	0.01	0.29	0.07	0.44	0.03	0.11	0.01	0.12	0.00	0.49	0.02
Fluorescence reflectance index																								
CUR	0.75	0.58	0.53	0.58	0.07	0.64	0.12	0.19	0.43	0.00	0.21	0.10	0.06	0.05	0.12	0.22	0.31	0.27	0.14	0.56	0.04	0.51	0.05	0.65

p-value < 0.005	*p*-value < 0.01	*p*-value < 0.05	not significant

Generally speaking, SIF quantified from airborne data and plant traits derived via RTM from hyperspectral imagery outperformed vegetation indices in nutrient assessment, yielding stronger correlations with higher significance levels. As shown in Table 2.6, C_{ab} and C_{car} had the strongest relationships with nutrients, closely followed by C_x and SIF. Nevertheless, all of them showed significant correlations with N at the 0.005 level, whereas C_{ab} and C_{car} (*p*-values < 0.01) had more significant correlations with P concentration than C_x and SIF (*p*-values < 0.05) did across both years. Despite this, these biochemical constituents (i.e., C_{ab}, C_{car}, and C_x) also displayed strong relationships with K (*p*-values < 0.005) and a number of micro-nutrients and nutrient ratios in 2021. There are also prominent relationships (*p*-values < 0.05) between C_{car} and Mn, as well as between C_x and Zn, over the two years. Further, statistically significant correlations were most evident between Anth and N (r^2 = 0.58, *p*-values < 0.005), as well as between Anth and P (r^2 = 0.46, *p*-values < 0.01), in 2020 but their correlations were not significant in 2021, which is consistent with the results obtained from the *in situ* leaf measurements. Nonetheless, it appears that C_{dm} was a reliable indicator of Ca/Mg and B/N ratios (*p*-values < 0.05) over the two years. No significant correlation was observed between LAI and nutrients or their ratios for both years.

Table 2.6. Correlations (r^2) between RTM-inverted plant traits from airborne hyperspectral imagery and nutrient concentrations and ratios for the 15 study plots in 2020 and 2021. Traits derived from airborne data include leaf chlorophyll a+b (C_{ab}), carotenoids (C_{car}), anthocyanin (Anth), photochemical reflectance parameter (C_x), dry matter content (C_{dm}), leaf area index (LAI) by inversion algorithm, and solar-induced fluorescence (SIF). Background color represents the *p*-value: dark green for $p < 0.005$, medium green for $0.005 \leq p < 0.01$, light green for $0.01 \leq p < 0.05$, and white for $p \geq 0.05$ (not significant).

Nutrients \ Airborne derived traits		RTM-derived plant traits												SIF	
		C_{ab} (µg/cm^2)		C_{car} (µg/cm^2)		Anth (µg/cm^2)		C_x		C_{dm} (g/cm^2)		LAI		SIF	
		2020	2021	2020	2021	2020	2021	2020	2021	2020	2021	2020	2021	2020	2021
Macro-nutrient concentration (%w/w)	N	0.73	0.66	0.75	0.56	0.58	0.09	0.61	0.62	0.36	0.20	0.02	0.05	0.60	0.55
	P	0.43	0.61	0.43	0.55	0.46	0.05	0.38	0.49	0.18	0.17	0.00	0.06	0.51	0.29
	K	0.07	0.66	0.12	0.58	0.02	0.06	0.10	0.51	0.08	0.25	0.23	0.09	0.30	0.44
	Ca	0.03	0.23	0.04	0.17	0.12	0.01	0.24	0.09	0.00	0.17	0.01	0.11	0.10	0.13
	Mg	0.16	0.00	0.16	0.00	0.34	0.05	0.34	0.00	0.43	0.00	0.06	0.00	0.15	0.00
	S	0.05	0.06	0.04	0.01	0.17	0.23	0.07	0.11	0.41	0.01	0.07	0.09	0.07	0.01
	C	0.20	0.06	0.24	0.14	0.02	0.01	0.08	0.12	0.04	0.04	0.17	0.02	0.11	0.23
Micro-nutrient concentration (10^{-6}%, mg/kg)	Fe	0.20	0.21	0.22	0.18	0.12	0.00	0.19	0.39	0.01	0.08	0.00	0.01	0.02	0.17
	Mn	0.26	0.24	0.26	0.29	0.12	0.02	0.14	0.24	0.00	0.25	0.00	0.14	0.33	0.28
	Zn	0.16	0.62	0.19	0.55	0.17	0.04	0.35	0.53	0.01	0.26	0.01	0.13	0.25	0.35
	Cu	0.02	0.47	0.04	0.36	0.04	0.01	0.09	0.42	0.02	0.24	0.12	0.11	0.34	0.30
	B	0.07	0.64	0.10	0.59	0.01	0.04	0.05	0.46	0.09	0.39	0.09	0.24	0.24	0.49
Ratios	N/P	0.12	0.07	0.13	0.08	0.02	0.00	0.08	0.02	0.10	0.01	0.04	0.02	0.01	0.00
	N/K	0.00	0.46	0.00	0.47	0.02	0.02	0.00	0.34	0.30	0.20	0.18	0.09	0.09	0.29
	N/(N+P+K)	0.00	0.47	0.00	0.46	0.01	0.02	0.00	0.34	0.29	0.22	0.16	0.10	0.09	0.29
	K/Ca	0.08	0.65	0.12	0.54	0.06	0.06	0.20	0.44	0.05	0.27	0.08	0.11	0.24	0.39
	K/(Ca+Mg)	0.10	0.63	0.14	0.52	0.08	0.06	0.23	0.43	0.03	0.26	0.08	0.10	0.26	0.39
	Ca/Mg	0.07	0.47	0.05	0.38	0.09	0.00	0.02	0.22	0.53	0.30	0.02	0.25	0.01	0.19
	Fe/Mn	0.12	0.14	0.13	0.15	0.08	0.07	0.06	0.08	0.05	0.20	0.00	0.14	0.37	0.15
	Fe/N (10^{-6}%)	0.00	0.00	0.00	0.00	0.00	0.02	0.01	0.03	0.17	0.00	0.01	0.01	0.06	0.00
	Zn/N (10^{-6}%)	0.00	0.49	0.00	0.46	0.01	0.02	0.07	0.41	0.11	0.23	0.00	0.14	0.03	0.22
	B/N (10^{-6}%)	0.18	0.27	0.14	0.29	0.23	0.00	0.16	0.12	0.60	0.34	0.05	0.33	0.02	0.18

p-value < 0.005	*p*-value < 0.01	*p*-value < 0.05	not significant

Throughout both years, SIF exhibited significant correlations with leaf K values (*p*-values < 0.05), and with N and P values, which is consistent with the leaf-level Ft result, implying that chlorophyll fluorescence could serve as a more reliable indicator of K than biochemical constituent testing or vegetation indices. Fig. 2.8 illustrates the relationships and trendlines between SIF and the macro-nutrients N, P, and K. Despite weaker relationships from SIF than from *in situ* Ft results, which may be related to the aggregated pixels representing soil and other background, the clustered trendlines of SIF vs. N, as well as the similar slopes of SIF vs. K across the two years, stand out. Likewise, when aggregated data for two years were analyzed, the correlation between SIF and leaf N ($r^2 = 0.74$) and K ($r^2 = 0.46$) was significant at the 0.005 level, with a better fit than leaf P, which is in agreement with Ft results at leaf level. Additionally, SIF also demonstrated consistently strong

relationships with certain micro-nutrients and ratios (i.e., Mn, Cu, K/(Ca+Mg)) for both years, with *p*-values less than 0.05. Overall, SIF and the fluorescence reflectance index CUR demonstrated consistent relationships with nutrients which were stronger than those demonstrated by vegetation indices.

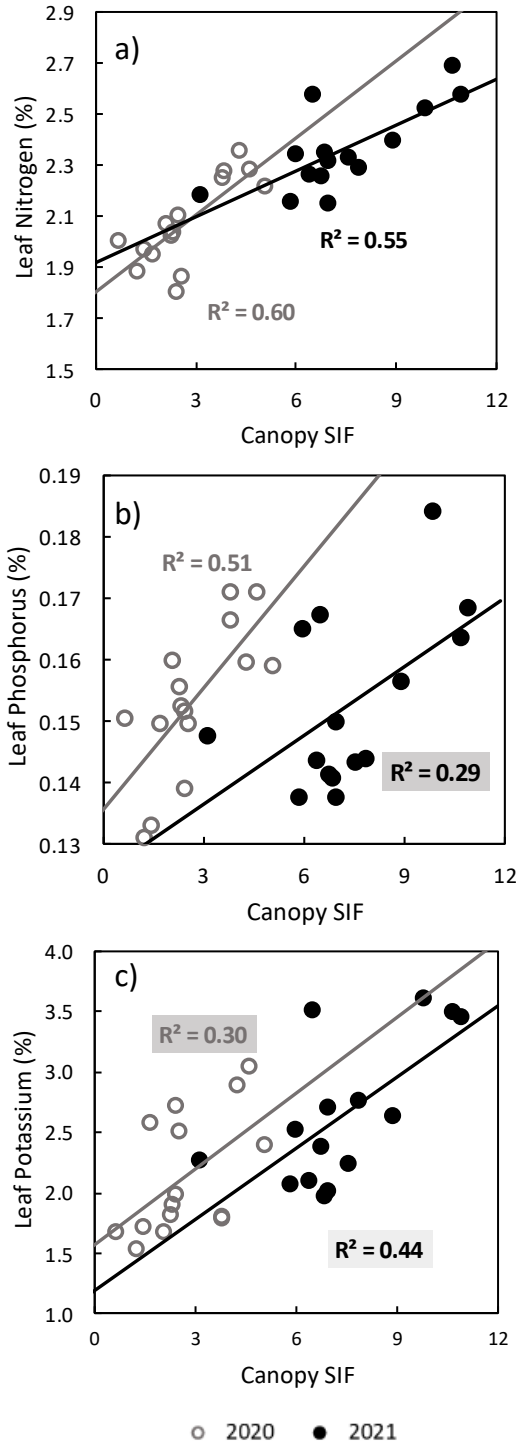

Fig. 2.8. Relationships between canopy solar-induced fluorescence (SIF) and biochemically derived leaf macro-nutrient levels of: a) Nitrogen; b) Phosphorus; c) Potassium concentration (%w/w) in 2020 (hollow gray circle) and 2021 (solid black circle). The highlighted text represents the *p*-value – below 0.005 (white), 0.01 (light gray), up to 0.05 (medium gray).

2.4. Discussions

C_{ab} has long been widely used as a measure of plant vigor and health condition (Ciganda *et al.*, 2008, Xue and Su, 2017, Haboudane *et al.*, 2008), as well as a nutrient deficiency indicator (Wood *et al.*, 1993, Herrmann *et al.*, 2010, Bojović and Marković, 2009, Yoder and Pettigrew-Crosby, 1995). However, at leaf level, rapid C_{ab} readings from field-portable chlorophyll meters are based on a limited number of bands to assess leaf greenness and are affected by several factors, specifically plant species, fertilizer application timing, phenological stages, and growing seasons (Schepers *et al.*, 1992, Masoni *et al.*, 1996). Thus, C_{ab} readings fail to consistently explain the variability of nutrients across years, as found by Xiong *et al.* (2015). This is also the case with most of the vegetation indices, which are calculated from only a few spectral bands and are further constrained by factors like soil background, leaf inclination angle, and atmospheric conditions (Baret and Guyot, 1991). However, our results demonstrated that, rather than relying upon the C_{ab} proxy, the actual values for C_{ab} content and other biochemical constituents derived from physical models exhibited more consistent relationships with nutrients over both years, considering the presence of multiple varieties, ages, and management practices within the orchard. These results are in agreement with other studies that report the superior performance of modeling approaches compared to the methods based on standard vegetation indices (Camino *et al.*, 2018).

In addition, our results are in accordance with other studies (Parkhill *et al.*, 2001, Kalaji *et al.*, 2018, Kalaji *et al.*, 2014, Camino *et al.*, 2018) that have suggested that chlorophyll fluorescence is a good proxy for photosynthesis and is closely related to nutrients, especially nitrogen. The results of our study reinforce this finding because we found that the measurements of Ft at leaf level displayed statistically significant correlations with nutrient values (i.e., N, P, and K) at the level of 0.005 across both years, outperforming C_{ab} readings and vegetation indices. These

significant relationships and consistent slopes are also found with the SIF quantified at canopy level for both years. Further, when combining the data from the two years, the relationship with N is even stronger, yielding $r^2 = 0.74$ (p-values < 0.005) at both the leaf and canopy levels. The close relationship between N and chlorophyll fluorescence indicates that N availability plays a greater role in photosynthesis and fluorescence emission than P and K availability do. C_{ab} is a pigment that is crucial to photosynthesis and N is an essential component of C_{ab}, whereas chlorophyll fluorescence is a measure of the amount of light energy emitted by chlorophyll molecules upon returning to their ground state following light excitation (Bolhàr-Nordenkampf and Öquist, 1993). So, when plants have inadequate nitrogen content, their C_{ab} levels decrease, which results in a reduction in photosynthetic performance and can negatively impact the amount of chlorophyll fluorescence emitted by the plant. However, even though P and K are also essential nutrients for plant growth, they do not have as direct an influence on chlorophyll levels or photosynthetic efficiency as N does. Therefore, it is unlikely that the presence of these nutrients has the same significant and consistent impact on chlorophyll fluorescence over time as N does. In addition, the P concentration (%) is lower (< 0.18%) and displays less variation (standard deviation of 0.01) than the N and K concentrations do (Table 2.2), resulting in a lower level of sensitivity to N and K.

In comparison to primary macro-nutrients, the values for secondary macro-nutrients (e.g., Ca, Mg) and for micro-nutrients (e.g., Fe, Cu) demonstrated weaker relationships with C_{ab} and chlorophyll fluorescence. This is generally due to their indirect and secondary roles in the photosynthetic process interfering with enzyme activity, protein synthesis, and membrane stability (Römheld and Marschner, 1991, Maathuis, 2009). These ‘assistant’ roles may not be as closely linked to C_{ab} and chlorophyll fluorescence as factors like light intensity and water availability, which directly affect

the photosynthetic process. Furthermore, it is possible that the relationships between these nutrients and C_{ab} or chlorophyll fluorescence, which are only indirect, do not hold across growth stages, variations in fertilizer application, or environmental conditions. For example, Cu was only applied at the beginning of the growing season, so the end of the season might not be the most appropriate time to assess its effects on the leaf pigment pool.

There is evidence of strong relationships between chlorophyll fluorescence and nutrient ratios (e.g., K/(Ca+Mg)), yielding significant results, 0.005 and 0.05 at leaf and canopy levels, respectively. The robustness of these relationships was not strongly demonstrated in this study over time, so further testing is needed to determine their validity. The timing of fertilizer applications and environmental conditions could also contribute to changes in nutrients' availability in the soil, their interactions, and plant uptake of them. Therefore, leaf nutrient assessment is not necessarily a reflection of nutrient availability in the soil. Nevertheless, nutrient ratio measurements can still be useful in assessing plant nutrient status, potential limitations of photosynthetic performance, and changes in nutrient availability, which can inform fertilizer application management.

2.5. Conclusions

This study examines the sensitivity of plant traits and vegetation indices to macro- and micro-nutrient concentrations and their ratios in almond orchards, at both the leaf and canopy levels, over the course of two years. The RTM-derived biochemical constituent levels (i.e., C_{ab}, C_{car}, C_x) calculated from airborne hyperspectral imagery outperformed vegetation indices in explaining nutrient variability across both years. In particular, the biochemical constituents showed significant correlations with leaf N (p-values < 0.005) for both years. Chlorophyll fluorescence emission demonstrated consistently significant correlations with the primary macro-nutrients (i.e., N, P, and

K) throughout the two years, at both leaf and canopy levels, suggesting it is a reliable indicator of nutrient variability, especially when considering data across years. For instance, the relationships of both leaf Ft and canopy SIF with leaf N yielded $r^2 = 0.74$ (p-values < 0.005) when combining the data from the two years. In addition, the relationships of pigment-related indices with leaf N were stronger than with structural indices and indices like CTRI1 (p-values < 0.005) and PRI_{m4} (p-values < 0.05), yielding consistently strong correlations over two years at both leaf and canopy levels. The relationships of leaf P and K with fluorescence and trait identification were weaker than those of leaf N, but they were still statistically significant (p-values < 0.05).

References

ABRÀMOFF, M. D., MAGALHÃES, P. J. & RAM, S. J. 2004. Image processing with ImageJ. *Biophotonics international,* 11**,** 36-42.

AFTAB, T. & HAKEEM, K. R. 2020. *Plant micronutrients: deficiency and toxicity management*, Springer Nature.

BARET, F. & GUYOT, G. 1991. Potentials and limits of vegetation indices for LAI and APAR assessment. *Remote sensing of environment,* 35**,** 161-173.

BARNES, J. D., BALAGUER, L., MANRIQUE, E., ELVIRA, S. & DAVISON, A. 1992. A reappraisal of the use of DMSO for the extraction and determination of chlorophylls a and b in lichens and higher plants. *Environmental and Experimental botany,* 32**,** 85-100.

BELWALKAR, A., POBLETE, T., LONGMIRE, A., HORNERO, A., HERNANDEZ-CLEMENTE, R. & ZARCO-TEJADA, P. 2022. Evaluation of SIF retrievals from narrow-band and sub-nanometer airborne hyperspectral imagers flown in tandem: Modelling and validation in the context of plant phenotyping. *Remote Sensing of Environment,* 273**,** 112986.

BLACKBURN, G. A. 1998. Spectral indices for estimating photosynthetic pigment concentrations: a test using senescent tree leaves. *International Journal of remote sensing,* 19**,** 657-675.

BLOOM, A. J., CHAPIN, F. S. & MOONEY, H. A. 1985. Resource limitation in plants--an economic analogy. *Annual review of Ecology and Systematics***,** 363-392.

BOJOVIĆ, B. & MARKOVIĆ, A. 2009. Correlation between nitrogen and chlorophyll content in wheat (Triticum aestivum L.). *Kragujevac Journal of Science,* 31**,** 69-74.

BOLHÀR-NORDENKAMPF, H. & ÖQUIST, G. 1993. Chlorophyll fluorescence as a tool in photosynthesis research. *Photosynthesis and production in a changing environment: a field and laboratory manual***,** 193-206.

CADET, É. & SAMSON, G. 2011. Detection and discrimination of nutrient deficiencies in sunflower by blue-green and chlorophyll-a fluorescence imaging. *Journal of plant nutrition,* 34**,** 2114-2126.

CALDERÓN, R., NAVAS-CORTÉS, J. A., LUCENA, C. & ZARCO-TEJADA, P. J. 2013. High-resolution airborne hyperspectral and thermal imagery for early detection of Verticillium wilt of olive using fluorescence, temperature and narrow-band spectral indices. *Remote Sensing of Environment,* 139**,** 231-245.

CAMINO, C., GONZÁLEZ-DUGO, V., HERNÁNDEZ, P., SILLERO, J. & ZARCO-TEJADA, P. J. 2018. Improved nitrogen retrievals with airborne-derived fluorescence and plant traits quantified from VNIR-SWIR hyperspectral imagery in the context of precision agriculture. *International journal of applied earth observation and geoinformation,* 70**,** 105-117.

CARTER, G. A. 1994. Ratios of leaf reflectances in narrow wavebands as indicators of plant stress. *Int. J. of Remote Sensing,* 15**,** 697-703.

CHAPIN, F. S., BLOOM, A. J., FIELD, C. B. & WARING, R. H. 1987. Plant responses to multiple environmental factors. *Bioscience,* 37**,** 49-57.

CIGANDA, V., GITELSON, A. & SCHEPERS, J. 2008. Vertical profile and temporal variation of chlorophyll in maize canopy: Quantitative "crop vigor" indicator by means of reflectance-based techniques. *Agronomy Journal,* 100**,** 1409-1417.

COMBAL, B., BARET, F., WEISS, M., TRUBUIL, A., MACE, D., PRAGNERE, A., MYNENI, R., KNYAZIKHIN, Y. & WANG, L. 2003. Retrieval of canopy biophysical variables from bidirectional reflectance: Using prior information to solve the ill-posed inverse problem. *Remote sensing of environment,* 84**,** 1-15.

DATT, B. 1998. Remote sensing of chlorophyll a, chlorophyll b, chlorophyll a+ b, and total carotenoid content in eucalyptus leaves. *Remote Sensing of Environment,* 66**,** 111-121.

DAUGHTRY, C. S., WALTHALL, C., KIM, M., DE COLSTOUN, E. B. & MCMURTREY III, J. 2000. Estimating corn leaf chlorophyll concentration from leaf and canopy reflectance. *Remote sensing of Environment,* 74**,** 229-239.

DE MAGALHÃES, J., ALVES, V., DE NOVAIS, R., MOSQUIM, P., MAGALHÃES, J., FILHO, A. B. & HUBERT, D. 1998. Nitrate uptake by corn under increasing periods of phosphorus starvation. *Journal of Plant Nutrition,* 21**,** 1753-1763.

EMBLETON, T. W., JONES, W. W., LABANAUSKAS, C. K. & REUTHER, W. 1973. Leaf analysis as a diagnostic tool and guide to fertilization. *The citrus industry,* 3**,** 183-210.

GAMON, J., PENUELAS, J. & FIELD, C. 1992. A narrow-waveband spectral index that tracks diurnal changes in photosynthetic efficiency. *Remote Sensing of environment,* 41**,** 35-44.

GARRITY, S. R., EITEL, J. U. & VIERLING, L. A. 2011. Disentangling the relationships between plant pigments and the photochemical reflectance index reveals a new approach for remote estimation of carotenoid content. *Remote Sensing of Environment,* 115**,** 628-635.

GEORGE, E. F., HALL, M. A. & KLERK, G.-J. D. 2008. The components of plant tissue culture media I: macro-and micro-nutrients. *Plant propagation by tissue culture.* Springer.

GITELSON, A. A., VIÑA, A., CIGANDA, V., RUNDQUIST, D. C. & ARKEBAUER, T. J. 2005. Remote estimation of canopy chlorophyll content in crops. *Geophysical research letters,* 32.

GNIAZDOWSKA, A. & RYCHTER, A. 2000. Nitrate uptake by bean (Phaseolus vulgaris L.) roots under phosphate deficiency. *Plant and Soil,* 226**,** 79-85.

GRUNES, D. 1959. Effect of nitrogen on the availability of soil and fertilizer phosphorus to plants. *Advances in Agronomy,* 11**,** 369-396.

GUEYMARD, C. A. 1995. *SMARTS2: a simple model of the atmospheric radiative transfer of sunshine: algorithms and performance assessment*, Florida Solar Energy Center Cocoa, FL.

GUEYMARD, C. A. 2001. Parameterized transmittance model for direct beam and circumsolar spectral irradiance. *Solar Energy,* 71**,** 325-346.

GÜSEWELL, S. 2004. N: P ratios in terrestrial plants: variation and functional significance. *New phytologist,* 164**,** 243-266.

HABOUDANE, D., MILLER, J. R., TREMBLAY, N., ZARCO-TEJADA, P. J. & DEXTRAZE, L. 2002. Integrated narrow-band vegetation indices for prediction of crop chlorophyll content for application to precision agriculture. *Remote sensing of environment,* 81**,** 416-426.

HABOUDANE, D., TREMBLAY, N., MILLER, J. R. & VIGNEAULT, P. 2008. Remote estimation of crop chlorophyll content using spectral indices derived from hyperspectral data. *IEEE Transactions on Geoscience and Remote Sensing,* 46**,** 423-437.

HASSOUN, M. H. 1995. *Fundamentals of artificial neural networks*, MIT press.

HERNÁNDEZ-CLEMENTE, R., NAVARRO-CERRILLO, R. M., SUÁREZ, L., MORALES, F. & ZARCO-TEJADA, P. J. 2011. Assessing structural effects on PRI for stress detection in conifer forests. *Remote Sensing of Environment,* 115**,** 2360-2375.

HERRMANN, I., KARNIELI, A., BONFIL, D., COHEN, Y. & ALCHANATIS, V. 2010. SWIR-based spectral indices for assessing nitrogen content in potato fields. *International Journal of Remote Sensing,* 31**,** 5127-5143.

HORUZ, A., KORKMAZ, A., KARAMAN, M. R., DIZMAN, M. & TURAN, M. 2013. The evaluation of leaf nutrient contents and element ratios of different raspberry varieties. *J. Food Agric. Environ,* 11**,** 588-593.

JONES, J. B. & JANICK, J. 1984. Soil testing and plant analysis: guides to the fertilization of horticultural crops. *Horticultural reviews. Vol. 7***,** 1-67.

KALAJI, H. M., BĄBA, W., GEDIGA, K., GOLTSEV, V., SAMBORSKA, I. A., CETNER, M. D., DIMITROVA, S., PISZCZ, U., BIELECKI, K. & KARMOWSKA, K. 2018. Chlorophyll fluorescence as a tool for nutrient status identification in rapeseed plants. *Photosynthesis Research,* 136**,** 329-343.

KALAJI, H. M., OUKARROUM, A., ALEXANDROV, V., KOUZMANOVA, M., BRESTIC, M., ZIVCAK, M., SAMBORSKA, I. A., CETNER, M. D., ALLAKHVERDIEV, S. I. & GOLTSEV, V. 2014. Identification of nutrient deficiency in maize and tomato plants by in vivo chlorophyll a fluorescence measurements. *Plant physiology and biochemistry,* 81**,** 16-25.

KOERSELMAN, W. & MEULEMAN, A. F. 1996. The vegetation N: P ratio: a new tool to detect the nature of nutrient limitation. *Journal of applied Ecology*, 1441-1450.

KROUK, G. & KIBA, T. 2020. Nitrogen and phosphorus interactions in plants: from agronomic to physiological and molecular insights. *Current opinion in plant biology*, 57, 104-109.

KUMAR, S., KUMAR, S. & MOHAPATRA, T. 2021. Interaction between macro-and micro-nutrients in plants. *Frontiers in Plant Science*, 12, 665583.

LI, D., WANG, C., JIANG, H., PENG, Z., YANG, J., SU, Y., SONG, J. & CHEN, S. 2018. Monitoring litchi canopy foliar phosphorus content using hyperspectral data. *Computers And Electronics In Agriculture*, 154, 176-186.

LIU, H. Q. & HUETE, A. 1995. A feedback based modification of the NDVI to minimize canopy background and atmospheric noise. *IEEE transactions on geoscience and remote sensing*, 33, 457-465.

LU, J., YANG, T., SU, X., QI, H., YAO, X., CHENG, T., ZHU, Y., CAO, W. & TIAN, Y. 2020. Monitoring leaf potassium content using hyperspectral vegetation indices in rice leaves. *Precision Agriculture*, 21, 324-348.

MAATHUIS, F. J. 2009. Physiological functions of mineral macronutrients. *Current opinion in plant biology*, 12, 250-258.

MAIER, S. W., GÜNTHER, K. P. & STELLMES, M. 2004. Sun-induced fluorescence: A new tool for precision farming. *Digital imaging and spectral techniques: Applications to precision agriculture and crop physiology*, 66, 207-222.

MARSCHNER, H. 2011. *Marschner's mineral nutrition of higher plants*, Academic press.

MASONI, A., ERCOLI, L. & MARIOTTI, M. 1996. Spectral properties of leaves deficient in iron, sulfur, magnesium, and manganese. *Agronomy journal*, 88, 937-943.

MCGRODDY, M. E., DAUFRESNE, T. & HEDIN, L. O. 2004. Scaling of C: N: P stoichiometry in forests worldwide: Implications of terrestrial redfield-type ratios. *Ecology*, 85, 2390-2401.

MENESATTI, P., ANTONUCCI, F., PALLOTTINO, F., ROCCUZZO, G., ALLEGRA, M., STAGNO, F. & INTRIGLIOLO, F. 2010. Estimation of plant nutritional status by Vis–NIR spectrophotometric analysis on orange leaves [Citrus sinensis (L) Osbeck cv Tarocco]. *biosystems engineering*, 105, 448-454.

MORAIS, M. C., AIRES, A., BARREALES, D., RODRIGUES, M. Â., RIBEIRO, A. C., GONÇALVES, B. & SILVA, A. P. 2020. Combined Soil and Foliar Nitrogen Fertilization Effects on Rainfed Almond Tree Performance. *Journal of Soil Science and Plant Nutrition*, 20, 2552-2565.

MUHAMMAD, S., SANDEN, B. L., LAMPINEN, B. D., SAA, S., SIDDIQUI, M. I., SMART, D. R., OLIVOS, A., SHACKEL, K. A., DEJONG, T. & BROWN, P. H. 2015. Seasonal changes in nutrient content and concentrations in a mature deciduous tree species: Studies in almond (Prunus dulcis (Mill.) DA Webb). *European Journal of Agronomy*, 65, 52-68.

MUNYATI, C., BALZTER, H. & ECONOMON, E. 2020. Correlating Sentinel-2 MSI-derived vegetation indices with in-situ reflectance and tissue macronutrients in savannah grass. *International Journal of Remote Sensing*, 41, 3820-3844.

NIBLACK, W. 1985. *An introduction to digital image processing*, Strandberg Publishing Company.

O'CONNELL, M., WHITFIELD, D. & ABUZAR, M. Satellite remote sensing of vegetation cover and nitrogen status in almond. XXIX International Horticultural Congress on Horticulture: Sustaining Lives, Livelihoods and Landscapes (IHC2014): 1130, 2014. 559-566.

PARKHILL, J. P., MAILLET, G. & CULLEN, J. J. 2001. Fluorescence-based maximal quantum yield for PSII as a diagnostic of nutrient stress. *Journal of Phycology*, 37, 517-529.

PENUELAS, J., BARET, F. & FILELLA, I. 1995. Semi-empirical indices to assess carotenoids/chlorophyll a ratio from leaf spectral reflectance. *Photosynthetica*, 31, 221-230.

PHANSALKAR, N., MORE, S., SABALE, A. & JOSHI, M. Adaptive local thresholding for detection of nuclei in diversity stained cytology images. 2011 International conference on communications and signal processing, 2011. IEEE, 218-220.

PLASCYK, J. A. 1975. The MK II Fraunhofer line discriminator (FLD-II) for airborne and orbital remote sensing of solar-stimulated luminescence. *Optical Engineering,* 14**,** 144339.

PLASCYK, J. A. & GABRIEL, F. C. 1975. The Fraunhofer line discriminator MKII-an airborne instrument for precise and standardized ecological luminescence measurement. *IEEE Transactions on Instrumentation and measurement,* 24**,** 306-313.

PRANANTO, J. A., MINASNY, B. & WEAVER, T. 2021. Rapid and cost-effective nutrient content analysis of cotton leaves using near-infrared spectroscopy (NIRS). *PeerJ,* 9**,** e11042.

RÖMHELD, V. & MARSCHNER, H. 1991. Function of micronutrients in plants. *Micronutrients in agriculture,* 4**,** 297-328.

RONDEAUX, G., STEVEN, M. & BARET, F. 1996. Optimization of soil-adjusted vegetation indices. *Remote sensing of environment,* 55**,** 95-107.

ROUSE, J. W., HAAS, R. H., SCHELL, J. A. & DEERING, D. W. 1974. Monitoring vegetation systems in the Great Plains with ERTS. *NASA special publication,* 351**,** 309.

ROY, R. N., FINCK, A., BLAIR, G. & TANDON, H. 2006. Plant nutrition for food security. *A guide for integrated nutrient management. FAO Fertilizer and Plant Nutrition Bulletin,* 16**,** 368.

RUFTY JR, T. W., MACKOWN, C. T. & ISRAEL, D. W. 1990. Phosphorus stress effects on assimilation of nitrate. *Plant Physiology,* 94**,** 328-333.

SAA, S. & BROWN, P. H. 2014. Fruit presence negatively affects photosynthesis by reducing leaf nitrogen in almond. *Functional Plant Biology,* 41**,** 884-891.

SAA, S., BROWN, P. H., MUHAMMAD, S., RIO, O.-D., SANDEN, B. L. & LACA, E. A. 2014. Prediction of leaf nitrogen from early season samples and development of field sampling protocols for nitrogen management in Almond (Prunus dulcis [Mill.] DA Webb). *Plant and soil,* 380**,** 153-163.

SCHEPERS, J., FRANCIS, D., VIGIL, M. & BELOW, F. 1992. Comparison of corn leaf nitrogen concentration and chlorophyll meter readings. *Communications in soil science and plant analysis,* 23**,** 2173-2187.

SHARMA, C. P. 2006. *Plant micronutrients,* CRC Press.

SMITH, F. W. & JACKSON, W. A. 1987. Nitrogen enhancement of phosphate transport in roots of Zea mays L: II. Kinetic and inhibitor studies. *Plant physiology,* 84**,** 1319-1324.

SMITH, P. F. 1962. Mineral analysis of plant tissues. *Annual Review of Plant Physiology,* 13**,** 81-108.

TESSIER, J. T. & RAYNAL, D. J. 2003. Use of nitrogen to phosphorus ratios in plant tissue as an indicator of nutrient limitation and nitrogen saturation. *Journal of Applied Ecology,* 40**,** 523-534.

ULRICH, A. 1952. Physiological bases for assessing the nutritional requirements of plants. *Annual Review of Plant Physiology,* 3**,** 207-228.

VERHOEF, W., JIA, L., XIAO, Q. & SU, Z. 2007. Unified optical-thermal four-stream radiative transfer theory for homogeneous vegetation canopies. *IEEE Transactions on geoscience and remote sensing,* 45**,** 1808-1822.

VILFAN, N., VAN DER TOL, C., YANG, P., WYBER, R., MALENOVSKÝ, Z., ROBINSON, S. A. & VERHOEF, W. 2018. Extending Fluspect to simulate xanthophyll driven leaf reflectance dynamics. *Remote sensing of environment,* 211**,** 345-356.

WANG, Y., SUAREZ, L., POBLETE, T., GONZALEZ-DUGO, V., RYU, D. & ZARCO-TEJADA, P. 2022. Evaluating the role of solar-induced fluorescence (SIF) and plant physiological traits for leaf nitrogen assessment in almond using airborne hyperspectral imagery. *Remote Sensing of Environment,* 279**,** 113141.

WANG, Y., SUAREZ, L., QIAN, X., POBLETE, T., GONZALEZ-DUGO, V., RYU, D. & ZARCO-TEJADA, P. Assessing the Contribution of Airborne-Retrieved Chlorophyll Fluorescence for Nitrogen Assessment in Almond Orchards. 2021 IEEE International Geoscience and Remote Sensing Symposium IGARSS, 2021. IEEE, 5853-5856.

WANG, Z., SKIDMORE, A. K., DARVISHZADEH, R., HEIDEN, U., HEURICH, M. & WANG, T. 2015. Leaf nitrogen content indirectly estimated by leaf traits derived from the PROSPECT model. *IEEE Journal of selected topics in applied earth observations and remote sensing,* 8**,** 3172-3182.

WOOD, C., REEVES, D. & HIMELRICK, D. Relationships between chlorophyll meter readings and leaf chlorophyll concentration, N status, and crop yield: a review. Proceedings of the Agronomy Society of New Zealand, 1993. 1-9.

XIONG, D., CHEN, J., YU, T., GAO, W., LING, X., LI, Y., PENG, S. & HUANG, J. 2015. SPAD-based leaf nitrogen estimation is impacted by environmental factors and crop leaf characteristics. *Scientific reports,* 5**,** 1-12.

XUE, J. & SU, B. 2017. Significant remote sensing vegetation indices: A review of developments and applications. *Journal of sensors,* 2017.

YODER, B. J. & PETTIGREW-CROSBY, R. E. 1995. Predicting nitrogen and chlorophyll content and concentrations from reflectance spectra (400–2500 nm) at leaf and canopy scales. *Remote sensing of environment,* 53**,** 199-211.

ZARATE-VALDEZ, J. L., MUHAMMAD, S., SAA, S., LAMPINEN, B. D. & BROWN, P. H. 2015. Light interception, leaf nitrogen and yield prediction in almonds: a case study. *European Journal of Agronomy,* 66**,** 1-7.

ZARCO-TEJADA, P. J., BERJÓN, A., LOPEZ-LOZANO, R., MILLER, J. R., MARTÍN, P., CACHORRO, V., GONZÁLEZ, M. & DE FRUTOS, A. 2005. Assessing vineyard condition with hyperspectral indices: Leaf and canopy reflectance simulation in a row-structured discontinuous canopy. *Remote Sensing of Environment,* 99**,** 271-287.

ZARCO-TEJADA, P. J., GONZÁLEZ-DUGO, V. & BERNI, J. A. 2012. Fluorescence, temperature and narrow-band indices acquired from a UAV platform for water stress detection using a micro-hyperspectral imager and a thermal camera. *Remote sensing of environment,* 117**,** 322-337.

ZARCO-TEJADA, P. J., MILLER, J. R., MOHAMMED, G. H. & NOLAND, T. L. 2000. Chlorophyll fluorescence effects on vegetation apparent reflectance: I. Leaf-level measurements and model simulation. *Remote Sensing of Environment,* 74**,** 582-595.

ZARCO-TEJADA, P. J., MILLER, J. R., NOLAND, T. L., MOHAMMED, G. H. & SAMPSON, P. H. 2001. Scaling-up and model inversion methods with narrowband optical indices for chlorophyll content estimation in closed forest canopies with hyperspectral data. *IEEE Transactions on Geoscience and Remote Sensing,* 39**,** 1491-1507.

ZARCO-TEJADA, P. J., MORALES, A., TESTI, L. & VILLALOBOS, F. J. 2013. Spatio-temporal patterns of chlorophyll fluorescence and physiological and structural indices acquired from hyperspectral imagery as compared with carbon fluxes measured with eddy covariance. *Remote Sensing of Environment,* 133**,** 102-115.

Chapter 3 : Evaluating the role of solar-induced fluorescence (SIF) and plant physiological traits for leaf nitrogen assessment in almond using airborne hyperspectral imagery

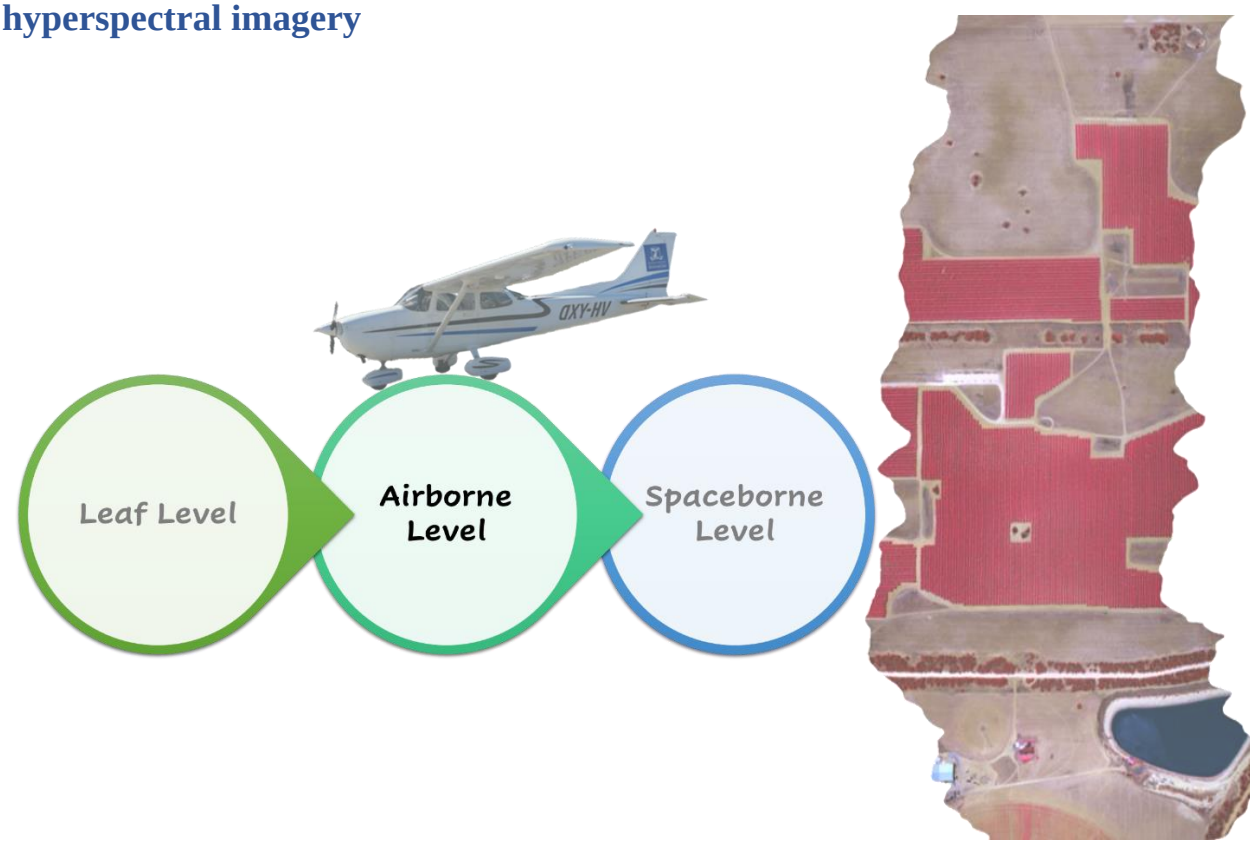

This chapter has been published in Remote Sensing of Environment:

Wang, Y., Suarez, L., Poblete, T., Gonzalez-Dugo, V., Ryu, D., Zarco-Tejada, P.J., Evaluating the role of solar-induced fluorescence (SIF) and plant physiological traits for leaf nitrogen assessment in almond using airborne hyperspectral imagery, Remote Sensing of Environment, 279, 113141. https://doi.org/10.1016/j.rse.2022.113141.

Abstract

Accurate, spatially extensive, and frequent assessments of plant nitrogen (N) enabled by remote sensing allow growers to optimize fertilizer applications and reduce environmental impacts. Standard remote sensing methods for N assessment typically involve the use of chlorophyll-sensitive vegetation indices calculated from multispectral or hyperspectral reflectance data. However, the chlorophyll *a*+*b* derived from spectral indices is indirectly related to leaf N and saturates at high leaf N levels, dramatically reducing the sensitivity with leaf N under these conditions. Furthermore, these relationships are heavily influenced by canopy structure, variability in leaf area density, proportion of sunlit-shaded tree-crown components, soil background, and understory. Recent studies in uniform crops have demonstrated that estimation of plant N can be improved by considering leaf biochemical constituents derived from radiative transfer model (RTM) and solar-induced fluorescence (SIF). However, it is unclear whether these methods are transferable to tree crops due to their intrinsic physiological differences, structural complexity, and within-tree crown heterogeneity. We investigated how various hyperspectrally derived proxies for leaf N, including RTM-based traits and SIF, could be combined to assess N status on a 1,200-ha almond orchard across two growing seasons. RTM-based chlorophyll *a*+*b* content (C_{ab}) and SIF were found to be the most important and consistent predictors for leaf N compared to other leaf biochemical and biophysical traits. C_{ab} alone was a modest predictor of leaf N variability (r^2 = 0.49, RMSE = 0.16%, *p*-value < 0.001), but when the non-collinear SIF and C_{ab} traits were coupled together, predictions improved dramatically (r^2 = 0.95, RMSE = 0.05%, *p*-value < 0.001). Leaf area index (LAI) was poorly associated with leaf N, suggesting that leaf physiological traits may be more important than structural traits in quantifying leaf N in well-managed orchards characterized by high N levels. Consistent results across the 2 years suggests the importance of

airborne SIF coupled with C_{ab} for precision agriculture and leaf N status assessment in almond orchards.

Keywords: Chlorophyll Fluorescence, SIF, Nitrogen, Chlorophyll, FluSAIL RTM, Hyperspectral, Gaussian Process Regression, Random Forest, Almond, Tree Orchard

3.1 Introduction

Nitrogen (N) is an essential nutrient for plant growth, productivity, and quality and is often the major limiting factor for photosynthesis (Evans, 1989). However, more N fertilizer than needed is often applied to maximize yield and quality (Conant *et al.*, 2013). In addition to the economic costs of N over-fertilization, excess N has detrimental effects on the environment, leading to pollution of the atmosphere and water systems (Stevenson and Cole, 1999, Shcherbak *et al.*, 2014, Zebarth *et al.*, 2009). Monitoring crop N status is essential for optimizing N applications and maintaining productivity while minimizing environmental impacts for sustainable agriculture (Matson *et al.*, 1998, Snyder *et al.*, 2009, Manna *et al.*, 2005, Panhwar *et al.*, 2019).

The concentration of leaf nitrogen can be determined through various approaches. The chemical analysis of leaf tissue via destructive sampling, such as the traditional Kjeldahl-digestion method (Kjeldahl, 1883) or the simpler and faster Dumas combustion method to avoid using toxic chemicals (Dumas, 1831), has been the standard method for the assessment of leaf N. Although this approach is very accurate, it is not cost- or time-effective for the continuous monitoring of N status over large areas. In recent decades, imaging spectroscopy has been used as an alternative to lab-based assays from the leaf, enabling rapid N monitoring at a range of spatio-temporal scales (Schepers *et al.*, 1992, Chapman and Barreto, 1997, Nageswara Rao *et al.*, 2001, Dong *et al.*, 2020, Romina *et al.*, 2019) to canopy level (Pinter Jr *et al.*, 2003, Nigon *et al.*, 2020, Inoue *et al.*, 2012, Clevers and Kooistra, 2011, Clevers and Gitelson, 2013, Gnyp *et al.*, 2014, Haboudane *et al.*, 2002).

Most remote sensing (RS) studies of leaf N depend on an assumed strong correlation between leaf chlorophyll $a+b$ (C_{ab}) and N (Evans, 1989). Thus, C_{ab} has been proposed as a common RS-based indicator for N assessment (Wood *et al.*, 1992, Yoder and Pettigrew-Crosby, 1995, Schlemmer *et*

al., 2013, Clevers and Gitelson, 2013). The conventional approach in these studies has been to determine an empirical relationship between destructively sampled tissue N and non-destructive proxy measurements, including hand-held spectral readings at visible, red-edge, and near-infrared spectral bands (Cerovic *et al.*, 2015, Cerovic *et al.*, 2012, Bullock and Anderson, 1998, Chang and Robison, 2003, Jongschaap and Booij, 2004, Padilla *et al.*, 2018, Wood *et al.*, 1992) or chlorophyll-sensitive vegetation indices derived from multispectral or hyperspectral reflectance at leaf and canopy levels (Filella *et al.*, 1995, Fitzgerald *et al.*, 2010, Cummings *et al.*, 2021, Nigon *et al.*, 2020, Inoue *et al.*, 2012, Clevers and Gitelson, 2013, Gnyp *et al.*, 2014). Although leaf chlorophyll meters are valuable tools for quick on-farm determination of leaf N status, the relationship between chlorophyll meter readings and N content differs across plant genotypes and environmental contexts (Xiong *et al.*, 2015). Furthermore, these chlorophyll indicators from chlorophyll meters or vegetation indices are not the actual chlorophyll content, but rather the proxy for leaf greenness. Although they are generally related to leaf N, these proxies saturate at high N levels, resulting in reduced sensitivity to increased N values (Padilla *et al.*, 2018, Romina *et al.*, 2019, Li *et al.*, 2020, Schlemmer *et al.*, 2013). In addition to these leaf greenness indicators, vegetation indices widely used in RS such as the Normalized Difference Vegetation Index (NDVI) (Rouse *et al.*, 1974), are also indirectly related to N (Yoder and Pettigrew-Crosby, 1995). They have been demonstrated to lack sensitivity and to saturate at high plant densities and under overfertilization levels (Matsushita *et al.*, 2007, Flowers *et al.*, 2003, Nguy-Robertson *et al.*, 2012). To prevent these effects, proxies directly linked to leaf N through pathways other than via the quantification of chlorophyll content are required.

Moreover, spectral indices that incorporate red-edge spectra are thought to be improved ways to derive N status due to the higher sensitivity of this spectral region to moderate and high chlorophyll

content levels (Gitelson *et al.*, 1996, Gitelson *et al.*, 2003). Fitzgerald *et al.* (2006) found that the Normalized Difference Red-Edge (NDRE) index, which is calculated by replacing the red band of NDVI with the red-edge band, was a reliable indicator of chlorophyll and N status. Another index termed the Canopy Chlorophyll Content Index (CCCI) is based on a two-dimensional planar extension of NDVI and NDRE and has been proposed as a method for improved estimation of N in annual crops (e.g., wheat (*Triticum aestivum*)) (Fitzgerald *et al.*, 2010, Perry *et al.*, 2012, Li *et al.*, 2014). Another approach combining the information in the red-edge with a structural index is the use of the Transformed Chlorophyll Absorption in Reflectance Index (TCARI) with the Optimized Soil-Adjusted Vegetation Index (TCARI/OSAVI) (Haboudane *et al.*, 2002). These indices tend to be sensitive to chlorophyll $a+b$ induced by N variability while also accounting for background effects (Gabriel *et al.*, 2017, Wu *et al.*, 2008). Nevertheless, empirical relationships are required to estimate N from these vegetation indices.

As leaf N content is associated with many other physiological traits besides C_{ab} content, the use of radiative transfer model (RTM)-based retrievals of plant physiological traits is a promising alternative to spectral indices for assessing leaf N. Due to the fact that leaf N is not an input in the RTM, nutrient variability was described through a wide range of model-simulated plant traits, including leaf constituents (e.g., C_{ab}, dry matter (C_{dm}), water content (C_w)), and canopy structural parameters (Wang *et al.*, 2018, Thorp *et al.*, 2012, Baret *et al.*, 2007, Camino *et al.*, 2018a, Wang *et al.*, 2021). Traits derived from RTMs are considered more accurate and transferrable than index-based empirical algorithms (Kimes *et al.*, 2000), although this has only been tested for uniform crops. For orchards, this method is more complex due to the tree crown heterogeneity and clumping effects with mixed crown-shadow-soil backgrounds. Radiative transfer model inversion also allows inverting for other non-photosynthetic plant pigments, such as carotenoids (C_{car}) and

xanthophylls (C_x), which are involved in photosynthetic light-harvesting (Niyogi *et al.*, 1997, Jacquemoud *et al.*, 2009, Vilfan *et al.*, 2016, Vilfan *et al.*, 2018). Plants prevent photodamage by deoxidizing the xanthophyll violaxanthin (V) into antheraxanthin (A) and zeaxanthin (Z) in response to excess excitation energy (Demmig *et al.*, 1987, Gilmore, 1997). Therefore, xanthophyll composition is linked to photosynthetic efficiency and may thus relate to leaf N status, particularly under abiotic stress conditions (Verhoeven *et al.*, 1999, Tóth *et al.*, 2002, Cheng, 2003, Ramalho *et al.*, 2000). Thus, based on their links with photosynthesis under stress conditions, the complete set of photosynthetic and non-photosynthetic pigments, along with structural traits, can lead to a more informed assessment of N.

In the last few decades, solar-induced fluorescence (SIF) has been proposed as a trait for monitoring plant physiology, vegetation functioning, and plant biotic and abiotic stress detection due to the dynamic changes in photochemical and non-photochemical quenching in the photosynthetic process (see review paper by Mohammed *et al.* (2019) and studies from Mohammed *et al.* (1995), Porcar-Castell *et al.* (2014), Maxwell and Johnson (2000), Murchie and Lawson (2013), Sayed (2003), Zarco-Tejada *et al.* (2018)). It is well known that abiotic-induced stress conditions such as light intensity, water status, and temperature extremes modulate the photosynthetic performance (Ashraf and Harris, 2013, Biswal *et al.*, 2011, Saibo *et al.*, 2009). Most importantly, SIF is considered a direct proxy for electron transport rate and thus a direct measure of photosynthesis (Krause and Weis, 1991, Walker *et al.*, 2014, Genty *et al.*, 1989, Middleton *et al.*, 2016). N modulates the fluorescence-photosynthesis link, thus several studies propose SIF as a potential proxy for the assessment of leaf N status at both the leaf (Lu and Zhang, 2000, Huang *et al.*, 2004) and the canopy levels (Cendrero-Mateo *et al.*, 2016, Middleton *et al.*, 2016, Corp *et al.*, 2003, Mohammed *et al.*, 2019, Wang *et al.*, 2021). For example, Camino *et al.*

(2018a) showed that SIF improved predictions of N content in wheat. However, in tree orchards, SIF is affected by canopy structure and the mixing of within-crown sunlit and shaded components. This adds complexity to the accurate SIF quantification in tree orchards (Camino *et al.*, 2018b). The combined use of RTM-based leaf biochemistry estimates with SIF for N assessment is poorly studied in structurally complex tree orchards. Such a methodology may have important uses in precision agriculture when using commercial hyperspectral sensors with 5- to 6-nm spectral resolution, which have been shown to be sensitive to SIF emission and thus are useful for quantifying abiotic sources of stress (Belwalkar *et al.*, 2022, Zarco-Tejada *et al.*, 2012, Zarco-Tejada *et al.*, 2016, Zarco-Tejada *et al.*, 2013, Raya-Sereno *et al.*, 2021, Belwalkar *et al.*, 2021).

In this study, we explored the contribution of various hyperspectrally derived proxies for leaf N status assessment in almond orchards across two consecutive growing seasons, including airborne-quantified plant physiological traits estimated by RTM inversion and canopy SIF. We evaluated the accuracy and robustness of the retrieved plant physiological traits and the collinearity among plant pigments, SIF, and structural traits when assessing leaf N variability across the field. Rather than a data driven approach, our study advances the mechanistic understanding of the responses of RS-derived plant traits to leaf N content changes.

3.2 Material and methods

3.2.1 Study area and field data collection

This study was conducted in a commercial almond orchard in northwest Victoria, Australia, at the pre-harvest stage of the growing season in 2019/2020 and 2020/2021 when the leaves are mature and have reached their maximum N uptake capacity. The region has a Mediterranean climate with

hot, dry summers and mild, wet winters. Average annual precipitation is 300 mm. The summer of 2020/2021 was milder than that of 2019/2020, with an average maximum air temperature of 29.5°C in December 2020, compared to 34.3°C in December 2019. The almond orchard (Fig. 3.1) covers approximately 1,240 hectares with trees planted between 2006 (Northern blocks facing N-S) and 2007 (Southern blocks mixed in N-S and E-W orientations) on sandy loam soils. Generally, trees planted in the eastern blocks tend to have larger tree crowns than those in the west. Three almond varieties were planted in alternating blocks of six rows to facilitate cross-pollination (Hill *et al.*, 1985, Asai *et al.*, 1996). Varieties included Nonpareil (50%), Carmel (33%), and Price (17%). A drip fertigation system was used to supply the same amount of water and nutrients to the tree root zones for each variety at the same time and was established at 1-hour intervals between varieties across the entire orchard. Fertigation was supplied as needed based on weather and plant responses over the growing season. In summer of 2020/2021, irrigation volume was 10% higher (12,795 m^3/ha) than in 2019/2020 (11,465 m^3/ha), but total N fertilizer applications (330 kg/ha in 2020/2021 and 326 kg/ha in 2019/2020) were similar. In summer of 2020/2021, Nonpareil was treated with 10% less fertigation than Carmel and Price varieties across the orchard based on the difference observed along the 2019/2020 season.

Fifteen homogeneous plots consisting of six rows of seven to eight trees were monitored throughout the experiment in 2019/2020 and 2020/2021 (Fig. 3.2). In each plot, four adjacent trees from Nonpareil and Carmel varieties (two each; yellow dashed rectangle in Fig. 3.2a) were sampled *in situ* prior to harvest in both years. Leaf C_{ab}, anthocyanins (Anth), flavonoid (Flav) content, and the nitrogen balance index (NBI) were measured from 20 representative sunlit mature leaves per tree using a Dualex 4 Scientific sensor (FORCE-A, Orsay, France). Leaf steady-state chlorophyll fluorescence (Ft) and leaf reflectance spectra within the visible (VIS) and near-infrared

(NIR) regions were measured with FluorPen FP 110 and PolyPen RP 410 instruments (PSI, Brno, Czech Republic) on the same leaves with the Dualex sensor. A series of vegetation pigment indices (see Table 3.1 for the complete list of indices used in this study) were calculated based on the leaf reflectance spectra measured from the PolyPen handheld instrument. An additional set of 20 leaves per plot were collected for biochemical laboratory analyses using Dumas Combustion (Etheridge *et al.*, 1998, Buckee, 1994, Dumas, 1831) with a LECO TruMac CNS Macro Analyzer (LECO Corporation, MI, USA) and an inductively coupled plasma optical emission spectrometer (ICP-OES Optima 8300, Perkin Elmer, USA). Thirteen macro and micro-nutrients (e.g., nitrogen, carbon, phosphorus, and potassium) were measured. The ranges of variation of field data collected over 2 years were compared against Ft-measured quartiles. The correlations between leaf measurement and laboratory N concentration were calculated for both years.

3.2.2 Airborne hyperspectral and thermal imagery

Airborne campaigns were conducted concurrently with the field measurements on February 17, 2020, and January 31, 2021. Both campaigns occurred at solar noon under clear skies. Field sampling and auxiliary data collection required for the calibration and atmospheric correction of the images were conducted simultaneously with airborne campaigns. A hyperspectral line-scanning sensor (Micro-Hyperspec VNIR E-Series model, Headwall Photonics, Fitchburg, MA, USA) and a thermal infrared camera (A655sc model, FLIR Systems, Wilsonville, OR, USA) were flown in tandem on a manned aircraft operated by the HyperSens Remote Sensing Laboratory, the Airborne Remote Sensing Facility of The University of Melbourne. The hyperspectral imager covers 371 spectral bands in the visible and near-infrared regions (400-1000 nm) with a full-width at half-maximum (FWHM) of 5.8 nm and a spectral sampling interval of 1.626 nm. Hyperspectral

and thermal images with an angular field of view (FOV) of 66° and 45° (8- and 13.1-mm focal length), respectively, were collected by the aircraft at 550 m above ground level (AGL), yielding spatial resolutions of 40 and 60 cm, respectively, enabling the differentiation of sunlit and shaded components of tree crowns and soil areas. SMARTS (Gueymard, 2001, Gueymard *et al.*, 2002, Gueymard, 1995) irradiance simulations were used to correct for atmospheric effects of the hyperspectral imagery based on aerosol optical measurements at 500 nm taken with a Microtops II sunphotometer (Solar Light, PA, USA) connected to a GPS-12 navigator (Garmin, Olathe, KS, USA) at the time of each flight. Air temperatures and relative humidity were calculated based on the average of three nearby weather stations (Robinvale, Lake Powell and Wemen) less than 15 km from the study site. Hyperspectral line-scanned image orthorectification was performed using PARGE software (ReSe Applications Schläpfe, Wil, Switzerland) with readings from the onboard inertial measuring unit (IMU) (VectorNav VN-300 dual-antenna GNSS/INS, Dallas, TX, USA). Empirical line calibration was conducted by measuring the reflectance spectra and temperature of bare soil and green and dry vegetation. Spectra were measured with an ASD Handheld-2 field spectrometer (FieldSpec Handheld Pro, ASD Inc., CO, USA), and temperature was measured with a thermal gun (LaserSight, Optris, Germany). Hyperspectral and thermal imagery were mosaicked (Figs. 3.1 and 3.3) using ENVI (Boulder, Colorado) and Pix4D (Lausanne, Switzerland) photogrammetry software, respectively.

Fig. 3.1. Color-infrared (CIR) overview of the hyperspectral mosaic acquired with the VNIR hyperspectral sensor over the 1,200-ha study site collected on January 31, 2021. Spectral bands at 860 (R), 650 (G), and 550 (B) nm are shown with a spatial resolution of 40 cm per pixel.

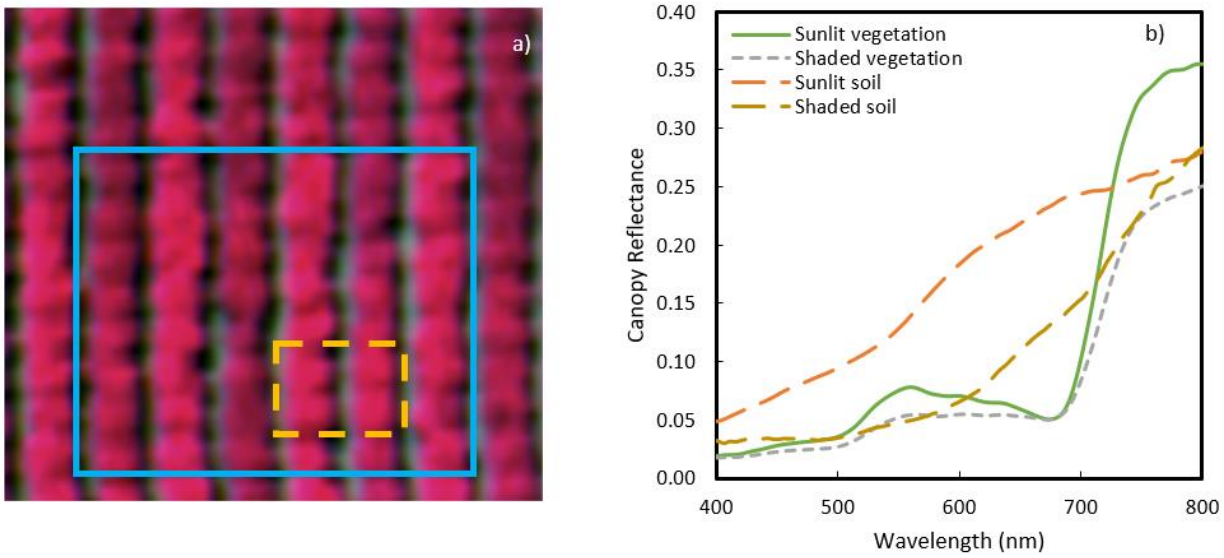

Fig. 3.2. (a) Study plot consisting of six rows by eight trees within the blue solid line. Leaves from four trees within the yellow dashed rectangle were measured in the field. (b) The reflectance spectra of different scene components extracted from the airborne hyperspectral imager, including sunlit (green solid line) and shaded (grey dashed line) tree crown, and sunlit (orange dashed line) and shaded soil (brown dashed line) pixels.

Automatic segmentation of the hyperspectral reflectance imagery was conducted using Fiji (Abràmoff *et al.*, 2004) combining Niblack's (Niblack, 1985) thresholding method on the NIR band, and Phansalkar's thresholding method (Phansalkar *et al.*, 2011) on a structural index (NDVI > 0.72). This method enabled the discrimination of sunlit pure tree crowns from the soil background, as well as the separation of within-crown shadows (see reflectance spectra in Fig. 3.2b). Considering the sensitivity of SIF to the illumination levels, a more selective segmentation (10% restricted) was applied to the hyperspectral radiance data when segmenting the sunlit crown component. The thermal segmentation of the tree canopy was performed with Niblack's thresholding method (Niblack, 1985) to eliminate the soil and background effects. The resulting pure vegetation pixels obtained in the previous step were clustered into tree-crown features using a watershed segmentation approach based on Euclidean distance (as in Zarco-Tejada *et al.* (2018)).

In Fig. 3.4, an example of the segmentation conducted on the hyperspectral and the thermal mosaics is presented.

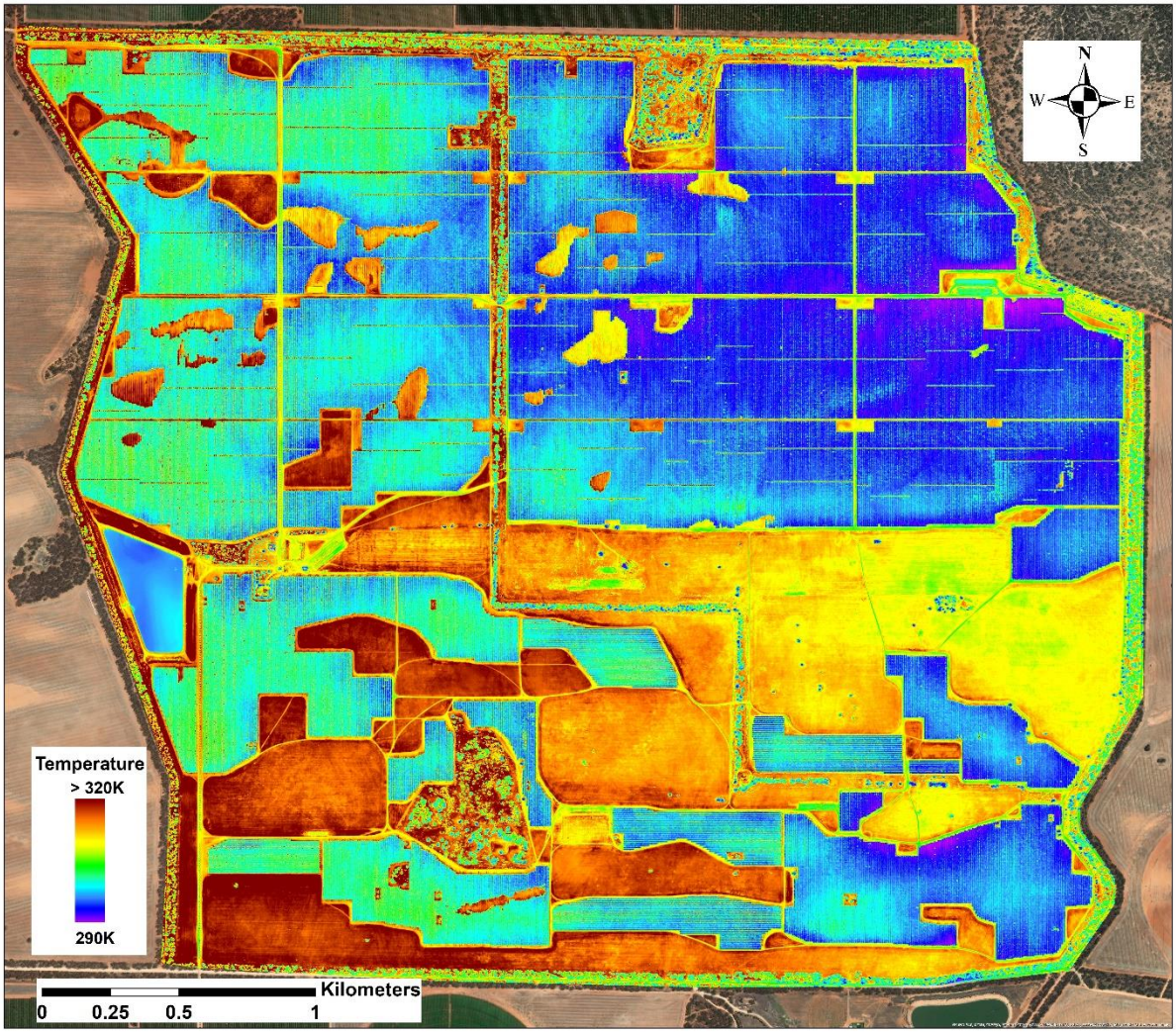

Fig. 3.3. Thermal mosaic collected over the entire study area captured on January 31, 2021 at a spatial resolution of 60 cm. Cooler colors (purple and blue) indicate plant canopies, and yellow/brown colors indicate soil.

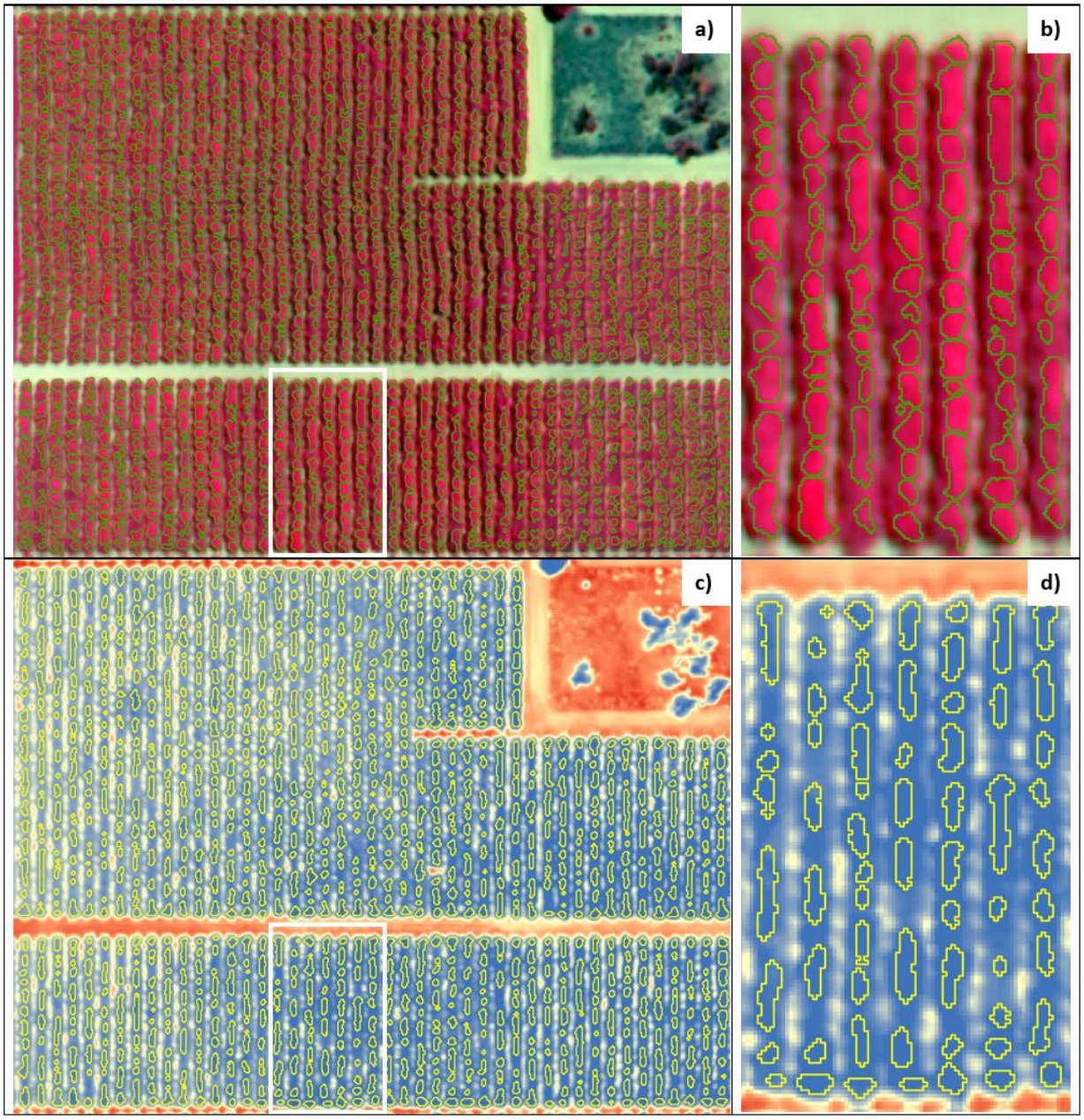

Fig. 3.4. Overview of the tree-crown segmentation applied to the hyperspectral mosaic (a, upper image in color-infrared, crown in green outline) and the thermal mosaic (c, bottom image displaying cooler canopy in blue and hot soil in red color, crown in yellow outline). Right column contains zoomed-in views (b and d) of the scenes within the white rectangle on the left.

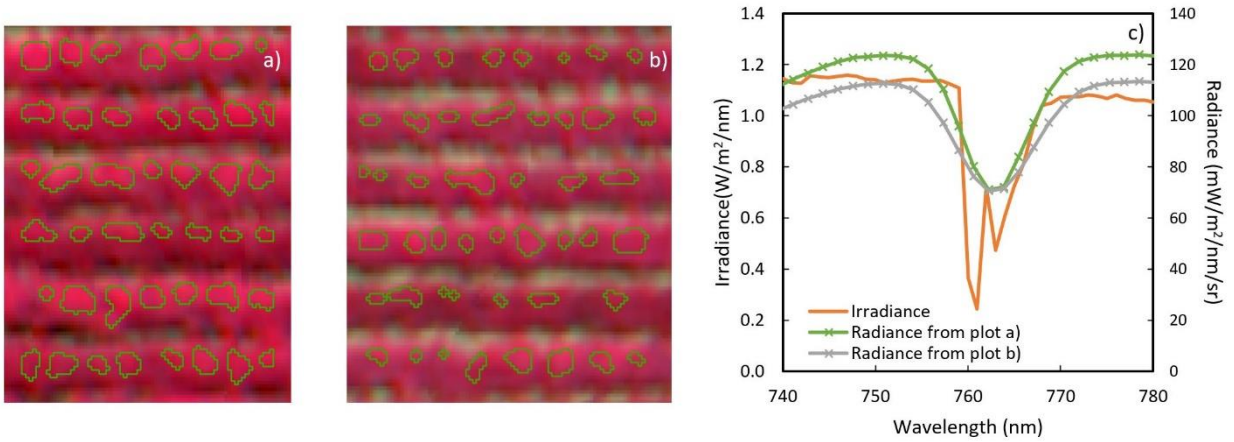

Fig. 3.5. Segmentation of the sunlit crown area for SIF quantification on two study plots (a) higher nutrient level and (b) lower nutrient level. The irradiance spectrum (orange color) was used along with the radiance spectra (example shown in (c) for two study plots (green and grey lines) to calculate SIF. Crosses denote the spectral position of the sensor bands (c).

The mean radiance and reflectance spectra, and temperature were extracted from tree crown pixels by hyperspectral and thermal imagery for each study plot. The crop water stress index (CWSI) (Idso *et al.*, 1981) was calculated based on the canopy-air temperature difference and the water vapor pressure deficit (VPD) at the time of image acquisition for assessing the tree-crown water stress levels. A non-water-stressed baseline (NWSB) for almond trees suggested by Bellvert *et al.* (2018) was used.

SIF was quantified using the Fraunhofer line depth (FLD) principle (Plascyk and Gabriel, 1975) based on three spectral bands (3FLD) (Maier *et al.*, 2004) located inside and outside the O_2-A absorption features. Specifically, we compared canopy radiance values L_{in} at 762 nm and L_{out} at 750 and 778 nm extracted from the hyperspectral imagery to the corresponding incoming irradiance E_{in} (E_{762}) and E_{out} (E_{750}, E_{778}) derived from the field measurements during the flight and resampled to match the spectral specifications of the airborne hyperspectral sensor. To account for the effects of negative values from atmospheric and calibration factors, SIF was scaled using the offset from non-fluorescence targets (e.g., soil) extracted from the imagery. Fig. 3.5 shows the

irradiance and the mean radiance spectra from two study plots (in Figs. 5a and 5b) at the oxygen-A absorption region around 760 nm. Average tree-crown reflectance (R) spectra extracted from pure vegetation pixels were used to estimate plant traits through RTM inversion and to calculate narrow-band hyperspectral indices (Table 3.1) for comparison. The set of indices used comprised structural indices (e.g., NDVI), pigment indices (e.g., Modified Chlorophyll Absorption in Reflectance Index (MCARI), TCARI/OSAVI, and Carter Index 1 (CTRI1)), and indices in the visible region (e.g., Photochemical Reflectance Index (PRI)) that track the dynamics of photoprotective mechanisms. Indices calculated from airborne imagery were also compared against leaf N, C_{ab}, NBI, and Ft measured in the field.

2646 Table 3.1. Spectral vegetation index equations used in this study.

Index	Equation	Reference
Structural indices		
NDVI	$(R_{800} - R_{670})/(R_{800} + R_{670})$	Rouse *et al.* (1974)
EVI	$2.5 \cdot (R_{800} - R_{670})/(R_{800} + 6 \cdot R_{670} - 7.5 \cdot R_{500} + 1)$	Liu and Huete (1995)
MCARI2	$\frac{1.5 \cdot (2.5 \cdot (R_{800} - R_{670}) - 1.3 \cdot (R_{800} - R_{550}))}{\sqrt{(2 \cdot R_{800} + 1)^2 - (6 \cdot R_{800} - 5 \cdot R_{670}) - 0.5}}$	Haboudane *et al.* (2004)
RDVI	$(R_{800} - R_{670})/\sqrt{R_{800} + R_{670}}$	Roujean and Breon (1995)
OSAVI	$(1 + 0.16) \cdot (R_{800} - R_{670})/(R_{800} + R_{670} + 0.16)$	Rondeaux *et al.* (1996)
Chlorophyll a+b indices		
MCARI	$((R_{700} - R_{670}) - 0.2 \cdot (R_{700} - R_{550})) \cdot (R_{700}/R_{670})$	Daughtry *et al.* (2000)
TCARI/OSAVI	$\frac{3 \cdot ((R_{700} - R_{670}) - 0.2 \cdot (R_{700} - R_{550}) \cdot (R_{700}/R_{670}))}{(1 + 0.16) \cdot (R_{800} - R_{670})/(R_{800} + R_{670} + 0.16)}$	Haboudane *et al.* (2002)
NPQI	$(R_{415} - R_{435})/(R_{415} + R_{435})$	Barnes *et al.* (1992)
PSSRa	R_{800}/R_{675}	Blackburn (1998)
PSSRb	R_{800}/R_{650}	Blackburn (1998)
PSSRc	R_{800}/R_{500}	Blackburn (1998)
SIPI	$(R_{800} - R_{445})/(R_{800} - R_{680})$	Penuelas *et al.* (1995)
CTRI1	R_{695}/R_{420}	Carter (1994)
Indices based on the green region		
PRI	$(R_{570} - R_{531})/(R_{570} + R_{531})$	Gamon *et al.* (1992)
PRI_{515}	$(R_{515} - R_{531})/(R_{515} + R_{531})$	Hernández-Clemente *et al.* (2011)
PRI·CI	$((R_{570} - R_{531})/(R_{570} + R_{531})) \cdot ((R_{760}/R_{700}) - 1)$	Garrity *et al.* (2011)
Fluorescence quantification		
SIF	$\frac{E_{out} \cdot L_{in} - E_{in} \cdot L_{out}}{E_{out} - E_{in}}$ Where E and L represent the incoming irradiance and canopy radiance, 'in' band refers to 762 nm, and 'out' band refers to the average value in 750 and 778 nm	Plascyk and Gabriel (1975)
Canopy temperature		
CWSI	$\frac{(T_c - T_a) - (T_c - T_a)_{LL}}{(T_c - T_a)_{UL} - (T_c - T_a)_{LL}}$ Where LL and UL represent the upper limit and lower limit of canopy (T_c) and air (T_a) temperatures	Jackson *et al.* (1981)

3.2.3 Modeling methods for plant trait retrieval and N assessment

The coupled leaf-level Fluspect-Cx model (Vilfan *et al.*, 2018) and 4SAIL (Verhoef, 1984) canopy radiative transfer model, referred to here as FluSAIL, were employed to derive plant biophysical and biochemical parameters by inverting the average canopy reflectance extracted from pure vegetation pixels. The de-epoxidation state of the xanthophyll cycle (C_x) as well as C_{ab}, C_{car}, and Anth pigment content were retrieved by the inversion of the Fluspect-Cx model. A look-up table (LUT) was generated by running 50,000 simulations using randomly generated input parameters drawn from uniform distributions (Table 3.2). Parameter ranges were adjusted for the viewing geometries due to the slightly different solar zenith angles (SZAs) for each airborne dataset. Biochemical constituents and biophysical parameters were estimated simultaneously for all study plots using a 10-hidden layer artificial neural network (ANN) model (Hassoun, 1995, Combal *et al.*, 2003). The model was trained using 70% of the LUT spectra and tested using the remaining 30% with the mean squared error (MSE) as a performance measure. The model was fit in MATLAB (MATLAB; Statistics and Machine Learning Toolbox and Deep Learning Toolbox; Natick, Massachusetts, USA). Retrieved parameters were used to simulate reflectance spectra with the FluSAIL model using the retrieved parameters and compared with the observed reflectance spectra obtained from the imagery in the 400–900-nm range based upon the root-mean-square deviation (RMSE) assessment. Additionally, the correlations of field leaf-level measurements against estimated plant traits derived from the inversion of the FluSAIL model were compared with those obtained from hyperspectral indices.

Table 3.2. Ranges of input parameters for the LUT of FluSAIL model.

Parameter	Symbol	Unit	Range/Value
Leaf thickness and constituents			
Chlorophyll *a*+*b* content	C_{ab}	µg/cm^2	20–70
Carotenoid content	C_{car}	µg/cm^2	3–20
Anthocyanin content	Anth	µg/cm^2	0–10
Leaf water content	C_w	g/cm^2	0.001–0.05
Leaf dry matter content	C_{dm}	g/cm^2	0.001–0.05
Brown pigment content	C_s	µg/cm^2	0
Leaf mesophyll structural parameter	N-struct	-	1.3–2.5
Leaf dynamic biochemistry			
De-epoxidation state of the xanthophyll cycle (photochemical reflectance parameter)	C_x	-	0–3
Fraction of photons partitioned to PSI	$f_{qe}I$	-	0.002
Fraction of photons partitioned to PSII	$f_{qe}II$	-	0.02
Canopy structural parameters			
Leaf area index	LAI	m^2/m^2	1–7
Hot spot parameter	q	-	0.03
Leaf inclination distribution function parameter *a*	$LIDF_a$	-	−1–1
Leaf inclination distribution function parameter *b*	$LIDF_b$	-	−1–1

To predict leaf N concentration, a pool of representative plant traits and parameters was considered as inputs in the N model, including (1) leaf biochemical and canopy biophysical traits retrieved from pure reflectance spectra with FluSAIL model inversion, (2) airborne-quantified SIF from sunlit-crown radiance spectra, and (3) the water stress indicator CWSI calculated from the thermal imagery. Random Forest (Breiman, 2001) and Gaussian process regression (Williams and Rasmussen, 1996, Williams and Rasmussen, 2006) algorithms were built with fine-tunning of hyperparameter optimization with 1,000 iterations incorporated in the leave-one-out-cross-validation (LOOCV, 15-fold) training and testing steps for each year's dataset. Previously, input collinearity was evaluated using the variance inflation factor (VIF) analysis (O'brien, 2007) following the approach in Zarco-Tejada *et al.* (2018) conducted using the 'fmsb' package (Gareth

et al., 2013) in R. Out-of-bag (OOB) predictor importance was implemented to rank the input relative contribution to the models (as in Zarco-Tejada *et al.* (2021)). Input parameters with a high degree of collinearity (VIF > 5) (Akinwande *et al.*, 2015) and therefore less informative contribution were filtered out to avoid redundancy. Both Random Forest and Gaussian process regression models were evaluated using the final selection of input parameters. The model performance was evaluated based on the coefficient of determination (r^2) and RMSE. In addition, models with different combination of any two non-collinear parameters were evaluated. In particular, models using leaf biochemical constituents and biophysical parameters with and without SIF were compared to assess the contribution of SIF to N assessments.

A final evaluation was conducted with the LOOCV (30-fold) method using the non-collinear airborne-quantified C_{ab} and SIF for N assessment from both datasets. Model performance was determined using r^2 and RMSE against the validation data from the 2 years. The best Gaussian process regression model was applied at the tree-crown level to obtain the spatial variability of the tree-based N concentration for the entire 1,200-ha almond orchard using the airborne-quantified SIF and C_{ab} content from FluSAIL RTM inversion. The continuous map of N concentration for each management unit were generated using the Kernel interpolation with barriers (KIB) algorithm (Worton, 1989) in ESRI ArcGIS Desktop (Redlands, CA, USA) to visualize the variability across the entire orchard.

3.3 Results

3.1 Field and laboratory data analyses

Leaf nutrient and pigment content varied widely within the study site and across the two growing seasons. Mean leaf N concentration was 2.07% in 2020 and 2.36% in 2021. The Dualex measured

C_{ab} and Flav were more variable in 2021 than in 2020. Mean C_{ab} was 32.53 units in 2020 and 30.71 units in 2021. Mean Flav was 2.04 units in 2020 and 1.84 units in 2021. Anth range was higher in 2021 than in 2020, with a mean value of 0.24 units compared to 0.19 in 2020. NBI was 16.46 in 2020 and 17.18 in 2021. Ft was highly variable throughout the orchard and was higher in 2021 than in 2020, ranging from 1,648 to 2,751 units in 2020 and from 2,574 to 3,970 units in 2021.

The relationships between leaf steady-state chlorophyll fluorescence quartiles and derived spectral and physiological metrics varied across seasons (Fig. 3.6). Similar linear relationships were observed across seasons for leaf N concentration (Fig. 3.6a), Flav (Fig. 3.6c), NBI (Fig. 3.6d), and leaf spectral indices (Fig. 3.6f-i). By contrast, Anth (Fig. 3.6e) exhibited opposite trends with Ft quartiles between 2020 (negative) and 2021 (positive). Unexpectedly, leaf C_{ab} (Fig. 3.6b) did not exhibit consistent trends relative to leaf Ft quartiles, with generally positive and negative trends for 2020 and 2021 (n.s.), respectively.

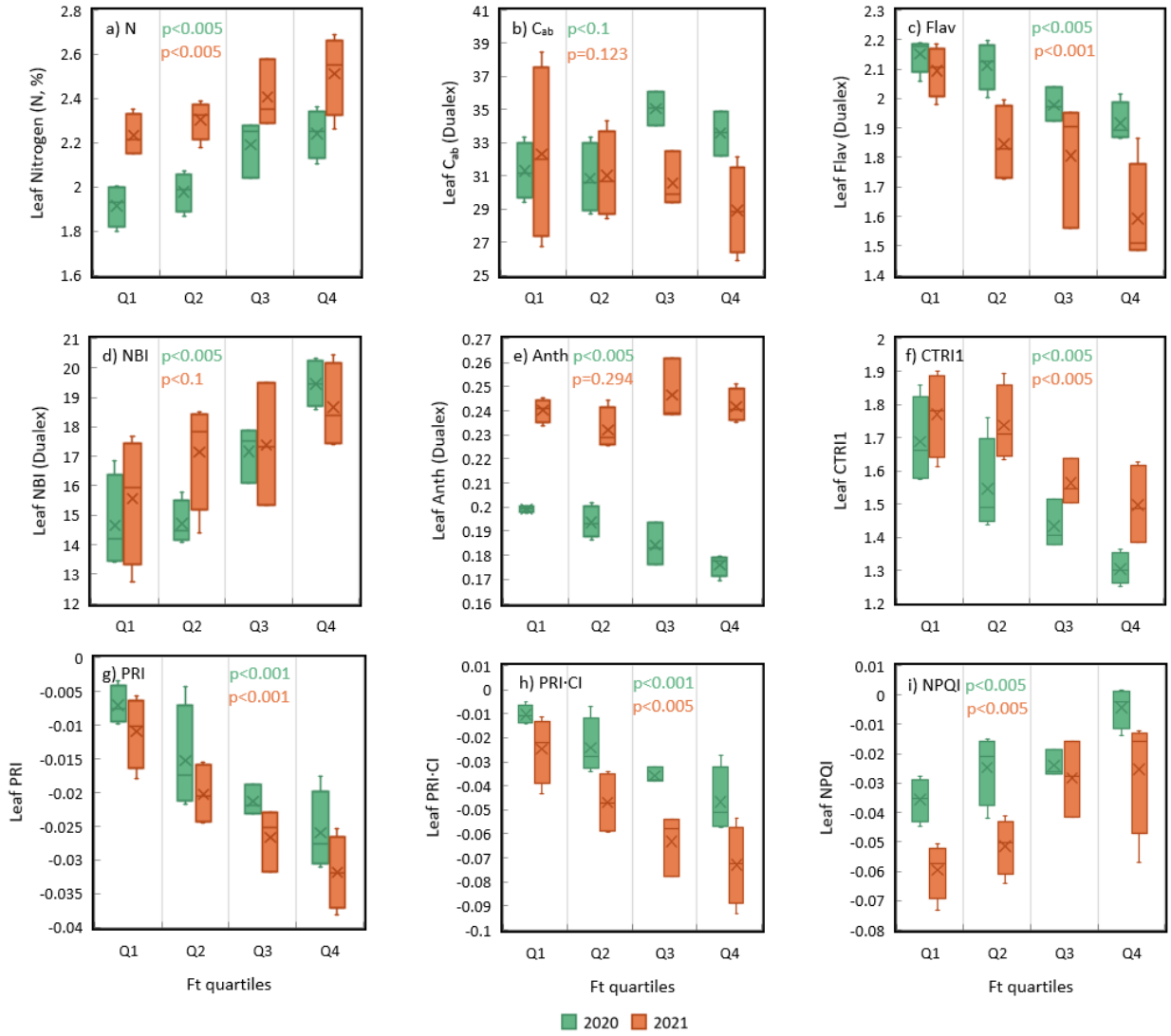

Fig. 3.6. Ranges of variation based on leaf steady-state chlorophyll fluorescence (Ft) quartiles for leaf phenotypes measured at the pre-harvest stage in 2020 (green) and 2021 (orange): a) nitrogen concentration, b) chlorophyll a+b (C_{ab}), c) flavonoid (Flav), d) Nitrogen Balance Index (NBI), e) anthocyanins (Anth), f) CTRI1, g) PRI, h) PRI·CI, and i) NPQI. The line through the box and marker 'x' refer to the median and mean value, respectively.

In general, leaf measurements were correlated with each other across years (Fig. 3.7). Chlorophyll content and leaf N were strongly correlated in 2020 ($r^2 = 0.60$, p-value < 0.005, Fig. 3.7a). However, this correlation was not statistically significant in 2021 ($r^2 = 0.04$, n.s.). Leaf N was more consistently correlated with Dualex-measured NBI (Fig. 3.7b) for both years ($r^2 = 0.68$ for 2020

and r^2 = 0.64 for 2021; *p*-values < 0.005), since the index calculation incorporates both chlorophyll and flavonoids. Leaf PRI (related to xanthophyll composition changes) was also correlated with leaf N across seasons (r^2 = 0.49 in 2020 and r^2 = 0.58 in 2021; *p*-values < 0.005, Fig. 3.7c) as was Ft (r^2 = 0.54 in 2020 and r^2 = 0.52 in 2021; *p*-values < 0.005, Fig. 3.7d). Leaf fluorescence (Fig. 3.7d) was strongly correlated with N when using combined 2-year data (r^2 = 0.74, *p*-value < 0.005), outperforming the rest of the leaf traits (e.g., r^2 = 0.50 for PRI and NBI; *p*-values < 0.005).

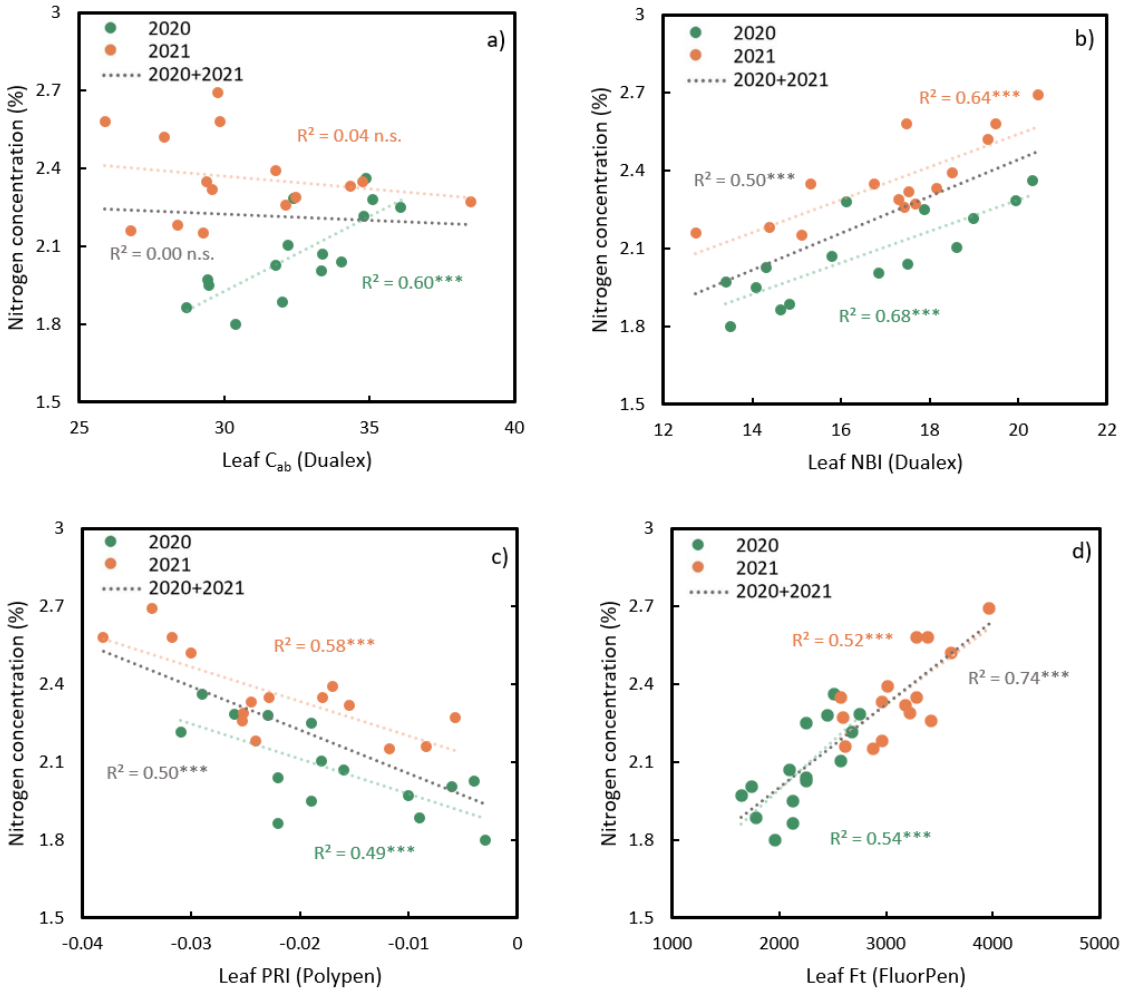

Fig. 3.7. Relationships between leaf N concentration (%) and a) leaf chlorophyll content, b) Nitrogen Balance Index (NBI), c) photochemical reflectance index (PRI), and d) steady-state chlorophyll fluorescence (Ft). Green and orange represent data in 2020 and 2021, respectively. Grey is used to represent correlation when combining data of 2 years. **p*-value < 0.05; ***p*-value < 0.01; ****p*-value < 0.005; n.s. = not significant.

3.2 Narrow-band indices calculated from airborne hyperspectral imagery

Relationships between narrow-band reflectance indices, airborne SIF, and field-based leaf measurements are summarized in Table 3.3. The results present a wide range of correlation and significance levels between leaf physiological measurements and indicators of canopy structure, pigments, airborne-quantified fluorescence, and CWSI temperature-based stress indicator. Airborne-quantified SIF (Fig. 3.8a) was significantly correlated with Ft in both 2020 (r^2 = 0.73, *p*-value < 0.005) and 2021 (r^2 = 0.30, *p*-value < 0.05). The relationship was stronger when combining datasets across 2 years (r^2 = 0.77, *p*-value < 0.005; shown by the grey dashed line in Fig. 3.8). SIF was also significantly correlated with leaf N (r^2 = 0.60 in 2020 and 0.55 in 2021, *p*-values < 0.005), and the relationships remained strong when combining data from both years (r^2 = 0.74, *p*-value < 0 .005, Fig. 3.8b). Strong correlations were also evident between SIF and leaf NBI (r^2 = 0.46 and 0.67, *p*-values < 0.01) in 2020 and 2021, respectively. Fluorescence, as a proxy of photosynthesis, both at the leaf (Fig. 3.7d) and canopy levels (Fig. 3.8b), achieved steady and strong relationships with leaf N (r^2 = 0.74, *p*-value < 0.005).

Hyperspectral indices related to vegetation structure (e.g., NDVI) and pigment concentration (e.g., MCARI) were generally correlated with leaf chlorophyll measured by Dualex in 2020, but not in 2021 (Table 3.3). This pattern was reversed for leaf NBI, where canopy structure (e.g., EVI) and pigment indices (e.g., MCARI) were more correlated in 2021 than in 2020. Leaf N was more strongly related to pigment indices (i.e., MCARI and CTRI1, Figs. 9b and 9c) than structural indices (i.e., NDVI and EVI) in both years. These strong relationships were not always consistent over 2 years, as illustrated in Table 3.3. For example, the chlorophyll index TCARI/OSAVI was unable to capture the existing N variability in 2021 (r^2 = 0, n.s.) as it did in 2020 (r^2 = 0.57, *p*-value < 0.01).

Some pigment indices in Table 3.3 stand out in terms of their high correlations with N for both years. For example, MCARI had an r^2 of 0.61 and 0.48 (p-values < 0.005, Fig. 3.9b) in 2020 and 2021, respectively. PRI_{515} (PRI index using reference band at 515 nm to minimize structural effects) (Stagakis *et al.*, 2012, Zarco-Tejada *et al.*, 2012, Hernández-Clemente *et al.*, 2011) was superior to PRI (at 570 nm) in both 2020 and 2021(Fig. 3.9d).

Many structural and pigment indices showed inconsistent trends across seasons, as shown in Fig. 3.9 and Table 3.3. When looking at data from the 2 years combined, no variables from Fig. 3.9 were significantly correlated with leaf N. NDVI had relatively weak associations with leaf N in each year throughout this heterogeneous orchard. By contrast, airborne SIF calculated from the illuminated crown pixels was consistently related to leaf N across years (Fig. 3.8). CWSI was not consistently correlated with leaf N or pigment content in either year (Table 3.3).

Table 3.3. Coefficients of determination (r^2) for the intercorrelations among standard indices at canopy level from the same 15 study plots in two consecutive years and leaf N concentration (%), Dualex-derived leaf chlorophyll content (C_{ab}), nitrogen balance index (NBI), and steady-state chlorophyll fluorescence (Ft) measured with FluorPen.

	N (%)		**C_{ab}**		**NBI**		**Ft**	
	2020	**2021**	**2020**	**2021**	**2020**	**2021**	**2020**	**2021**
Structural indices								
NDVI	0.25*	0.13	0.49***	0.10	0.07	0.12	0.04	0.05
EVI	0.37**	0.29**	0.56***	0.01	0.14	0.43***	0.07	0.17
MCARI2	0.40**	0.28**	0.58***	0.03	0.16	0.36**	0.09	0.15
RDVI	0.36**	0.25*	0.58***	0.01	0.15	0.36**	0.07	0.13
OSAVI	0.34**	0.22*	0.57***	0.03	0.13	0.29**	0.06	0.10
Chlorophyll a+b indices								
MCARI	0.61***	0.48***	0.54***	0.00	0.55***	0.39**	0.44***	0.31**
TCARI/OSAVI	0.57***	0.00	0.15	0.04	0.46***	0.00	0.48***	0.01
NPQI	0.38**	0.00	0.37**	0.12	0.39**	0.00	0.36**	0.05
PSSRa	0.24*	0.15	0.49***	0.08	0.08	0.16	0.04	0.06
PSSRb	0.14	0.12	0.43***	0.06	0.03	0.14	0.01	0.05
PSSRc	0.23*	0.16	0.58***	0.02	0.12	0.21*	0.02	0.05
SIPI	0.17	0.05	0.37**	0.16	0.02	0.03	0.02	0.02
CTRI1	0.61***	0.52***	0.35**	0.03	0.76***	0.51***	0.45***	0.18
Indices calculated in the green region								
PRI	0.10	0.27**	0.01	0.13	0.24*	0.36**	0.10	0.08
PRI_{515}	0.69***	0.47***	0.61***	0.11	0.43***	0.38**	0.33**	0.25*
PRI·CI	0.13	0.18	0.49***	0.15	0.03	0.21*	0.00	0.05
Fluorescence quantification								
SIF	0.60***	0.55***	0.28**	0.00	0.46***	0.67***	0.73***	0.30**
Canopy temperature								
CWSI	0.05	0.03	0.00	0.23*	0.31**	0.01	0.10	0.03

*p-value < 0.1; **p-value < 0.05; ***p-value < 0.01.

C_{ab}: Chlorophyll $a+b$ content; NBI: Nitrogen Balance Index; Ft: steady-state chlorophyll fluorescence.

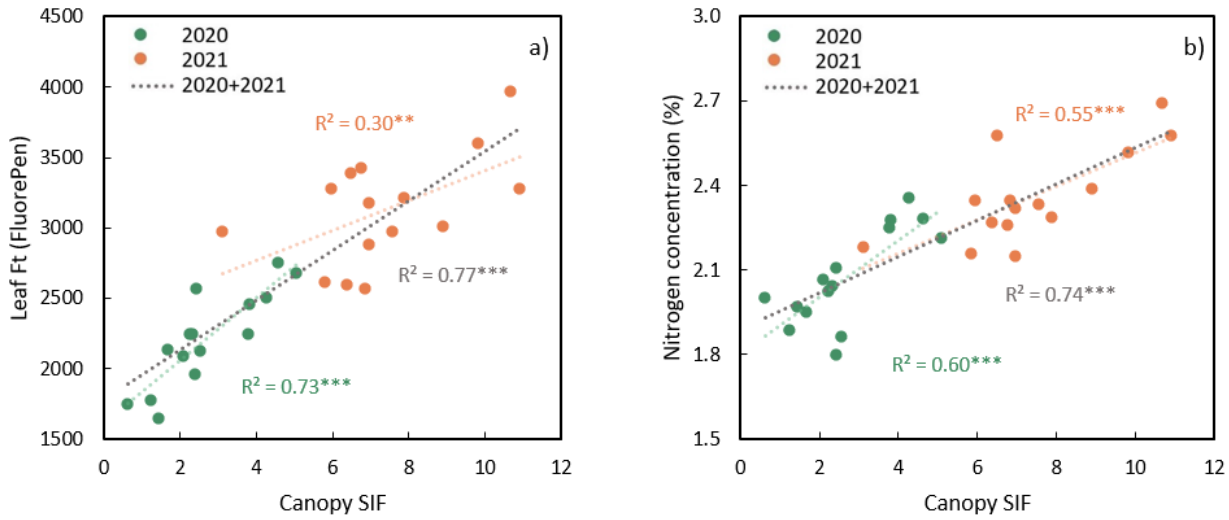

Fig. 3.8. Relationships between canopy SIF and a) leaf steady-state chlorophyll fluorescence (Ft) and b) leaf N concentration (%) in 2020 (green), 2021 (orange), and the combined years (grey). **p*-value < 0.5; ***p*-value < 0.05; ****p*-value < 0.005.

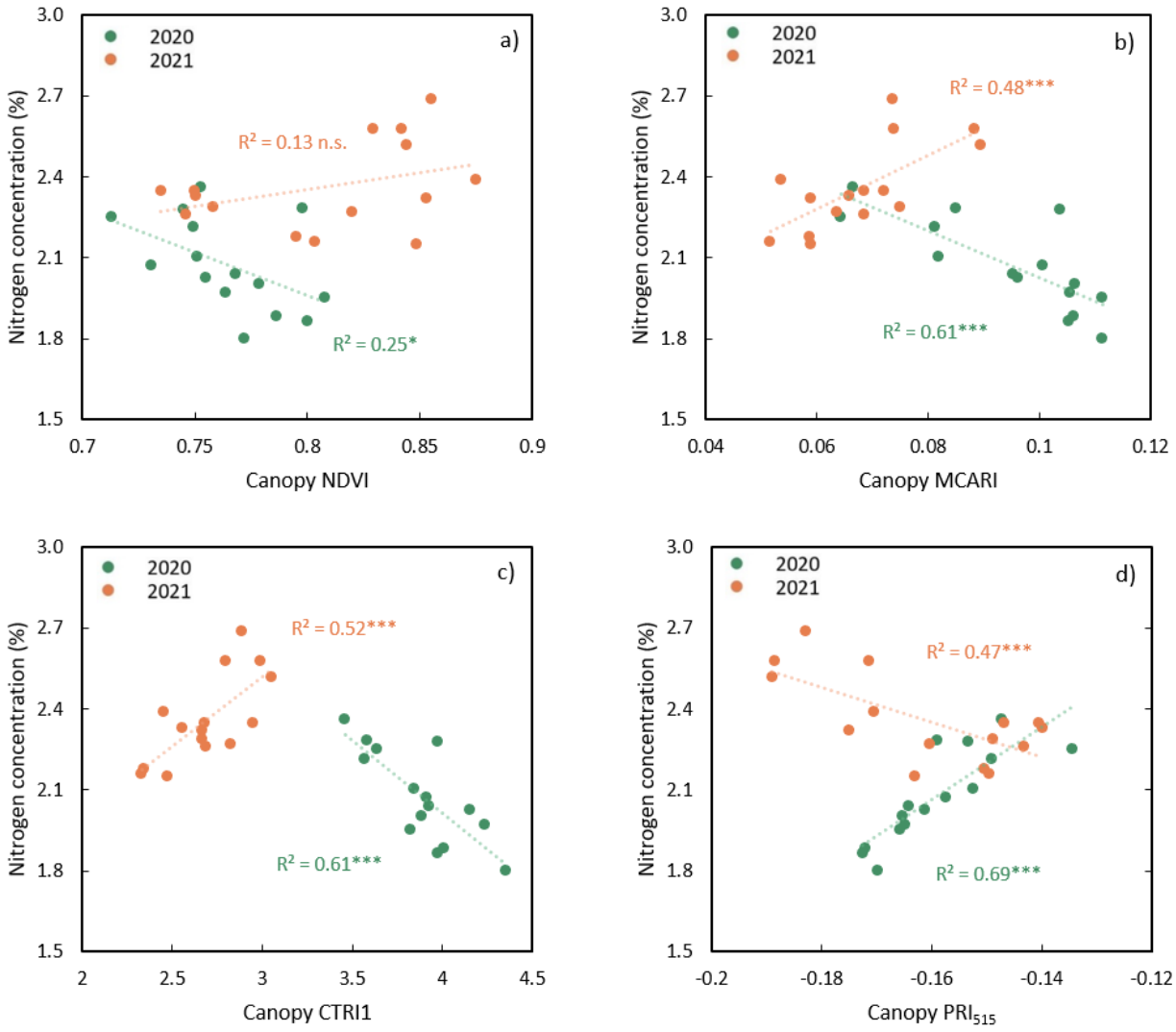

Fig. 3.9. Leaf N against a) NDVI, b) MCARI, c) CTRI1, and d) PRI_{515} calculated from hyperspectral imagery acquired in 2020 (green) and 2021 (orange). *p-value < 0.05; **p-value < 0.01; ***p-value < 0.005; n.s. = not significant.

3.3 Plant trait retrieval from the FluSAIL radiative transfer model

Modelled reflectance spectra from FluSAIL showed close agreement with observed spectra extracted from pure tree crown vegetation pixels in airborne hyperspectral imagery, yielding average RMSE values of 0.008 and 0.007 for 2020 and 2021, respectively. Fig. 3.10 illustrates a simulated and observed spectra as well as a range of simulated spectra from the FluSAIL LUT.

In 2020, leaf C_{ab} from model inversion was strongly correlated to both the Dualex chlorophyll measurement (r^2 = 0.66, p-value < 0.001) and leaf N (r^2 = 0.73, p-value < 0.001). As with the hyperspectral indices, no model-derived measures were significantly correlated with Dualex chlorophyll in 2021 (Table 3.4). In addition to C_{ab}, other pigments (i.e., C_{car} and C_x) also presented significant relationships with leaf N.

C_x, which is sensitive to the de-epoxidation state of the xanthophyll cycle, was significantly correlated with canopy PRI_{515} (r^2 = 0.68 and 0.60 in 2020 and 2021, p-values < 0.001) and with leaf N (r^2 = 0.61 and 0.62 in 2020 and 2021, p-values < 0.001). C_{ab} was also closely related to canopy PRI_{515} (r^2 = 0.80, p-value < 0.001) and SIF (r^2 = 0.51, p-value < 0.005). No significant relationship was detected between the retrieved LAI and leaf N throughout the orchard across years. These results suggest that pigment content and N were highly correlated with biochemical constituents and SIF but showed little effects on the crown structure.

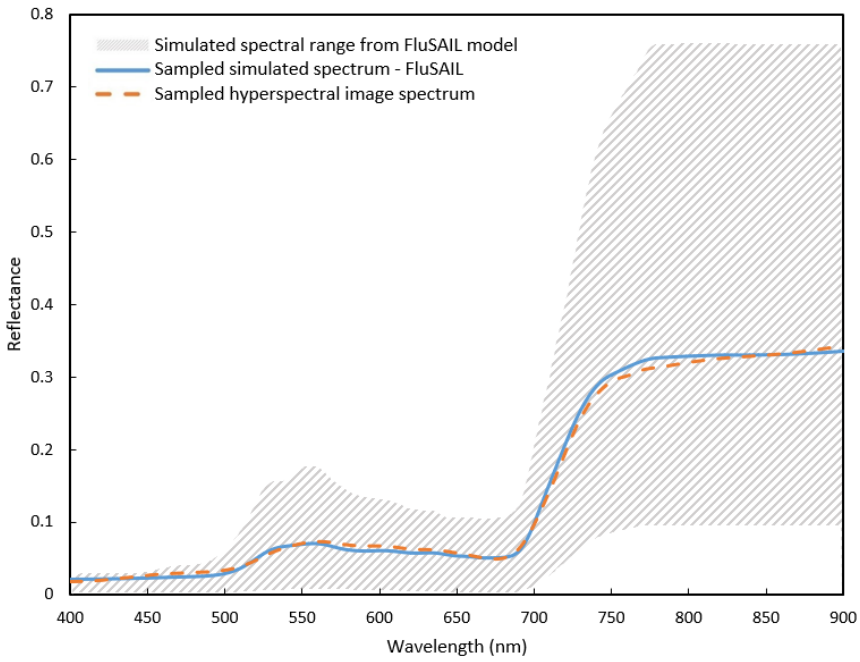

Fig. 3.10. Comparison of the average hyperspectral image spectrum (orange dashed line) and the corresponding spectrum obtained from the FluSAIL model inversion (blue solid line) for one monitored plot. The simulated FluSAIL spectral range is shown in the shaded grey area.

Table 3.4. Coefficients of determination (r^2) for correlations among model-derived estimates from the same 15 study plots in two consecutive years, including leaf chlorophyll a+b (C_{ab}), carotenoids (C_{car}), anthocyanin (Anth), dry matter content (C_{dm}), photochemical reflectance parameter (C_x), leaf area index (LAI), measured leaf N concentration (%), Dualex-measured chlorophyll content, canopy SIF, and canopy photochemical reflectance index (PRI_{515}).

Estimated parameter	N (%)		Leaf C_{ab}		Canopy SIF		Canopy PRI_{515}	
	2020	2021	2020	2021	2020	2021	2020	2021
C_{ab} (µg/cm^2)	0.73***	0.66***	0.66***	0.10	0.51**	0.52**	0.80***	0.82***
C_{car} (µg/cm^2)	0.75***	0.56**	0.65***	0.15	0.56**	0.43*	0.72***	0.50**
Anth (µg/cm^2)	0.58***	0.09	0.63***	0.00	0.45*	0.04	0.85***	0.00
C_x	0.61***	0.62***	0.50**	0.01	0.54**	0.57**	0.68***	0.60***
C_{dm} (g/cm^2)	0.36*	0.20	0.58**	0.04	0.20	0.31*	0.59***	0.79***
LAI	0.02	0.05	0.02	0.16	0.07	0.06	0.02	0.49**

*p-value < 0.05; **p-value < 0.005; ***p-value < 0.001.

3.4 Leaf N status assessment from the airborne-estimated plant traits and SIF

The final model for leaf N using traits derived from hyperspectral imagery was strongly correlated to field-measured N across years (r^2 = 0.96, p-value < 0.001). FluSAIL-inverted C_{ab} and airborne-derived SIF had the greatest OOB predictor scores, followed by other biochemical constituents (e.g., C_{car} and C_x), as illustrated in Fig. 3.11a. While the structural trait LAI (p-value > 0.1) and the thermal-based water stress indicator CWSI (p-value > 0.05) were not statistically significant predictors of N. VIF analysis revealed that C_{ab} and SIF were not collinear, but other biochemical constituents (C_{car}, C_x, and C_{dm}) were discarded from further analysis with a VIF > 5 (empty bars in Fig. 3.11a). Fig. 3.11b shows that C_{ab} and SIF were the most important predictors of N for both years, yielding r^2 and RMSE of 0.95 and 0.05%, respectively.

When using combined data from both years, the Gaussian regression model using chlorophyll exclusively as a predictor explained 49% (p-value < 0.001) of the variability in N (Fig. 3.12a) across the almond orchard. A Gaussian process regression model including C_{ab} and SIF

considerably increased the performance (r^2 = 0.95, p-value < 0.001, RMSE = 0.05%, Fig. 3.12b). This model with C_{ab} and SIF outperformed any other combination of traits quantified from the hyperspectral imagery for predicting leaf N. As an example, the addition of a structural parameter (LAI) to the model only resulted in a slight increase of 0.02 in r^2 and a 0.01% reduction in RMSE (Fig. 3.12c) but yielded reasonable results when coupled to SIF (r^2 = 0.81, p-value < 0.001, RMSE = 0.1%, Fig. 3.12d). The consistency in the results obtained from the two growing seasons suggests the importance of combining C_{ab} and SIF to assess leaf N status as opposed to standard methods based on individual traits or single vegetation indices, which are generally affected by management practices and the changing growing conditions naturally varying across seasons.

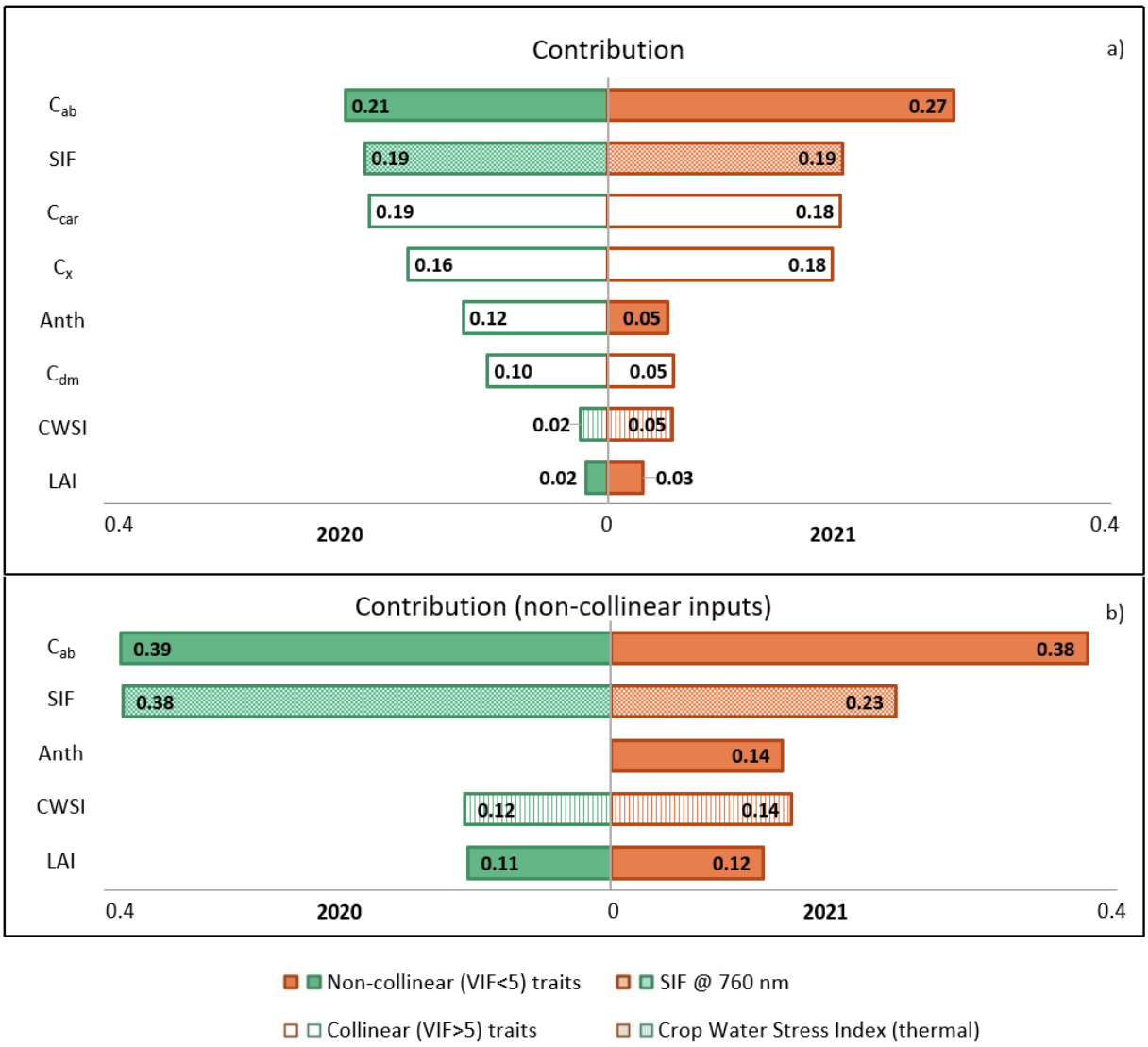

2823 Fig. 3.11. The relative contribution from OOB importance scores of each variable to the predicted
2824 N concentration from a) all plant traits estimated from hyperspectral and thermal imagery and b)
2825 a non-collinear subset of variables (VIF < 5).

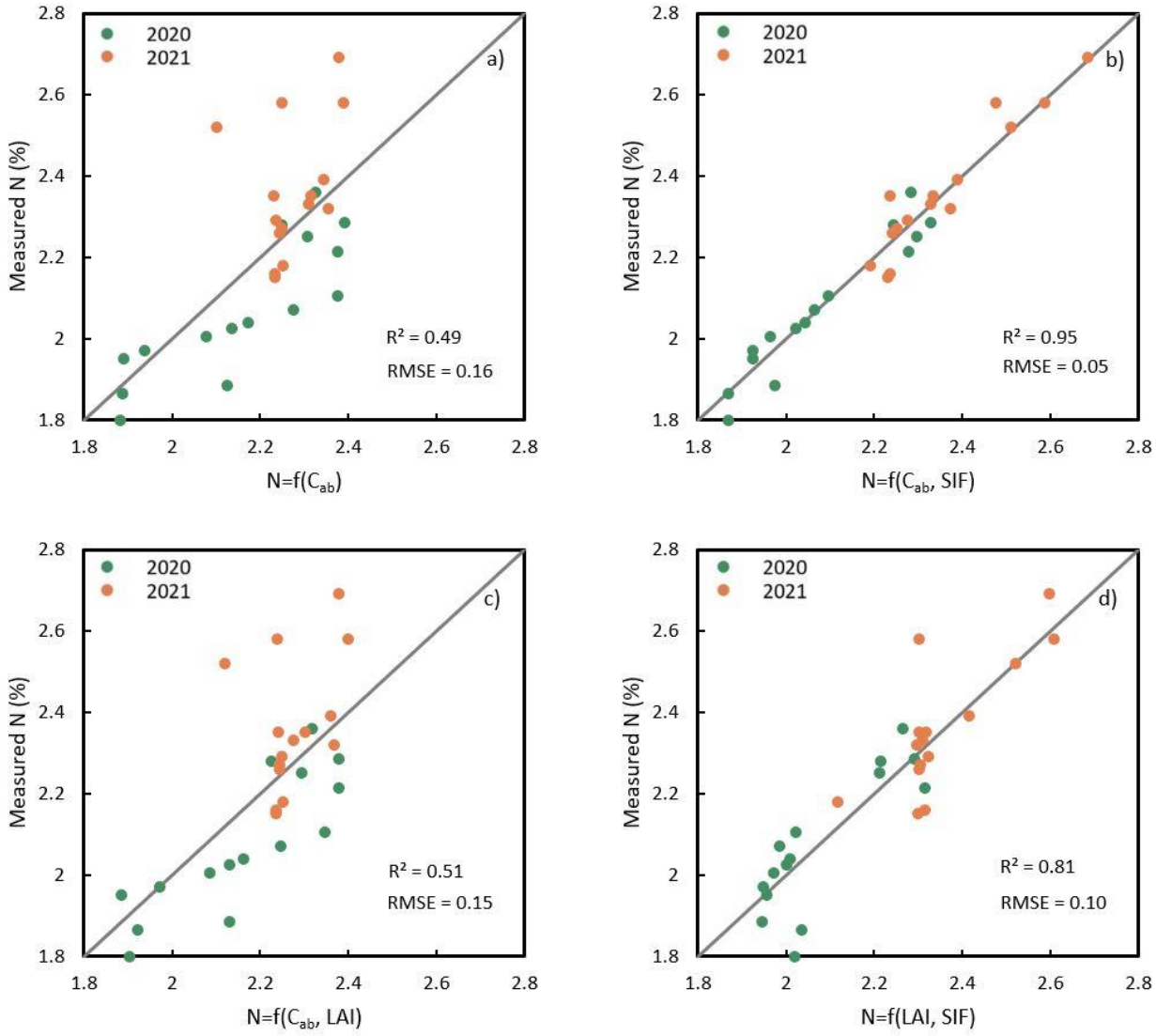

Fig. 3.12. Correlations between leaf N concentration (%) and predicted N using models based on a) chlorophyll a+b content alone, b) chlorophyll a+b content with canopy SIF, c) chlorophyll a+b content with leaf area index (LAI), and d) LAI with canopy SIF. The grey diagonal line is the 1:1 line. All *p*-values < 0.001.

The N prediction map based on a model using C_{ab} and SIF as predictors revealed that tree N was spatially variable across the orchard in 2021 (Fig. 3.13). As expected, the pattern of N predictions integrates trends in chlorophyll *a+b* content and SIF.

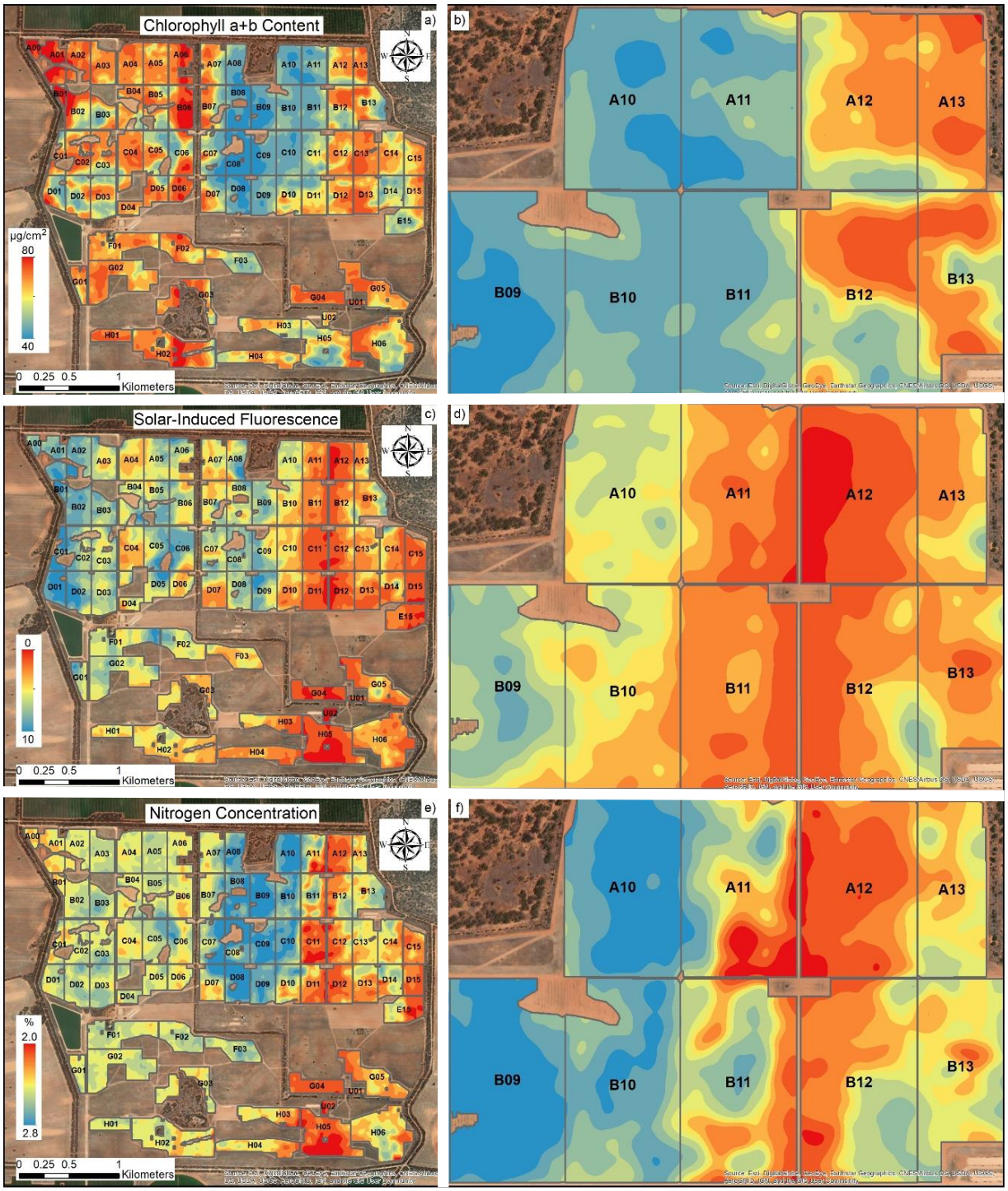

Fig. 3.13. Interpolated map of a) chlorophyll a+b content, c) solar-induced fluorescence, and e) predicted N concentration derived from C_{ab} and SIF in 2021. Right column contains zoomed-in views (b, d and f) of the scenes on the left in the northeast blocks. Block numbers are displayed in the centers.

3.4 Discussion

Previous studies using RS spectroscopy to estimate leaf N have often focused on developing multispectral indices or proxies from leaf or canopy spectra. These methods usually require the development of empirical models relating leaf N to chlorophyll-sensitive vegetation indices (Clevers and Kooistra, 2011, Inoue *et al.*, 2012, Schlemmer *et al.*, 2013, Pancorbo *et al.*, 2021, Fitzgerald *et al.*, 2010, Gabriel *et al.*, 2017) or combinations of bands and indices (Haboudane *et al.*, 2002, Fitzgerald *et al.*, 2010). However, these methods fail to explain leaf N variability in woody crops that are characterized by structurally complex canopies that are managed to increase productivity. In these highly managed orchard canopies, the relationship between structure and nutrient levels is uncoupled; therefore, structural index-based models are not appropriate (Table 3.4). In these orchard canopies, the main drivers for the observed structural changes are the planting density and the fractional cover, which add additional complexity to the use of structural RS vegetation indices as indicators of nutrient levels. In these structurally complex orchards, the spectral indices are heavily affected by the canopy architecture and by structural parameters, such as leaf density, which in turn interact with the illumination and observation geometry within the canopy (Haboudane *et al.*, 2002, Broge and Leblanc, 2001, Wang *et al.*, 2018). Therefore, the variability observed with standard vegetation indices such as NDVI and other structurally sensitive indicators may not necessarily represent the nutrient variability, but instead the heterogeneity due to different tree ages, crown densities, and planting grids that usually coexist in large well-managed orchards such as the one used in this study.

The assessment of the physiological status, independent from the structure and canopy architecture using plant traits through RTM model inversion, is particularly beneficial in the case of structurally complex canopies (Malenovský *et al.*, 2013) when trying to capture the within-field spatial

variability of the leaf nutrient status independent from the structural variability. In this study, we found that plant physiological estimates derived from RTM inversion using VNIR hyperspectral imagery were generally stronger and more consistent predictors of leaf N status than the empirical models built with vegetation indices. In particular, RTM-retrieved pigment C_{ab} was the strongest predictor (Fig. 3.11), consistent with the results of Camino *et al.* (2018a) for wheat. RTM-based carotenoid content and the xanthophyll cycle (C_x) parameter were also more strongly related to leaf N than vegetation indices in our study, as both are involved in light-harvesting regulation that is associated with photosynthetic efficiency (Ruban *et al.*, 1999). For instance, RTM-based chlorophyll *a*+*b* content was strongly correlated with leaf N for both years of study (r^2 = 0.73 in 2020 and 0.66 in 2021, *p*-values < 0.001), whereas the chlorophyll-sensitive index TCARI/OSAVI was not correlated with N in 2021 (r^2 = 0, n.s.), suggesting those indices are not reliable indicators for N assessment across seasons. Spectral indices are greatly affected by management practices and background changes across orchards and years, leading to inconsistencies that may make them inappropriate for operational purposes.

The fact that both model-inverted LAI and structural hyperspectral indices were poorly related to leaf N supports the idea that canopy structure is not driven by nutrient availability in well-managed intensive orchards. As a consequence, it is not surprising that the widely used structural index NDVI was inadequate for predicting leaf N in this context. Ground-based leaf chlorophyll measurements were poorly related to leaf N when leaf N was high in 2021. This is consistent with the results of Jifon *et al.* (2005), who found the relationship between chlorophyll meter readings and leaf N was stronger at low chlorophyll concentrations than at higher chlorophyll concentrations. At high N concentrations, there is a possibility that some N may be allocated to soluble protein rather than pigment-protein complexes (Evans, 1989). And the soluble protein and

pigment complexes in leaves can be imbalanced depending on leaf physical characteristics, plant age, environmental factors, and management practices (Bondada and Syvertsen, 2003, Evans and Poorter, 2001, Syvertsen and Smith Jr, 1984, Syvertsen *et al.*, 1995). In our study, leaf nitrogen balance index was more strongly correlated with leaf N and canopy indices as it incorporated the ratio of a second pigment flavonoid into the calculation. This phenomenon was also observed at the canopy level for both chlorophyll-sensitive vegetation indices and RTM-based pigment concentrations. C_{ab} at the canopy level was more strongly related to leaf N than C_{ab} at the leaf level, which may be attributed to the fact that the field-collected leaf measurements came from lower layers of the tree crown, whereas the imagery captured the upper layers. Our results provide evidence that RTM-based leaf physiological traits provide additional benefits over standard structural indices for assessing leaf N in orchards, particularly when multiple varieties, ages, and management practices coexist within the orchard.

Several studies have shown that SIF derived from sub-meter narrow-band imagery, in which the depth of the oxygen absorption feature can be quantified, is an effective tool for detecting plant stress in precision agriculture (Zarco-Tejada *et al.*, 2012, Calderón *et al.*, 2013, Quemada *et al.*, 2014, Camino *et al.*, 2018b, Camino *et al.*, 2018a, Raya-Sereno *et al.*, 2021). In this study, we also found a strong association between fluorescence and leaf N, consistent with the literature (Corp *et al.*, 2003, Cendrero-Mateo *et al.*, 2016, Schächtl *et al.*, 2005), yielding $r^2 = 0.74$ (p-value < 0.005) over the course of 2 years at both leaf and canopy levels. Airborne-quantified SIF was the second most important predictor of leaf N after C_{ab} and outperformed any other vegetation index or structural and temperature-based plant traits in terms of correlation and consistency across years. When combined with RTM-based traits, SIF significantly improved model performance for predicting leaf N. The model that included C_{ab} and SIF explained 95% of the leaf N variability (p-

value < 0.001), improving upon results obtained with C_{ab} alone (r^2 = 0.49, *p*-value < 0.001) accounting for different plant varieties, ages, planting patterns, water status levels, and fertilizer management practices across 2 years.

CWSI, a thermal canopy water status index, was poorly associated with leaf N and relatively inconsistent across years. Overall, we found no evidence of a relationship between CWSI and leaf N, suggesting that leaf N variability was not driven by water status in this well-managed intensive almond orchard.

3.5 Conclusions

This study demonstrates that leaf N estimation conducted in an almond orchard across 2 years was significantly improved when SIF was included alongside RTM-based leaf chlorophyll *a*+*b* content. Among all spectral plant traits evaluated from hyperspectral imagery, including all RTM-derived leaf biochemical constituents, SIF, and structural and water stress traits, the retrieved leaf chlorophyll *a*+*b* and SIF were the two most important predictors to explain leaf N variability. The model that incorporated both chlorophyll *a*+*b* content and SIF traits explained 95% of the variability in leaf N (*p*-value < 0.001) consistently across 2 years of airborne hyperspectral data collection. Together, these results provide important insights into the quantification of leaf N content in well-managed structurally complex canopies, such as discontinuous tree orchards, demonstrating that traditional vegetation indices and individual plant traits do not sufficiently track leaf N content over well-managed intensive crops typically reaching high N levels.

References

ABRÀMOFF, M. D., MAGALHÃES, P. J. & RAM, S. J. 2004. Image processing with ImageJ. *Biophotonics international,* 11**,** 36-42.

AKINWANDE, M. O., DIKKO, H. G. & SAMSON, A. 2015. Variance inflation factor: as a condition for the inclusion of suppressor variable (s) in regression analysis. *Open Journal of Statistics,* 5**,** 754.

ASAI, W., MICKE, W., KESTER, D. & ROUGH, D. 1996. The evaluation and selection of current varieties; almond production manual, University of California (system). Division of Agriculture and Natural Resources. ANR Publications, California.

ASHRAF, M. & HARRIS, P. J. 2013. Photosynthesis under stressful environments: an overview. *Photosynthetica,* 51**,** 163-190.

BARET, F., HOULÈS, V. & GUERIF, M. 2007. Quantification of plant stress using remote sensing observations and crop models: the case of nitrogen management. *Journal of Experimental Botany,* 58**,** 869-880.

BARNES, J. D., BALAGUER, L., MANRIQUE, E., ELVIRA, S. & DAVISON, A. 1992. A reappraisal of the use of DMSO for the extraction and determination of chlorophylls a and b in lichens and higher plants. *Environmental and Experimental botany,* 32**,** 85-100.

BELLVERT, J., ADELINE, K., BARAM, S., PIERCE, L., SANDEN, B. L. & SMART, D. R. 2018. Monitoring crop evapotranspiration and crop coefficients over an almond and pistachio orchard throughout remote sensing. *Remote Sensing,* 10**,** 2001.

BELWALKAR, A., POBLETE, T., LONGMIRE, A., HORNERO, A., HERNANDEZ-CLEMENTE, R. & ZARCO-TEJADA, P. 2022. Evaluation of SIF retrievals from narrow-band and sub-nanometer airborne hyperspectral imagers flown in tandem: modelling and validation in the context of plant phenotyping. *Remote Sensing of Environment,* 273.

BELWALKAR, A., POBLETE, T., LONGMIRE, A., HORNERO, A. & ZARCO-TEJADA, P. Comparing the Retrieval of Chlorophyll Fluorescence from Two Airborne Hyperspectral Imagers with Different Spectral Resolutions for Plant Phenotyping Studies. 2021 IEEE International Geoscience and Remote Sensing Symposium IGARSS, 2021. IEEE, 5845-5848.

BISWAL, B., JOSHI, P., RAVAL, M. & BISWAL, U. 2011. Photosynthesis, a global sensor of environmental stress in green plants: stress signalling and adaptation. *Current Science***,** 47-56.

BLACKBURN, G. A. 1998. Spectral indices for estimating photosynthetic pigment concentrations: a test using senescent tree leaves. *International Journal of remote sensing,* 19**,** 657-675.

BONDADA, B. R. & SYVERTSEN, J. P. 2003. Leaf chlorophyll, net gas exchange and chloroplast ultrastructure in citrus leaves of different nitrogen status. *Tree Physiology,* 23**,** 553-559.

BREIMAN, L. 2001. Random forests. *Machine learning,* 45**,** 5-32.

BROGE, N. H. & LEBLANC, E. 2001. Comparing prediction power and stability of broadband and hyperspectral vegetation indices for estimation of green leaf area index and canopy chlorophyll density. *Remote sensing of environment,* 76**,** 156-172.

BUCKEE, G. 1994. Determination of total nitrogen in barley, malt and beer by Kjeldahl procedures and the dumas combustion methodcollaborative trial. *Journal of the Institute of Brewing,* 100**,** 57-64.

BULLOCK, D. & ANDERSON, D. 1998. Evaluation of the Minolta SPAD-502 chlorophyll meter for nitrogen management in corn. *Journal of Plant Nutrition,* 21**,** 741-755.

CALDERÓN, R., NAVAS-CORTÉS, J. A., LUCENA, C. & ZARCO-TEJADA, P. J. 2013. High-resolution airborne hyperspectral and thermal imagery for early detection of Verticillium wilt of olive using fluorescence, temperature and narrow-band spectral indices. *Remote Sensing of Environment,* 139**,** 231-245.

CAMINO, C., GONZÁLEZ-DUGO, V., HERNÁNDEZ, P., SILLERO, J. & ZARCO-TEJADA, P. J. 2018a. Improved nitrogen retrievals with airborne-derived fluorescence and plant traits quantified from VNIR-SWIR hyperspectral imagery in the context of precision agriculture. *International journal of applied earth observation and geoinformation,* 70**,** 105-117.

CAMINO, C., ZARCO-TEJADA, P. J. & GONZALEZ-DUGO, V. 2018b. Effects of heterogeneity within tree crowns on airborne-quantified SIF and the CWSI as indicators of water stress in the context of precision agriculture. *Remote Sensing,* 10**,** 604.

CARTER, G. A. 1994. Ratios of leaf reflectances in narrow wavebands as indicators of plant stress. *Int. J. of Remote Sensing,* 15**,** 697-703.

CENDRERO-MATEO, M. P., MORAN, M. S., PAPUGA, S. A., THORP, K., ALONSO, L., MORENO, J., PONCE-CAMPOS, G., RASCHER, U. & WANG, G. 2016. Plant chlorophyll fluorescence: active and passive measurements at canopy and leaf scales with different nitrogen treatments. *Journal of Experimental Botany,* 67**,** 275-286.

CEROVIC, Z. G., GHOZLEN, N. B., MILHADE, C., OBERT, M. L., DEBUISSON, S. B. & MOIGNE, M. L. 2015. Nondestructive diagnostic test for nitrogen nutrition of grapevine (Vitis vinifera L.) based on dualex leaf-clip measurements in the field. *Journal of agricultural and food chemistry,* 63**,** 3669-3680.

CEROVIC, Z. G., MASDOUMIER, G., GHOZLEN, N. B. & LATOUCHE, G. 2012. A new optical leaf-clip meter for simultaneous non-destructive assessment of leaf chlorophyll and epidermal flavonoids. *Physiologia plantarum,* 146**,** 251-260.

CHANG, S. X. & ROBISON, D. J. 2003. Nondestructive and rapid estimation of hardwood foliar nitrogen status using the SPAD-502 chlorophyll meter. *Forest Ecology and Management,* 181**,** 331-338.

CHAPMAN, S. C. & BARRETO, H. J. 1997. Using a chlorophyll meter to estimate specific leaf nitrogen of tropical maize during vegetative growth. *Agronomy Journal,* 89**,** 557-562.

CHENG, L. 2003. Xanthophyll cycle pool size and composition in relation to the nitrogen content of apple leaves. *Journal of Experimental Botany,* 54**,** 385-393.

CLEVERS, J. G. & GITELSON, A. A. 2013. Remote estimation of crop and grass chlorophyll and nitrogen content using red-edge bands on Sentinel-2 and-3. *International Journal of Applied Earth Observation and Geoinformation,* 23**,** 344-351.

CLEVERS, J. G. & KOOISTRA, L. 2011. Using hyperspectral remote sensing data for retrieving canopy chlorophyll and nitrogen content. *IEEE Journal of selected topics in applied earth observations and remote sensing,* 5**,** 574-583.

COMBAL, B., BARET, F., WEISS, M., TRUBUIL, A., MACE, D., PRAGNERE, A., MYNENI, R., KNYAZIKHIN, Y. & WANG, L. 2003. Retrieval of canopy biophysical variables from bidirectional reflectance: Using prior information to solve the ill-posed inverse problem. *Remote sensing of environment,* 84**,** 1-15.

CONANT, R. T., BERDANIER, A. B. & GRACE, P. R. 2013. Patterns and trends in nitrogen use and nitrogen recovery efficiency in world agriculture. *Global Biogeochemical Cycles,* 27**,** 558-566.

CORP, L. A., MCMURTREY, J. E., MIDDLETON, E. M., MULCHI, C. L., CHAPPELLE, E. W. & DAUGHTRY, C. S. 2003. Fluorescence sensing systems: In vivo detection of biophysical variations in field corn due to nitrogen supply. *Remote sensing of environment,* 86**,** 470-479.

CUMMINGS, C., MIAO, Y., PAIAO, G. D., KANG, S. & FERNÁNDEZ, F. G. 2021. Corn nitrogen status diagnosis with an innovative multi-parameter crop circle phenom sensing system. *Remote Sensing,* 13**,** 401.

DAUGHTRY, C. S., WALTHALL, C., KIM, M., DE COLSTOUN, E. B. & MCMURTREY III, J. 2000. Estimating corn leaf chlorophyll concentration from leaf and canopy reflectance. *Remote sensing of Environment,* 74**,** 229-239.

DEMMIG, B., WINTER, K., KRÜGER, A. & CZYGAN, F.-C. 1987. Photoinhibition and zeaxanthin formation in intact leaves: a possible role of the xanthophyll cycle in the dissipation of excess light energy. *Plant physiology,* 84**,** 218-224.

DONG, R., MIAO, Y., WANG, X., CHEN, Z., YUAN, F., ZHANG, W. & LI, H. 2020. Estimating plant nitrogen concentration of maize using a leaf fluorescence sensor across growth stages. *Remote Sensing,* 12**,** 1139.

DUMAS, J. B. A. 1831. Procedes de l'analyse Organic. *Annales de Chimie et de Physique (Annals of Chemistry and of Physics),* 247**,** 198-213.

ETHERIDGE, R., PESTI, G. & FOSTER, E. 1998. A comparison of nitrogen values obtained utilizing the Kjeldahl nitrogen and Dumas combustion methodologies (Leco CNS 2000) on samples typical of an animal nutrition analytical laboratory. *Animal Feed Science and Technology,* 73**,** 21-28.

EVANS, J. 1989. Photosynthesis and nitrogen relationships in leaves of C 3 plants. *Oecologia,* 78**,** 9-19.

EVANS, J. & POORTER, H. 2001. Photosynthetic acclimation of plants to growth irradiance: the relative importance of specific leaf area and nitrogen partitioning in maximizing carbon gain. *Plant, cell & environment,* 24**,** 755-767.

FILELLA, I., SERRANO, L., SERRA, J. & PENUELAS, J. 1995. Evaluating wheat nitrogen status with canopy reflectance indices and discriminant analysis. *Crop Science,* 35**,** 1400-1405.

FITZGERALD, G., RODRIGUEZ, D., CHRISTENSEN, L., BELFORD, R., SADRAS, V. & CLARKE, T. 2006. Spectral and thermal sensing for nitrogen and water status in rainfed and irrigated wheat environments. *Precision Agriculture,* 7**,** 233-248.

FITZGERALD, G., RODRIGUEZ, D. & O'LEARY, G. 2010. Measuring and predicting canopy nitrogen nutrition in wheat using a spectral index—The canopy chlorophyll content index (CCCI). *Field Crops Research,* 116**,** 318-324.

FLOWERS, M., WEISZ, R. & HEINIGER, R. 2003. Quantitative approaches for using color infrared photography for assessing in-season nitrogen status in winter wheat. *Agronomy journal,* 95**,** 1189-1200.

GABRIEL, J. L., ZARCO-TEJADA, P. J., LÓPEZ-HERRERA, P. J., PÉREZ-MARTÍN, E., ALONSO-AYUSO, M. & QUEMADA, M. 2017. Airborne and ground level sensors for monitoring nitrogen status in a maize crop. *Biosystems Engineering,* 160**,** 124-133.

GAMON, J., PENUELAS, J. & FIELD, C. 1992. A narrow-waveband spectral index that tracks diurnal changes in photosynthetic efficiency. *Remote Sensing of environment,* 41**,** 35-44.

GARETH, J., DANIELA, W., TREVOR, H. & ROBERT, T. 2013. *An introduction to statistical learning: with applications in R,* Spinger.

GARRITY, S. R., EITEL, J. U. & VIERLING, L. A. 2011. Disentangling the relationships between plant pigments and the photochemical reflectance index reveals a new approach for remote estimation of carotenoid content. *Remote Sensing of Environment,* 115**,** 628-635.

GENTY, B., BRIANTAIS, J.-M. & BAKER, N. R. 1989. The relationship between the quantum yield of photosynthetic electron transport and quenching of chlorophyll fluorescence. *Biochimica et Biophysica Acta (BBA)-General Subjects,* 990**,** 87-92.

GILMORE, A. M. 1997. Mechanistic aspects of xanthophyll cycle-dependent photoprotection in higher plant chloroplasts and leaves. *Physiologia Plantarum,* 99**,** 197-209.

GITELSON, A. A., GRITZ, Y. & MERZLYAK, M. N. 2003. Relationships between leaf chlorophyll content and spectral reflectance and algorithms for non-destructive chlorophyll assessment in higher plant leaves. *Journal of plant physiology,* 160**,** 271-282.

GITELSON, A. A., MERZLYAK, M. N. & LICHTENTHALER, H. K. 1996. Detection of red edge position and chlorophyll content by reflectance measurements near 700 nm. *Journal of plant physiology,* 148**,** 501-508.

GNYP, M. L., MIAO, Y., YUAN, F., USTIN, S. L., YU, K., YAO, Y., HUANG, S. & BARETH, G. 2014. Hyperspectral canopy sensing of paddy rice aboveground biomass at different growth stages. *Field Crops Research,* 155**,** 42-55.

GUEYMARD, C. A. 1995. *SMARTS2: a simple model of the atmospheric radiative transfer of sunshine: algorithms and performance assessment,* Florida Solar Energy Center Cocoa, FL.

GUEYMARD, C. A. 2001. Parameterized transmittance model for direct beam and circumsolar spectral irradiance. *Solar Energy,* 71**,** 325-346.

GUEYMARD, C. A., MYERS, D. & EMERY, K. 2002. Proposed reference irradiance spectra for solar energy systems testing. *Solar energy,* 73**,** 443-467.

HABOUDANE, D., MILLER, J. R., PATTEY, E., ZARCO-TEJADA, P. J. & STRACHAN, I. B. 2004. Hyperspectral vegetation indices and novel algorithms for predicting green LAI of crop canopies:

Modeling and validation in the context of precision agriculture. *Remote sensing of environment,* 90**,** 337-352.

HABOUDANE, D., MILLER, J. R., TREMBLAY, N., ZARCO-TEJADA, P. J. & DEXTRAZE, L. 2002. Integrated narrow-band vegetation indices for prediction of crop chlorophyll content for application to precision agriculture. *Remote sensing of environment,* 81**,** 416-426.

HASSOUN, M. H. 1995. *Fundamentals of artificial neural networks*, MIT press.

HERNÁNDEZ-CLEMENTE, R., NAVARRO-CERRILLO, R. M., SUÁREZ, L., MORALES, F. & ZARCO-TEJADA, P. J. 2011. Assessing structural effects on PRI for stress detection in conifer forests. *Remote Sensing of Environment,* 115**,** 2360-2375.

HILL, S., STEPHENSON, D. & TAYLOR, B. 1985. Almond pollination studies: pollen production and viability, flower emergence and cross-pollination tests. *Australian Journal of Experimental Agriculture,* 25**,** 697-704.

HUANG, Z.-A., JIANG, D.-A., YANG, Y., SUN, J.-W. & JIN, S.-H. 2004. Effects of nitrogen deficiency on gas exchange, chlorophyll fluorescence, and antioxidant enzymes in leaves of rice plants. *Photosynthetica,* 42**,** 357-364.

IDSO, S., JACKSON, R., PINTER JR, P., REGINATO, R. & HATFIELD, J. 1981. Normalizing the stress-degree-day parameter for environmental variability. *Agricultural meteorology,* 24**,** 45-55.

INOUE, Y., SAKAIYA, E., ZHU, Y. & TAKAHASHI, W. 2012. Diagnostic mapping of canopy nitrogen content in rice based on hyperspectral measurements. *Remote Sensing of Environment,* 126**,** 210-221.

JACKSON, R. D., IDSO, S., REGINATO, R. & PINTER JR, P. 1981. Canopy temperature as a crop water stress indicator. *Water resources research,* 17**,** 1133-1138.

JACQUEMOUD, S., VERHOEF, W., BARET, F., BACOUR, C., ZARCO-TEJADA, P. J., ASNER, G. P., FRANÇOIS, C. & USTIN, S. L. 2009. PROSPECT+ SAIL models: A review of use for vegetation characterization. *Remote sensing of environment,* 113**,** S56-S66.

JIFON, J. L., SYVERTSEN, J. P. & WHALEY, E. 2005. Growth environment and leaf anatomy affect nondestructive estimates of chlorophyll and nitrogen in Citrus sp. leaves. *Journal of the American Society for Horticultural Science,* 130**,** 152-158.

JONGSCHAAP, R. E. & BOOIJ, R. 2004. Spectral measurements at different spatial scales in potato: relating leaf, plant and canopy nitrogen status. *International Journal of Applied Earth Observation and Geoinformation,* 5**,** 205-218.

KIMES, D. S., KNYAZIKHIN, Y., PRIVETTE, J., ABUELGASIM, A. & GAO, F. 2000. Inversion methods for physically-based models. *Remote Sensing Reviews,* 18**,** 381-439.

KJELDAHL, J. 1883. A new method for the estimation of nitrogen in organic compounds. *Z. Anal. Chem,* 22**,** 366.

KRAUSE, G. & WEIS, E. 1991. Chlorophyll fluorescence and photosynthesis: the basics. *Annual review of plant biology,* 42**,** 313-349.

LI, F., MIAO, Y., FENG, G., YUAN, F., YUE, S., GAO, X., LIU, Y., LIU, B., USTIN, S. L. & CHEN, X. 2014. Improving estimation of summer maize nitrogen status with red edge-based spectral vegetation indices. *Field Crops Research,* 157**,** 111-123.

LI, H., ZHANG, Y., LEI, Y., ANTONIUK, V. & HU, C. 2020. Evaluating different non-destructive estimation methods for winter wheat (Triticum aestivum L.) nitrogen status based on canopy spectrum. *Remote Sensing,* 12**,** 95.

LIU, H. Q. & HUETE, A. 1995. A feedback based modification of the NDVI to minimize canopy background and atmospheric noise. *IEEE transactions on geoscience and remote sensing,* 33**,** 457-465.

LU, C. & ZHANG, J. 2000. Photosynthetic CO2 assimilation, chlorophyll fluorescence and photoinhibition as affected by nitrogen deficiency in maize plants. *Plant Science,* 151**,** 135-143.

MAIER, S. W., GÜNTHER, K. P. & STELLMES, M. 2004. Sun-induced fluorescence: A new tool for precision farming. *Digital imaging and spectral techniques: Applications to precision agriculture and crop physiology,* 66**,** 207-222.

MALENOVSKÝ, Z., HOMOLOVÁ, L., ZURITA-MILLA, R., LUKEŠ, P., KAPLAN, V., HANUŠ, J., GASTELLU-ETCHEGORRY, J.-P. & SCHAEPMAN, M. E. 2013. Retrieval of spruce leaf chlorophyll content from airborne image data using continuum removal and radiative transfer. *Remote Sensing of Environment,* 131**,** 85-102.

MANNA, M., SWARUP, A., WANJARI, R., RAVANKAR, H., MISHRA, B., SAHA, M., SINGH, Y., SAHI, D. & SARAP, P. 2005. Long-term effect of fertilizer and manure application on soil organic carbon storage, soil quality and yield sustainability under sub-humid and semi-arid tropical India. *Field crops research,* 93**,** 264-280.

MATSON, P. A., NAYLOR, R. & ORTIZ-MONASTERIO, I. 1998. Integration of environmental, agronomic, and economic aspects of fertilizer management. *Science,* 280**,** 112-115.

MATSUSHITA, B., YANG, W., CHEN, J., ONDA, Y. & QIU, G. 2007. Sensitivity of the enhanced vegetation index (EVI) and normalized difference vegetation index (NDVI) to topographic effects: a case study in high-density cypress forest. *Sensors,* 7**,** 2636-2651.

MAXWELL, K. & JOHNSON, G. N. 2000. Chlorophyll fluorescence—a practical guide. *Journal of experimental botany,* 51**,** 659-668.

MIDDLETON, E. M., HUEMMRICH, K. F., CHENG, Y.-B. & MARGOLIS, H. A. 2016. 12 spectral bioindicators of photosynthetic efficiency and vegetation stress. *Hyperspectral remote sensing of vegetation.* CRC Press.

MOHAMMED, G. H., BINDER, W. & GILLIES, S. 1995. Chlorophyll fluorescence: a review of its practical forestry applications and instrumentation. *Scandinavian Journal of Forest Research,* 10**,** 383-410.

MOHAMMED, G. H., COLOMBO, R., MIDDLETON, E. M., RASCHER, U., VAN DER TOL, C., NEDBAL, L., GOULAS, Y., PÉREZ-PRIEGO, O., DAMM, A. & MERONI, M. 2019. Remote sensing of solar-induced chlorophyll fluorescence (SIF) in vegetation: 50 years of progress. *Remote sensing of environment,* 231**,** 111177.

MURCHIE, E. H. & LAWSON, T. 2013. Chlorophyll fluorescence analysis: a guide to good practice and understanding some new applications. *Journal of experimental botany,* 64**,** 3983-3998.

NAGESWARA RAO, R., TALWAR, H. & WRIGHT, G. 2001. Rapid assessment of specific leaf area and leaf nitrogen in peanut (Arachis hypogaea L.) using a chlorophyll meter. *Journal of Agronomy and Crop Science,* 186**,** 175-182.

NGUY-ROBERTSON, A., GITELSON, A., PENG, Y., VIÑA, A., ARKEBAUER, T. & RUNDQUIST, D. 2012. Green leaf area index estimation in maize and soybean: Combining vegetation indices to achieve maximal sensitivity. *Agronomy Journal,* 104**,** 1336-1347.

NIBLACK, W. 1985. *An introduction to digital image processing*, Strandberg Publishing Company.

NIGON, T. J., YANG, C., DIAS PAIAO, G., MULLA, D. J., KNIGHT, J. F. & FERNÁNDEZ, F. G. 2020. Prediction of Early Season Nitrogen Uptake in Maize Using High-Resolution Aerial Hyperspectral Imagery. *Remote Sensing,* 12**,** 1234.

NIYOGI, K. K., BJÖRKMAN, O. & GROSSMAN, A. R. 1997. The roles of specific xanthophylls in photoprotection. *Proceedings of the National Academy of Sciences,* 94**,** 14162-14167.

O'BRIEN, R. M. 2007. A caution regarding rules of thumb for variance inflation factors. *Quality & quantity,* 41**,** 673-690.

PADILLA, F. M., DE SOUZA, R., PEÑA-FLEITAS, M. T., GALLARDO, M., GIMENEZ, C. & THOMPSON, R. B. 2018. Different responses of various chlorophyll meters to increasing nitrogen supply in sweet pepper. *Frontiers in plant science,* 9**,** 1752.

PANCORBO, J., CAMINO, C., ALONSO-AYUSO, M., RAYA-SERENO, M., GONZALEZ-FERNANDEZ, I., GABRIEL, J., ZARCO-TEJADA, P. & QUEMADA, M. 2021. Simultaneous assessment of nitrogen and water status in winter wheat using hyperspectral and thermal sensors. *European Journal of Agronomy,* 127**,** 126287.

PANHWAR, Q. A., ALI, A., NAHER, U. A. & MEMON, M. Y. 2019. Fertilizer management strategies for enhancing nutrient use efficiency and sustainable wheat production. *Organic Farming.* Elsevier.

PENUELAS, J., BARET, F. & FILELLA, I. 1995. Semi-empirical indices to assess carotenoids/chlorophyll a ratio from leaf spectral reflectance. *Photosynthetica,* 31**,** 221-230.

PERRY, E. M., FITZGERALD, G. J., NUTTALL, J. G., O'LEARY, G. J., SCHULTHESS, U. & WHITLOCK, A. 2012. Rapid estimation of canopy nitrogen of cereal crops at paddock scale using a Canopy Chlorophyll Content Index. *Field Crops Research,* 134**,** 158-164.

PHANSALKAR, N., MORE, S., SABALE, A. & JOSHI, M. Adaptive local thresholding for detection of nuclei in diversity stained cytology images. 2011 International conference on communications and signal processing, 2011. IEEE, 218-220.

PINTER JR, P. J., HATFIELD, J. L., SCHEPERS, J. S., BARNES, E. M., MORAN, M. S., DAUGHTRY, C. S. & UPCHURCH, D. R. 2003. Remote sensing for crop management. *Photogrammetric Engineering & Remote Sensing,* 69**,** 647-664.

PLASCYK, J. A. & GABRIEL, F. C. 1975. The Fraunhofer line discriminator MKII-an airborne instrument for precise and standardized ecological luminescence measurement. *IEEE Transactions on Instrumentation and measurement,* 24**,** 306-313.

PORCAR-CASTELL, A., TYYSTJÄRVI, E., ATHERTON, J., VAN DER TOL, C., FLEXAS, J., PFÜNDEL, E. E., MORENO, J., FRANKENBERG, C. & BERRY, J. A. 2014. Linking chlorophyll a fluorescence to photosynthesis for remote sensing applications: mechanisms and challenges. *Journal of experimental botany,* 65**,** 4065-4095.

QUEMADA, M., GABRIEL, J. L. & ZARCO-TEJADA, P. 2014. Airborne hyperspectral images and ground-level optical sensors as assessment tools for maize nitrogen fertilization. *Remote sensing,* 6**,** 2940-2962.

RAMALHO, J. C., PONS, T. L., GROENEVELD, H. W., AZINHEIRA, H. G. & NUNES, M. A. 2000. Photosynthetic acclimation to high light conditions in mature leaves of Coffea arabica L.: role of xanthophylls, quenching mechanisms and nitrogen nutrition. *Functional Plant Biology,* 27**,** 43-51.

RAYA-SERENO, M. D., ALONSO-AYUSO, M., PANCORBO, J. L., GABRIEL, J. L., CAMINO, C., ZARCO-TEJADA, P. J. & QUEMADA, M. 2021. Residual Effect and N Fertilizer Rate Detection by High-Resolution VNIR-SWIR Hyperspectral Imagery and Solar-Induced Chlorophyll Fluorescence in Wheat. *IEEE Transactions on Geoscience and Remote Sensing*.

ROMINA, D. S., TERESA, P.-F., RODNEY, B. T., MARISA, G., RAFAEL, G. & FRANCISCO, M. P. 2019. The use of chlorophyll meters to assess crop N status and derivation of sufficiency values for sweet pepper. *Sensors,* 19**,** 2949.

RONDEAUX, G., STEVEN, M. & BARET, F. 1996. Optimization of soil-adjusted vegetation indices. *Remote sensing of environment,* 55**,** 95-107.

ROUJEAN, J.-L. & BREON, F.-M. 1995. Estimating PAR absorbed by vegetation from bidirectional reflectance measurements. *Remote sensing of Environment,* 51**,** 375-384.

ROUSE, J. W., HAAS, R. H., SCHELL, J. A. & DEERING, D. W. 1974. Monitoring vegetation systems in the Great Plains with ERTS. *NASA special publication,* 351**,** 309.

RUBAN, A. V., LEE, P. J., WENTWORTH, M., YOUNG, A. J. & HORTON, P. 1999. Determination of the stoichiometry and strength of binding of xanthophylls to the photosystem II light harvesting complexes. *Journal of Biological Chemistry,* 274**,** 10458-10465.

SAIBO, N. J., LOURENÇO, T. & OLIVEIRA, M. M. 2009. Transcription factors and regulation of photosynthetic and related metabolism under environmental stresses. *Annals of botany,* 103**,** 609-623.

SAYED, O. 2003. Chlorophyll fluorescence as a tool in cereal crop research. *Photosynthetica,* 41**,** 321-330.

SCHÄCHTL, J., HUBER, G., MAIDL, F.-X., STICKSEL, E., SCHULZ, J. & HASCHBERGER, P. 2005. Laser-induced chlorophyll fluorescence measurements for detecting the nitrogen status of wheat (Triticum aestivum L.) canopies. *Precision Agriculture,* 6**,** 143-156.

SCHEPERS, J., FRANCIS, D., VIGIL, M. & BELOW, F. 1992. Comparison of corn leaf nitrogen concentration and chlorophyll meter readings. *Communications in soil science and plant analysis,* 23**,** 2173-2187.

SCHLEMMER, M., GITELSON, A., SCHEPERS, J., FERGUSON, R., PENG, Y., SHANAHAN, J. & RUNDQUIST, D. 2013. Remote estimation of nitrogen and chlorophyll contents in maize at leaf and canopy levels. *International Journal of Applied Earth Observation and Geoinformation,* 25**,** 47-54.

SHCHERBAK, I., MILLAR, N. & ROBERTSON, G. P. 2014. Global metaanalysis of the nonlinear response of soil nitrous oxide (N2O) emissions to fertilizer nitrogen. *Proceedings of the National Academy of Sciences,* 111**,** 9199-9204.

SNYDER, C. S., BRUULSEMA, T. W., JENSEN, T. L. & FIXEN, P. E. 2009. Review of greenhouse gas emissions from crop production systems and fertilizer management effects. *Agriculture, Ecosystems & Environment,* 133**,** 247-266.

STAGAKIS, S., GONZÁLEZ-DUGO, V., CID, P., GUILLÉN-CLIMENT, M. L. & ZARCO-TEJADA, P. J. 2012. Monitoring water stress and fruit quality in an orange orchard under regulated deficit irrigation using narrow-band structural and physiological remote sensing indices. *ISPRS Journal of Photogrammetry and Remote Sensing,* 71**,** 47-61.

STEVENSON, F. J. & COLE, M. A. 1999. *Cycles of soils: carbon, nitrogen, phosphorus, sulfur, micronutrients*, John Wiley & Sons.

SYVERTSEN, J., LLOYD, J., MCCONCHIE, C., KRIEDEMANN, P. & FARQUHAR, G. 1995. On the relationship between leaf anatomy and CO2 diffusion through the mesophyll of hypostomatous leaves. *Plant, Cell & Environment,* 18**,** 149-157.

SYVERTSEN, J. & SMITH JR, M. 1984. Light acclimation in citrus leaves. I: Changes in physical characteristics, chlorophyll, and nitrogen content. *Journal of the American Society for Horticultural Science,* 109**,** 807-812.

THORP, K., WANG, G., WEST, A., MORAN, M., BRONSON, K., WHITE, J. & MON, J. 2012. Estimating crop biophysical properties from remote sensing data by inverting linked radiative transfer and ecophysiological models. *Remote Sensing of Environment,* 124**,** 224-233.

TÓTH, V. R., MÉSZÁROS, I., VERES, S. & NAGY, J. 2002. Effects of the available nitrogen on the photosynthetic activity and xanthophyll cycle pool of maize in field. *Journal of Plant Physiology,* 159**,** 627-634.

VERHOEF, W. 1984. Light scattering by leaf layers with application to canopy reflectance modeling: The SAIL model. *Remote sensing of environment,* 16**,** 125-141.

VERHOEVEN, A. S., ADAMS III, W. W., DEMMIG-ADAMS, B., CROCE, R. & BASSI, R. 1999. Xanthophyll cycle pigment localization and dynamics during exposure to low temperatures and light stress in Vinca major. *Plant Physiology,* 120**,** 727-738.

VILFAN, N., VAN DER TOL, C., MULLER, O., RASCHER, U. & VERHOEF, W. 2016. Fluspect-B: A model for leaf fluorescence, reflectance and transmittance spectra. *Remote Sensing of Environment,* 186**,** 596-615.

VILFAN, N., VAN DER TOL, C., YANG, P., WYBER, R., MALENOVSKÝ, Z., ROBINSON, S. A. & VERHOEF, W. 2018. Extending Fluspect to simulate xanthophyll driven leaf reflectance dynamics. *Remote sensing of environment,* 211**,** 345-356.

WALKER, A. P., BECKERMAN, A. P., GU, L., KATTGE, J., CERNUSAK, L. A., DOMINGUES, T. F., SCALES, J. C., WOHLFAHRT, G., WULLSCHLEGER, S. D. & WOODWARD, F. I. 2014. The relationship of leaf photosynthetic traits–Vcmax and Jmax–to leaf nitrogen, leaf phosphorus, and specific leaf area: a meta-analysis and modeling study. *Ecology and evolution,* 4**,** 3218-3235.

WANG, Y., SUAREZ, L., QIAN, X., POBLETE, T., GONZALEZ-DUGO, V., RYU, D. & ZARCO-TEJADA, P. Assessing the Contribution of Airborne-Retrieved Chlorophyll Fluorescence for Nitrogen Assessment in Almond Orchards. 2021 IEEE International Geoscience and Remote Sensing Symposium IGARSS, 2021. IEEE, 5853-5856.

WANG, Z., SKIDMORE, A. K., DARVISHZADEH, R. & WANG, T. 2018. Mapping forest canopy nitrogen content by inversion of coupled leaf-canopy radiative transfer models from airborne hyperspectral imagery. *Agricultural and forest meteorology,* 253**,** 247-260.

WILLIAMS, C. K. & RASMUSSEN, C. E. 1996. Gaussian processes for regression.

WILLIAMS, C. K. & RASMUSSEN, C. E. 2006. *Gaussian processes for machine learning*, MIT press Cambridge, MA.

WOOD, C., REEVES, D., DUFFIELD, R. & EDMISTEN, K. 1992. Field chlorophyll measurements for evaluation of corn nitrogen status. *Journal of Plant Nutrition,* 15**,** 487-500.

WORTON, B. J. 1989. Kernel methods for estimating the utilization distribution in home-range studies. *Ecology,* 70**,** 164-168.

WU, C., NIU, Z., TANG, Q. & HUANG, W. 2008. Estimating chlorophyll content from hyperspectral vegetation indices: Modeling and validation. *Agricultural and forest meteorology,* 148**,** 1230-1241.

XIONG, D., CHEN, J., YU, T., GAO, W., LING, X., LI, Y., PENG, S. & HUANG, J. 2015. SPAD-based leaf nitrogen estimation is impacted by environmental factors and crop leaf characteristics. *Scientific reports,* 5**,** 1-12.

YODER, B. J. & PETTIGREW-CROSBY, R. E. 1995. Predicting nitrogen and chlorophyll content and concentrations from reflectance spectra (400–2500 nm) at leaf and canopy scales. *Remote sensing of environment,* 53**,** 199-211.

ZARCO-TEJADA, P. J., CAMINO, C., BECK, P., CALDERON, R., HORNERO, A., HERNÁNDEZ-CLEMENTE, R., KATTENBORN, T., MONTES-BORREGO, M., SUSCA, L. & MORELLI, M. 2018. Previsual symptoms of Xylella fastidiosa infection revealed in spectral plant-trait alterations. *Nature Plants,* 4**,** 432-439.

ZARCO-TEJADA, P. J., GONZÁLEZ-DUGO, M. & FERERES, E. 2016. Seasonal stability of chlorophyll fluorescence quantified from airborne hyperspectral imagery as an indicator of net photosynthesis in the context of precision agriculture. *Remote Sensing of Environment,* 179**,** 89-103.

ZARCO-TEJADA, P. J., GONZÁLEZ-DUGO, V. & BERNI, J. A. 2012. Fluorescence, temperature and narrow-band indices acquired from a UAV platform for water stress detection using a micro-hyperspectral imager and a thermal camera. *Remote sensing of environment,* 117**,** 322-337.

ZARCO-TEJADA, P. J., MORALES, A., TESTI, L. & VILLALOBOS, F. J. 2013. Spatio-temporal patterns of chlorophyll fluorescence and physiological and structural indices acquired from hyperspectral imagery as compared with carbon fluxes measured with eddy covariance. *Remote Sensing of Environment,* 133**,** 102-115.

ZARCO-TEJADA, P. J., POBLETE, T., CAMINO, C., GONZALEZ-DUGO, V., CALDERON, R., HORNERO, A., HERNANDEZ-CLEMENTE, R., ROMÁN-ÉCIJA, M., VELASCO-AMO, M. & LANDA, B. 2021. Divergent abiotic spectral pathways unravel pathogen stress signals across species. *Nature Communications,* 12**,** 1-11.

ZEBARTH, B., DRURY, C., TREMBLAY, N. & CAMBOURIS, A. 2009. Opportunities for improved fertilizer nitrogen management in production of arable crops in eastern Canada: A review. *Canadian Journal of Soil Science,* 89**,** 113-132.

Chapter 4 : Quantification of leaf nitrogen in almond orchards from the spaceborne DESIS hyperspectral sensor: modeling and assessment with airborne hyperspectral and Sentinel-2 imagery

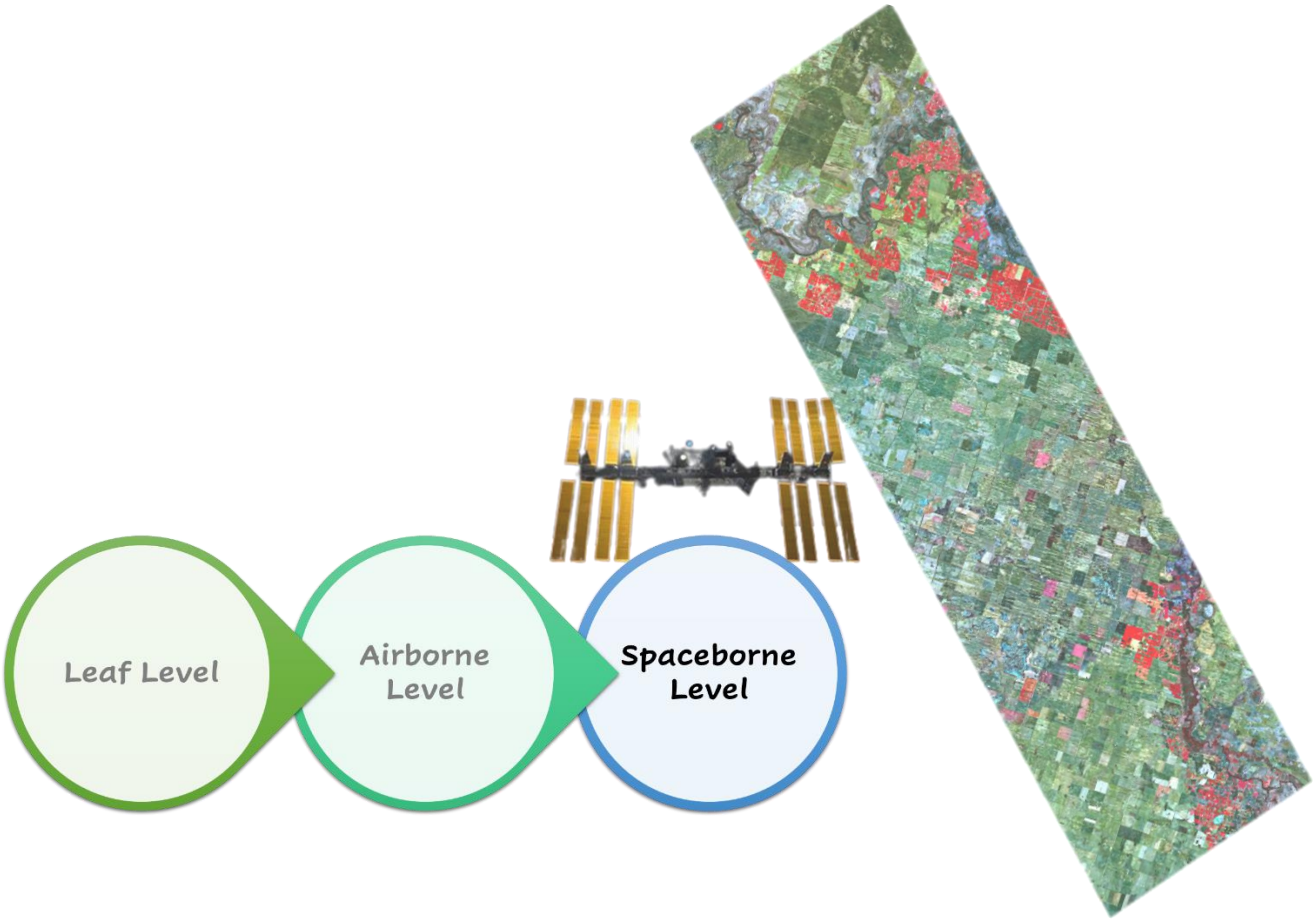

This chapter is under review in IEEE Transactions on Geoscience and Remote Sensing.

Abstract

To ensure the quality and yield in almond orchards, it is essential to accurately monitor leaf nitrogen (N) status both spatially across orchards and temporally throughout the growing season. Remote sensing approaches are well suited for this need and typically assess leaf N through proxies such as leaf chlorophyll a+b (Cab) content estimated from vegetation indices or radiative transfer model (RTM) inversion techniques. Hyperspectral sensors allow the estimation of other biochemical plant traits besides Cab, which enhance our understanding of plant photosynthetic performance and physiological condition. Previous work has shown that solar-induced fluorescence (SIF) and Cab are strong predictors of leaf N, but these assessments were based exclusively on high-resolution airborne imagery. This study evaluates the performance of leaf N estimation using hyperspectral imagery collected from the spaceborne DESIS. We compare spaceborne retrievals to field measurements and the retrievals from both airborne hyperspectral and spaceborne multispectral imagery (Sentinel-2). We found that Cab and SIF derived from DESIS were strongly associated with leaf N, consistent with airborne hyperspectral observations. A DESIS-based model predicted field-measured leaf N with an r2 of 0.83 and RMSE of 0.06%. Sentinel-2 yielded inferior results (r2 = 0.72, RMSE = 0.08%) to those from hyperspectral imagery, despite having a higher nominal spatial resolution (up to 10 m) than DESIS (30 m). This work demonstrates that spaceborne hyperspectral imagery can be useful for the operational monitoring of N content in almond orchards. It also highlights the importance of Cab, SIF, and other physiological plant pigments in nutrient assessment.

Keywords: Chlorophyll Fluorescence, SIF, Nitrogen, ISS DESIS, Spaceborne Imaging, ESA Sentinel-2, Chlorophyll, FluSAIL RTM, Hyperspectral, HSI, Large Scale, Dense Canopy, Almond, Tree Orchard

4.1 Introduction

Nitrogen (N) is an essential macronutrient for plants (Lemaire *et al.*, 2008). In agricultural settings, N fertilizer inputs enhance plant growth and yield via improved photosynthetic rate and light use efficiency (Jones, 1999). However, excessive N inputs lead to resource waste, economic losses, and environmental problems (e.g., soil contamination, and atmospheric and water pollution) (Stewart *et al.*, 2005, Stevenson and Cole, 1999, Matson *et al.*, 1998). Leaf N content is typically determined by destructive sampling followed by laboratoryf-based assays, such as Kjeldahl digestion (Kjeldahl, 1883) or Dumas combustion (Dumas, 1831). Although reliable, these methods are costly in terms of time, samples, and laboratory equipment. These costs limit the practical extent to which N may be measured over an area such as an orchard. For this reason, the accurate measurement of leaf N via remote sensing (RS) has been widely studied (Peterson *et al.*, 1988, Peñuelas *et al.*, 1994, Yoder and Pettigrew-Crosby, 1995). RS imaging spectroscopy techniques enable the creation of spatially continuous maps of plant traits, including the potential quantification of leaf N. However, for crop monitoring, these assessments need to be both precise and repeatable.

Recent advances in RS-based monitoring of plant N have relied on the use of physical models rather than empirical relationships between plant N and vegetation indices derived from specific spectra (Verrelst *et al.*, 2016, Kimes *et al.*, 2000). For instance, solar-induced fluorescence (SIF) has been shown to improve the RS-based quantification of leaf nutrient levels (Wang *et al.*, 2022, Camino *et al.*, 2018a). Physical models are more capable of adapting local variability in specific crop fields due to the fitting process involved and thus are arguably more scalable than vegetation index-based models. Most of these techniques, however, require high-spatial-resolution

hyperspectral imagery captured from airborne platforms, which is costly and limited in the spatial extent that can be sampled, particularly when SIF is required.

Spaceborne imaging spectrometers provide valuable RS data at a relatively high temporal frequency across large spatial scales (Rast and Painter, 2019, Atzberger, 2013). Yet, spaceborne imagery often has the disadvantage of limited spatial and/or spectral resolution. Trade-offs between spatial and spectral resolutions limit the applicability of hyperspectral sensors operated at lower altitudes (Teillet *et al.*, 1997). However, spaceborne sensor technology is rapidly developing, and several hyperspectral sensors onboard spaceborne systems have recently come online.

Recent spaceborne hyperspectral sensors include the Environmental Mapping and Analysis Program (EnMAP), launched in April 2022 (Guanter *et al.*, 2015), and the PRecursore IperSpettrale della Missione Applicativa (PRISMA), launched in March 2019 (Labate *et al.*, 2009). More missions are under development, including the Hyperspectral Infrared Imager (HysplRI, with a 150-km swath) onboard NASA's Earth Observing-1 (EO-1), now part of NASA's Surface Biology and Geology (SBG) mission (Lee *et al.*, 2015, Team, 2018), the Copernicus Hyperspectral Imaging Mission for the Environment (CHIME, with 20-30 m spatial resolution) satellite from the European Space Agency (ESA) (Rast *et al.*, 2021), and the ESA's high-spectral-resolution (around 0.3 nm) Fluorescence explorer FLEX with a 500-780 nm spectral range (Drusch *et al.*, 2016). In addition, the new-generation German Aerospace Center (DLR) Earth Sensing Imaging Spectrometer (DESIS) (Eckardt *et al.*, 2015), operating since August 2018 onboard the International Space Station (ISS), collects hyperspectral imagery (HSI) over 235 narrow spectral bands in the VNIR at a 30-m spatial resolution (Krutz *et al.*, 2019). In this study, we investigate the utility of DESIS imagery for plant N monitoring.

Although DESIS was not explicitly designed for retrieving SIF, it captures spectra within the Fraunhofer lines centered at photosystem (PS) I (PS-I) and PS-II emission regions, making SIF calculations technically possible (Gupana *et al.*, 2021). SIF has been found to correlate with leaf C_{ab} content and photosynthetic activity and has been considered to be a close proxy for leaf N (Genty *et al.*, 1989, Weis and Berry, 1987). SIF has been used to detect both biotic and abiotic plant stress (Ač *et al.*, 2015, Hernández-Clemente *et al.*, 2017) and improve the predictive accuracy of models estimating leaf N (Camino *et al.*, 2018a, Tremblay *et al.*, 2012, Wang *et al.*, 2021). Using high-resolution airborne imagery, Camino *et al.* (2018a) and Wang *et al.* (2022) assessed leaf N in wheat and almond, respectively, demonstrating that SIF combined with other leaf traits outperformed standard models based on leaf C_{ab} alone. Despite much previous research using SIF quantification from airborne platforms, the effectiveness of using spaceborne SIF for stress detection in precision agriculture, especially in non-homogeneous and discontinuous crop canopies, has yet to be thoroughly tested (Paul-Limoges *et al.*, 2018).

In this study, we evaluate the potential use of the spaceborne DESIS hyperspectral sensor to assess leaf N content, photosynthetic pigment content, and SIF in a heterogeneous almond orchard. Further, we compare the performance of DESIS-based assessment against estimates based on high-spatial-resolution airborne hyperspectral imagery. We evaluate the influence of image spectral and spatial resolution, as well as SIF and other physically modeled variables, on the reliability and consistency of leaf N prediction.

Lastly, we compare leaf N estimates from hyperspectral-based data sources to those from the ESA's Sentinel-2 multispectral instrument (MSI), which is increasingly used for agricultural monitoring. Sentinel-2 data is freely available and provides high-spatial-resolution imagery (up to 10 m) over 13 discrete spectral bands in the visible near-infrared to short-wave infrared (VNIR-

SWIR) spectral ranges. Most standard C_{ab} and N estimation methods from Sentinel-2 imagery rely on vegetation indices derived from red-edge spectral bands (Clevers and Gitelson, 2013), such as $CI_{red\text{-}edge}$, $TCARI/OSAVI_{705, 750}$, NDRE, and S2REP. Although Sentinel-2 data are insufficient for quantifying SIF, they include the SWIR spectral domain, which covers features related to leaf protein and water absorption and hence can potentially be used to model physical parameters related to leaf N content (Curran, 1989, Kumar *et al.*, 2002) at large spatial scales (Söderström *et al.*, 2017, Clevers and Gitelson, 2013, Delloye *et al.*, 2018). We assess the performance of leaf N prediction models based on all three data sources (airborne hyperspectral, spaceborne hyperspectral, and spaceborne multispectral), considering trade-offs of accuracy, resolution, and scalability.

4.2 Material and methods

4.2.1 Study area and field data collection

This study was carried out in a commercial almond orchard (yellow dashed line in Fig. 4.1) located on the south bank of the Murray River in northwestern Victoria, Australia. At the study site, the average annual precipitation is 310 mm, and the climate is Mediterranean, marked by hot, dry summers and mild, wet winters. These conditions are favorable for almond production, making northwestern Victoria one of the largest almond-producing regions in Australia. The almond orchard is 1200 ha with 67 blocks of trees planted in the north-south direction and six blocks in the east-west direction. Soils at the site are sandy loams. Three varieties were planted between 2006 and 2007 in alternating rows spaced 7 m apart with 4.4 m between trees in a row. Three varieties were planted in groups of six rows, Nonpareil (1/2 of the rows), Carmel (1/3 of rows), and Price (1/6 of the rows). Tree crowns typically span 4-6.5 m in diameter, resulting in a nearly

closed canopy between trees. Water and nutrients were optimized for each variety and were applied via drip fertigation. Fertigation amounts were tuned each year based on species-specific observation of varietal performance in the previous season. Following this approach, the same rate of fertigation (325.6 kg N/ha and 11,465 m^3 water/ha) was applied to all varieties during the 2019/2020 growing season, whereas Nonpareil (318.7 kg N/ha and 12,255 m^3 water/ha) was treated with about 10% less fertigation than the Carmel and Price varieties (340.7 kg N/ha and 13,335 m^3 water/ha) during the growing season of 2020/2021.

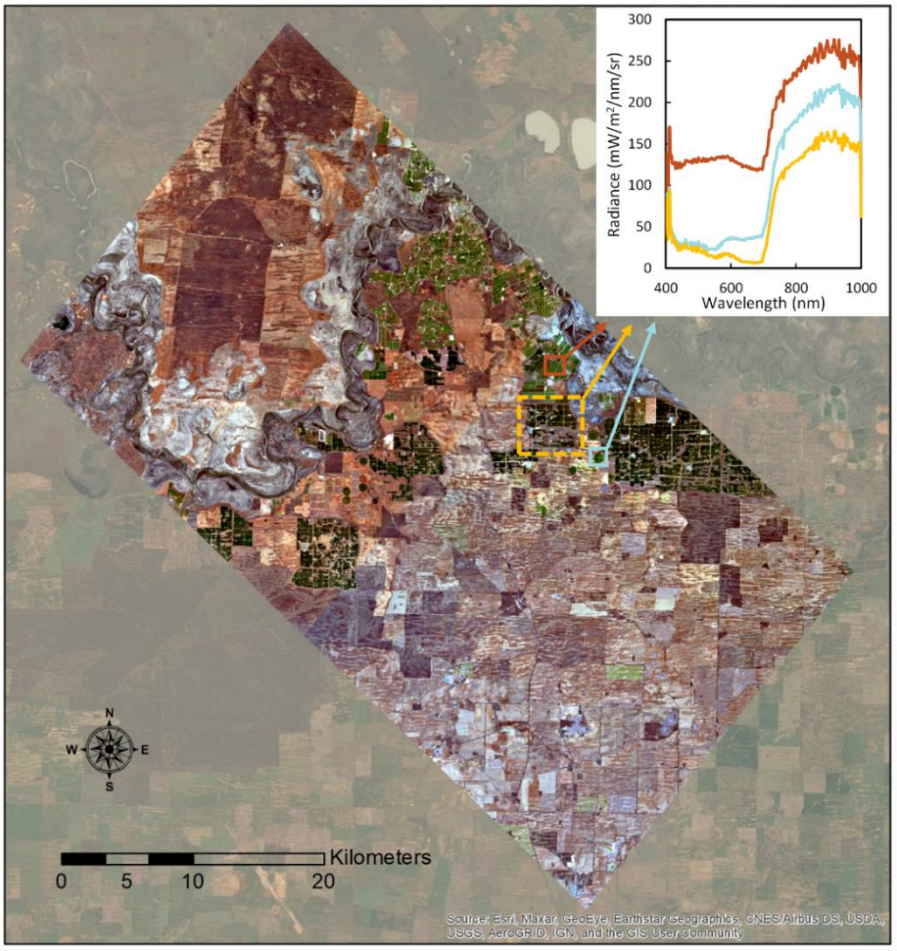

Fig. 4.1. Two adjacent scenes from the spaceborne DESIS hyperspectral sensor (30-m spatial resolution). The radiance spectra from randomly chosen fields are shown in the inset. The study site is demarcated by the yellow dashed line.

Field measurements were conducted at the pre-harvest stage over two consecutive growing seasons: 2019/2020 and 2020/2021. Twelve study plots were monitored in February 2020 and 24 study plots in February 2021. Each plot consisted of six rows of seven to eight trees, of which four adjacent trees (two Nonpareil and two Carmel) were subject to *in situ* samplings. Leaf steady-state chlorophyll fluorescence (Ft) and leaf reflectance spectra within the VNIR region were measured with a FluorPen FP 110 and a PolyPen RP 410 (PSI, Brno, Czech Republic), respectively, on 20 representative leaves from each tree. Leaf C_{ab}, anthocyanin (Anth), flavonoid content, and nitrogen balance index were measured with a Dualex 4 Scientific sensor (FORCE-A, Orsay, France). Twenty additional leaves per plot (100 leaves in total) were collected for chemical analysis using Dumas combustion (Etheridge *et al.*, 1998, Buckee, 1994, Dumas, 1831) with a LECO TruMac CNS Macro Analyzer (LECO Corporation, MI, USA) and an inductively coupled plasma optical emission spectrometer (ICP-OES Optima 8300, Perkin Elmer, USA).

4.2.2 Airborne and spaceborne hyperspectral datasets

4.2.2.1 High-spatial-resolution airborne hyperspectral imagery

Airborne campaigns were conducted concurrently with field measurements on February 17, 2020 and January 31, 2021, which were previously conducted by Wang *et al.* (2022). To minimize atmospheric effects and tree shading, both campaigns were carried out at solar noon under clear skies. A manned aircraft operated by the HyperSens Remote Sensing Laboratory, The University of Melbourne's Airborne Remote Sensing Facility, carried a hyperspectral line-scanning sensor (Micro-Hyperspec VNIR E-Series model, Headwall Photonics, Fitchburg, MA, USA) with an angular field of view of 66° flying at 550 m above ground level. This resulted in a spatial resolution of 40 cm, enabling the separation of sunlit and shaded components of tree crowns and soil features.

The hyperspectral sensor collects imagery in the VNIR spectral region (400-1000 nm) with a full-width at half-maximum (FWHM) of 5.8 nm and a spectral sampling interval of 1.626 nm, resulting in 371 spectral-band images (detailed specifications in Table 4.1). Auxiliary data were collected over the same area as the aircraft passed over; these were later used for image calibration and atmospheric correction. Airborne HSI was atmospherically corrected using the SMARTS model (Gueymard, 1995, Gueymard, 2001). Aerosol optical measurements were taken with a Microtops II sunphotometer (Solar Light, PA, USA) on the ground during the flight, and several other parameters for the model were derived from the average observations (i.e., air temperature and relative humidity) from three weather stations (Robinvale, Lake Powell, and Wemen) between 4 and 15 km away. Reflectance was measured *in situ* for vegetation and soil targets with a FieldSpec Handheld Pro spectrometer (ASD Inc., CO, USA) to validate and correct imagery. Images were orthorectified and mosaiced with PARGE (ReSe Applications Schlapfe, Wil, Switzerland) and ENVI (Boulder, Colorado), respectively. A false-colour airborne hyperspectral mosaic of the study site from 2021 is shown in Fig. 4.2a. Tree crowns were segmented in the HSI following Wang *et al.* (2022) to differentiate the canopy from soil and shade background. Mean spectra were calculated for each individual tree crown for use in subsequent analyses.

Table 4.1. Specifications of the sensors used in this study.

	Airborne Hyperspectral	ISS DESIS Hyperspectral	ESA Sentinel-2 MSI
Spectral range	400–1000 nm (VNIR)	402–1000 nm (VNIR)	433–2280 nm (VNIR-SWIR)
FWHM	5.8 nm	3.5 nm	15–180 nm
Spectral sampling distance	1.626 nm	2.55 nm	N/A
Spectral bands	371	235	13
Radiometric resolution	16 bits	12 bits + 1 bit gain	12 bits
Spatial resolution	40 cm	30 m	10, 20, 60 m
Flight altitude	550 m	400 km	786 km
Image swath	640 m	30 km	290 km
Acquisition date	February 17, 2020 January 31, 2021	January 23, 2021	February 13, 2020 January 23, 2021
Flight time (local)	11.30 am–1 pm	Around 12.33 pm	Around 10.33 am

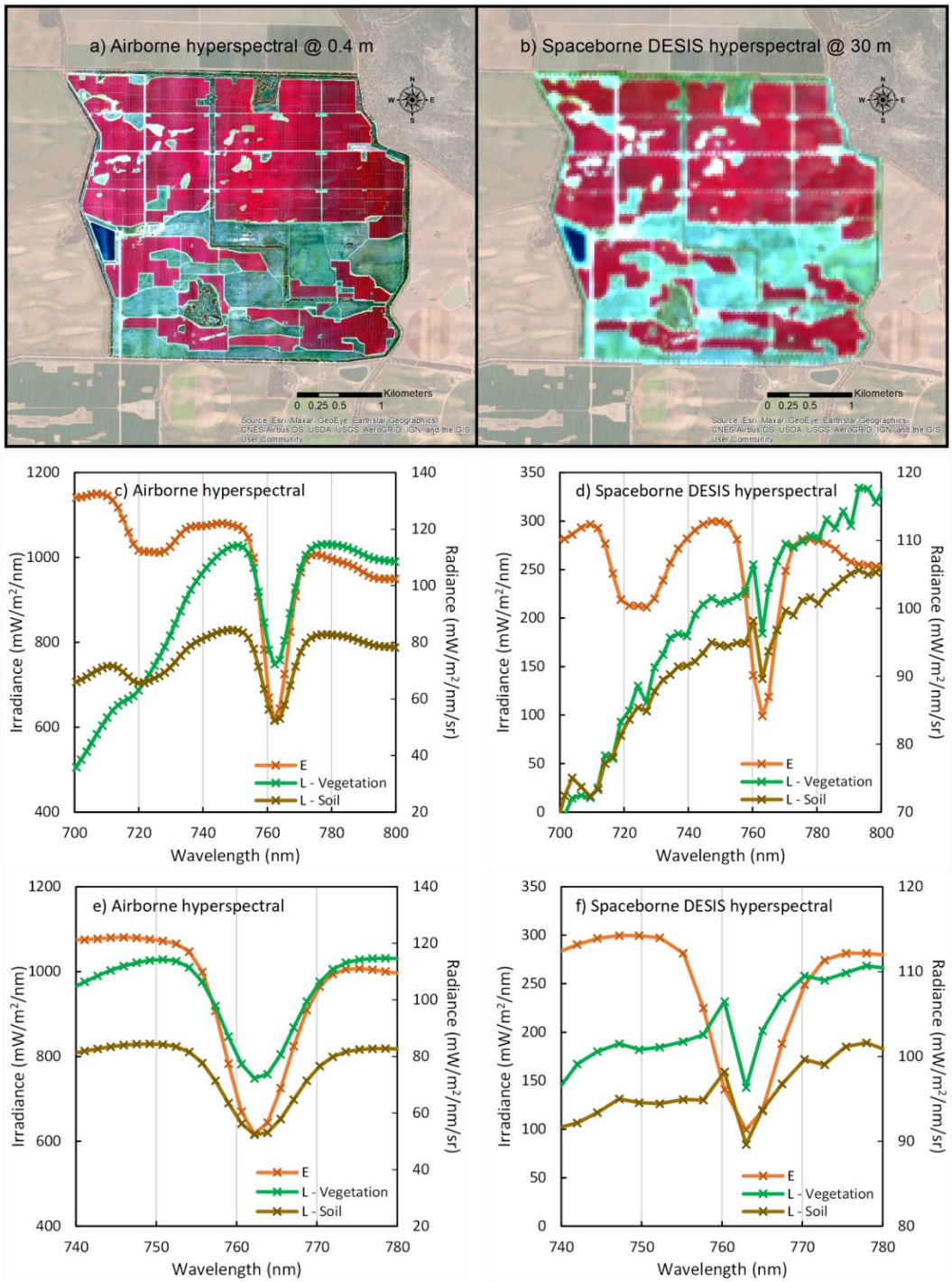

Fig. 4.2. Colour-infrared (CIR-R: 860, G: 650, B: 550) overview of a) airborne VNIR hyperspectral image (HSI) acquired at 0.4-m pixel size on January 31, 2021 and b) spaceborne DESIS VNIR HSI collected at 30-m pixel size on January 23, 2021 over the 1200-ha study site. (c-f) The irradiance (E) spectrum at each data collection date and the radiance (L) spectra of vegetation and soil from c) airborne HSI and d) spaceborne DESIS HSI over the 700-800 nm spectral region and e-f) their spectra over the O_2-A feature around 760 nm.

4.2.2.2 Spaceborne DESIS hyperspectral imagery

Spaceborne HSI was collected by DESIS onboard the ISS (Fig. 4.1). As part of the Multi-User System for Earth Sensing (MUSES) platform, DESIS was jointly developed by Teledyne Brown Engineering and DLR and launched on June 29, 2018. A cloud-free DESIS image over the study area from January 23, 2021 (within one week of the airborne campaign) was selected for analysis (Fig. 4.2b). DESIS contains 235 spectral bands in the VNIR spectral region (400-1000 nm) with an FWHM of 3.5 nm and a spectral sampling interval of 2.55 nm (Krutz *et al.*, 2019) (detailed specifications in Table 4.1). An orbit of the ISS at 400-km altitude results in a 30-m ground sampling distance (Alonso *et al.*, 2019). Orthorectified top-of-atmosphere (TOA) radiance (L1C) and reflectance (L2A) DESIS products were used without spectral binning. The DESIS image together with the radiance spectra from randomly selected vegetation features are depicted in Fig. 4.1. Due to the low surface reflectance in the blue spectral region, DESIS reflectance imagery was post-calibrated based on airborne HSI via an empirical line for 42 feature targets randomly selected throughout the orchard consisting of soil, water, and vegetation areas. Fig. 4.3 shows the reflectance spectrum of one of the targets before and after calibration. The irradiance simulation for the day of DESIS acquisition (Fig. 4.2d) was produced using the data collected from the three nearby weather stations. Aerosol optical depth (AOD) data at processing level 1.5 was obtained from Fowlers Gap, the nearest Aeronet station (https://aeronet.gsfc.nasa.gov/new_web/index.html).

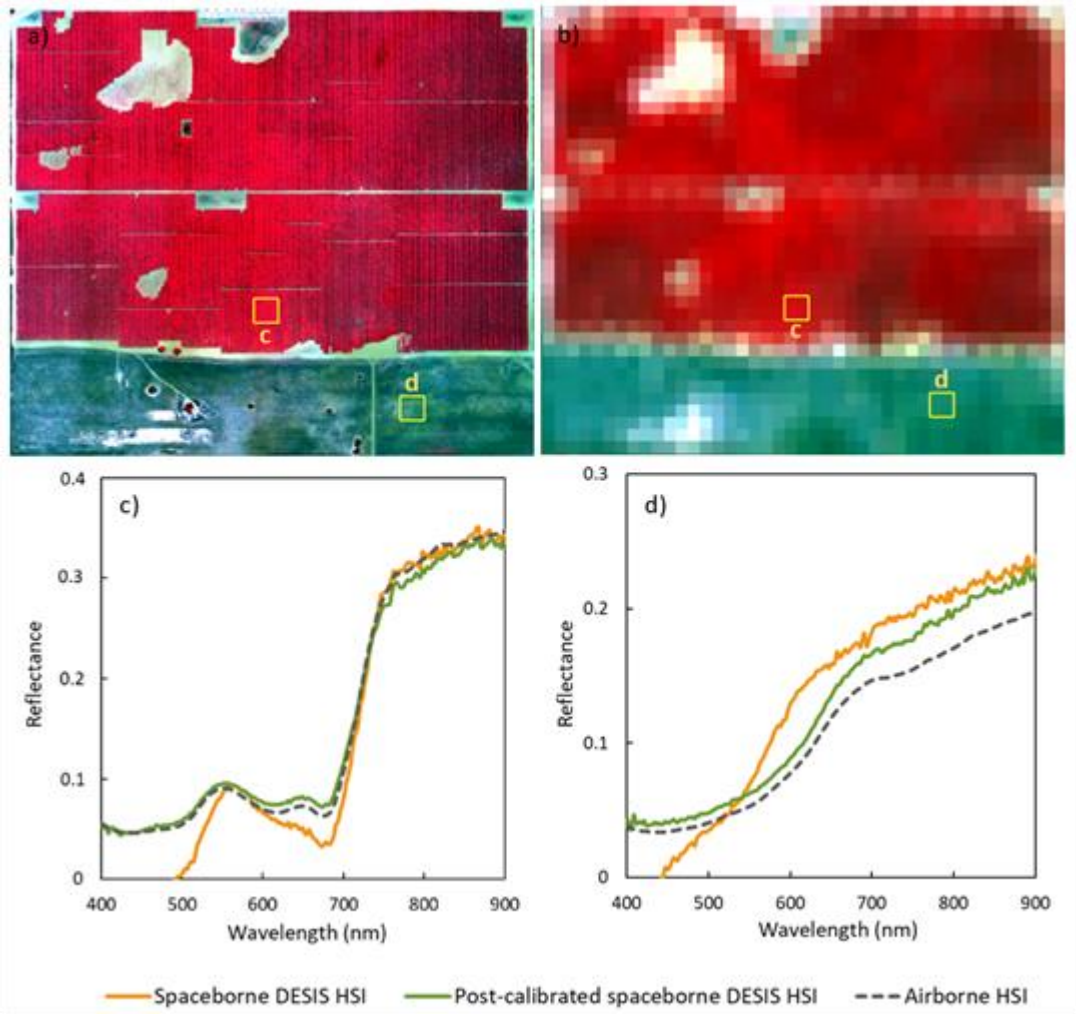

Fig. 4.3. Comparison of colour-infrared a) airborne and b) DESIS hyperspectral image (HSI), and the reflectance spectra for c) vegetation and d) soil, from the original spaceborne DESIS HSI (solid orange line), post-calibrated spaceborne DESIS HSI (solid green line), and airborne HSI (grey dashed line).

The airborne HSI (see a closed view in Fig. 4.4a) was resampled to 30-m resolution using the Pixel Aggregate method in ENVI (Boulder, Colorado) by averaging all the surrounding pixels. In this regard, the resampled airborne hyperspectral pixels maintained all 371 spectral bands, incorporating soil, vegetation, and shadow features. Spatially resampled airborne pixels were aligned to the extent of DESIS pixels using the Snap Raster feature in ESRI ArcGIS Desktop (Redlands, CA, USA). A comparison of pixel sizes and alignments is shown in Figs. 4.5a to 4.5c.

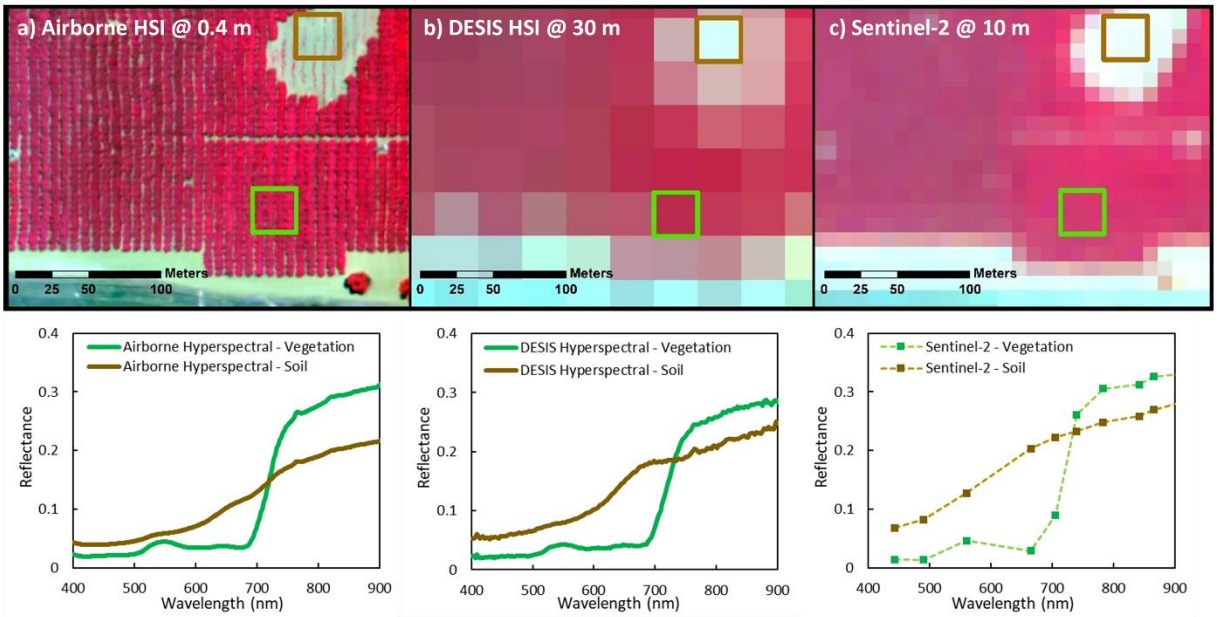

Fig. 4.4. Colour-infrared image from the a) airborne VNIR hyperspectral image (HSI) acquired at 0.4 m per pixel on January 31, 2021, b) post-calibrated DESIS HSI acquired at 30 m per pixel on January 23, 2021, and c) Sentinel-2 multispectral image at 10 m per pixel collected on January 23, 2021, with the reflectance spectra of vegetation (in green) and soil (in brown) within the DESIS pixel in the VNIR region.

4.2.3 Plant trait retrieval and SIF quantification from airborne and DESIS hyperspectral

Plant physiological traits were derived from HSI by inverting canopy reflectance spectra using the Fluspect-Cx (Vilfan *et al.*, 2018) leaf optical properties model coupled with the 4SAIL (Verhoef *et al.*, 2007) canopy bidirectional reflectance model (henceforth FluSAIL). For airborne HSI, reflectance spectra from pure vegetation pixels were selected for modeling (segmentation shown in Fig. 4.5a). For imagery with coarser spatial resolution, pixels overlapping the ground measurements but not edges of the planting blocks were selected. Reflectance spectra from each study plot were used as inputs for the modeling inversion. To perform the inversion, a synthetic dataset was first created from the FluSAIL forward model in order to derive the reflectance spectrum. The result of this process is the generation of a look-up table (LUT) containing 500,000 simulations, integrating the output spectrum with randomly assigned input parameters drawn from

uniform distributions (see Table 4.2 for input parameter ranges used by Wang *et al.* (2022)) along with the solar zenith and relative azimuth angles for each data source. Based on this LUT, model training, testing, and validation were conducted using the Statistics and Machine Learning Toolbox and Deep Learning Toolbox in MATLAB R2020a version (Natick, MA, USA), with 70%, 15%, and 15% of the LUT samples, respectively (Xie *et al.*, 2019). During the training phase, which is the backward model, it is intended to determine the relationship between the input reflectance spectrum and the output plant parameters. Consequently, leaf constituents (i.e., C_{ab}, C_{car}, Anth, and C_{dm}), the de-epoxidation state of the xanthophyll cycle (C_x), and structural trait LAI were simultaneously inverted through a 10-hidden layer artificial neural network (ANN) (Hassoun, 1995, Combal *et al.*, 2003) for each data source. The inverted parameters were then compared using field measurements from all study plots. The FluSAIL model was also run in the forward mode for the final inverted parameters to compare against observed image spectra using the root mean square error (RMSE).

Table 4.2. Ranges of input parameters for the LUT of the FluSAIL Model.

Parameter	Symbol	Range/Value
Leaf thickness and constituents		
Chlorophyll *a*+*b* content (µg/cm^2)	C_{ab}	20–70
Carotenoid content (µg/cm^2)	C_{car}	3–20
Anthocyanin content (µg/cm^2)	Anth	0–10
Leaf water content (g/cm^2)	C_w	0.001–0.05
Leaf dry matter content (g/cm^2)	C_{dm}	0.001–0.05
Brown pigment content (µg/cm^2)	C_s	0
Leaf mesophyll structural parameter	N-struct	1.3–2.5
Leaf dynamic biochemistry		
De-epoxidation state of the xanthophyll cycle (photochemical reflectance parameter)	C_x	0–3
Fraction of photons partitioned to PSI	$f_{qe}I$	0.002
Fraction of photons partitioned to PSII	$f_{qe}II$	0.02
Canopy structural parameters		
Leaf area index (m^2/m^2)	LAI	1–7
Hot spot parameter	q	0.03
Leaf inclination distribution function parameter *a*	$LIDF_a$	-1–1
Leaf inclination distribution function parameter *b*	$LIDF_b$	-1–1

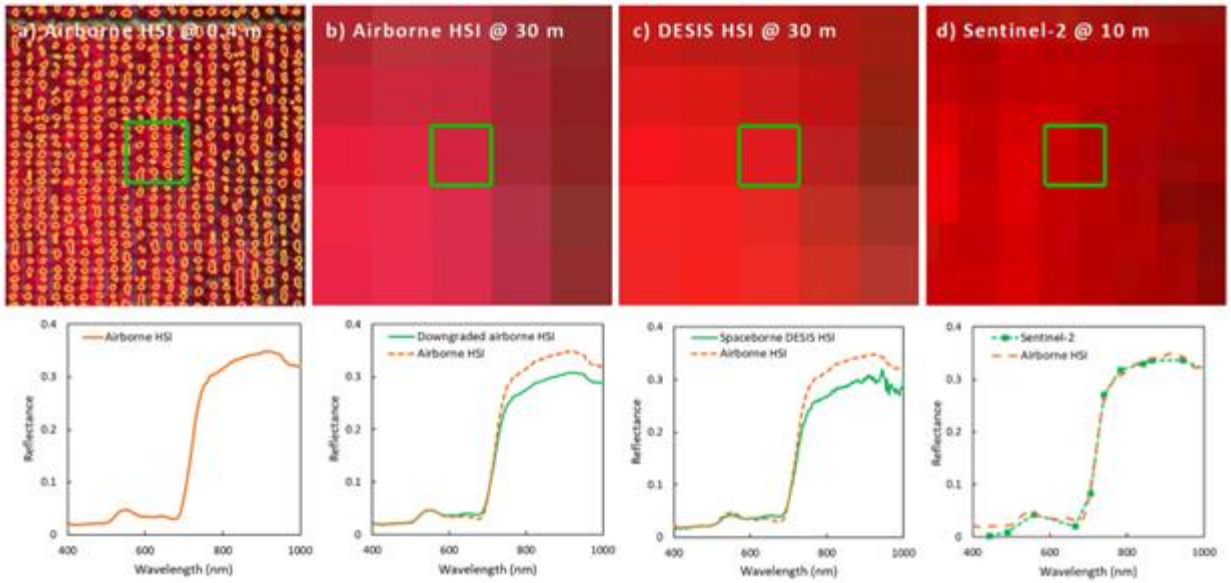

Fig. 4.5. Colour-infrared overview of a 5-by-5 DESIS pixel window of a) the tree-crown segmentation in yellow colour and the average tree-crown reflectance spectrum (in orange) from an airborne hyperspectral image (HSI) at 0.4-m resolution, b) airborne HSI resampled to 30-m per pixel, c) post-calibrated DESIS HSI at 30 m per pixel, and d) Sentinel-2 multispectral image at 10 m per pixel. VNIR reflectance spectra within each green box are shown below each image. The solid green line represents the reflectance spectrum within the central DESIS pixel (in green) from different images compared with the tree-crown reflectance spectrum (orange dashed line).

SIF was calculated from the oxygen (O_2) A-band absorption feature near 760 nm, following the Fraunhofer line depth principle (Plascyk and Gabriel, 1975, Plascyk, 1975). For each data source, SIF quantification using the O_2-A in-filling method was performed by comparing the spectral windows for 'in' and 'out' of the peak irradiance (E) and radiance (L). It was observed that the minimum value within the 755-765 nm region of E and L was at 762 nm (used as E_{in}/L_{in}) for both airborne and DESIS HSI, as shown in Figs. 2e and 2f. Here, the E_{out}/L_{out} corresponds to their maximum E/L values within the spectral regions of 744–754 nm and 770–780 nm, respectively. A correction based on values of non-fluorescence soil features was added to reduce atmospheric and calibration effects (Belwalkar *et al.*, 2022). Due to the limited availability of AOD data from the nearby Aeronet station on the date of the DESIS imagery, SIF values from DESIS were treated as SIF proxies rather than absolute values.

4.2.4 Sentinel-2 datasets for vegetation indices calculation and plant traits retrievals

Cloud-free scenes from Sentinel-2B on February 13, 2020, and Sentinel-2A on January 23, 2021 were considered for potential leaf N estimation. Twelve-bit images with a swath width of 290 km and 13 spectral bands over VNIR-SWIR spectral regions were acquired at three spatial resolutions of 10, 20, and 60 m (detailed specifications can be found in Table 4.1 and Drusch *et al.* (2012)). Level-1C images (orthorectified TOA reflectance) were processed into level-2A (bottom-of-atmosphere reflectance) using Sen2Cor, version 2.8.0 (Louis *et al.*, 2016). The lower-spatial-resolution bands (20 and 60 m) were then resampled to 10 m to create a uniform-resolution multispectral image over the study site. Fig. 4.4 illustrates VNIR images as well as soil and vegetation spectra from the three sensors used in this study. The comparison of reflectance spectra (RMSE = 0.01) over the dense canopy of tree crowns from Sentinel-2 (in green) and airborne (in orange) is shown in Fig. 4.5d.

Sixteen vegetation indices related to canopy structure and pigment content were calculated from the uniform-resolution images (see Table 4.3 for the list of indices and their formulas). Some of them were the indices compatible with Sentinel-2 spectral bands proposed by Clevers and Gitelson (2013), such as Sentinel-2 red-edge position (S2REP) (Frampton *et al.*, 2013). Other indices using bands in the SWIR were also tested in this study, such as the Aerosol free vegetation index ($AFRI_{1510}$ and $AFRI_{2100}$) (Karnieli *et al.*, 2001).

Table 4.3. Vegetation indices calculated in this study from Sentinel-2 data.

Index	Equation	Reference
VNIR indices for Sentinel-2		
NDVI	$(R_{842} - R_{665})/(R_{842} + R_{665})$	Rouse *et al.* (1974)
EVI	$\frac{2.5 \cdot (R_{842} - R_{665})}{R_{842} + 6 \cdot R_{665} - 7.5 \cdot R_{490} + 1}$	Liu and Huete (1995)
$CI_{red\text{-}edge}$	$(R_{783}/R_{705}) - 1$	Gitelson *et al.* (2003)
CI_{green}	$(R_{783}/R_{560}) - 1$	Gitelson *et al.* (2003)
S2REP	$705 + \frac{35 \cdot (R_{665} + R_{783})/2 - R_{705}}{R_{740} - R_{705}}$	Frampton *et al.* (2013)
MTCI	$(R_{740} - R_{705})/(R_{705} - R_{665})$	Dash and Curran (2007)
$MCARI/OSAVI_{705,750}$	$\frac{((R_{740} - R_{705}) - 0.2 \cdot (R_{740} - R_{560})) \cdot (R_{740}/R_{705})}{(1 + 0.16) \cdot (R_{740} - R_{705})/(R_{740} + R_{705} + 0.16)}$	Wu *et al.* (2008)
$TCARI/OSAVI_{705,750}$	$\frac{3 \cdot ((R_{740} - R_{705}) - 0.2 \cdot (R_{740} - R_{560}) \cdot (R_{740}/R_{705}))}{(1 + 0.16) \cdot (R_{740} - R_{705})/(R_{740} + R_{705} + 0.16)}$	Wu *et al.* (2008)
NDRE1	$(R_{740} - R_{705})/(R_{740} + R_{705})$	Sims and Gamon (2002)
NDRE2	$(R_{783} - R_{705})/(R_{783} + R_{705})$	Barnes *et al.* (2000)
PSSRa	R_{783}/R_{665}	Blackburn (1998)
PSSRc2	R_{842}/R_{490}	Blackburn (1998)
SWIR indices for Sentinel-2		
STI	R_{1610}/R_{2190}	Van Deventer *et al.* (1997)
NDWI	$(R_{842} - R_{1610})/(R_{842} + R_{1610})$	Gao (1996)
$AFRI_{1510}$	$R_{865} - \frac{0.66 \cdot R_{1610}}{R_{865} + 0.66 \cdot R_{1610}}$	Karnieli *et al.* (2001)
$AFRI_{2100}$	$R_{865} - \frac{0.5 \cdot R_{2190}}{R_{865} + 0.56 \cdot R_{2190}}$	Karnieli *et al.* (2001)

As with the other two datasets, a LUT with 500,000 FluSAIL simulations using the same ranges of input parameters in Table 4.2 was built for the Sentinel-2 dataset. As Sentinel-2 has only one band in the green spectral region where most pigments are active, making it difficult to accurately determine minor pigments and the xanthophyll epoxidation state (C_x), hence only C_{ab} retrieval was attempted. A selection of plant traits (i.e., C_{ab}, C_w, C_{dm}, and LAI) were extracted using the ANN from Sentinel-2 LUT.

4.2.5 Leaf N estimation

For HSI-derived data, leaf N prediction models were built using RTM inverted plant traits (i.e., C_{ab}, C_{car}, Anth, C_{dm}, C_x, and LAI) and SIF as inputs (see STAGE 2 at the bottom of Fig. 4.6). For

Sentinel-2 data, two separate models were established, one using the estimated plant traits (i.e., C_{ab}, C_w, C_{dm}, and LAI) and the other using the vegetation indices (Table 4.3) as inputs. Data were fit with random forest (RF) (Breiman, 2001) regression models with fine-tuning of hyperparameters, using leave-one-out cross-validation for the training and testing steps, following the method described by Wang *et al.* (2022). Predictions from the model based on airborne imagery were previously validated by Wang *et al.* (2022) and explained 95% of the variability of field-measured leaf N throughout the orchard over 2 years of study. Due to the high resolution and accuracy of this model, its spatially resolved predictions were used as a baseline for the models from coarser resolution data. Randomly selected pixels across the orchard were employed for training (60%) and testing (40%) based on the airborne N map for both DESIS and Sentinel-2. Finally, all models were compared against field-derived leaf N concentration.

To reduce the redundancy of the inputs, a variance inflation factor (VIF) (O'brien, 2007) collinearity assessment was conducted when building the regression model. To understand the relative importance of the inputs to each model, out-of-bag predictor importance scores were evaluated. The final model was constructed using the most important predictors, which are non-collinear for each year of data sources. More specifically, the airborne and spaceborne DESIS hyperspectral models were built with C_{ab} and SIF, whereas C_{ab}, C_{dm}, and C_w were employed for Sentinel-2-based models. As an alternative to the plant traits, a second N model using non-collinear VNIR and SWIR vegetation indices was constructed for the Sentinel-2 dataset. Using r^2 and RMSE as performance measures, the models were evaluated against the validation data. To conclude, leaf N estimation from DESIS hyperspectral and Sentinel-2 were compared with high-resolution airborne estimates throughout the orchard to determine the RMSE based on individual planting blocks.

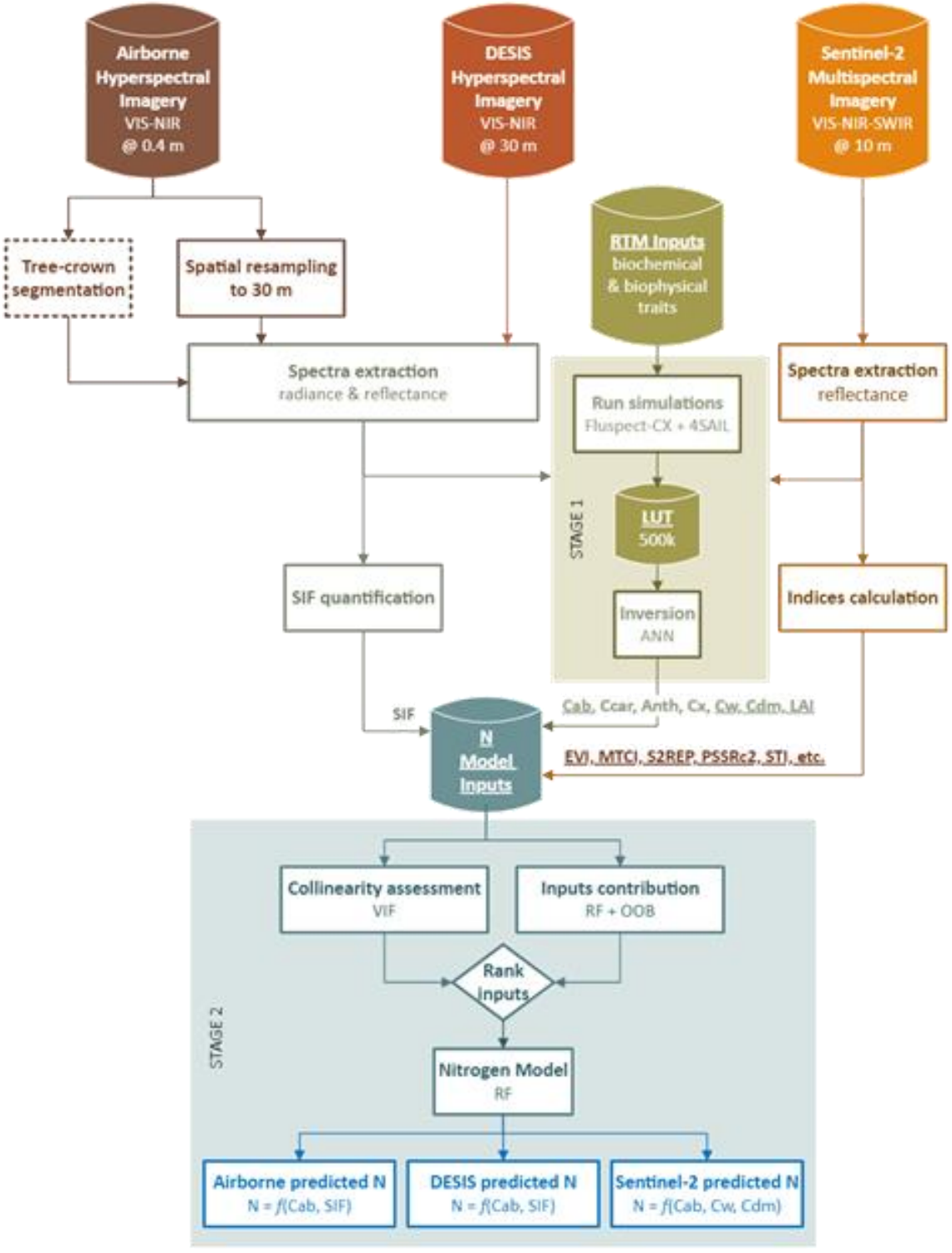

Fig. 4.6. Schematic representation of the leaf N assessment from airborne hyperspectral, spaceborne DESIS hyperspectral imagery, and Sentinel-2 multispectral image in a dense canopy almond orchard. Underlined parameters were retrieved and used in the Sentinel-2 model.

4.3 Results

4.3.1 Assessment of trait retrievals with airborne and spaceborne hyperspectral datasets

A comparison of C_{ab} and SIF from airborne hyperspectral imagery in native vs. downsampled resolutions is presented in Figs. 7a and 7b. Values across spatial resolutions were highly correlated for both C_{ab} (e.g., $r^2 = 0.93$, RMSE = 1.99, p-value < 0.001 in 2021) and SIF (e.g., $r^2 = 0.97$, RMSE = 0.61, p-value < 0.001 in 2021). When both years of data were considered simultaneously, associations remained strong for SIF ($r^2 = 0.93$, RMSE = 0.77, p-value < 0.001) and to a lesser extent for C_{ab} ($r^2 = 0.72$, RMSE = 4.81, p-value < 0.001). The structural vegetation indices (e.g., NDVI) and SIF and were not correlated with each other ($r^2 < 0.1$, not significant for both years), suggesting that canopy structural effects were not the dominant driver of SIF differences between years. Associations were weaker between airborne and DESIS-derived C_{ab} ($r^2 = 0.33$, RMSE = 8.07, p-value < 0.005 in 2021) and SIF index ($r^2 = 0.53$, p-value < 0.001 in 2021) (Figs. 7c to 7f). When compared to airborne observations, DESIS-derived C_{ab} contents were biased towards higher C_{ab} contents.

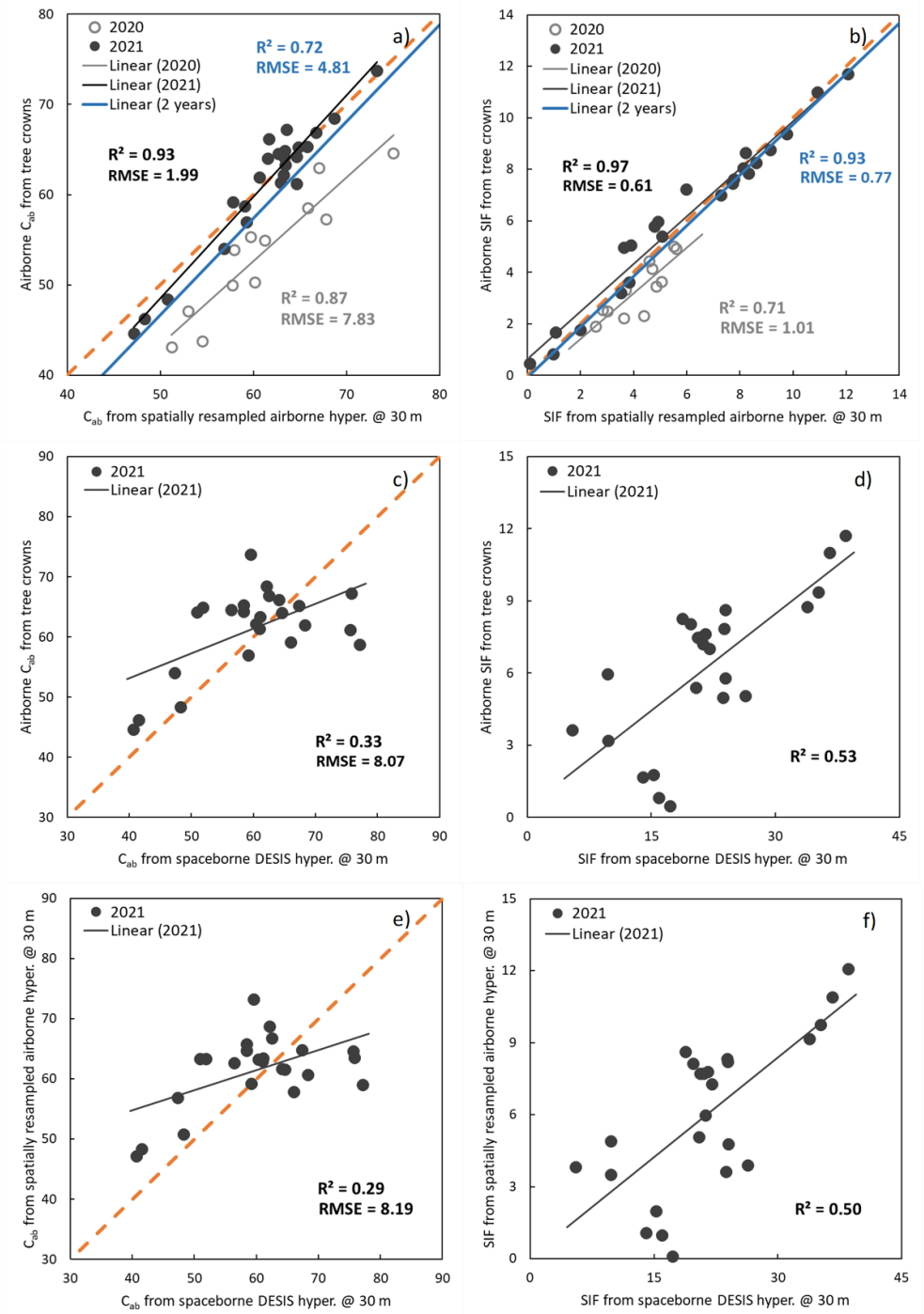

Fig. 4.7. Relationships between estimates of plant characteristics by measurement methodology. Top row: spatially resampled (aggregated to 30 m) airborne hyperspectral vs. tree crown-based estimates for a) C_{ab}, and b) SIF in 2020 (12 points in the hollow grey circle) and 2021 (24 points in solid black circle). The solid blue line represents correlation when combining data from 2 years. Middle row: DESIS hyperspectral vs. tree crown-based estimates of c) C_{ab} and d) SIF in 2021. Bottom row: e) C_{ab} and f) SIF index between DESIS hyperspectral and the spatially resampled airborne hyperspectral at 30 m. The orange dashed diagonal line is the 1:1 line.

SIF and RTM-derived plant traits were strongly correlated with leaf pigment content and leaf N concentration obtained from *in situ* measurements (Table 4.4). Statistically significant correlations were found between HSI-estimated C_{ab} and both Dualex-measured C_{ab} (all p-values < 0.005) and laboratory-derived leaf N concentration (all p-values < 0.001). SIF (p-values < 0.005) and C_{dm} (p-values < 0.005) were also significantly correlated with leaf N. As expected, C_x had greater correspondence with N measures when estimated from high-spatial-resolution imagery, allowing the extraction of pure vegetation features from tree crowns rather than mixed features derived from low-spatial-resolution pixels of DESIS. Airborne-derived traits (esp. SIF, C_{ab}, C_{car}, and C_x) were also more correlated with *in situ* leaf Ft measurements than spaceborne-derived traits. RTM-inverted plant traits were more closely correlated with field measurements than vegetation indices derived from either airborne or DESIS hyperspectral imagery (e.g., TCARI/OSAVI vs. leaf N concentration: r^2 < 0.23, data not shown).

Table 4.4. Correlations (r^2) between image-derived spectral traits and field measurements. Rows indicate modeled traits, and columns indicate pairing of field data source (top row), year (second row), and HSI source (third row).

Field data	Leaf C_{ab} (µg/cm²)			Leaf Ft (a.u.)			Leaf N (%)		
	2020	2021		2020	2021		2020	2021	
Image-derived spectral traits	**Airborne HSI**	**Airborne HSI**	**DESIS HSI**	**Airborne HSI**	**Airborne HSI**	**DESIS HSI**	**Airborne HSI**	**Airborne HSI**	**DESIS HSI**
Model-derived plant traits from hyperspectral imagery									
C_{ab} (µg/cm²)	0.66	0.52	0.52	0.35	0.41	0.17	0.71	0.50	0.50
C_{car} (µg/cm²)	0.66	0.35	0.01	0.41	0.50	0.19	0.73	0.27	0.20
Anth (µg/cm²)	0.65	0.00	0.17	0.33	0.00	0.13	0.75	0.04	0.18
C_x	0.58	0.40	0.28	0.42	0.61	0.14	0.77	0.30	0.16
C_{dm} (g/cm²)	0.60	0.20	0.60	0.12	0.00	0.14	0.62	0.37	0.47
LAI	0.06	0.09	0.32	0.01	0.08	0.02	0.02	0.11	0.18
Fluorescence quantification from hyperspectral imagery									
SIF	0.36	0.18	0.34	0.71	0.33	0.25	0.65	0.45	0.59

p-value < 0.001	p-value < 0.005	p-value < 0.05	not significant

Field measurements are Dualex-derived leaf C_{ab} (µg/cm²), FluorPen-derived steady-state chlorophyll fluorescence (Ft, a.u.), and leaf N concentration (%).
Data from 2020 (12 study plots) and 2021 (24 study plots).
Background colour represents the p-value: dark blue for $p < 0.001$, medium blue for $0.001 \leq p < 0.005$, light blue for $0.005 \leq p < 0.05$, and white for $p \geq 0.05$ (not significant).

4.3.2 Leaf nitrogen assessment using SIF and plant traits derived from airborne and DESIS hyperspectral data

Predictor importance scores for models based on spaceborne DESIS HSI and airborne HSI from 2021 are exhibited in Fig. 4.8. DESIS-derived SIF (p-value < 0.001) and FluSAIL RTM-inverted C_{ab} (p-value < 0.001) were the highest ranked predictors for both platforms, followed by other leaf biochemical constituents and biophysical traits. SIF and C_{ab} were not collinear when assessed for variance inflation (VIF < 5) for both airborne and spaceborne DESIS and thus were kept in the final prediction model. However, C_{dm}, $C_{ca,}$, and C_x were collinear with C_{ab}. The structural trait LAI was markedly more important in the DESIS-based model than the airborne-based model. As a result, final models for both HSI datasets were constructed using C_{ab} and SIF. The DESIS model yielded an r^2 of 0.83 (p-value < 0.001) and RMSE of 0.06% when validated against *in situ* leaf N in 2021. The prediction against the airborne-based model had an r^2 of 0.88 (p-value < 0.001) and RMSE of 0.05% throughout the entire orchard.

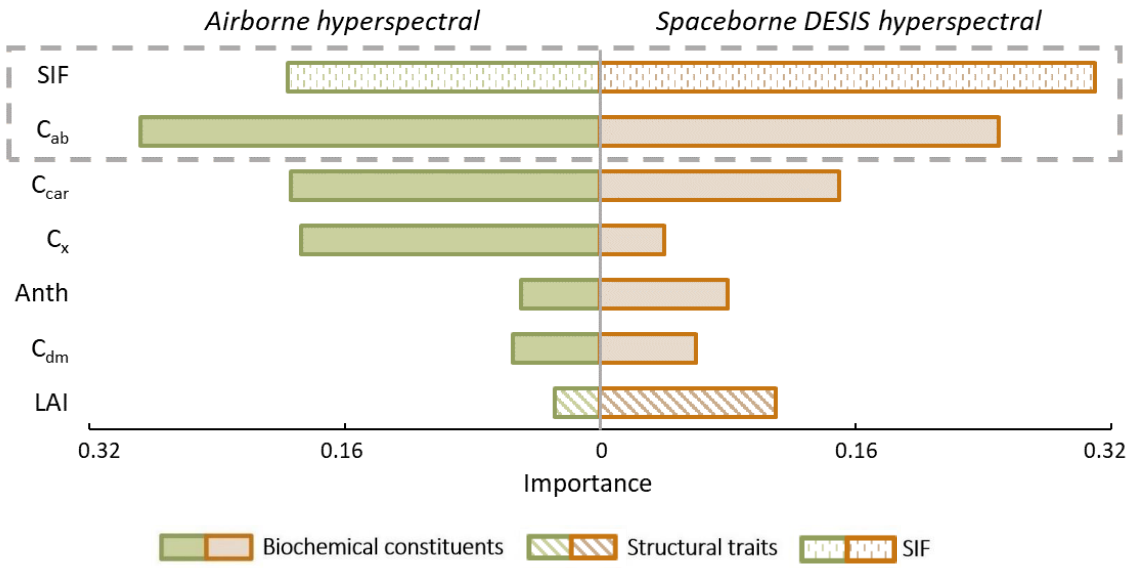

Fig. 4.8. Importance of FluSAIL RTM-inverted traits and SIF used as predictors for leaf N. Models used traits derived from either DESIS (in orange) or airborne (in green) hyperspectral imagery in 2021. The two most important variables (non-collinear) are marked in a grey dashed rectangle.

4.3.3 Performance of Sentinel-2-derived plant traits and vegetation indices

Correlations between Sentinel-2-derived indices and field measurements are presented in Table 4.5. Overall, plant traits (e.g., C_{ab} and C_{dm}) tended to be more consistently significant correlated with field measures than vegetation indices across the 2 years of study. Vegetation indices were more correlated with field measures in 2021 than in 2020. RTM-derived C_{ab} from Sentinel-2 was biased at higher C_{ab} contents compared to *in situ* measures with an r^2 of 0.41 (p-value < 0.001) and RMSE of 1.63 in 2021 (Fig. 4.9a). Nevertheless, RTM-derived C_{ab} was consistently significant correlated with leaf N for both years (r^2 = 0.68 and 0.64 in 2020 and 2021, respectively, p-values < 0.001). $CI_{red\text{-}edge}$ was weakly correlated with leaf N in 2020 (r^2 = 0.18, n.s.) but strongly correlated in 2021 (r^2 = 0.56, p-value < 0.001, Fig. 4.9b). Additionally, indices derived from spectra in the SWIR region tended to be more correlated with field measurements than those from the VNIR region. For example, $AFRI_{1500}$, a SWIR-based index, was correlated with leaf N in both 2020 (r^2 = 0.54, p-value < 0.05) and 2021 (r^2 = 0.69, p-value < 0.001).

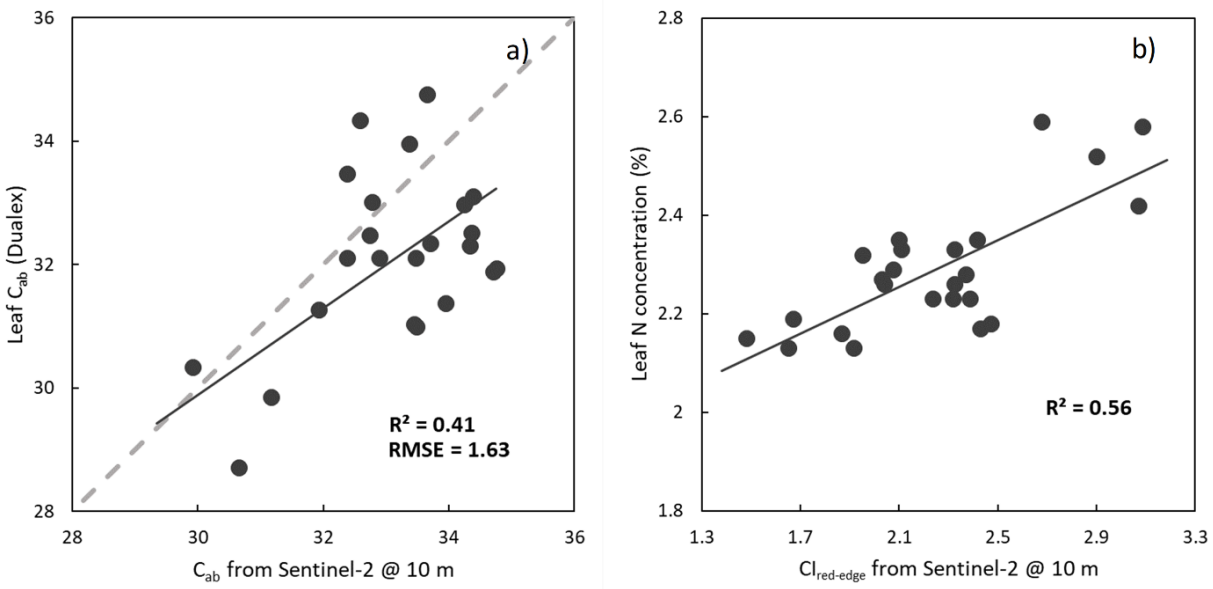

Fig. 4.9. Relationships between a) RTM-derived C_{ab} content from Sentinel-2 and leaf C_{ab} measured by Dualex, and b) $CI_{red\text{-}edge}$ calculated from Sentinel-2 and leaf N concentration (%) in 2021 (24 points). The grey dashed diagonal line is the 1:1 line.

Sentinel-2-based C_{ab} and C_{dm} were consistently correlated with leaf N across years (Table 4.5), as with hyperspectral-derived C_{ab} and C_{dm}. However, correlations with Dualex-measured C_{ab} were lower than those derived from hyperspectral imagery. LAI determined from Sentinel-2 was more strongly correlated with GNDVI ($r^2 = 0.71$, p-value < 0.001) and RDVI ($r^2 = 0.40$, p-value < 0.005) (data not shown) than LAI obtained from hyperspectral sources in 2021. Sentinel-2-derived LAI was more correlated with leaf N concentration ($r^2 = 0.28$, p-value < 0.05 in 2021) than DESIS-derived LAI ($r^2 = 0.18$, p-value < 0.05 in 2021). Nevertheless, the structural trait LAI did not explain much N variability in this well-managed dense orchard compared to other traits.

Table 4.5. Correlations (r^2) between model-derived plant traits and vegetation indices from Sentinel-2 against field measurements.

Field data / Sentinel-2 indicators	Leaf C_{ab} (µg/cm²)		Leaf Ft (a.u.)		Leaf N (%)	
	2020	2021	2020	2021	2020	2021
Model-derived plant traits						
C_{ab} (µg/cm²)	0.55	0.41	0.43	0.43	0.68	0.64
C_w (g/cm²)	0.37	0.01	0.32	0.00	0.66	0.07
C_{dm} (g/cm²)	0.33	0.31	0.24	0.27	0.58	0.60
LAI	0.28	0.11	0.44	0.07	0.41	0.28
VNIR vegetation indices						
NDVI	0.29	0.29	0.08	0.26	0.37	0.52
EVI	0.43	0.53	0.13	0.39	0.47	0.63
$CI_{red\text{-}edge}$	0.11	0.41	0.00	0.25	0.18	0.56
CI_{green}	0.28	0.35	0.03	0.24	0.33	0.62
S2REP	0.20	0.24	0.29	0.06	0.13	0.31
MTCI	0.03	0.36	0.23	0.12	0.02	0.40
$MCARI/OSAVI_{705,\ 750}$	0.33	0.55	0.07	0.35	0.39	0.65
$TCARI/OSAVI_{705,\ 750}$	0.00	0.32	0.04	0.21	0.02	0.50
NDRE1	0.15	0.36	0.01	0.23	0.21	0.53
NDRE2	0.12	0.34	0.00	0.22	0.18	0.53
PSSRa	0.28	0.45	0.08	0.35	0.39	0.61
PSSRc2	0.41	0.18	0.16	0.22	0.54	0.55
SWIR vegetation indices						
STI	0.16	0.41	0.02	0.29	0.26	0.62
NDWI	0.21	0.39	0.07	0.28	0.36	0.58
$AFRI_{1500}$	0.43	0.53	0.17	0.38	0.54	0.69
$AFRI_{2100}$	0.44	0.52	0.15	0.38	0.53	0.71

p-value < 0.001	p-value < 0.005	p-value < 0.05	not significant

Field measurements are Dualex-derived leaf C_{ab} (µg/cm²), FluorPen-derived steady-state chlorophyll fluorescence (Ft, a.u.), and leaf N concentration (%).
Data from 2020 (12 study plots) and 2021 (24 study plots).
Background colour represents the p-value: dark blue for $p < 0.001$, medium blue for $0.001 \leq p < 0.005$, light blue for $0.005 \leq p < 0.05$, and white for $p \geq 0.05$ (not significant).

4.3.4 Leaf nitrogen assessment from Sentinel-2: comparison against hyperspectral imagery

For predictions of leaf N using Sentinel-2 data, C_{ab}, C_{dm}, and C_w were found to be more important than LAI across years (Fig. 4.10). Importance scores of vegetation indices were inconsistent across years. Nevertheless, vegetation indices derived from the SWIR region (i.e., 2190 and 1610 nm) tended to be more important than VNIR vegetation indices.

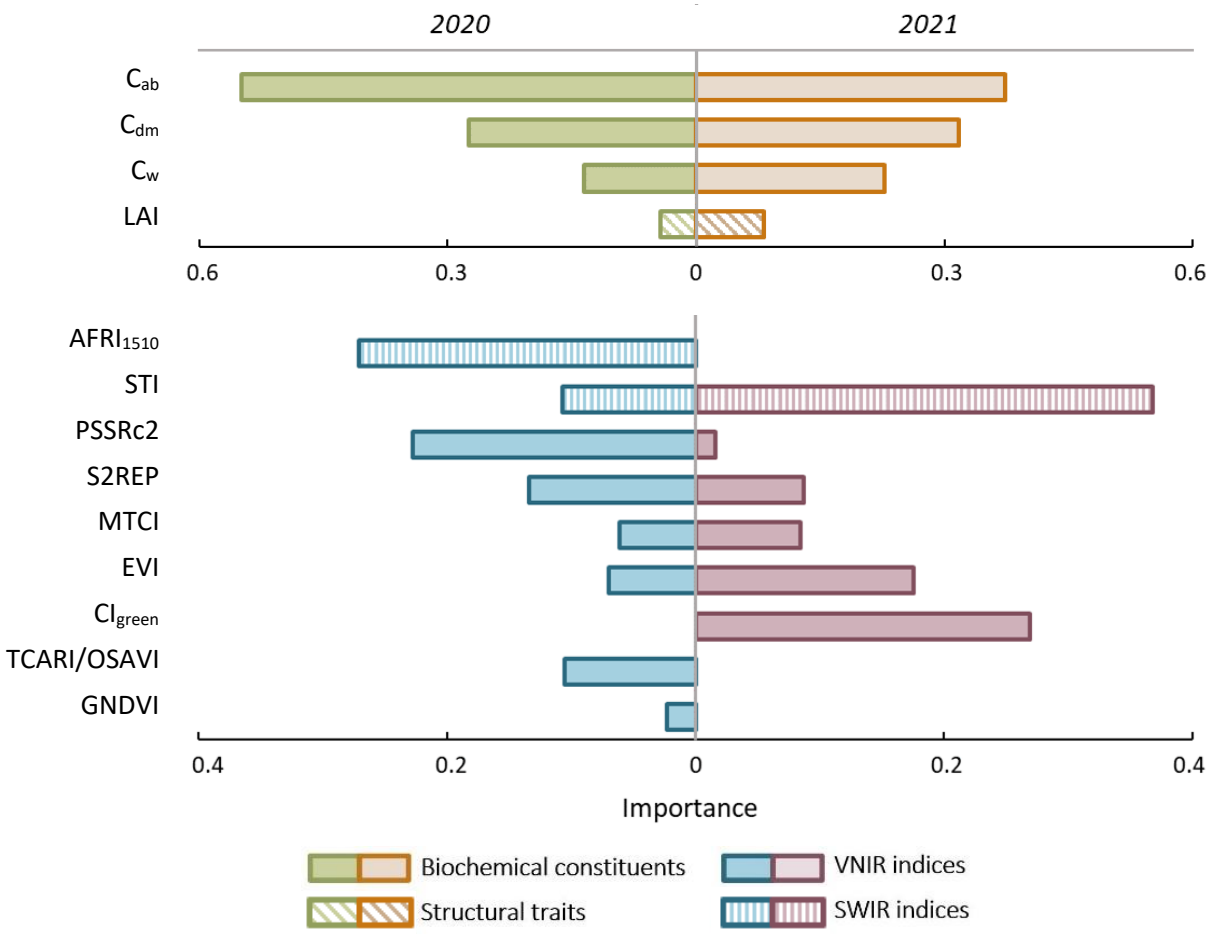

Fig. 4.10. Importance of model-derived plant traits and vegetation indices (non-collinear, VIF < 5) calculated from Sentinel-2 in 2020 and 2021.

The final N prediction model using plant traits from Sentinel-2 (N = f(C_{ab}, C_w, C_{dm})) had an r^2 of 0.79 (p-value < 0.001) and RMSE of 0.08% for 2020, and an r^2 of 0.72 (p-value < 0.001) and

RMSE of 0.12% for 2021. Similar performance was found for the model based on the non-collinear vegetation indices (N = *f*(STI, PSSRc2, S2REP, MTCI, EVI, CI_{green})). Across all models, those built with hyperspectral-derived datasets (e.g., r^2 = 0.86, RMSE = 0.05%, *p*-value < 0.001 from airborne HSI in 2021, and r^2 = 0.83, RMSE = 0.06%, *p*-value < 0.001 from spaceborne DESIS HSI in 2021) outperformed Sentinel-2-based models (e.g., r^2 = 0.72, RMSE = 0.08%, *p*-value < 0.001 in 2021, Fig. 4.11) each year. Combining data over both years, the airborne-based regression model (r^2 = 0.91, RMSE = 0.05%, *p*-value < 0.001) performed much better than Sentinel-2 (r^2 = 0.82, RMSE = 0.09%, *p*-value < 0.001).

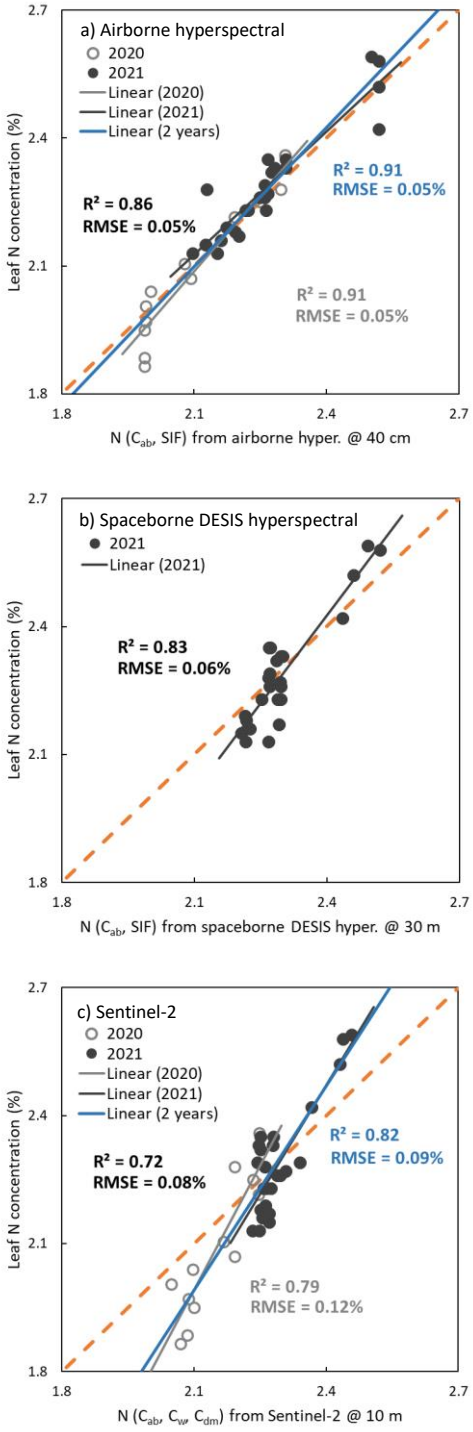

Fig. 4.11. Relationships between leaf N concentration model predictions based on a) airborne hyperspectral-derived N (C_{ab}, SIF) from tree crowns, b) Sentinel-2-derived N (C_{ab}, C_w, C_{dm}), and c) spaceborne DESIS hyperspectral-derived N (C_{ab}, SIF). Data from 2020 (12 points) are shown as hollow grey circles, and data from 2021 (24 points) are shown as solid black circles. The solid blue line represents the linear fit when combining data from 2 years. The orange dashed diagonal line is the 1:1 line.

Spatial patterns in predicted N were similar between models based on spaceborne and airborne imagery (Fig. 4.12). Pixel values from the airborne-derived N map were highly correlated with both the DESIS (r^2 = 0.88 and RMSE = 0.03%, *p*-value < 0.001, *n* (number of pixels) = 5030) and Sentinel-2 (r^2 = 0.82 and RMSE = 0.07%, *p*-value < 0.001, *n* = 54661) N maps. The largest discrepancies between N maps were observed in areas with extreme N levels, possibly due to the influence of soil and shadows in coarser imagery and to fewer extreme-valued samples being used in model training. When using an average aggregated value per management block, DESIS estimates had greater correspondence with high-resolution airborne estimates than Sentinel-2 estimates, with 67 out of 71 blocks having an RMSE under 0.1% for DESIS (compared to 62 out of 73 blocks for Sentinel-2). Subsequent examination revealed that blocks with high RMSEs also tended to have high N levels.

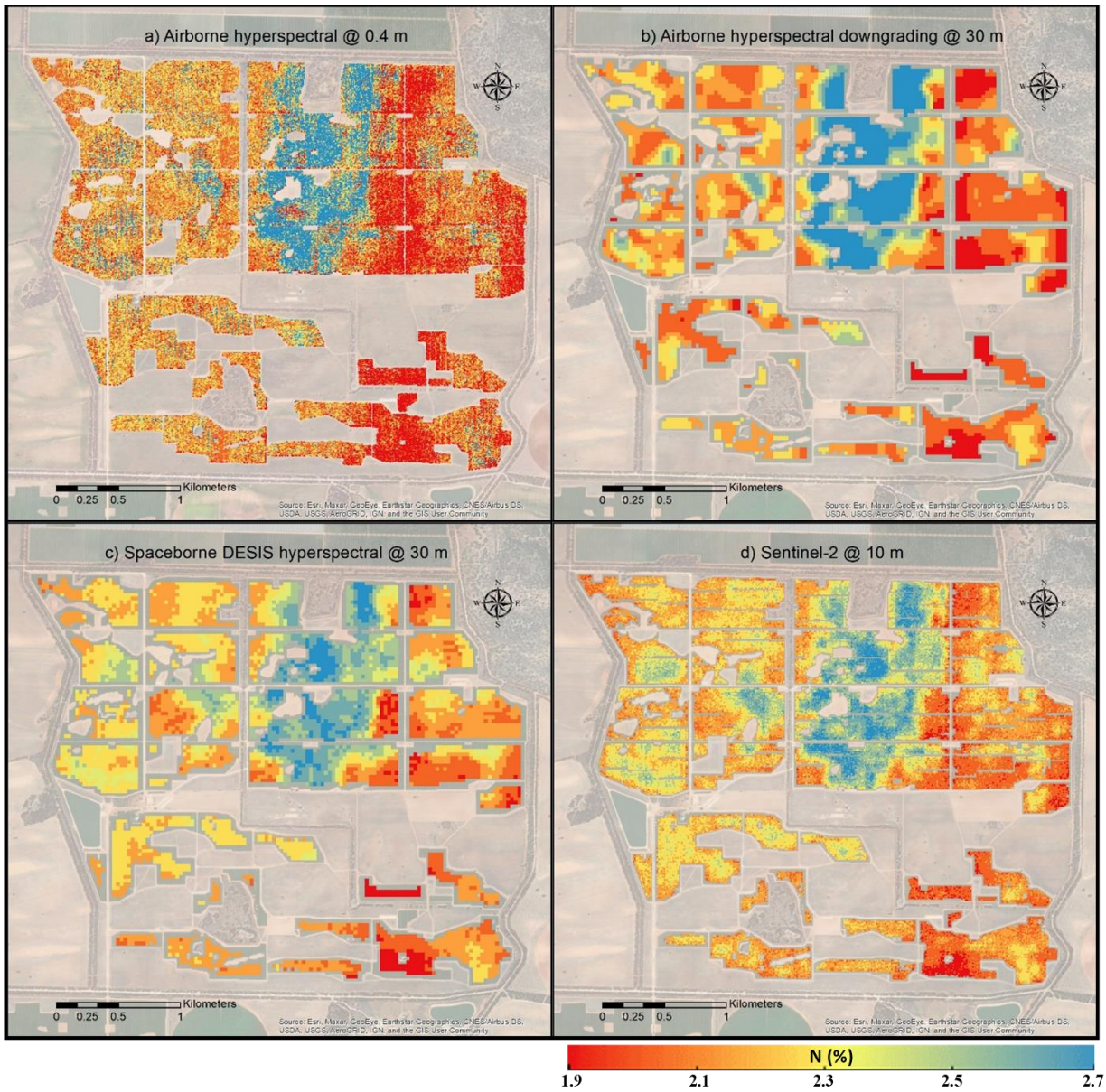

Fig. 4.12. Estimated leaf N maps for the 2021 pre-harvest season based on models using a) airborne hyperspectral-derived C_{ab} and SIF from tree crowns, b) spatially resampled airborne hyperspectral imagery-derived C_{ab} and SIF, c) spaceborne DESIS hyperspectral imagery-derived C_{ab} and SIF, and d) Sentinel-2-derived plant traits C_{ab}, C_w, and C_{dm}.

4.4 Discussion

Monitoring and quantification of leaf N at both the local and large-area scales require a comprehensive understanding of the drivers and plant traits that can best explain N stress. For both

hyperspectral image datasets (airborne and spaceborne DESIS) tested in this study, SIF and C_{ab} were the most important spectrally derived traits for predicting leaf N, followed by C_{car} and C_x (Fig. 4.8). By contrast, LAI was only modestly important and only for the model based on the DESIS dataset. One possible explanation is that at the pre-harvest stage, foliage growth slows (Clark and Smith, 1990, Brown, 1994) and becomes more uniform, especially in well-managed orchards. Thus, LAI would not be expected to vary much, especially in pure vegetation pixels.

The spatial resolution of each sensor influenced both trait retrievals and model predictions in this study. In particular, medium-resolution satellite imagery is known to suffer from greater mixing effects from shadow and soil backgrounds on vegetation signals within pixels (Zarco-Tejada *et al.*, 2013). In this study, C_x, a dynamic trait approximating the xanthophyll cycle as a function of stress, was not found to be important for predicting leaf N at coarse spatial resolutions. According to Jia *et al.* (2021), SIF was found to be important for predicting leaf N, outperforming other spectral indices (e.g., $CI_{red\text{-}edge}$ and NDRE). However, this result was somewhat sensitive to the N measurement technique (area-based vs. mass-based leaf N content). In this study, RTM-derived C_{ab} and SIF were found to be important for predicting leaf N in models from both airborne (40-cm resolution) and DESIS (30-m resolution) imagery, suggesting that both C_{ab} and SIF are strong candidates for leaf N estimates across spatial resolutions.

Many studies have shown that it is possible to estimate LAI from Sentinel-2 data (Richter *et al.*, 2009, Verrelst *et al.*, 2015, Herrmann *et al.*, 2011, Atzberger and Richter, 2012); however, estimates of actual leaf pigment content or other biochemical constituents are more difficult due to the limited number of spectral bands available in these data. In this study, we found strong correlations between estimated plant physiological traits and field measurements, suggesting that it is possible to use RTM inversion with Sentinel-2 data to estimate key physiological traits (i.e.,

C_{ab}, C_w, C_{dm}, and LAI). When we compared RTM-derived C_{ab} and C_{dm} to field-measured C_{ab}, we observed relatively strong correlations over both years (*p*-values < 0.05) and even stronger correlations with leaf N (*p*-values < 0.005) (Table 4.5). Although LAI can reflect changes in plant growth due to nutrient or water availability (Albaugh *et al.*, 2004), sustained stress is uncommon in well-managed orchards, and it is thus unlikely that LAI will be sensitive to the relatively low nutrient variability found in production settings. In this study, we found that LAI was not correlated with leaf C_{ab} or N. C_w was also not consistently associated with leaf N across seasons, which could be explained by the actual differences in fertigation management between seasons. Li *et al.* (2010) found that the utility of vegetation indices for predicting plant N was inconsistent and particularly contingent on the plant phenological stage. Similarly, there was evidence of a significant correlation between vegetation indices and *in situ* leaf measurements in 2021, but not in 2020. This inconsistency suggests that vegetation indices may not be appropriate for long-term N monitoring. Regardless, consistent contribution of vegetation indices across years was not observed (Fig. 4.10), which is important when attempting to monitor C_{ab} and N status over phenological stages across multiple years.

Sensor spatial and spectral resolution strongly influences the accuracy of any downstream leaf N predictions, especially in heterogeneous orchards. Among the three platforms tested in this study, the imager with the highest resolution (airborne) provided the best leaf N predictions. The model built with Sentinel-2 multispectral imagery had nearly double the RMSE of the airborne-derived model. Interestingly, in 2021, the model based on DESIS hyperspectral imagery (N = f(C_{ab}, SIF) with r^2 = 0.83, RMSE = 0.06%, *p*-value < 0.001 when assessed against field measurements) was more accurate than the Sentinel-2 models (N = f(C_{ab}, C_w, C_{dm}) with r^2 = 0.72, RMSE = 0.08%, *p*-value < 0.001 against field measurements), despite having a lower spatial resolution and shorter

spectral range. The DESIS model (94% of RMSE ≥ 0.1%) also had greater correspondence with the airborne model at the block level than the Sentinel-2 model (85% of RMSE ≥ 0.1%). These results suggest that spectral resolution may be more important than spatial resolution in predicting leaf N. Nevertheless, the performance of Sentinel 2 ($N = f(C_{ab}, C_w, C_{dm})$) is still acceptable, and provides a reasonable alternative approach for estimating N from Sentinel-2derived C_{ab}, C_w, and C_{dm} when hyperspectral imagery cannot be utilized to derive SIF.

The presence of stem elements, crown architecture, and bare soil in a scene can result in model inaccuracies (Verstraete *et al.*, 1990, Law *et al.*, 2001). Nevertheless, RTMs considering the canopy as a turbid medium have already been successfully used to retrieve plant traits. An earlier study by Zarco-Tejada *et al.* (2001) demonstrated that coupled PROSPECT and SAILH models could be used to estimate C_{ab} in high-density closed forest canopies, particularly after selecting the brightest 25% pixels in the NIR region from high-resolution airborne imagery. In the well-managed orchard used for this study, tree canopies were dense and uniform, thus minimizing the impact of the canopy structural variation. In prior work using the same data as this study, Wang *et al.* (2022) demonstrated that plant traits can be successfully estimated through a one-dimensional canopy RTM (4SAIL) using such high-density closed tree canopy data. Models in the current study did not take into account the effects of woody material and foliar clumping required for a more detailed estimate of LAI (Chen *et al.*, 1997). With coarse spatial resolution data (over 10 m), however, these effects are difficult to detect and unlikely to be a significant issue.

Another limitation of this study was the empirical line post-calibration needed to correct the abnormal values found in the blue and parts of green region of the DESIS reflectance imagery. An improved radiometry calibration of the DESIS imagery, especially in the Southern Hemisphere, would be beneficial in the future. Raw radiance spectra with no further calibration were used for

SIF calculation in this study. Although SIF retrieval is known to be affected by spatial resolution and illumination differences (Camino *et al.*, 2018b, Zarco-Tejada *et al.*, 2013), SIF estimates based on 30-m resolution DESIS imagery were shown to be associated with leaf N in this study, possibly due to the dense tree canopy in the orchard. Nevertheless, this study illustrates the potential use of DESIS for monitoring N across large areas.

4.5 Conclusions

We demonstrated that it is possible to estimate leaf N in a discontinuous tree-structured orchard using 30-m spatial resolution DESIS hyperspectral imagery. High-resolution airborne hyperspectral imagery and field data were used for validation. We found that SIF and RTM-derived Cab were the most important for predicting leaf N across spatial resolutions. Furthermore, the model based on airborne and spaceborne hyperspectral data outperformed Sentinel-2-based models (using either vegetation indices or RTM-derived traits). Our results suggest that the newly available spaceborne hyperspectral sensor can be used to assess N across large areas via models using RTM-derived leaf biochemical trait retrievals and SIF. One important finding of this study was that models based on hyperspectral data outperformed models based on Sentinel-2 data, even though Sentinel-2 data has a higher spatial resolution and represent reflectance in the SWIR spectral region.

References

AČ, A., MALENOVSKÝ, Z., OLEJNÍČKOVÁ, J., GALLÉ, A., RASCHER, U. & MOHAMMED, G. 2015. Meta-analysis assessing potential of steady-state chlorophyll fluorescence for remote sensing detection of plant water, temperature and nitrogen stress. *Remote sensing of environment,* 168**,** 420-436.

ALBAUGH, T. J., ALLEN, H. L., DOUGHERTY, P. M. & JOHNSEN, K. H. 2004. Long term growth responses of loblolly pine to optimal nutrient and water resource availability. *Forest ecology and management,* 192**,** 3-19.

ALONSO, K., BACHMANN, M., BURCH, K., CARMONA, E., CERRA, D., DE LOS REYES, R., DIETRICH, D., HEIDEN, U., HÖLDERLIN, A. & ICKES, J. 2019. Data products, quality and validation of the DLR earth sensing imaging spectrometer (DESIS). *Sensors,* 19**,** 4471.

ATZBERGER, C. 2013. Advances in remote sensing of agriculture: Context description, existing operational monitoring systems and major information needs. *Remote sensing,* 5**,** 949-981.

ATZBERGER, C. & RICHTER, K. 2012. Spatially constrained inversion of radiative transfer models for improved LAI mapping from future Sentinel-2 imagery. *Remote Sensing of Environment,* 120**,** 208-218.

BARNES, J. D., BALAGUER, L., MANRIQUE, E., ELVIRA, S. & DAVISON, A. 1992. A reappraisal of the use of DMSO for the extraction and determination of chlorophylls a and b in lichens and higher plants. *Environmental and Experimental botany,* 32**,** 85-100.

BELWALKAR, A., POBLETE, T., LONGMIRE, A., HORNERO, A., HERNANDEZ-CLEMENTE, R. & ZARCO-TEJADA, P. 2022. Evaluation of SIF retrievals from narrow-band and sub-nanometer airborne hyperspectral imagers flown in tandem: Modelling and validation in the context of plant phenotyping. *Remote Sensing of Environment,* 273**,** 112986.

BLACKBURN, G. A. 1998. Spectral indices for estimating photosynthetic pigment concentrations: a test using senescent tree leaves. *International Journal of remote sensing,* 19**,** 657-675.

BREIMAN, L. 2001. Random forests. *Machine learning,* 45**,** 5-32.

BROWN, P. H. 1994. Seasonal variations in fig (Ficus carica L.) leaf nutrient concentrations. *HortScience,* 29**,** 871-873.

BUCKEE, G. 1994. Determination of total nitrogen in barley, malt and beer by Kjeldahl procedures and the dumas combustion methodcollaborative trial. *Journal of the Institute of Brewing,* 100**,** 57-64.

CAMINO, C., GONZÁLEZ-DUGO, V., HERNÁNDEZ, P., SILLERO, J. & ZARCO-TEJADA, P. J. 2018a. Improved nitrogen retrievals with airborne-derived fluorescence and plant traits quantified from VNIR-SWIR hyperspectral imagery in the context of precision agriculture. *International journal of applied earth observation and geoinformation,* 70**,** 105-117.

CAMINO, C., ZARCO-TEJADA, P. J. & GONZALEZ-DUGO, V. 2018b. Effects of heterogeneity within tree crowns on airborne-quantified SIF and the CWSI as indicators of water stress in the context of precision agriculture. *Remote Sensing,* 10**,** 604.

CARTER, G. A. 1994. Ratios of leaf reflectances in narrow wavebands as indicators of plant stress. *Int. J. of Remote Sensing,* 15**,** 697-703.

CHEN, J. M., RICH, P. M., GOWER, S. T., NORMAN, J. M. & PLUMMER, S. 1997. Leaf area index of boreal forests: Theory, techniques, and measurements. *Journal of Geophysical Research: Atmospheres,* 102**,** 29429-29443.

CLARK, C. & SMITH, G. 1990. Seasonal changes in the mineral nutrient content of persimmon leaves. *Scientia Horticulturae,* 42**,** 85-97.

CLEVERS, J. G. & GITELSON, A. A. 2013. Remote estimation of crop and grass chlorophyll and nitrogen content using red-edge bands on Sentinel-2 and-3. *International Journal of Applied Earth Observation and Geoinformation,* 23**,** 344-351.

COMBAL, B., BARET, F., WEISS, M., TRUBUIL, A., MACE, D., PRAGNERE, A., MYNENI, R., KNYAZIKHIN, Y. & WANG, L. 2003. Retrieval of canopy biophysical variables from

bidirectional reflectance: Using prior information to solve the ill-posed inverse problem. *Remote sensing of environment,* 84**,** 1-15.
CURRAN, P. J. 1989. Remote sensing of foliar chemistry. *Remote sensing of environment,* 30**,** 271-278.
DAUGHTRY, C. S., WALTHALL, C., KIM, M., DE COLSTOUN, E. B. & MCMURTREY III, J. 2000. Estimating corn leaf chlorophyll concentration from leaf and canopy reflectance. *Remote sensing of Environment,* 74**,** 229-239.
DELLOYE, C., WEISS, M. & DEFOURNY, P. 2018. Retrieval of the canopy chlorophyll content from Sentinel-2 spectral bands to estimate nitrogen uptake in intensive winter wheat cropping systems. *Remote Sensing of Environment,* 216**,** 245-261.
DRUSCH, M., DEL BELLO, U., CARLIER, S., COLIN, O., FERNANDEZ, V., GASCON, F., HOERSCH, B., ISOLA, C., LABERINTI, P. & MARTIMORT, P. 2012. Sentinel-2: ESA's optical high-resolution mission for GMES operational services. *Remote sensing of Environment,* 120**,** 25-36.
DRUSCH, M., MORENO, J., DEL BELLO, U., FRANCO, R., GOULAS, Y., HUTH, A., KRAFT, S., MIDDLETON, E. M., MIGLIETTA, F. & MOHAMMED, G. 2016. The fluorescence explorer mission concept—ESA's earth explorer 8. *IEEE Transactions on Geoscience and Remote Sensing,* 55**,** 1273-1284.
DUMAS, J. B. A. 1831. Procedes de l'analyse Organic. *Annales de Chimie et de Physique (Annals of Chemistry and of Physics),* 247**,** 198-213.
ECKARDT, A., HORACK, J., LEHMANN, F., KRUTZ, D., DRESCHER, J., WHORTON, M. & SOUTULLO, M. Desis (dlr earth sensing imaging spectrometer for the iss-muses platform). 2015 IEEE international geoscience and remote sensing symposium (IGARSS), 2015. IEEE, 1457-1459.
ETHERIDGE, R., PESTI, G. & FOSTER, E. 1998. A comparison of nitrogen values obtained utilizing the Kjeldahl nitrogen and Dumas combustion methodologies (Leco CNS 2000) on samples typical of an animal nutrition analytical laboratory. *Animal Feed Science and Technology,* 73**,** 21-28.
FRAMPTON, W. J., DASH, J., WATMOUGH, G. & MILTON, E. J. 2013. Evaluating the capabilities of Sentinel-2 for quantitative estimation of biophysical variables in vegetation. *ISPRS journal of photogrammetry and remote sensing,* 82**,** 83-92.
GAMON, J., PENUELAS, J. & FIELD, C. 1992. A narrow-waveband spectral index that tracks diurnal changes in photosynthetic efficiency. *Remote Sensing of environment,* 41**,** 35-44.
GARRITY, S. R., EITEL, J. U. & VIERLING, L. A. 2011. Disentangling the relationships between plant pigments and the photochemical reflectance index reveals a new approach for remote estimation of carotenoid content. *Remote Sensing of Environment,* 115**,** 628-635.
GENTY, B., BRIANTAIS, J.-M. & BAKER, N. R. 1989. The relationship between the quantum yield of photosynthetic electron transport and quenching of chlorophyll fluorescence. *Biochimica et Biophysica Acta (BBA)-General Subjects,* 990**,** 87-92.
GUANTER, L., KAUFMANN, H., SEGL, K., FOERSTER, S., ROGASS, C., CHABRILLAT, S., KUESTER, T., HOLLSTEIN, A., ROSSNER, G. & CHLEBEK, C. 2015. The EnMAP spaceborne imaging spectroscopy mission for earth observation. *Remote Sensing,* 7**,** 8830-8857.
GUEYMARD, C. A. 1995. *SMARTS2: a simple model of the atmospheric radiative transfer of sunshine: algorithms and performance assessment*, Florida Solar Energy Center Cocoa, FL.
GUEYMARD, C. A. 2001. Parameterized transmittance model for direct beam and circumsolar spectral irradiance. *Solar Energy,* 71**,** 325-346.
GUPANA, R. S., ODERMATT, D., CESANA, I., GIARDINO, C., NEDBAL, L. & DAMM, A. 2021. Remote sensing of sun-induced chlorophyll-a fluorescence in inland and coastal waters: Current state and future prospects. *Remote Sensing of Environment,* 262**,** 112482.
HABOUDANE, D., MILLER, J. R., PATTEY, E., ZARCO-TEJADA, P. J. & STRACHAN, I. B. 2004. Hyperspectral vegetation indices and novel algorithms for predicting green LAI of crop canopies: Modeling and validation in the context of precision agriculture. *Remote sensing of environment,* 90**,** 337-352.

HABOUDANE, D., MILLER, J. R., TREMBLAY, N., ZARCO-TEJADA, P. J. & DEXTRAZE, L. 2002. Integrated narrow-band vegetation indices for prediction of crop chlorophyll content for application to precision agriculture. *Remote sensing of environment,* 81**,** 416-426.

HASSOUN, M. H. 1995. *Fundamentals of artificial neural networks*, MIT press.

HERNÁNDEZ-CLEMENTE, R., NAVARRO-CERRILLO, R. M., SUÁREZ, L., MORALES, F. & ZARCO-TEJADA, P. J. 2011. Assessing structural effects on PRI for stress detection in conifer forests. *Remote Sensing of Environment,* 115**,** 2360-2375.

HERNÁNDEZ-CLEMENTE, R., NORTH, P. R., HORNERO, A. & ZARCO-TEJADA, P. J. 2017. Assessing the effects of forest health on sun-induced chlorophyll fluorescence using the FluorFLIGHT 3-D radiative transfer model to account for forest structure. *Remote Sensing of Environment,* 193**,** 165-179.

HERRMANN, I., PIMSTEIN, A., KARNIELI, A., COHEN, Y., ALCHANATIS, V. & BONFIL, D. 2011. LAI assessment of wheat and potato crops by VENμS and Sentinel-2 bands. *Remote Sensing of Environment,* 115**,** 2141-2151.

JACKSON, R. D., IDSO, S., REGINATO, R. & PINTER JR, P. 1981. Canopy temperature as a crop water stress indicator. *Water resources research,* 17**,** 1133-1138.

JIA, M., COLOMBO, R., ROSSINI, M., CELESTI, M., ZHU, J., COGLIATI, S., CHENG, T., TIAN, Y., ZHU, Y. & CAO, W. 2021. Estimation of leaf nitrogen content and photosynthetic nitrogen use efficiency in wheat using sun-induced chlorophyll fluorescence at the leaf and canopy scales. *European Journal of Agronomy,* 122**,** 126192.

JONES, H. 1999. Physicochemical and Environmental Plant Physiology, 2nd edn. *Journal of Applied Ecology,* 36**,** 1076-1077.

KARNIELI, A., KAUFMAN, Y. J., REMER, L. & WALD, A. 2001. AFRI—Aerosol free vegetation index. *Remote Sensing of Environment,* 77**,** 10-21.

KIMES, D. S., KNYAZIKHIN, Y., PRIVETTE, J., ABUELGASIM, A. & GAO, F. 2000. Inversion methods for physically-based models. *Remote Sensing Reviews*, 18**,** 381-439.

KJELDAHL, J. 1883. A new method for the estimation of nitrogen in organic compounds. *Z. Anal. Chem,* 22**,** 366.

KRUTZ, D., MÜLLER, R., KNODT, U., GÜNTHER, B., WALTER, I., SEBASTIAN, I., SÄUBERLICH, T., REULKE, R., CARMONA, E. & ECKARDT, A. 2019. The instrument design of the DLR earth sensing imaging spectrometer (DESIS). *Sensors,* 19**,** 1622.

KUMAR, L., SCHMIDT, K., DURY, S. & SKIDMORE, A. 2002. Imaging spectrometry and vegetation science. *Imaging spectrometry.* Springer.

LABATE, D., CECCHERINI, M., CISBANI, A., DE COSMO, V., GALEAZZI, C., GIUNTI, L., MELOZZI, M., PIERACCINI, S. & STAGI, M. 2009. The PRISMA payload optomechanical design, a high performance instrument for a new hyperspectral mission. *Acta Astronautica,* 65**,** 1429-1436.

LAW, B. E., CESCATTI, A. & BALDOCCHI, D. D. 2001. Leaf area distribution and radiative transfer in open-canopy forests: implications for mass and energy exchange. *Tree Physiology,* 21**,** 777-787.

LEE, C. M., CABLE, M. L., HOOK, S. J., GREEN, R. O., USTIN, S. L., MANDL, D. J. & MIDDLETON, E. M. 2015. An introduction to the NASA Hyperspectral InfraRed Imager (HyspIRI) mission and preparatory activities. *Remote Sensing of Environment,* 167**,** 6-19.

LEMAIRE, G., JEUFFROY, M.-H. & GASTAL, F. 2008. Diagnosis tool for plant and crop N status in vegetative stage: Theory and practices for crop N management. *European Journal of agronomy,* 28**,** 614-624.

LI, F., MIAO, Y., HENNIG, S. D., GNYP, M. L., CHEN, X., JIA, L. & BARETH, G. 2010. Evaluating hyperspectral vegetation indices for estimating nitrogen concentration of winter wheat at different growth stages. *Precision Agriculture,* 11**,** 335-357.

LIU, H. Q. & HUETE, A. 1995. A feedback based modification of the NDVI to minimize canopy background and atmospheric noise. *IEEE transactions on geoscience and remote sensing,* 33**,** 457-465.

LOUIS, J., DEBAECKER, V., PFLUG, B., MAIN-KNORN, M., BIENIARZ, J., MUELLER-WILM, U., CADAU, E. & GASCON, F. Sentinel-2 Sen2Cor: L2A processor for users. Proceedings living planet symposium 2016, 2016. Spacebooks Online, 1-8.

MATSON, P. A., NAYLOR, R. & ORTIZ-MONASTERIO, I. 1998. Integration of environmental, agronomic, and economic aspects of fertilizer management. *Science,* 280**,** 112-115.

O'BRIEN, R. M. 2007. A caution regarding rules of thumb for variance inflation factors. *Quality & quantity,* 41**,** 673-690.

PAUL-LIMOGES, E., DAMM, A., HUENI, A., LIEBISCH, F., EUGSTER, W., SCHAEPMAN, M. E. & BUCHMANN, N. 2018. Effect of environmental conditions on sun-induced fluorescence in a mixed forest and a cropland. *Remote Sensing of Environment,* 219**,** 310-323.

PENUELAS, J., BARET, F. & FILELLA, I. 1995. Semi-empirical indices to assess carotenoids/chlorophyll a ratio from leaf spectral reflectance. *Photosynthetica,* 31**,** 221-230.

PEÑUELAS, J., GAMON, J., FREDEEN, A., MERINO, J. & FIELD, C. 1994. Reflectance indices associated with physiological changes in nitrogen-and water-limited sunflower leaves. *Remote sensing of Environment,* 48**,** 135-146.

PETERSON, D. L., ABER, J. D., MATSON, P. A., CARD, D. H., SWANBERG, N., WESSMAN, C. & SPANNER, M. 1988. Remote sensing of forest canopy and leaf biochemical contents. *Remote Sensing of Environment,* 24**,** 85-108.

PLASCYK, J. A. 1975. The MK II Fraunhofer line discriminator (FLD-II) for airborne and orbital remote sensing of solar-stimulated luminescence. *Optical Engineering,* 14**,** 144339.

PLASCYK, J. A. & GABRIEL, F. C. 1975. The Fraunhofer line discriminator MKII-an airborne instrument for precise and standardized ecological luminescence measurement. *IEEE Transactions on Instrumentation and measurement,* 24**,** 306-313.

RAST, M., NIEKE, J., ADAMS, J., ISOLA, C. & GASCON, F. Copernicus Hyperspectral Imaging Mission for the Environment (Chime). 2021 IEEE International Geoscience and Remote Sensing Symposium IGARSS, 2021. IEEE, 108-111.

RAST, M. & PAINTER, T. H. 2019. Earth observation imaging spectroscopy for terrestrial systems: An overview of its history, techniques, and applications of its missions. *Surveys in Geophysics,* 40**,** 303-331.

RICHTER, K., ATZBERGER, C., VUOLO, F., WEIHS, P. & D'URSO, G. 2009. Experimental assessment of the Sentinel-2 band setting for RTM-based LAI retrieval of sugar beet and maize. *Canadian Journal of Remote Sensing,* 35**,** 230-247.

RONDEAUX, G., STEVEN, M. & BARET, F. 1996. Optimization of soil-adjusted vegetation indices. *Remote sensing of environment,* 55**,** 95-107.

ROUJEAN, J.-L. & BREON, F.-M. 1995. Estimating PAR absorbed by vegetation from bidirectional reflectance measurements. *Remote sensing of Environment,* 51**,** 375-384.

ROUSE, J. W., HAAS, R. H., SCHELL, J. A. & DEERING, D. W. 1974. Monitoring vegetation systems in the Great Plains with ERTS. *NASA special publication,* 351**,** 309.

SÖDERSTRÖM, M., PIIKKI, K., STENBERG, M., STADIG, H. & MARTINSSON, J. 2017. Producing nitrogen (N) uptake maps in winter wheat by combining proximal crop measurements with Sentinel-2 and DMC satellite images in a decision support system for farmers. *Acta Agriculturae Scandinavica, Section B—Soil & Plant Science,* 67**,** 637-650.

STEVENSON, F. J. & COLE, M. A. 1999. *Cycles of soils: carbon, nitrogen, phosphorus, sulfur, micronutrients,* John Wiley & Sons.

STEWART, W., DIBB, D., JOHNSTON, A. & SMYTH, T. 2005. The contribution of commercial fertilizer nutrients to food production. *Agronomy journal,* 97**,** 1-6.

TEAM, H. M. C. 2018. HyspIRI Final Report. *Jet Propulsion Laboratory, California Institute of Technology, Pasadena, California***,** 1-87.

TEILLET, P., STAENZ, K. & WILLIAM, D. 1997. Effects of spectral, spatial, and radiometric characteristics on remote sensing vegetation indices of forested regions. *Remote Sensing of Environment,* 61**,** 139-149.

TREMBLAY, N., WANG, Z. & CEROVIC, Z. G. 2012. Sensing crop nitrogen status with fluorescence indicators. A review. *Agronomy for sustainable development,* 32**,** 451-464.

VERHOEF, W., JIA, L., XIAO, Q. & SU, Z. 2007. Unified optical-thermal four-stream radiative transfer theory for homogeneous vegetation canopies. *IEEE Transactions on geoscience and remote sensing,* 45**,** 1808-1822.

VERRELST, J., RIVERA, J. P., VEROUSTRAETE, F., MUÑOZ-MARÍ, J., CLEVERS, J. G., CAMPS-VALLS, G. & MORENO, J. 2015. Experimental Sentinel-2 LAI estimation using parametric, non-parametric and physical retrieval methods–A comparison. *ISPRS Journal of Photogrammetry and Remote Sensing,* 108**,** 260-272.

VERRELST, J., SABATER, N., RIVERA, J. P., MUÑOZ-MARÍ, J., VICENT, J., CAMPS-VALLS, G. & MORENO, J. 2016. Emulation of leaf, canopy and atmosphere radiative transfer models for fast global sensitivity analysis. *Remote Sensing,* 8**,** 673.

VERSTRAETE, M. M., PINTY, B. & DICKINSON, R. E. 1990. A physical model of the bidirectional reflectance of vegetation canopies: 1. Theory. *Journal of Geophysical Research: Atmospheres,* 95**,** 11755-11765.

VILFAN, N., VAN DER TOL, C., YANG, P., WYBER, R., MALENOVSKÝ, Z., ROBINSON, S. A. & VERHOEF, W. 2018. Extending Fluspect to simulate xanthophyll driven leaf reflectance dynamics. *Remote sensing of environment,* 211**,** 345-356.

WANG, Y., SUAREZ, L., POBLETE, T., GONZALEZ-DUGO, V., RYU, D. & ZARCO-TEJADA, P. 2022. Evaluating the role of solar-induced fluorescence (SIF) and plant physiological traits for leaf nitrogen assessment in almond using airborne hyperspectral imagery. *Remote Sensing of Environment,* 279**,** 113141.

WANG, Y., SUAREZ, L., QIAN, X., POBLETE, T., GONZALEZ-DUGO, V., RYU, D. & ZARCO-TEJADA, P. Assessing the Contribution of Airborne-Retrieved Chlorophyll Fluorescence for Nitrogen Assessment in Almond Orchards. 2021 IEEE International Geoscience and Remote Sensing Symposium IGARSS, 2021. IEEE, 5853-5856.

WEIS, E. & BERRY, J. A. 1987. Quantum efficiency of photosystem II in relation to 'energy'-dependent quenching of chlorophyll fluorescence. *Biochimica et Biophysica Acta (BBA)-Bioenergetics,* 894**,** 198-208.

XIE, Q., DASH, J., HUETE, A., JIANG, A., YIN, G., DING, Y., PENG, D., HALL, C. C., BROWN, L. & SHI, Y. 2019. Retrieval of crop biophysical parameters from Sentinel-2 remote sensing imagery. *International Journal of Applied Earth Observation and Geoinformation,* 80**,** 187-195.

YODER, B. J. & PETTIGREW-CROSBY, R. E. 1995. Predicting nitrogen and chlorophyll content and concentrations from reflectance spectra (400–2500 nm) at leaf and canopy scales. *Remote sensing of environment,* 53**,** 199-211.

ZARCO-TEJADA, P. J., MILLER, J. R., NOLAND, T. L., MOHAMMED, G. H. & SAMPSON, P. H. 2001. Scaling-up and model inversion methods with narrowband optical indices for chlorophyll content estimation in closed forest canopies with hyperspectral data. *IEEE Transactions on Geoscience and Remote Sensing,* 39**,** 1491-1507.

ZARCO-TEJADA, P. J., SUÁREZ, L. & GONZALEZ-DUGO, V. 2013. Spatial resolution effects on chlorophyll fluorescence retrieval in a heterogeneous canopy using hyperspectral imagery and radiative transfer simulation. *IEEE Geoscience and Remote Sensing Letters,* 10**,** 937-941.

Chapter 5 : Conclusions

5.1 Summary and main conclusions

The primary objective of this PhD thesis was to assess the role of chlorophyll fluorescence in leaf nutrient estimation for almond orchards at the leaf and the canopy levels using leaf-scanning instruments and airborne and spaceborne imagery. The study evaluated models based on a series of plant parameters over the course of two growing seasons with different fertigation applications in a discontinuous tree-structured almond orchard.

The thesis starts with a general exploration of spectral traits as predictors for a series of leaf nutrient elements (e.g., N, P, and K) and nutrient ratios measured by destructive testing of leaves sampled in the field, followed by focusing on the assessment of nitrogen content, the most abundant primary element in plants. Analysis of airborne imagery and ground measurements indicated that vegetation indices calculated from the visible spectral region (e.g., NPQI, CTRI1, BGI1, and PRI series) were more closely related to nutrients than structural indices calculated from the visible and near-infrared regions (e.g., NDVI). Based on hyperspectral imagery collected in the visible and near-infrared regions, biochemical constituents such as photosynthetic pigments (e.g., C_{ab}, C_{car}, C_x) derived from the FluSAIL radiative transfer model were found to be reliable predictors of nutrient levels (especially for primary macronutrients), outperforming the results of empirical models based on single vegetation indices. In addition, this PhD thesis demonstrates that chlorophyll fluorescence, used as a proxy for photosynthesis, is sensitive to deficiencies of the three primary macro-nutrients (i.e., N, P, and K), especially when considering data across years under varying management practices, yielding $r^2 = 0.74$ (p-values < 0.005) for the relationships of both leaf steady-state measurements and canopy SIF with leaf N.

The study emphasizes the importance of examining other proxies for nutrients in addition to chlorophyll alone, particularly when N levels are high, because C_{ab} shows reverse trends with N across different fertigation applications during different years. At the leaf level, the Dualex leaf-measurement of chlorophyll alone was not as sensitive and consistent as the NBI indicator based on both Flav and C_{ab} parameters. Alternatively, steady-state chlorophyll fluorescence results demonstrated consistently stronger correlation and trend with primary macro-nutrient results than did the leaf-measured C_{ab} results. This stronger correlation and trend remained consistent at the canopy level, whereas spectral vegetation indices showed inconsistent trends. However, airborne SIF calculated from the illuminated crown pixels was correlated with leaf N results across growing seasons. For leaf nitrogen estimation in almond trees, C_{ab} and SIF were found to be the most effective predictors of N for individual years, at both high-resolution airborne scale and spaceborne scale, outperforming other biochemical tests and biophysical plant trait assessments. SIF exhibited performance in terms of primary macro-nutrients superior to that of RTM-based plant traits across years, with an $r^2 = 0.74$ (p-values < 0.005) for both steady-state measurements and canopy SIF of leaf N. The performance of N estimation improved when SIF was coupled with photosynthetic plant traits derived by both airborne and spaceborne platforms, making combined C_{ab} and SIF superior to any other combinations for this purpose. The model using C_{ab} alone showed modest predictivity for leaf N variability ($r^2 = 0.49$, RMSE = 0.16%, p-value < 0.001) over the two years of data, but when SIF and C_{ab} traits (non-collinear) were coupled, predictions improved dramatically ($r^2 = 0.95$, RMSE = 0.05%, p-value < 0.001). These findings suggest that chlorophyll fluorescence is a promising and reliable indicator for nutrient assessment, and that the combination of C_{ab} and SIF provides the most robust assessment of leaf N concentration.

Additionally, this work demonstrates that spaceborne hyperspectral imagery, such as the newly developed DESIS onboard the International Space Station (ISS) with a 30-m spatial resolution, is useful for the operational monitoring of N content via models using RTM-derived leaf biochemical trait determinations and SIF in almond tree orchards. Also, N assessments of discontinuous dense canopies are more accurate with greater spectral resolution than with greater spatial resolution, and hyperspectral imaging provides the most accurate N estimations. These results demonstrate the vital contribution of hyperspectral spaceborne missions to large-area N monitoring and precision agriculture.

5.2 Implications and contributions

Over two growing seasons with different fertigation applications monitored at various scales, this PhD thesis demonstrates a consistent method for assessing leaf nitrogen in a dense discontinuous tree-structured almond orchard. As compared to the standard method of using C_{ab} alone, the combination of C_{ab} and SIF provides a more robust and improved assessment of leaf nitrogen, eliminating the saturation effects and instability caused by the variation of fertigation practices. As a result of this research, SIF has been further proven as a means of assessing leaf nutrients in heterogeneous canopies and monitoring vegetation health before harvest. A subsequent analysis of leaf nutrient status can also be conducted during other phenological stages. In Chapter 4, the effects of image spatial resolution are evaluated by comparing the results obtained from pure tree-crown pixels and from downsampled resolutions resulting in mixed features, both for SIF and N content assessment. Considering that the tree canopies in this almond orchard are quite dense and clustered, the effects of canopy discontinuity did not impede the assessment. The results presented in this thesis provide us with new insights which can be applied to assessing the performance of

SIF techniques for other tree species and structures, particularly when using coarser spatial resolution sensors at the regional scale.

An assessment of the PRI family of indices as a measure of the dynamics of the xanthophylls was carried out. Throughout two growing seasons in the almond orchard, PRI_{515} (PRI index using as reference the signal at 515 nm), developed to minimize structural effects, was superior to PRI (at 570 nm). As part of this thesis, FluSAIL RTM was employed to retrieve C_x data for the assessment of the de-epoxidation state of the xanthophyll cycle, as well as the standard major leaf photosynthetic pigments C_{ab}, C_{car}, and Anth. The modeling of the C_x parameter is based on *in vivo* absorption coefficients for two extreme states of the carotenoid pool, corresponding to the two extremes of xanthophyll de-epoxidation, and describes the intermediate states as a lineal mixture of these two extreme states. The C_x data retrieved from airborne hyperspectral imagery was significantly correlated with PRI_{515} results (r^2 = 0.68 and 0.60 in 2020 and 2021, *p*-values <0.001) and with leaf N results (r^2 = 0.61 and 0.62 in 2020 and 2021, *p*-values <0.001). In addition, C_x was found to be the next best non-collinear (VIF<10) predictor for leaf N after C_{ab} and SIF. The model incorporating C_x, C_{ab}, and SIF outperformed any other combinations with plant traits derived from high-resolution airborne hyperspectral imagery across both years. These results suggest that RTM-derived C_x estimates from airborne hyperspectral imagery, serving as a measure of xanthophyll status, are important predictors for leaf N levels in almond orchards, the model's performance improving when combined with C_{ab} and SIF.

RTM-inverted plant traits identified from VNIR hyperspectral images are found to be more accurate N estimators than single vegetation indices at both high (airborne at 0.4-m) and coarse (DESIS at 30-m) spatial resolutions. Compared to biochemical constituent results, LAI based on vegetation pixels from the airborne scale was less effective for leaf N estimates, whereas LAI

derived from spaceborne DESIS, where pixels comprise crowns, soil, and shaded background, gave more accurate N assessment than did plant traits derived from high-resolution airborne imagery. Based on these results, LAI was not the primary indicator of leaf nutrient content when using high-resolution imagery, but it should be considered with coarser spatial resolutions.

Even though this thesis is primarily focused on the use of hyperspectral imagery for nutrient assessment, the results from the multispectral Sentinel-2 imagery, a widely used free satellite source, are also evaluated. In the absence of SIF quantification, other biochemical constituents (e.g., C_w and C_{dm}) can be coupled with C_{ab} for estimation of leaf nitrogen using the SWIR spectral region.

The potential effect of water stress under varying fertigation was also considered. Based on the two-year dataset, it was observed that the water stress indicator, CWSI, did not show any correlation with leaf nitrogen variability, revealing different variability patterns throughout the orchard. These results indicate that leaf nitrogen variability is not driven by water status in this managed intensive almond orchard, even when both water and fertilizer are applied together via fertigation.

This study also demonstrates the high correlation between chlorophyll fluorescence and primary macro-nutrients, including P and K, and provides guidance on estimating these nutrients using the proposed method. From a physiological perspective, it is believed that the SIF signal is closely related to the photosynthetic capacity of leaves, which is in turn dependent on the availability of micro-nutrients. Particularly evident are the correlations of SIF data with results for plants that are capable of absorbing large amounts of nutrients, suggesting that these nutrient elements may be of particular importance to photosynthesis. As a result of their indirect and secondary roles in the

photosynthetic process, results for secondary macro-nutrients (e.g., Ca, Mg) and micro-nutrients (e.g., Fe, Cu) demonstrate less correlation with C_{ab} and chlorophyll fluorescence data.

5.3 Recommendations for further research

This thesis contributes to the development of future research in the fields of fertilizer use efficiency optimization and precision agriculture in heterogeneous orchards using airborne and spaceborne remote sensing. Future research could focus on:

- ⇨ Investigating the sensitivity of SWIR spectral bands to nitrogen and other nutrients through the use of high-resolution airborne and spaceborne hyperspectral imagery.
- ⇨ Evaluation of the contribution and robustness of C_{ab} and SIF in the assessment of the leaf nitrogen levels of other tree species at airborne and spaceborne levels.
- ⇨ Examining the performance of plant trait estimation using 3-D RTMs in heterogeneous orchards and its contribution to leaf N assessment.
- ⇨ Exploring plant spectral traits and performance in assessment of other macro-nutrients (i.e., P and K).
- ⇨ Improving the accuracy of SIF quantification via use of a variety of advanced methods and sensor technologies (e.g., sub-nanometer spectrometers) in heterogeneous orchards.
- ⇨ Investigating the feasibility and performance of satellite-borne spectrometers for the quantification of SIF in heterogeneous orchards, especially for less dense canopy, as well as investigating their contribution to nutrient assessment.

Appendix 1

Evaluating the role of solar-induced fluorescence (SIF) and plant physiological traits for leaf nitrogen assessment in almond using airborne hyperspectral imagery

This is the paper in its published format in Remote Sensing of Environment:

Wang, Y., Suarez, L., Poblete, T., Gonzalez-Dugo, V., Ryu, D., Zarco-Tejada, P.J., Evaluating the role of solar-induced fluorescence (SIF) and plant physiological traits for leaf nitrogen assessment in almond using airborne hyperspectral imagery, Remote Sensing of Environment, 279, 113141.

Remote Sensing of Environment 279 (2022) 113141

Contents lists available at ScienceDirect

Remote Sensing of Environment

journal homepage: www.elsevier.com/locate/rse

Evaluating the role of solar-induced fluorescence (SIF) and plant physiological traits for leaf nitrogen assessment in almond using airborne hyperspectral imagery

Y. Wang [a,*], L. Suarez [a,b], T. Poblete [a,b], V. Gonzalez-Dugo [c], D. Ryu [a], P.J. Zarco-Tejada [a,b,c]

[a] Department of Infrastructure Engineering, Faculty of Engineering and Information Technology (FEIT), University of Melbourne, Melbourne, VIC 3010, Australia
[b] School of Agriculture and Food, Faculty of Veterinary and Agricultural Sciences (FVAS), University of Melbourne, Melbourne, VIC 3010, Australia
[c] Instituto de Agricultura Sostenible (IAS), Consejo Superior de Investigaciones Cientificas (CSIC), Avenida Menendez Pidal s/n, 14004 Cordoba, Spain

ARTICLE INFO

Edited by Jing M. Chen

Keywords:
Chlorophyll fluorescence
SIF
Nitrogen
Chlorophyll
FluSAIL RTM
Hyperspectral
Gaussian process regression
Random Forest
Almond
Tree orchard

ABSTRACT

Accurate, spatially extensive, and frequent assessments of plant nitrogen (N) enabled by remote sensing allow growers to optimize fertilizer applications and reduce environmental impacts. Standard remote sensing methods for N assessment typically involve the use of chlorophyll-sensitive vegetation indices calculated from multispectral or hyperspectral reflectance data. However, the chlorophyll $a + b$ derived from spectral indices is indirectly related to leaf N and saturates at high leaf N levels, dramatically reducing the sensitivity with leaf N under these conditions. Furthermore, these relationships are heavily influenced by canopy structure, variability in leaf area density, proportion of sunlit-shaded tree-crown components, soil background, and understory. Recent studies in uniform crops have demonstrated that estimation of plant N can be improved by considering leaf biochemical constituents derived from radiative transfer model (RTM) and solar-induced fluorescence (SIF). However, it is unclear whether these methods are transferable to tree crops due to their intrinsic physiological differences, structural complexity, and within-tree crown heterogeneity. We investigated how various hyperspectrally derived proxies for leaf N, including RTM-based traits and SIF, could be combined to assess N status on a 1200-ha almond orchard across two growing seasons. RTM-based chlorophyll $a + b$ content (C_{ab}) and SIF were found to be the most important and consistent predictors for leaf N compared to other leaf biochemical and biophysical traits. C_{ab} alone was a modest predictor of leaf N variability ($r^2 = 0.49$, RMSE = 0.16%, p-value <0.001), but when the non-collinear SIF and C_{ab} traits were coupled together, predictions improved dramatically ($r^2 = 0.95$, RMSE = 0.05%, p-value <0.001). Leaf area index (LAI) was poorly associated with leaf N, suggesting that leaf physiological traits may be more important than structural traits in quantifying leaf N in well-managed orchards characterized by high N levels. Consistent results across the 2 years suggests the importance of airborne SIF coupled with C_{ab} for precision agriculture and leaf N status assessment in almond orchards.

1. Introduction

Nitrogen (N) is an essential nutrient for plant growth, productivity, and quality and is often the major limiting factor for photosynthesis (Evans, 1989). However, more N fertilizer than needed is often applied to maximize yield and quality (Conant et al., 2013). In addition to the economic costs of N over-fertilization, excess N has detrimental effects on the environment, leading to pollution of the atmosphere and water systems (Shcherbak et al., 2014; Stevenson and Cole, 1999; Zebarth et al., 2009). Monitoring crop N status is essential for optimizing N applications and maintaining productivity while minimizing environmental impacts for sustainable agriculture (Manna et al., 2005; Matson et al., 1998; Panhwar et al., 2019; Snyder et al., 2009).

The concentration of leaf nitrogen can be determined through various approaches. The chemical analysis of leaf tissue via destructive sampling, such as the traditional Kjeldahl-digestion method (Kjeldahl, 1883) or the simpler and faster Dumas combustion method to avoid using toxic chemicals (Dumas, 1831), has been the standard method for the assessment of leaf N. Although this approach is very accurate, it is not cost- or time-effective for the continuous monitoring of N status over large areas. In recent decades, imaging spectroscopy has been used as an alternative to lab-based assays from the leaf, enabling rapid N

* Corresponding author.
E-mail address: wang.y@unimelb.edu.au (Y. Wang).

https://doi.org/10.1016/j.rse.2022.113141
Received 13 December 2021; Received in revised form 11 April 2022; Accepted 18 June 2022

monitoring at a range of spatio-temporal scales (Chapman and Barreto, 1997; Dong et al., 2020; Nageswara Rao et al., 2001; Romina et al., 2019; Schepers et al., 1992) to canopy level (Clevers and Gitelson, 2013; Clevers and Kooistra, 2011; Gnyp et al., 2014; Haboudane et al., 2002; Inoue et al., 2012; Nigon et al., 2020; Pinter Jr et al., 2003).

Most remote sensing (RS) studies of leaf N depend on an assumed strong correlation between leaf chlorophyll $a + b$ (C_{ab}) and N (Evans, 1989). Thus, C_{ab} has been proposed as a common RS-based indicator for N assessment (Clevers and Gitelson, 2013; Schlemmer et al., 2013; Wood et al., 1992; Yoder and Pettigrew-Crosby, 1995). The conventional approach in these studies has been to determine an empirical relationship between destructively sampled tissue N and non-destructive proxy measurements, including hand-held spectral readings at visible, red-edge, and near-infrared spectral bands (Bullock and Anderson, 1998; Cerovic et al., 2015; Cerovic et al., 2012; Chang and Robison, 2003; Jongschaap and Booij, 2004; Padilla et al., 2018; Wood et al., 1992) or chlorophyll-sensitive vegetation indices derived from multispectral or hyperspectral reflectance at leaf and canopy levels (Clevers and Gitelson, 2013; Cummings et al., 2021; Filella et al., 1995; Fitzgerald et al., 2010; Gnyp et al., 2014; Inoue et al., 2012; Nigon et al., 2020). Although leaf chlorophyll meters are valuable tools for quick on-farm determination of leaf N status, the relationship between chlorophyll meter readings and N content differs across plant genotypes and environmental contexts (Xiong et al., 2015). Furthermore, these chlorophyll indicators from chlorophyll meters or vegetation indices are not the actual chlorophyll content, but rather the proxy for leaf greenness. Although they are generally related to leaf N, these proxies saturate at high N levels, resulting in reduced sensitivity to increased N values (Li et al., 2020; Padilla et al., 2018; Romina et al., 2019; Schlemmer et al., 2013). In addition to these leaf greenness indicators, vegetation indices widely used in RS such as the Normalized Difference Vegetation Index (NDVI) (Rouse et al., 1974), are also indirectly related to N (Yoder and Pettigrew-Crosby, 1995). They have been demonstrated to lack sensitivity and to saturate at high plant densities and under overfertilization levels (Flowers et al., 2003; Matsushita et al., 2007; Nguy-Robertson et al., 2012). To prevent these effects, proxies directly linked to leaf N through pathways other than via the quantification of chlorophyll content are required.

Moreover, spectral indices that incorporate red-edge spectra are thought to be improved ways to derive N status due to the higher sensitivity of this spectral region to moderate and high chlorophyll content levels (Gitelson et al., 2003; Gitelson et al., 1996). Fitzgerald et al. (2006) found that the Normalized Difference Red-Edge (NDRE) index, which is calculated by replacing the red band of NDVI with the red-edge band, was a reliable indicator of chlorophyll and N status. Another index termed the Canopy Chlorophyll Content Index (CCCI) is based on a two-dimensional planar extension of NDVI and NDRE and has been proposed as a method for improved estimation of N in annual crops (e.g., wheat (*Triticum aestivum*)) (Fitzgerald et al., 2010; Li et al., 2014; Perry et al., 2012). Another approach combining the information in the red-edge with a structural index is the use of the Transformed Chlorophyll Absorption in Reflectance Index (TCARI) with the Optimized Soil-Adjusted Vegetation Index (TCARI/OSAVI) (Haboudane et al., 2002). These indices tend to be sensitive to chlorophyll $a + b$ induced by N variability while also accounting for background effects (Gabriel et al., 2017; Wu et al., 2008). Nevertheless, empirical relationships are required to estimate N from these vegetation indices.

As leaf N content is associated with many other physiological traits besides C_{ab} content, the use of radiative transfer model (RTM)-based retrievals of plant physiological traits is a promising alternative to spectral indices for assessing leaf N. Due to the fact that leaf N is not an input in the RTM, nutrient variability was described through a wide range of model-simulated plant traits, including leaf constituents (e.g., C_{ab}, dry matter (C_{dm}), water content (C_w)), and canopy structural parameters (Baret et al., 2007; Camino et al., 2018a; Thorp et al., 2012; Wang et al., 2021; Wang et al., 2018). Traits derived from RTMs are considered more accurate and transferrable than index-based empirical algorithms (Kimes et al., 2000), although this has only been tested for uniform crops. For orchards, this method is more complex due to the tree crown heterogeneity and clumping effects with mixed crown-shadow-soil backgrounds. Radiative transfer model inversion also allows inverting for other non-photosynthetic plant pigments, such as carotenoids (C_{car}) and xanthophylls (C_x), which are involved in photosynthetic light-harvesting (Jacquemoud et al., 2009; Niyogi et al., 1997; Vilfan et al., 2016; Vilfan et al., 2018). Plants prevent photodamage by deoxidizing the xanthophyll violaxanthin (V) into antheraxanthin (A) and zeaxanthin (Z) in response to excess excitation energy (Demmig et al., 1987; Gilmore, 1997). Therefore, xanthophyll composition is linked to photosynthetic efficiency and may thus relate to leaf N status, particularly under abiotic stress conditions (Cheng, 2003; Ramalho et al., 2000; Tóth et al., 2002; Verhoeven et al., 1999). Thus, based on their links with photosynthesis under stress conditions, the complete set of photosynthetic and non-photosynthetic pigments, along with structural traits, can lead to a more informed assessment of N.

In the last few decades, solar-induced fluorescence (SIF) has been proposed as a trait for monitoring plant physiology, vegetation functioning, and plant biotic and abiotic stress detection due to the dynamic changes in photochemical and non-photochemical quenching in the photosynthetic process (see review paper by Mohammed et al. (2019) and studies from Maxwell and Johnson (2000); Mohammed et al. (1995); Murchie and Lawson (2013); Porcar-Castell et al. (2014); Sayed (2003); Zarco-Tejada et al. (2018)). It is well known that abiotic-induced stress conditions such as light intensity, water status, and temperature extremes modulate the photosynthetic performance (Ashraf and Harris, 2013; Biswal et al., 2011; Saibo et al., 2009). Most importantly, SIF is considered a direct proxy for electron transport rate and thus a direct measure of photosynthesis (Genty et al., 1989; Krause and Weis, 1991; Middleton et al., 2016; Walker et al., 2014). N modulates the fluorescence-photosynthesis link, thus several studies propose SIF as a potential proxy for the assessment of leaf N status at both the leaf (Huang et al., 2004; Lu and Zhang, 2000) and the canopy levels (Cendrero-Mateo et al., 2016; Corp et al., 2003; Middleton et al., 2016; Mohammed et al., 2019; Wang et al., 2021). For example, Camino et al. (2018a) showed that SIF improved predictions of N content in wheat. However, in tree orchards, SIF is affected by canopy structure and the mixing of within-crown sunlit and shaded components. This adds complexity to the accurate SIF quantification in tree orchards (Camino et al., 2018b). The combined use of RTM-based leaf biochemistry estimates with SIF for N assessment is poorly studied in structurally complex tree orchards. Such a methodology may have important uses in precision agriculture when using commercial hyperspectral sensors with 5- to 6-nm spectral resolution, which have been shown to be sensitive to SIF emission and thus are useful for quantifying abiotic sources of stress (Belwalkar et al., 2022; Belwalkar et al., 2021; Raya-Sereno et al., 2021; Zarco-Tejada et al., 2016; Zarco-Tejada et al., 2012; Zarco-Tejada et al., 2013).

In this study, we explored the contribution of various hyperspectrally derived proxies for leaf N status assessment in almond orchards across two consecutive growing seasons, including airborne-quantified plant physiological traits estimated by RTM inversion and canopy SIF. We evaluated the accuracy and robustness of the retrieved plant physiological traits and the collinearity among plant pigments, SIF, and structural traits when assessing leaf N variability across the field. Rather than a data driven approach, our study advances the mechanistic understanding of the responses of RS-derived plant traits to leaf N content changes.

2. Material and methods

2.1. Study area and field data collection

This study was conducted in a commercial almond orchard in

northwest Victoria, Australia, at the pre-harvest stage of the growing season in 2019/2020 and 2020/2021 when the leaves are mature and have reached their maximum N uptake capacity. The region has a Mediterranean climate with hot, dry summers and mild, wet winters. Average annual precipitation is 300 mm. The summer of 2020/2021 was milder than that of 2019/2020, with an average maximum air temperature of 29.5 °C in December 2020, compared to 34.3 °C in December 2019. The almond orchard (Fig. 1) covers approximately 1240 ha with trees planted between 2006 (Northern blocks facing N-S) and 2007 (Southern blocks mixed in N-S and *E*-W orientations) on sandy loam soils. Generally, trees planted in the eastern blocks tend to have larger tree crowns than those in the west. Three almond varieties were planted in alternating blocks of six rows to facilitate cross-pollination (Asai et al., 1996; Hill et al., 1985). Varieties included Nonpareil (50%), Carmel (33%), and Price (17%). A drip fertigation system was used to supply the same amount of water and nutrients to the tree root zones for each variety at the same time and was established at 1-h intervals between varieties across the entire orchard. Fertigation was supplied as needed based on weather and plant responses over the growing season. In summer of 2020/2021, irrigation volume was 10% higher (12,795 m^3/ha) than in 2019/2020 (11,465 m^3/ha), but total N fertilizer applications (330 kg/ha in 2020/2021 and 326 kg/ha in 2019/2020) were similar. In summer of 2020/2021, Nonpareil was treated with 10% less fertigation than Carmel and Price varieties across the orchard based on the difference observed along the 2019/2020 season.

Fifteen homogeneous plots consisting of six rows of seven to eight trees were monitored throughout the experiment in 2019/2020 and 2020/2021 (Fig. 2). In each plot, four adjacent trees from Nonpareil and Carmel varieties (two each; yellow dashed rectangle in Fig. 2a) were sampled in situ prior to harvest in both years. Leaf C_{ab}, anthocyanins (Anth), flavonoid (Flav) content, and the nitrogen balance index (NBI) were measured from 20 representative sunlit mature leaves per tree using a Dualex 4 Scientific sensor (FORCE-A, Orsay, France). Leaf steady-state chlorophyll fluorescence (Ft) and leaf reflectance spectra within the visible (VIS) and near-infrared (NIR) regions were measured with FluorPen FP 110 and PolyPen RP 410 instruments (PSI, Brno, Czech Republic) on the same leaves with the Dualex sensor. A series of vegetation pigment indices (see Table 1 for the complete list of indices used in this study) were calculated based on the leaf reflectance spectra measured from the PolyPen handheld instrument. An additional set of 20 leaves per plot were collected for biochemical laboratory analyses using Dumas Combustion (Buckee, 1994; Dumas, 1831; Etheridge et al., 1998) with a LECO TruMac CNS Macro Analyzer (LECO Corporation, MI, USA) and an inductively coupled plasma optical emission spectrometer (ICP-OES Optima 8300, Perkin Elmer, USA). Thirteen macro and micronutrients (e.g., nitrogen, carbon, phosphorus, and potassium) were measured. The ranges of variation of field data collected over 2 years were compared against Ft-measured quartiles. The correlations between leaf measurement and laboratory N concentration were calculated for both years.

Fig. 1. Colour-infrared (CIR) overview of the hyperspectral mosaic acquired with the VNIR hyperspectral sensor over the 1200-ha study site collected on January 31, 2021. Spectral bands at 860 (R), 650 (G), and 550 (B) nm are shown with a spatial resolution of 40 cm per pixel.

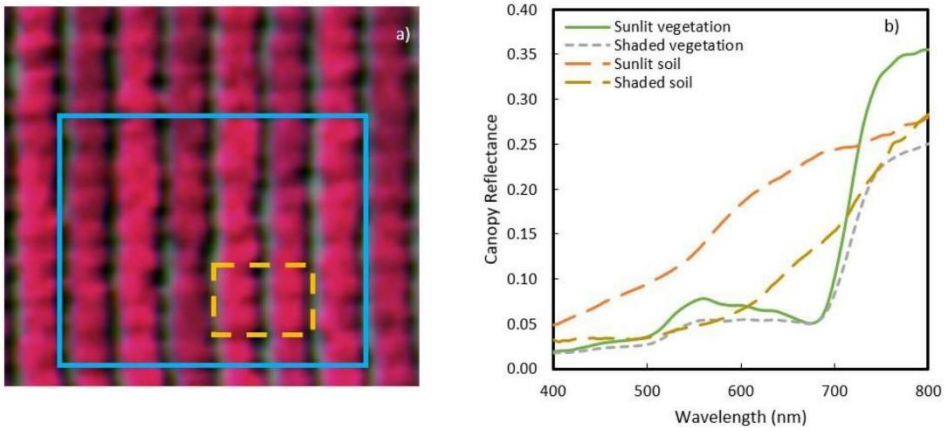

Fig. 2. (a) Study plot consisting of six rows by eight trees within the blue solid line. Leaves from four trees within the yellow dashed rectangle were measured in the field. (b) The reflectance spectra of different scene components extracted from the airborne hyperspectral imager, including sunlit (green solid line) and shaded (grey dashed line) tree crown, and sunlit (orange dashed line) and shaded soil (brown dashed line) pixels. (For interpretation of the references to colour in this figure legend, the reader is referred to the web version of this article.)

Table 1
Spectral vegetation index equations used in this study.

Index	Equation	Reference
Structural indices		
NDVI	$(R_{800} - R_{670})/(R_{800} + R_{670})$	Rouse et al. (1974)
EVI	$2.5 \bullet (R_{800} - R_{670})/(R_{800} + 6 \bullet R_{670} - 7.5 \bullet R_{500} + 1)$	Liu and Huete (1995)
MCARI2	$1.5 \bullet \{2.5 \bullet (R_{800} - R_{670}) - 1.3 \bullet (R_{800} - R_{550})\} \Big/ \sqrt{(2 \bullet R_{800} + 1)^2 - (6 \bullet R_{800} - 5 \bullet R_{670}) - 0.5}$	Haboudane et al. (2004)
RDVI	$(R_{800} - R_{670})/\sqrt{R_{800} + R_{670}}$	Roujean and Breon (1995)
OSAVI	$(1 + 0.16) \bullet (R_{800} - R_{670})/(R_{800} + R_{670} + 0.16)$	Rondeaux et al. (1996)
Chlorophyll a + b indices		
MCARI	$((R_{700} - R_{670}) - 0.2 \bullet (R_{700} - R_{550})) \bullet (R_{700}/R_{670})$	Daughtry et al. (2000)
TCARI/ OSAVI	$3 \bullet ((R_{700} - R_{670}) - 0.2 \bullet (R_{700} - R_{550}) \bullet (R_{700}/R_{670}))/(1 + 0.16) \bullet (R_{800} - R_{670})/(R_{800} + R_{670} + 0.16)$	Haboudane et al. (2002)
NPQI	$(R_{415} - R_{435})/(R_{415} + R_{435})$	Barnes et al. (1992)
PSSRa	R_{800}/R_{675}	Blackburn (1998)
PSSRb	R_{800}/R_{650}	Blackburn (1998)
PSSRc	R_{800}/R_{500}	Blackburn (1998)
SIPI	$(R_{800} - R_{445})/(R_{800} - R_{680})$	Penuelas et al. (1995)
CTRI1	R_{695}/R_{420}	Carter (1994)
Indices based on the green region		
PRI	$(R_{570} - R_{531})/(R_{570} + R_{531})$	Gamon et al. (1992)
PRI_{515}	$(R_{515} - R_{531})/(R_{515} + R_{531})$	Hernández-Clemente et al. (2011)
PRI•CI	$((R_{570} - R_{531})/(R_{570} + R_{531})) \bullet ((R_{760}/R_{700}) - 1)$	Garrity et al. (2011)
Fluorescence quantification		
SIF	$E_{out} \cdot L_{in} - E_{in} \cdot L_{out}/E_{out} - E_{in}$ Where E and L represent the incoming irradiance and canopy radiance, 'in' band refers to 762 nm, and 'out' band refers to the average value in 750 and 778 nm	Plascyk and Gabriel (1975)
Canopy temperature		
CWSI	$(T_c - T_a) - (T_c - T_a)_{LL}/(T_c - T_a)_{UL} - (T_c - T_a)_{LL}$ Where LL and UL represent the upper limit and lower limit of canopy (T_c) and air (T_a) temperatures	Jackson et al. (1981)

2.2. Airborne hyperspectral and thermal imagery

Airborne campaigns were conducted concurrently with the field measurements on February 17, 2020, and January 31, 2021. Both campaigns occurred at solar noon under clear skies. Field sampling and auxiliary data collection required for the calibration and atmospheric correction of the images were conducted simultaneously with airborne campaigns. A hyperspectral line-scanning sensor (Micro-Hyperspec VNIR E-Series model, Headwall Photonics, Fitchburg, MA, USA) and a thermal infrared camera (A655sc model, FLIR Systems, Wilsonville, OR, USA) were flown in tandem on a manned aircraft operated by the HyperSens Remote Sensing Laboratory, the Airborne Remote Sensing Facility of The University of Melbourne. The hyperspectral imager covers 371 spectral bands in the visible and near-infrared regions (400–1000 nm) with a full-width at half-maximum (FWHM) of 5.8 nm and a spectral sampling interval of 1.626 nm. Hyperspectral and thermal images with an angular field of view (FOV) of 66° and 45° (8- and 13.1-mm focal length), respectively, were collected by the aircraft at 550 m above ground level (AGL), yielding spatial resolutions of 40 and 60 cm, respectively, enabling the differentiation of sunlit and shaded components of tree crowns and soil areas. SMARTS (Gueymard, 1995, 2001; Gueymard et al., 2002) irradiance simulations were used to correct for atmospheric effects of the hyperspectral imagery based on aerosol optical measurements at 500 nm taken with a Microtops II sunphotometer (Solar Light, PA, USA) connected to a GPS – 12 navigator (Garmin, Olathe, KS, USA) at the time of each flight. Air temperatures and relative humidity were calculated based on the average of three nearby weather stations (Robinvale, Lake Powell and Wemen) less than 15 km from the study site. Hyperspectral line-scanned image orthorectification was performed using PARGE software (ReSe Applications Schläpfe, Wil, Switzerland) with readings from the onboard inertial measuring unit (IMU) (VectorNav VN-300 dual-antenna GNSS/INS, Dallas, TX, USA). Empirical line calibration was conducted by measuring the reflectance spectra and temperature of bare soil and green and dry vegetation. Spectra were measured with an ASD Handheld-2 field spectrometer (FieldSpec Handheld Pro, ASD Inc., CO, USA), and temperature was measured with a thermal gun (LaserSight, Optris, Germany). Hyperspectral and thermal imagery were mosaicked (Figs. 1 and 3) using ENVI (Boulder, Colorado) and Pix4D (Lausanne, Switzerland) photogrammetry software, respectively.

Automatic segmentation of the hyperspectral reflectance imagery was conducted using Fiji (Abràmoff et al., 2004) combining Niblack's (Niblack, 1985) thresholding method on the NIR band, and Phansalkar's thresholding method (Phansalkar et al., 2011) on a structural index (NDVI >0.72). This method enabled the discrimination of sunlit pure tree crowns from the soil background, as well as the separation of within-crown shadows (see reflectance spectra in Fig. 2b). Considering the sensitivity of SIF to the illumination levels, a more selective segmentation (10% restricted) was applied to the hyperspectral radiance data when segmenting the sunlit crown component. The thermal

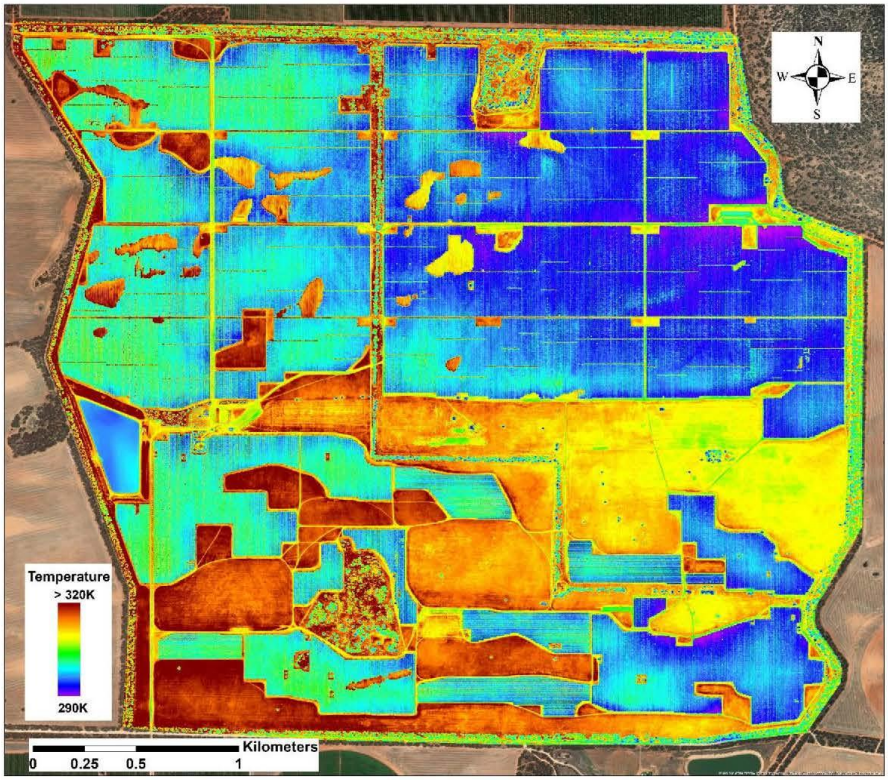

Fig. 3. Thermal mosaic collected over the entire study area captured on January 31, 2021 at a spatial resolution of 60 cm. Cooler colors (purple and blue) indicate plant canopies, and yellow/brown colors indicate soil. (For interpretation of the references to colour in this figure legend, the reader is referred to the web version of this article.)

segmentation of the tree canopy was performed with Niblack's thresholding method (Niblack, 1985) to eliminate the soil and background effects. The resulting pure vegetation pixels obtained in the previous step were clustered into tree-crown features using a watershed segmentation approach based on Euclidean distance (as in Zarco-Tejada et al. (2018)). In Fig. 4, an example of the segmentation conducted on the hyperspectral and the thermal mosaics is presented.

The mean radiance and reflectance spectra, and temperature were extracted from tree crown pixels by hyperspectral and thermal imagery for each study plot. The crop water stress index (CWSI) (Idso et al., 1981) was calculated based on the canopy-air temperature difference and the water vapor pressure deficit (VPD) at the time of image acquisition for assessing the tree-crown water stress levels. A non-water-stressed baseline (NWSB) for almond trees suggested by Bellvert et al. (2018) was used.

SIF was quantified using the Fraunhofer line depth (FLD) principle (Plascyk and Gabriel, 1975) based on three spectral bands (3FLD) (Maier et al., 2004) located inside and outside the O_2-A absorption features. Specifically, we compared canopy radiance values L_{in} at 762 nm and L_{out} at 750 and 778 nm extracted from the hyperspectral imagery to the corresponding incoming irradiance E_{in} (E_{762}) and E_{out} (E_{750}, E_{778}) derived from the field measurements during the flight and resampled to match the spectral specifications of the airborne hyperspectral sensor. To account for the effects of negative values from atmospheric and calibration factors, SIF was scaled using the offset from non-fluorescence targets (e.g., soil) extracted from the imagery. Fig. 5 shows the irradiance and the mean radiance spectra from two study plots (in Fig. 5a and b) at the oxygen-A absorption region around 760 nm. Average tree-crown reflectance (R) spectra extracted from pure vegetation pixels were used to estimate plant traits through RTM inversion and to calculate narrow-band hyperspectral indices (Table 1) for comparison. The set of indices used comprised structural indices (e.g., NDVI), pigment indices (e.g., Modified Chlorophyll Absorption in Reflectance Index (MCARI), TCARI/OSAVI, and Carter Index 1 (CTRI1)), and indices in the visible region (e.g., Photochemical Reflectance Index (PRI)) that track the dynamics of photoprotective mechanisms. Indices calculated

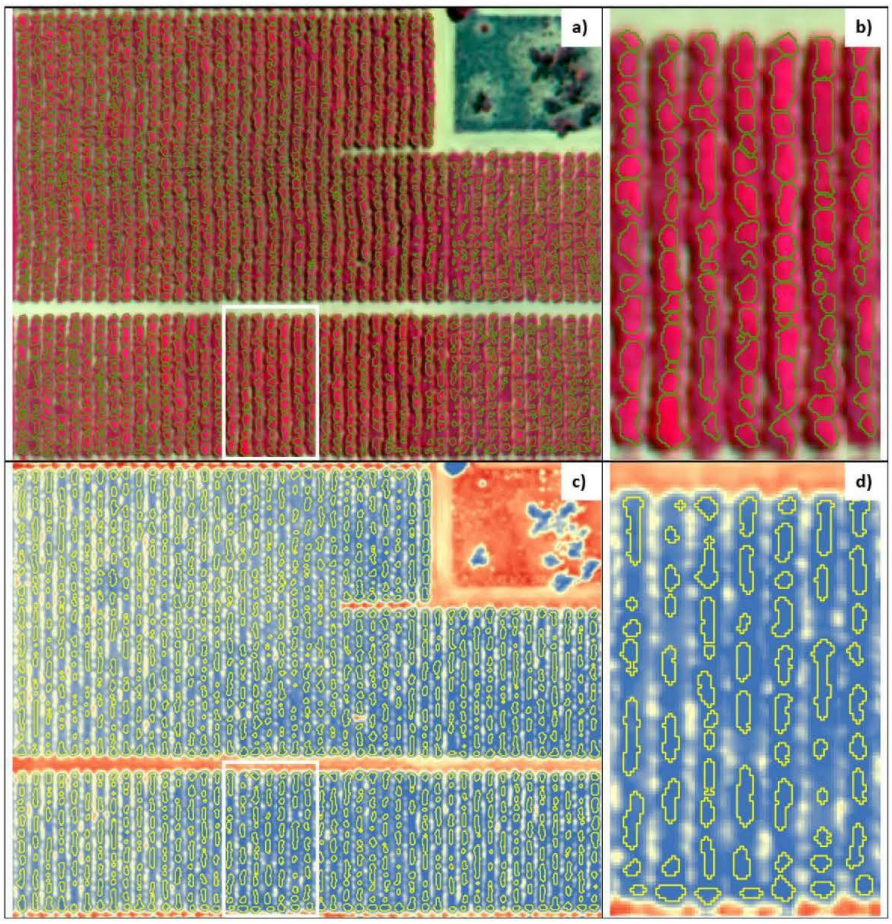

Fig. 4. Overview of the tree-crown segmentation applied to the hyperspectral mosaic (a, upper image in colour-infrared, crown in green outline) and the thermal mosaic (c, bottom image displaying cooler canopy in blue and hot soil in red colour, crown in yellow outline). Right column contains zoomed-in views (b and d) of the scenes within the white rectangle on the left. (For interpretation of the references to colour in this figure legend, the reader is referred to the web version of this article.)

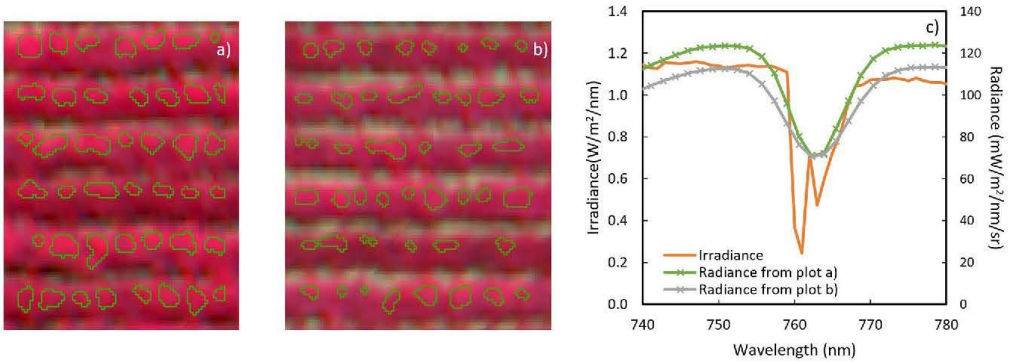

Fig. 5. Segmentation of the sunlit crown area for SIF quantification on two study plots (a) higher nutrient level and (b) lower nutrient level. The irradiance spectrum (orange colour) was used along with the radiance spectra (example shown in (c) for two study plots (green and grey lines) to calculate SIF. Crosses denote the spectral position of the sensor bands (c). (For interpretation of the references to colour in this figure legend, the reader is referred to the web version of this article.)

from airborne imagery were also compared against leaf N, C_{ab}, NBI, and Ft measured in the field.

2.3. Modeling methods for plant trait retrieval and N assessment

The coupled leaf-level Fluspect-Cx model (Vilfan et al., 2018) and 4SAIL (Verhoef, 1984) canopy radiative transfer model, referred to here as FluSAIL, were employed to derive plant biophysical and biochemical parameters by inverting the average canopy reflectance extracted from pure vegetation pixels. The de-epoxidation state of the xanthophyll cycle (C_x) as well as C_{ab}, C_{car}, and Anth pigment content were retrieved by the inversion of the Fluspect-Cx model. A look-up table (LUT) was generated by running 50,000 simulations using randomly generated input parameters drawn from uniform distributions (Table 2). Parameter ranges were adjusted for the viewing geometries due to the slightly different solar zenith angles (SZAs) for each airborne dataset. Biochemical constituents and biophysical parameters were estimated simultaneously for all study plots using a 10-hidden layer artificial neural network (ANN) model (Combal et al., 2003; Hassoun, 1995). The model was trained using 70% of the LUT spectra and tested using the remaining 30% with the mean squared error (MSE) as a performance measure. The model was fit in MATLAB (MATLAB; Statistics and Machine Learning Toolbox and Deep Learning Toolbox; Natick, Massachusetts, USA). Retrieved parameters were used to simulate reflectance spectra with the FluSAIL model using the retrieved parameters and compared with the observed reflectance spectra obtained from the imagery in the 400–900-nm range based upon the root-mean-square deviation (RMSE) assessment. Additionally, the correlations of field leaf-level measurements against estimated plant traits derived from the inversion of the FluSAIL model were compared with those obtained from hyperspectral indices.

To predict leaf N concentration, a pool of representative plant traits and parameters was considered as inputs in the N model, including (1) leaf biochemical and canopy biophysical traits retrieved from pure reflectance spectra with FluSAIL model inversion, (2) airborne-quantified SIF from sunlit-crown radiance spectra, and (3) the water stress indicator CWSI calculated from the thermal imagery. Random Forest (Breiman, 2001) and Gaussian process regression (Williams and Rasmussen, 1996, 2006) algorithms were built with fine-tunning of hyperparameter optimization with 1000 iterations incorporated in the leave-one-out-cross-validation (LOOCV, 15-fold) training and testing steps for each year's dataset. Previously, input collinearity was evaluated using the variance inflation factor (VIF) analysis (O'brien, 2007) following the approach in Zarco-Tejada et al. (2018) conducted using the 'fmsb' package (Gareth et al., 2013) in R. Out-of-bag (OOB) predictor importance was implemented to rank the input relative contribution to the models (as in Zarco-Tejada et al. (2021)). Input parameters with a high degree of collinearity (VIF > 5) (Akinwande et al., 2015) and therefore less informative contribution were filtered out to avoid redundancy. Both Random Forest and Gaussian process regression models were evaluated using the final selection of input parameters. The model performance was evaluated based on the coefficient of determination (r^2) and RMSE. In addition, models with different combination of any two non-collinear parameters were evaluated. In particular, models using leaf biochemical constituents and biophysical parameters with and without SIF were compared to assess the contribution of SIF to N

Table 2
Ranges of input parameters for the LUT of FluSAIL model.

Parameter	Symbol	Unit	Range/ Value
Leaf thickness and constituents			
Chlorophyll $a+b$ content	C_{ab}	µg/ cm^2	20–70
Carotenoid content	C_{car}	µg/ cm^2	3–20
Anthocyanin content	Anth	µg/ cm^2	0–10
Leaf water content	C_w	g/ cm^2	0.001–0.05
Leaf dry matter content	C_{dm}	g/ cm^2	0.001–0.05
Brown pigment content	C_s	µg/ cm^2	0
Leaf mesophyll structural parameter	N-struct	–	1.3–2.5
Leaf dynamic biochemistry			
De-epoxidation state of the xanthophyll cycle (photochemical reflectance parameter)	C_x	–	0–3
Fraction of photons partitioned to PSI	f_{qe}I	–	0.002
Fraction of photons partitioned to PSII	f_{qe}II	–	0.02
Canopy structural parameters			
Leaf area index	LAI	m^2/ m^2	1–7
Hot spot parameter	q	–	0.03
Leaf inclination distribution function parameter a	$LIDF_a$	–	−1–1
Leaf inclination distribution function parameter b	$LIDF_b$	–	−1–1

assessments.

A final evaluation was conducted with the LOOCV (30-fold) method using the non-collinear airborne-quantified C_{ab} and SIF for N assessment from both datasets. Model performance was determined using r^2 and RMSE against the validation data from the 2 years. The best Gaussian process regression model was applied at the tree-crown level to obtain the spatial variability of the tree-based N concentration for the entire 1200-ha almond orchard using the airborne-quantified SIF and C_{ab} content from FluSAIL RTM inversion. The continuous map of N concentration for each management unit were generated using the Kernel interpolation with barriers (KIB) algorithm (Worton, 1989) in ESRI ArcGIS Desktop (Redlands, CA, USA) to visualize the variability across the entire orchard.

3. Results

3.1. Field and laboratory data analyses

Leaf nutrient and pigment content varied widely within the study site and across the two growing seasons. Mean leaf N concentration was 2.07% in 2020 and 2.36% in 2021. The Dualex measured C_{ab} and Flav were more variable in 2021 than in 2020. Mean C_{ab} was 32.53 units in 2020 and 30.71 units in 2021. Mean Flav was 2.04 units in 2020 and 1.84 units in 2021. Anth range was higher in 2021 than in 2020, with a mean value of 0.24 units compared to 0.19 in 2020. NBI was 16.46 in 2020 and 17.18 in 2021. Ft was highly variable throughout the orchard and was higher in 2021 than in 2020, ranging from 1648 to 2751 units in 2020 and from 2574 to 3970 units in 2021.

The relationships between leaf steady-state chlorophyll fluorescence quartiles and derived spectral and physiological metrics varied across seasons (Fig. 6). Similar linear relationships were observed across seasons for leaf N concentration (Fig. 6a), Flav (Fig. 6c), NBI (Fig. 6d), and leaf spectral indices (Fig. 6f-i). By contrast, Anth (Fig. 6e) exhibited opposite trends with Ft quartiles between 2020 (negative) and 2021 (positive). Unexpectedly, leaf C_{ab} (Fig. 6b) did not exhibit consistent trends relative to leaf Ft quartiles, with generally positive and negative trends for 2020 and 2021 (n.s.), respectively.

In general, leaf measurements were correlated with each other across years (Fig. 7). Chlorophyll content and leaf N were strongly correlated in 2020 ($r^2 = 0.60$, p-value <0.005, Fig. 7a). However, this correlation was not statistically significant in 2021 ($r^2 = 0.04$, n.s.). Leaf N was more consistently correlated with Dualex-measured NBI (Fig. 7b) for both

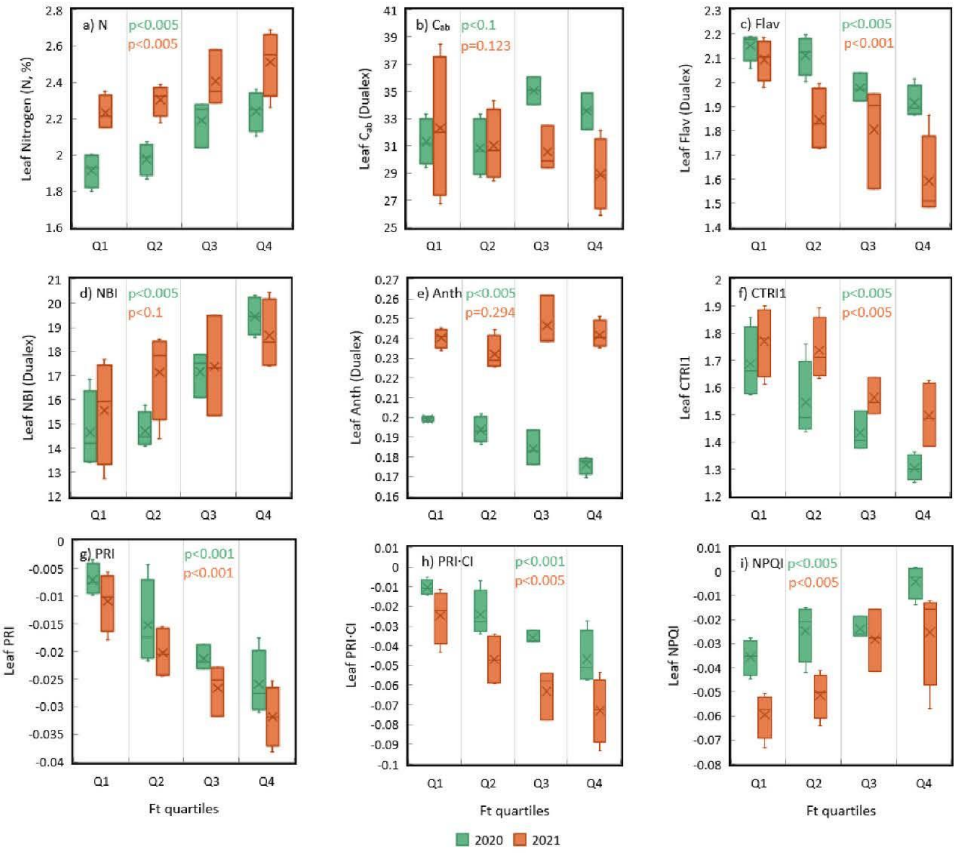

Fig. 6. Ranges of variation based on leaf steady-state chlorophyll fluorescence (Ft) quartiles for leaf phenotypes measured at the pre-harvest stage in 2020 (green) and 2021 (orange): a) nitrogen concentration, b) chlorophyll $a + b$ (C_{ab}), c) flavonoid (Flav), d) Nitrogen Balance Index (NBI), e) anthocyanins (Anth), f) CTRI1, g) PRI, h) PRI•CI, and i) NPQI. The line through the box and marker 'x' refer to the median and mean value, respectively. (For interpretation of the references to colour in this figure legend, the reader is referred to the web version of this article.)

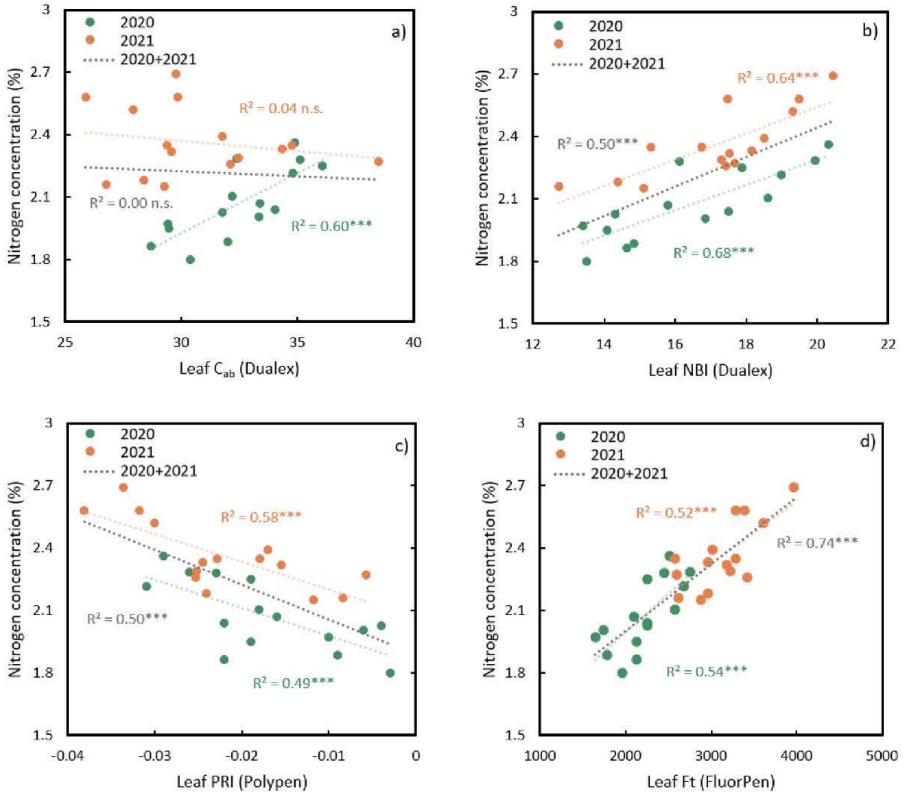

Fig. 7. Relationships between leaf N concentration (%) and a) leaf chlorophyll content, b) Nitrogen Balance Index (NBI), c) photochemical reflectance index (PRI), and d) steady-state chlorophyll fluorescence (Ft). Green and orange represent data in 2020 and 2021, respectively. Grey is used to represent correlation when combining data of 2 years. *p-value <0.05; **p-value <0.01; ***p-value <0.005; n.s. not significant. (For interpretation of the references to colour in this figure legend, the reader is referred to the web version of this article.)

years ($r^2 = 0.68$ for 2020 and $r^2 = 0.64$ for 2021; p-values <0.005), since the index calculation incorporates both chlorophyll and flavonoids. Leaf PRI (related to xanthophyll composition changes) was also correlated with leaf N across seasons ($r^2 = 0.49$ in 2020 and $r^2 = 0.58$ in 2021; p-values <0.005, Fig. 7c) as was Ft ($r^2 = 0.54$ in 2020 and $r^2 = 0.52$ in 2021; p-values <0.005, Fig. 7d). Leaf fluorescence (Fig. 7d) was strongly correlated with N when using combined 2-year data ($r^2 = 0.74$, p-value <0.005), outperforming the rest of the leaf traits (e.g., $r^2 = 0.50$ for PRI and NBI; p-values <0.005).

3.2. Narrow-band indices calculated from airborne hyperspectral imagery

Relationships between narrow-band reflectance indices, airborne SIF, and field-based leaf measurements are summarized in Table 3. The results present a wide range of correlation and significance levels between leaf physiological measurements and indicators of canopy structure, pigments, airborne-quantified fluorescence, and CWSI temperature-based stress indicator. Airborne-quantified SIF (Fig. 8a) was significantly correlated with Ft in both 2020 ($r^2 = 0.73$, p-value <0.005) and 2021 ($r^2 = 0.30$, p-value <0.05). The relationship was stronger when combining datasets across 2 years ($r^2 = 0.77$, p-value <0.005; shown by the grey dashed line in Fig. 8). SIF was also significantly correlated with leaf N ($r^2 = 0.60$ in 2020 and 0.55 in 2021, p-values <0.005), and the relationships remained strong when combining data from both years ($r^2 = 0.74$, p-value <0 0.005, Fig. 8b). Strong correlations were also evident between SIF and leaf NBI ($r^2 = 0.46$ and 0.67, p-values <0.01) in 2020 and 2021, respectively. Fluorescence, as a proxy of photosynthesis, both at the leaf (Fig. 7d) and canopy levels (Fig. 8b), achieved steady and strong relationships with leaf N ($r^2 = 0.74$, p-value <0.005).

Hyperspectral indices related to vegetation structure (e.g., NDVI) and pigment concentration (e.g., MCARI) were generally correlated with leaf chlorophyll measured by Dualex in 2020, but not in 2021 (Table 3). This pattern was reversed for leaf NBI, where canopy structure (e.g., EVI) and pigment indices (e.g., MCARI) were more correlated in 2021 than in 2020. Leaf N was more strongly related to pigment indices (i.e., MCARI and CTRI1, Fig. 9b and c) than structural indices (i.e., NDVI and EVI) in both years. These strong relationships were not always consistent over 2 years, as illustrated in Table 3. For example, the chlorophyll index TCARI/OSAVI was unable to capture the existing N variability in 2021 ($r^2 = 0$, n.s.) as it did in 2020 ($r^2 = 0.57$, p-value <0.01).

Some pigment indices in Table 3 stand out in terms of their high correlations with N for both years. For example, MCARI had an r^2 of 0.61 and 0.48 (p-values <0.005, Fig. 9b) in 2020 and 2021, respectively. PRI_{515} (PRI index using reference band at 515 nm to minimize structural effects) (Hernández-Clemente et al., 2011; Stagakis et al., 2012; Zarco-Tejada et al., 2012) was superior to PRI (at 570 nm) in both 2020 and 2021(Fig. 9d).

Table 3
Coefficients of determination (r^2) for the intercorrelations among standard indices at canopy level from the same 15 study plots in two consecutive years and leaf N concentration (%), Dualex-derived leaf chlorophyll content (C_{ab}), nitrogen balance index (NBI), and steady-state chlorophyll fluorescence (Ft) measured with FluorPen.

	N (%)		C_{ab}		NBI		Ft	
	2020	2021	2020	2021	2020	2021	2020	2021
Structural indices								
NDVI	0.25*	0.13	0.49***	0.10	0.07	0.12	0.04	0.05
EVI	0.37**	0.29**	0.56***	0.01	0.14	0.43***	0.07	0.17
MCARI2	0.40**	0.28**	0.58***	0.03	0.16	0.36**	0.09	0.15
RDVI	0.36**	0.25*	0.58***	0.01	0.15	0.36**	0.07	0.13
OSAVI	0.34**	0.22*	0.57***	0.03	0.13	0.29**	0.06	0.10
Chlorophyll a + b indices								
MCARI	0.61***	0.48***	0.54***	0.00	0.55***	0.39**	0.44***	0.31**
TCARI/OSAVI	0.57***	0.00	0.15	0.04	0.46***	0.00	0.48***	0.01
NPQI	0.38**	0.00	0.37**	0.12	0.39**	0.00	0.36**	0.05
PSSRa	0.24*	0.15	0.49***	0.08	0.08	0.16	0.04	0.06
PSSRb	0.14	0.12	0.43***	0.06	0.03	0.14	0.01	0.05
PSSRc	0.23*	0.16	0.58***	0.02	0.12	0.21*	0.02	0.05
SIPI	0.17	0.05	0.37**	0.16	0.02	0.03	0.02	0.02
CTRI1	0.61***	0.52***	0.35**	0.03	0.76***	0.51***	0.45***	0.18
Indices calculated in the green region								
PRI	0.10	0.27**	0.01	0.13	0.24*	0.36**	0.10	0.08
PRI_{515}	0.69***	0.47***	0.61***	0.11	0.43***	0.38**	0.33**	0.25*
PRI•CI	0.13	0.18	0.49***	0.15	0.03	0.21*	0.00	0.05
Fluorescence quantification								
SIF	0.60***	0.55***	0.28**	0.00	0.46***	0.67***	0.73***	0.30**
Canopy temperature								
CWSI	0.05	0.03	0.00	0.23*	0.31**	0.01	0.10	0.03

*p-value <0.1; **p-value <0.05; ***p-value <0.01.
C_{ab}: Chlorophyll $a + b$ content; NBI: Nitrogen Balance Index; Ft: steady-state chlorophyll fluorescence.

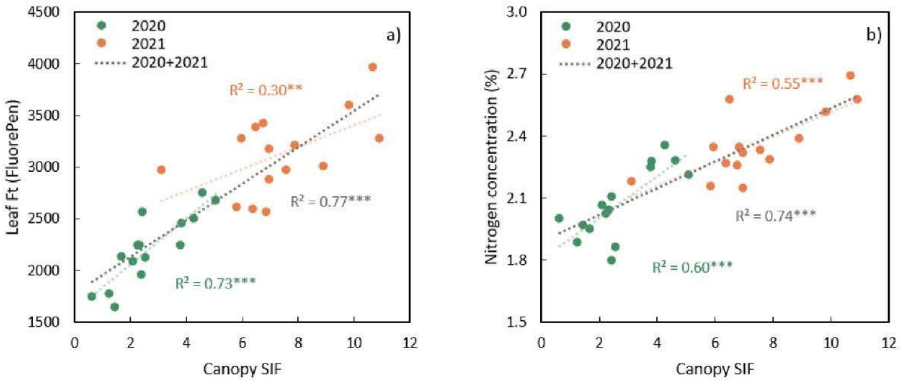

Fig. 8. Relationships between canopy SIF and a) leaf steady-state chlorophyll fluorescence (Ft) and b) leaf N concentration (%) in 2020 (green), 2021 (orange), and the combined years (grey). *p-value <0.5; **p-value <0.05; ***p-value <0.005. (For interpretation of the references to colour in this figure legend, the reader is referred to the web version of this article.)

Many structural and pigment indices showed inconsistent trends across seasons, as shown in Fig. 9 and Table 3. When looking at data from the 2 years combined, no variables from Fig. 9 were significantly correlated with leaf N. NDVI had relatively weak associations with leaf N in each year throughout this heterogeneous orchard. By contrast, airborne SIF calculated from the illuminated crown pixels was consistently related to leaf N across years (Fig. 8). CWSI was not consistently correlated with leaf N or pigment content in either year (Table 3).

3.3. *Plant trait retrieval from the FluSAIL radiative transfer model*

Modelled reflectance spectra from FluSAIL showed close agreement with observed spectra extracted from pure tree crown vegetation pixels in airborne hyperspectral imagery, yielding average RMSE values of

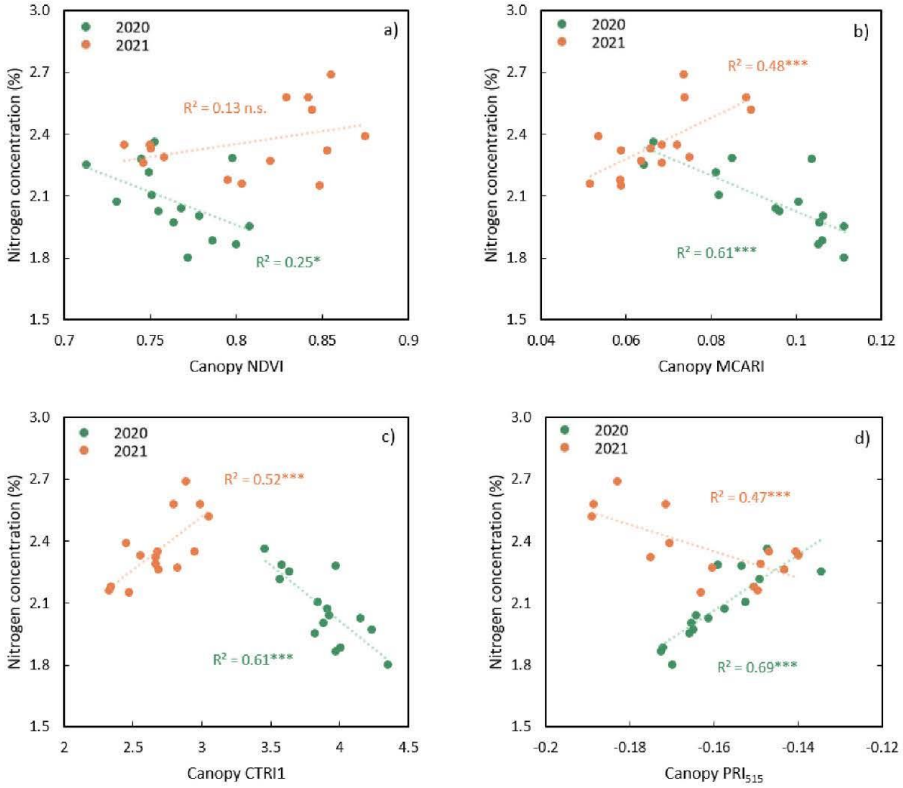

Fig. 9. Leaf N against a) NDVI, b) MCARI, c) CTRI1, and d) PRI_{515} calculated from hyperspectral imagery acquired in 2020 (green) and 2021 (orange). *p-value <0.05; **p-value <0.01; ***p-value <0.005; n.s. not significant. (For interpretation of the references to colour in this figure legend, the reader is referred to the web version of this article.)

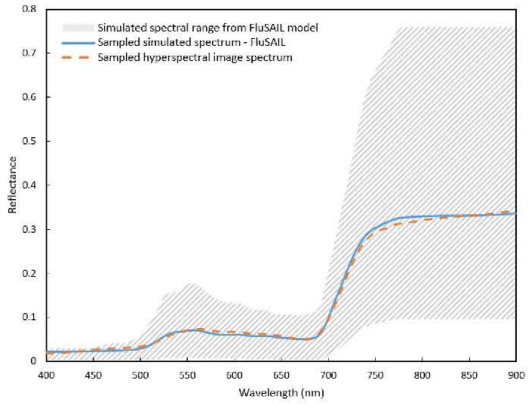

Fig. 10. Comparison of the average hyperspectral image spectrum (orange dashed line) and the corresponding spectrum obtained from the FluSAIL model inversion (blue solid line) for one monitored plot. The simulated FluSAIL spectral range is shown in the shaded grey area. (For interpretation of the references to colour in this figure legend, the reader is referred to the web version of this article.)

0.008 and 0.007 for 2020 and 2021, respectively. Fig. 10 illustrates a simulated and observed spectra as well as a range of simulated spectra from the FluSAIL LUT.

In 2020, leaf C_{ab} from model inversion was strongly correlated to both the Dualex chlorophyll measurement ($r^2 = 0.66$, p-value <0.001) and leaf N ($r^2 = 0.73$, p-value <0.001). As with the hyperspectral indices, no model-derived measures were significantly correlated with Dualex chlorophyll in 2021 (Table 4). In addition to C_{ab}, other pigments (i.e., C_{car} and C_x) also presented significant relationships with leaf N.

C_x, which is sensitive to the de-epoxidation state of the xanthophyll cycle, was significantly correlated with canopy PRI_{515} ($r^2 = 0.68$ and 0.60 in 2020 and 2021, p-values <0.001) and with leaf N ($r^2 = 0.61$ and 0.62 in 2020 and 2021, p-values <0.001). C_{ab} was also closely related to canopy PRI_{515} ($r^2 = 0.80$, p-value <0.001) and SIF ($r^2 = 0.51$, p-value <0.005). No significant relationship was detected between the retrieved LAI and leaf N throughout the orchard across years. These results suggest that pigment content and N were highly correlated with biochemical constituents and SIF but showed little effects on the crown structure.

3.4. *Leaf N status assessment from the airborne-estimated plant traits and SIF*

The final model for leaf N using traits derived from hyperspectral imagery was strongly correlated to field-measured N across years ($r^2 =$ 0.96, p-value <0.001). FluSAIL-inverted C_{ab} and airborne-derived SIF

Table 4
Coefficients of determination (r^2) for correlations among model-derived estimates from the same 15 study plots in two consecutive years, including leaf chlorophyll *a* + *b* (C_{ab}), carotenoids (C_{car}), anthocyanin (Anth), dry matter content (C_{dm}), photochemical reflectance parameter (C_x), leaf area index (LAI), measured leaf N concentration (%), Dualex-measured chlorophyll content, canopy SIF, and canopy photochemical reflectance index (PRI_{515}).

Estimated traits	N (%)		Leaf C_{ab}		Canopy SIF		Canopy PRI_{515}	
	2020	2021	2020	2021	2020	2021	2020	2021
C_{ab} (μg/cm^2)	0.73***	0.66***	0.66***	0.10	0.51**	0.52**	0.80***	0.82***
C_{car} (μg/cm^2)	0.75***	0.56**	0.65***	0.15	0.56**	0.43*	0.72***	0.50**
Anth (μg/cm^2)	0.58***	0.09	0.63***	0.00	0.45*	0.04	0.85***	0.00
C_x	0.61***	0.62***	0.50**	0.01	0.54**	0.57**	0.68***	0.60***
C_{dm} (g/cm^2)	0.36*	0.20	0.58**	0.04	0.20	0.31*	0.59***	0.79***
LAI	0.02	0.05	0.02	0.16	0.07	0.06	0.02	0.49**

*p-value <0.05; **p-value <0.005; ***p-value <0.001.

had the greatest OOB predictor scores, followed by other biochemical constituents (e.g., C_{car} and C_x), as illustrated in Fig. 11a. While the structural trait LAI (p-value >0.1) and the thermal-based water stress indicator CWSI (p-value >0.05) were not statistically significant predictors of N. VIF analysis revealed that C_{ab} and SIF were not collinear, but other biochemical constituents (C_{car}, C_x, and C_{dm}) were discarded from further analysis with a VIF > 5 (empty bars in Fig. 11a). Fig. 11b shows that C_{ab} and SIF were the most important predictors of N for both years, yielding r^2 and RMSE of 0.95 and 0.05%, respectively.

When using combined data from both years, the Gaussian regression model using chlorophyll exclusively as a predictor explained 49% (p-value <0.001) of the variability in N (Fig. 12a) across the almond orchard. A Gaussian process regression model including C_{ab} and SIF considerably increased the performance (r^2 = 0.95, p-value <0.001, RMSE = 0.05%, Fig. 12b). This model with C_{ab} and SIF outperformed any other combination of traits quantified from the hyperspectral imagery for predicting leaf N. As an example, the addition of a structural parameter (LAI) to the model only resulted in a slight increase of 0.02 in r^2 and a 0.01% reduction in RMSE (Fig. 12c) but yielded reasonable results when coupled to SIF (r^2 = 0.81, p-value <0.001, RMSE = 0.1%,

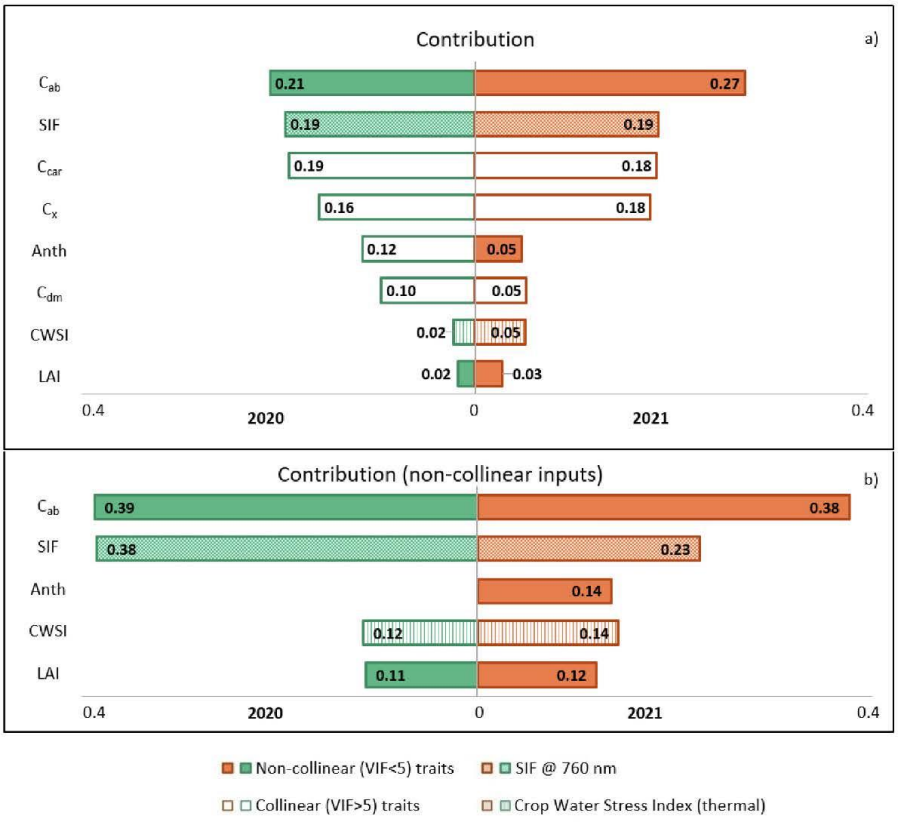

Fig. 11. The relative contribution from OOB importance scores of each variable to the predicted N concentration from a) all plant traits estimated from hyperspectral and thermal imagery and b) a non-collinear subset of variables (VIF < 5).

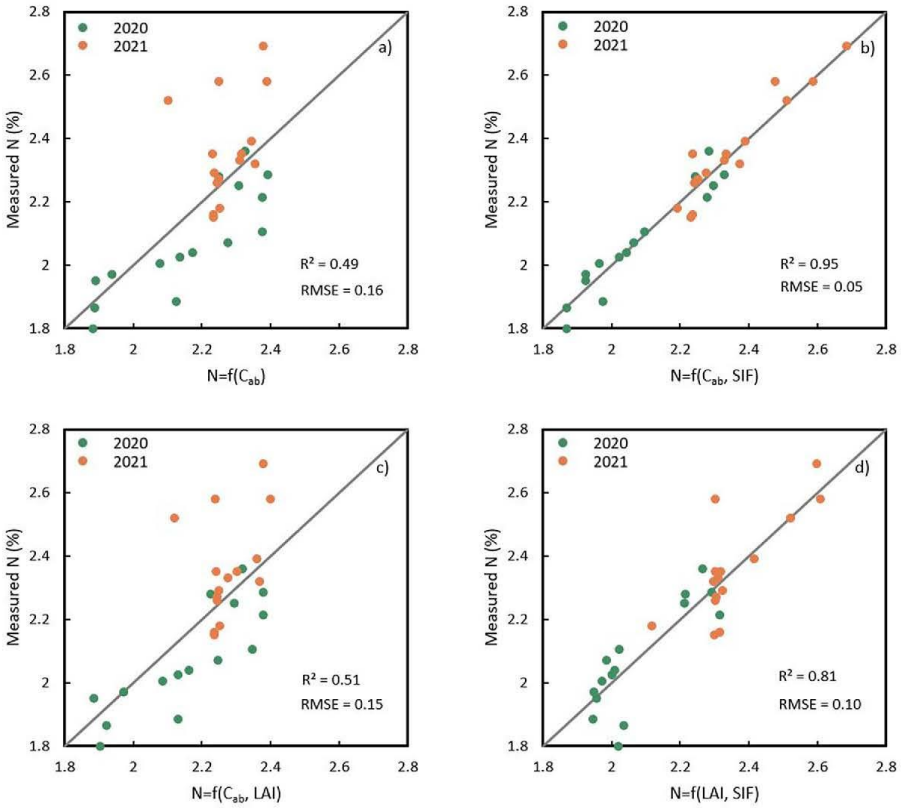

Fig. 12. Correlations between leaf N concentration (%) and predicted N using models based on a) chlorophyll $a+b$ content alone, b) chlorophyll $a+b$ content with canopy SIF, c) chlorophyll $a+b$ content with leaf area index (LAI), and d) LAI with canopy SIF. The grey diagonal line is the 1:1 line. All p-values <0.001.

Fig. 12d). The consistency in the results obtained from the two growing seasons suggests the importance of combining C_{ab} and SIF to assess leaf N status as opposed to standard methods based on individual traits or single vegetation indices, which are generally affected by management practices and the changing growing conditions naturally varying across seasons.

The N prediction map based on a model using C_{ab} and SIF as predictors revealed that tree N was spatially variable across the orchard in 2021 (Fig. 13). As expected, the pattern of N predictions integrates trends in chlorophyll $a+b$ content and SIF.

4. Discussion

Previous studies using RS spectroscopy to estimate leaf N have often focused on developing multispectral indices or proxies from leaf or canopy spectra. These methods usually require the development of empirical models relating leaf N to chlorophyll-sensitive vegetation indices (Clevers and Kooistra, 2011; Fitzgerald et al., 2010; Gabriel et al., 2017; Inoue et al., 2012; Pancorbo et al., 2021; Schlemmer et al., 2013) or combinations of bands and indices (Fitzgerald et al., 2010; Haboudane et al., 2002). However, these methods fail to explain leaf N variability in woody crops that are characterized by structurally complex canopies that are managed to increase productivity. In these highly managed orchard canopies, the relationship between structure and nutrient levels is uncoupled; therefore, structural index-based models are not appropriate (Table 4). In these orchard canopies, the main drivers for the observed structural changes are the planting density and the fractional cover, which add additional complexity to the use of structural RS vegetation indices as indicators of nutrient levels. In these structurally complex orchards, the spectral indices are heavily affected by the canopy architecture and by structural parameters, such as leaf density, which in turn interact with the illumination and observation geometry within the canopy (Broge and Leblanc, 2001; Haboudane et al., 2002; Wang et al., 2018). Therefore, the variability observed with standard vegetation indices such as NDVI and other structurally sensitive indicators may not necessarily represent the nutrient variability, but instead the heterogeneity due to different tree ages, crown densities, and planting grids that usually coexist in large well-managed orchards such as the one used in this study.

The assessment of the physiological status, independent from the structure and canopy architecture using plant traits through RTM model inversion, is particularly beneficial in the case of structurally complex canopies (Malenovský et al., 2013) when trying to capture the within-field spatial variability of the leaf nutrient status independent from the structural variability. In this study, we found that plant physiological estimates derived from RTM inversion using VNIR hyperspectral imagery were generally stronger and more consistent predictors of leaf N status than the empirical models built with vegetation indices. In particular, RTM-retrieved pigment C_{ab} was the strongest predictor (Fig. 11), consistent with the results of Camino et al. (2018a) for wheat.

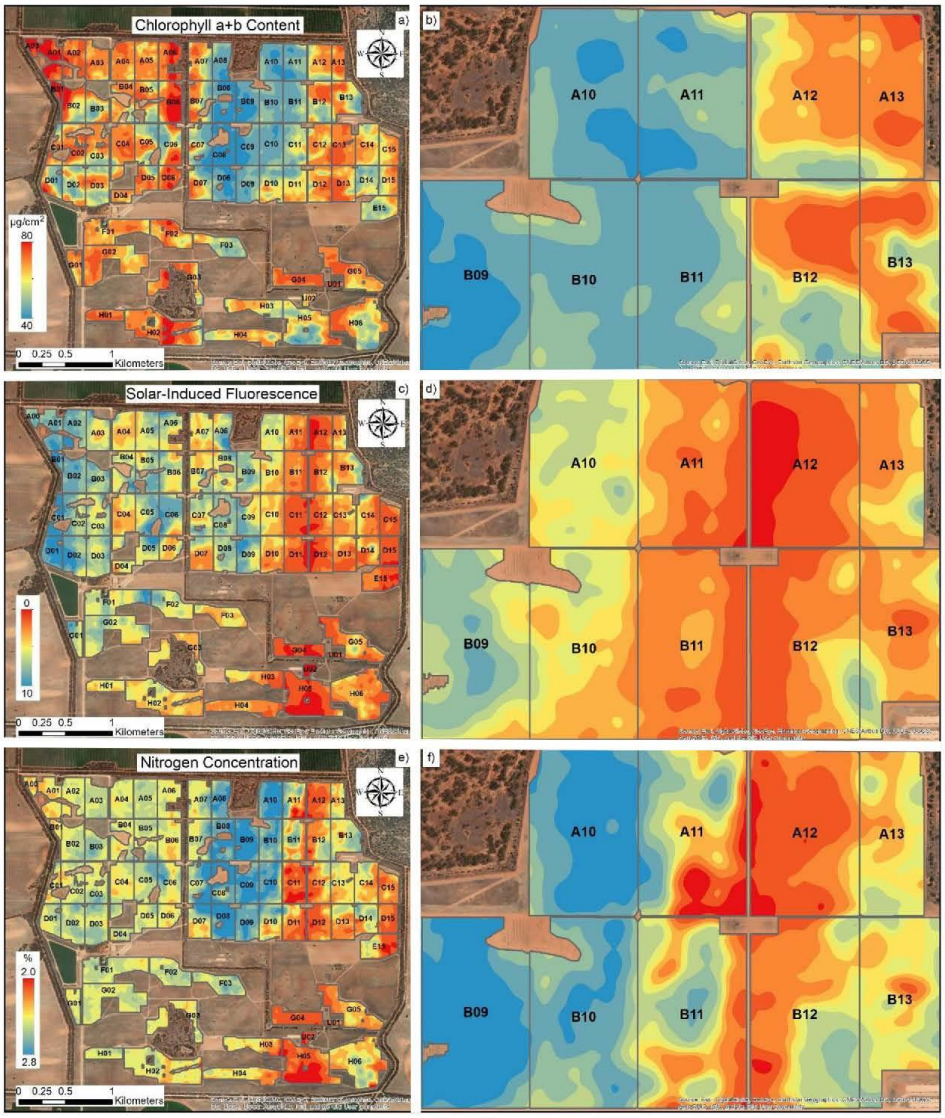

Fig. 13. Interpolated map of a) chlorophyll $a + b$ content, c) solar-induced fluorescence, and e) predicted N concentration derived from C_{ab} and SIF in 2021. Right column contains zoomed-in views (b, d and f) of the scenes on the left in the northeast blocks. Block numbers are displayed in the centers.

RTM-based carotenoid content and the xanthophyll cycle (C_x) parameter were also more strongly related to leaf N than vegetation indices in our study, as both are involved in light-harvesting regulation that is associated with photosynthetic efficiency (Ruban et al., 1999). For instance, RTM-based chlorophyll $a + b$ content was strongly correlated with leaf N for both years of study ($r^2 = 0.73$ in 2020 and 0.66 in 2021, p-values <0.001), whereas the chlorophyll-sensitive index TCARI/OSAVI was not correlated with N in 2021 ($r^2 = 0$, n.s.), suggesting those indices are not reliable indicators for N assessment across seasons. Spectral indices are greatly affected by management practices and background changes across orchards and years, leading to inconsistencies that may make them inappropriate for operational purposes.

The fact that both model-inverted LAI and structural hyperspectral indices were poorly related to leaf N supports the idea that canopy structure is not driven by nutrient availability in well-managed intensive orchards. As a consequence, it is not surprising that the widely used structural index NDVI was inadequate for predicting leaf N in this context. Ground-based leaf chlorophyll measurements were poorly related to leaf N when leaf N was high in 2021. This is consistent with the results of Jifon et al. (2005), who found the relationship between

chlorophyll meter readings and leaf N was stronger at low chlorophyll concentrations than at higher chlorophyll concentrations. At high N concentrations, there is a possibility that some N may be allocated to soluble protein rather than pigment-protein complexes (Evans, 1989). And the soluble protein and pigment complexes in leaves can be imbalanced depending on leaf physical characteristics, plant age, environmental factors, and management practices (Bondada and Syvertsen, 2003; Evans and Poorter, 2001; Syvertsen et al., 1995; Syvertsen, 1984). In our study, leaf nitrogen balance index was more strongly correlated with leaf N and canopy indices as it incorporated the ratio of a second pigment flavonoid into the calculation. This phenomenon was also observed at the canopy level for both chlorophyll-sensitive vegetation indices and RTM-based pigment concentrations. C_{ab} at the canopy level was more strongly related to leaf N than C_{ab} at the leaf level, which may be attributed to the fact that the field-collected leaf measurements came from lower layers of the tree crown, whereas the imagery captured the upper layers. Our results provide evidence that RTM-based leaf physiological traits provide additional benefits over standard structural indices for assessing leaf N in orchards, particularly when multiple varieties, ages, and management practices coexist within the orchard.

Several studies have shown that SIF derived from sub-meter narrowband imagery, in which the depth of the oxygen absorption feature can be quantified, is an effective tool for detecting plant stress in precision agriculture (Calderón et al., 2013; Camino et al., 2018a; Camino et al., 2018b; Quemada et al., 2014; Raya-Sereno et al., 2021; Zarco-Tejada et al., 2012). In this study, we also found a strong association between fluorescence and leaf N, consistent with the literature (Cendrero-Mateo et al., 2016; Corp et al., 2003; Schächtl et al., 2005), yielding $r^2 = 0.74$ (p-value <0.005) over the course of 2 years at both leaf and canopy levels. Airborne-quantified SIF was the second most important predictor of leaf N after C_{ab} and outperformed any other vegetation index or structural and temperature-based plant traits in terms of correlation and consistency across years. When combined with RTM-based traits, SIF significantly improved model performance for predicting leaf N. The model that included C_{ab} and SIF explained 95% of the leaf N variability (p-value <0.001), improving upon results obtained with C_{ab} alone ($r^2 = 0.49$, p-value <0.001) accounting for different plant varieties, ages, planting patterns, water status levels, and fertilizer management practices across 2 years.

CWSI, a thermal canopy water status index, was poorly associated with leaf N and relatively inconsistent across years. Overall, we found no evidence of a relationship between CWSI and leaf N, suggesting that leaf N variability was not driven by water status in this well-managed intensive almond orchard.

5. Conclusions

This study demonstrates that leaf N estimation conducted in an almond orchard across 2 years was significantly improved when SIF was included alongside RTM-based leaf chlorophyll $a + b$ content. Among all spectral plant traits evaluated from hyperspectral imagery, including all RTM-derived leaf biochemical constituents, SIF, and structural and water stress traits, the retrieved leaf chlorophyll $a + b$ and SIF were the two most important predictors to explain leaf N variability. The model that incorporated both chlorophyll $a + b$ content and SIF traits explained 95% of the variability in leaf N (p-value <0.001) consistently across 2 years of airborne hyperspectral data collection. Together, these results provide important insights into the quantification of leaf N content in well-managed structurally complex canopies, such as discontinuous tree orchards, demonstrating that traditional vegetation indices and individual plant traits do not sufficiently track leaf N content over well-managed intensive crops typically reaching high N levels.

Credit author statement

Y.W., L.S. and P.J.Z.-T. designed the objectives of this study and designed research; L.S. and P.J.Z.-T supervised the work; Y.W., L.S., and T.P. carried out field work and airborne data collections; Y.W. analysed data and performed research; Y.W. wrote the paper, and L.S., T.P., V.G.-D., D.R. and P.J.Z.-T. contributed and provided comments. All authors read and approved the final submission.

Declaration of Competing Interest

The authors declare that they have no known competing financial interests or personal relationships that could have appeared to influence the work reported in this paper.

Acknowledgment

The authors gratefully acknowledge McPherson Family and Invergowrie Foundation for the financial support and the assistant from the Mallee Regional Innovation Centre (MRIC). Special thanks to Xiaojin Qian from HyperSens Remote Sensing Laboratory for her support in the field, also extend to Rafael Romero, David Notario and Alberto Hornero from QuantaLab IAS-CSIC (Spain) for their contributions in the laboratory. And Brian Slater for allowing this research to be carried out in the Aroona Farms.

References

Abràmoff, M.D., Magalhães, P.J., Ram, S.J., 2004. Image processing with ImageJ. Biophoton. Int. 11 (7), 36–42.
Akinwande, M.O., Dikko, H.G., Samson, A., 2015. Variance inflation factor: as a condition for the inclusion of suppressor variable (s) in regression analysis. Open J. Stat. 5 (07), 754.
Asai, W., Micke, W., Kester, D., Rough, D., 1996. The Evaluation and Selection of Current Varieties; Almond Production Manual, University of California (System). Division of Agriculture and Natural Resources. ANR Publications, California.
Ashraf, M., Harris, P.J., 2013. Photosynthesis under stressful environments: an overview. Photosynthetica 51 (2), 163–190.
Baret, F., Houlès, V., Guerif, M., 2007. Quantification of plant stress using remote sensing observations and crop models: the case of nitrogen management. J. Exp. Bot. 58 (4), 869–880.
Barnes, J.D., Balaguer, L., Manrique, E., Elvira, S., Davison, A., 1992. A reappraisal of the use of DMSO for the extraction and determination of chlorophylls a and b in lichens and higher plants. Environ. Exp. Bot. 32 (2), 85–100.
Bellvert, J., Adeline, K., Baram, S., Pierce, L., Sanden, B.L., Smart, D.R., 2018. Monitoring crop evapotranspiration and crop coefficients over an almond and pistachio orchard throughout remote sensing. Remote Sens. 10 (12), 2001.
Belwalkar, A., Poblete, T., Longmire, A., Hornero, A., Zarco-Tejada, P., 2021. Comparing the retrieval of chlorophyll fluorescence from two airborne hyperspectral imagers with different spectral resolutions for plant phenotyping studies. In: Paper presented at the 2021 IEEE International Geoscience and Remote Sensing Symposium IGARSS.
Belwalkar, A., Poblete, T., Longmire, A., Hornero, A., Hernandez-Clemente, R., Zarco-Tejada, P., 2022. Evaluation of SIF retrievals from narrow-band and sub-nanometer airborne hyperspectral imagers flown in tandem: modelling and validation in the context of plant phenotyping. Remote Sens. Environ. 273 (112986).
Biswal, B., Joshi, P., Raval, M., Biswal, U., 2011. Photosynthesis, a global sensor of environmental stress in green plants: stress signalling and adaptation. Curr. Sci. 47–56.
Blackburn, G.A., 1998. Spectral indices for estimating photosynthetic pigment concentrations: a test using senescent tree leaves. Int. J. Remote Sens. 19 (4), 657–675.
Bondada, B.R., Syvertsen, J.P., 2003. Leaf chlorophyll, net gas exchange and chloroplast ultrastructure in citrus leaves of different nitrogen status. Tree Physiol. 23 (8), 553–559.
Breiman, L., 2001. Random forests. Mach. Learn. 45 (1), 5–32.
Broge, N.H., Leblanc, E., 2001. Comparing prediction power and stability of broadband and hyperspectral vegetation indices for estimation of green leaf area index and canopy chlorophyll density. Remote Sens. Environ. 76 (2), 156–172.
Buckee, G., 1994. Determination of total nitrogen in barley, malt and beer by Kjeldahl procedures and the dumas combustion methodcollaborative trial. J. Inst. Brew. 100 (2), 57–64.
Bullock, D., Anderson, D., 1998. Evaluation of the Minolta SPAD-502 chlorophyll meter for nitrogen management in corn. J. Plant Nutr. 21 (4), 741–755.
Calderón, R., Navas-Cortés, J.A., Lucena, C., Zarco-Tejada, P.J., 2013. High-resolution airborne hyperspectral and thermal imagery for early detection of Verticillium wilt of olive using fluorescence, temperature and narrow-band spectral indices. Remote Sens. Environ. 139, 231–245.
Camino, C., González-Dugo, V., Hernández, P., Sillero, J., Zarco-Tejada, P.J., 2018a. Improved nitrogen retrievals with airborne-derived fluorescence and plant traits quantified from VNIR-SWIR hyperspectral imagery in the context of precision agriculture. Int. J. Appl. Earth Obs. Geoinf. 70, 105–117.

Camino, C., Zarco-Tejada, P.J., Gonzalez-Dugo, V., 2018b. Effects of heterogeneity within tree crowns on airborne-quantified SIF and the CWSI as indicators of water stress in the context of precision agriculture. Remote Sens. 10 (4), 604.
Carter, G.A., 1994. Ratios of leaf reflectances in narrow wavebands as indicators of plant stress. Int. J. Remote Sens. 15 (3), 697–703.
Cendrero-Mateo, M.P., Moran, M.S., Papuga, S.A., Thorp, K., Alonso, L., Moreno, J., Wang, G., 2016. Plant chlorophyll fluorescence: active and passive measurements at canopy and leaf scales with different nitrogen treatments. J. Exp. Bot. 67 (1), 275–286.
Cerovic, Z.G., Masdoumier, G., Ghozlen, N.B., Latouche, G., 2012. A new optical leaf-clip meter for simultaneous non-destructive assessment of leaf chlorophyll and epidermal flavonoids. Physiol. Plant. 146 (3), 251–260.
Cerovic, Z.G., Ghozlen, N.B., Milhade, C., Obert, M., Debuisson, S.B., Moigne, M.L., 2015. Nondestructive diagnostic test for nitrogen nutrition of grapevine (Vitis vinifera L.) based on dualex leaf-clip measurements in the field. J. Agric. Food Chem. 63 (14), 3669–3680.
Chang, S.X., Robison, D.J., 2003. Nondestructive and rapid estimation of hardwood foliar nitrogen status using the SPAD-502 chlorophyll meter. For. Ecol. Manag. 181 (3), 331–338.
Chapman, S.C., Barreto, H.J., 1997. Using a chlorophyll meter to estimate specific leaf nitrogen of tropical maize during vegetative growth. Agron. J. 89 (4), 557–562.
Cheng, L., 2003. Xanthophyll cycle pool size and composition in relation to the nitrogen content of apple leaves. J. Exp. Bot. 54 (381), 385–393.
Clevers, J.G., Gitelson, A.A., 2013. Remote estimation of crop and grass chlorophyll and nitrogen content using red-edge bands on Sentinel-2 and-3. Int. J. Appl. Earth Obs. Geoinf. 23, 344–351.
Clevers, J.G., Kooistra, L., 2011. Using hyperspectral remote sensing data for retrieving canopy chlorophyll and nitrogen content. IEEE J. Sel. Top. Appl. Earth Obs. Remote Sens. 5 (2), 574–583.
Combal, B., Baret, F., Weiss, M., Trubuil, A., Mace, D., Pragnere, A., Wang, L., 2003. Retrieval of canopy biophysical variables from bidirectional reflectance: using prior information to solve the ill-posed inverse problem. Remote Sens. Environ. 84 (1), 1–15.
Conant, R.T., Berdanier, A.B., Grace, P.R., 2013. Patterns and trends in nitrogen use and nitrogen recovery efficiency in world agriculture. Glob. Biogeochem. Cycles 27 (2), 558–566.
Corp, L.A., McMurtrey, J.E., Middleton, E.M., Mulchi, C.L., Chappelle, E.W., Daughtry, C. S., 2003. Fluorescence sensing systems: in vivo detection of biophysical variations in field corn due to nitrogen supply. Remote Sens. Environ. 86 (4), 470–479.
Cummings, C., Miao, Y., Paiao, G.D., Kang, S., Fernández, F.G., 2021. Corn nitrogen status diagnosis with an innovative multi-parameter crop circle phenom sensing system. Remote Sens. 13 (3), 401.
Daughtry, C.S., Walthall, C., Kim, M., De Colstoun, E.B., McMurtrey Iii, J., 2000. Estimating corn leaf chlorophyll concentration from leaf and canopy reflectance. Remote Sens. Environ. 74 (2), 229–239.
Demmig, B., Winter, K., Krüger, A., Czygan, F.-C., 1987. Photoinhibition and zeaxanthin formation in intact leaves: a possible role of the xanthophyll cycle in the dissipation of excess light energy. Plant Physiol. 84 (2), 218–224.
Dong, R., Miao, Y., Wang, X., Chen, Z., Yuan, F., Zhang, W., Li, H., 2020. Estimating plant nitrogen concentration of maize using a leaf fluorescence sensor across growth stages. Remote Sens. 12 (7), 1139.
Dumas, J.B.A., 1831. Procedes de l'analyse organic. Ann. Chim. Phys. 247, 198–213.
Etheridge, R., Pesti, G., Foster, E., 1998. A comparison of nitrogen values obtained utilizing the Kjeldahl nitrogen and Dumas combustion methodologies (Leco CNS 2000) on samples typical of an animal nutrition analytical laboratory. Anim. Feed Sci. Technol. 73 (1–2), 21–28.
Evans, J., 1989. Photosynthesis and nitrogen relationships in leaves of C 3 plants. Oecologia 78 (1), 9–19.
Evans, J., Poorter, H., 2001. Photosynthetic acclimation of plants to growth irradiance: the relative importance of specific leaf area and nitrogen partitioning in maximizing carbon gain. Plant Cell Environ. 24 (8), 755–767.
Filella, I., Serrano, L., Serra, J., Penuelas, J., 1995. Evaluating wheat nitrogen status with canopy reflectance indices and discriminant analysis. Crop Sci. 35 (5), 1400–1405.
Fitzgerald, G., Rodriguez, D., Christensen, L., Belford, R., Sadras, V., Clarke, T., 2006. Spectral and thermal sensing for nitrogen and water status in rainfed and irrigated wheat environments. Precis. Agric. 7 (4), 233–248.
Fitzgerald, G., Rodriguez, D., O'Leary, G., 2010. Measuring and predicting canopy nitrogen nutrition in wheat using a spectral index—the canopy chlorophyll content index (CCCI). Field Crop Res. 116 (3), 318–324.
Flowers, M., Weisz, R., Heiniger, R., 2003. Quantitative approaches for using color infrared photography for assessing in-season nitrogen status in winter wheat. Agron. J. 95 (5), 1189–1200.
Gabriel, J.L., Zarco-Tejada, P.J., López-Herrera, P.J., Pérez-Martín, E., Alonso-Ayuso, M., Quemada, M., 2017. Airborne and ground level sensors for monitoring nitrogen status in a maize crop. Biosyst. Eng. 160, 124–133.
Gamon, J., Penuelas, J., Field, C., 1992. A narrow-waveband spectral index that tracks diurnal changes in photosynthetic efficiency. Remote Sens. Environ. 41 (1), 35–44.
Gareth, J., Daniela, W., Trevor, H., Robert, T., 2013. An Introduction to Statistical Learning: With Applications in R. Spinger.
Garrity, S.R., Eitel, J.U., Vierling, L.A., 2011. Disentangling the relationships between plant pigments and the photochemical reflectance index reveals a new approach for remote estimation of carotenoid content. Remote Sens. Environ. 115 (2), 628–635.
Genty, B., Briantais, J.-M., Baker, N.R., 1989. The relationship between the quantum yield of photosynthetic electron transport and quenching of chlorophyll fluorescence. Biochim. Biophys. Acta 990 (1), 87–92.
Gilmore, A.M., 1997. Mechanistic aspects of xanthophyll cycle-dependent photoprotection in higher plant chloroplasts and leaves. Physiol. Plant. 99 (1), 197–209.
Gitelson, A.A., Merzlyak, M.N., Lichtenthaler, H.K., 1996. Detection of red edge position and chlorophyll content by reflectance measurements near 700 nm. J. Plant Physiol. 148 (3–4), 501–508.
Gitelson, A.A., Gritz, Y., Merzlyak, M.N., 2003. Relationships between leaf chlorophyll content and spectral reflectance and algorithms for non-destructive chlorophyll assessment in higher plant leaves. J. Plant Physiol. 160 (3), 271–282.
Gnyp, M.L., Miao, Y., Yuan, F., Ustin, S.L., Yu, K., Yao, Y., Bareth, G., 2014. Hyperspectral canopy sensing of paddy rice aboveground biomass at different growth stages. Field Crop Res. 155, 42–55.
Gueymard, C.A., 1995. SMARTS2: A simple model of the atmospheric radiative transfer of sunshine. In: Algorithms and Performance Assessment. Florida Solar Energy Center Cocoa, FL.
Gueymard, C.A., 2001. Parameterized transmittance model for direct beam and circumsolar spectral irradiance. Sol. Energy 71 (5), 325–346.
Gueymard, C.A., Myers, D., Emery, K., 2002. Proposed reference irradiance spectra for solar energy systems testing. Sol. Energy 73 (6), 443–467.
Haboudane, D., Miller, J.R., Tremblay, N., Zarco-Tejada, P.J., Dextraze, L., 2002. Integrated narrow-band vegetation indices for prediction of crop chlorophyll content for application to precision agriculture. Remote Sens. Environ. 81 (2–3), 416–426.
Haboudane, D., Miller, J.R., Pattey, E., Zarco-Tejada, P.J., Strachan, I.B., 2004. Hyperspectral vegetation indices and novel algorithms for predicting green LAI of crop canopies: modeling and validation in the context of precision agriculture. Remote Sens. Environ. 90 (3), 337–352.
Hassoun, M.H., 1995. Fundamentals of Artificial Neural Networks. MIT press.
Hernández-Clemente, R., Navarro-Cerrillo, R.M., Suárez, L., Morales, F., Zarco-Tejada, P. J., 2011. Assessing structural effects on PRI for stress detection in conifer forests. Remote Sens. Environ. 115 (9), 2360–2375.
Hill, S., Stephenson, D., Taylor, B., 1985. Almond pollination studies: pollen production and viability, flower emergence and cross-pollination tests. Aust. J. Exp. Agric. 25 (3), 697–704.
Huang, Z.-A., Jiang, D.-A., Yang, Y., Sun, J.-W., Jin, S.-H., 2004. Effects of nitrogen deficiency on gas exchange, chlorophyll fluorescence, and antioxidant enzymes in leaves of rice plants. Photosynthetica 42 (3), 357–364.
Idso, S., Jackson, R., Pinter Jr., P., Reginato, R., Hatfield, J., 1981. Normalizing the stress-degree-day parameter for environmental variability. Agric. Meteorol. 24, 45–55.
Inoue, Y., Sakaiya, E., Zhu, Y., Takahashi, W., 2012. Diagnostic mapping of canopy nitrogen content in rice based on hyperspectral measurements. Remote Sens. Environ. 126, 210–221.
Jackson, R.D., Idso, S., Reginato, R., Pinter Jr., P., 1981. Canopy temperature as a crop water stress indicator. Water Resour. Res. 17 (4), 1133–1138.
Jacquemoud, S., Verhoef, W., Baret, F., Bacour, C., Zarco-Tejada, P.J., Asner, G.P., Ustin, S.L., 2009. PROSPECT+ SAIL models: a review of use for vegetation characterization. Remote Sens. Environ. 113, S56–S66.
Jifon, J.L., Syvertsen, J.P., Whaley, E., 2005. Growth environment and leaf anatomy affect nondestructive estimates of chlorophyll and nitrogen in Citrus sp. leaves. J. Am. Soc. Hortic. Sci. 130 (2), 152–158.
Jongschaap, R.E., Booij, R., 2004. Spectral measurements at different spatial scales in potato: relating leaf, plant and canopy nitrogen status. Int. J. Appl. Earth Obs. Geoinf. 5 (3), 205–218.
Kimes, D.S., Knyazikhin, Y., Privette, J., Abuelgasim, A., Gao, F., 2000. Inversion methods for physically-based models. Remote Sens. Rev. 18 (2–4), 381–439.
Kjeldahl, J., 1883. A new method for the estimation of nitrogen in organic compounds. Z. Anal. Chem. 22 (1), 366.
Krause, G., Weis, E., 1991. Chlorophyll fluorescence and photosynthesis: the basics. Annu. Rev. Plant Biol. 42 (1), 313–349.
Li, F., Miao, Y., Feng, G., Yuan, F., Yue, S., Gao, X., Chen, X., 2014. Improving estimation of summer maize nitrogen status with red edge-based spectral vegetation indices. Field Crop Res. 157, 111–123.
Li, H., Zhang, Y., Lei, Y., Antoniuk, V., Hu, C., 2020. Evaluating different non-destructive estimation methods for winter wheat (Triticum aestivum L.) nitrogen status based on canopy spectrum. Remote Sens. 12 (1), 95.
Liu, H.Q., Huete, A., 1995. A feedback based modification of the NDVI to minimize canopy background and atmospheric noise. IEEE Trans. Geosci. Remote Sens. 33 (2), 457–465.
Lu, C., Zhang, J., 2000. Photosynthetic CO2 assimilation, chlorophyll fluorescence and photoinhibition as affected by nitrogen deficiency in maize plants. Plant Sci. 151 (2), 135–143.
Maier, S.W., Günther, K.P., Stellmes, M., 2004. Sun-induced fluorescence: a new tool for precision farming. Digit. Imaging Spect. Tech. 66, 207–222.
Malenovský, Z., Homolová, L., Zurita-Milla, R., Lukeš, P., Kaplan, V., Hanuš, J., Schaepman, M.E., 2013. Retrieval of spruce leaf chlorophyll content from airborne image data using continuum removal and radiative transfer. Remote Sens. Environ. 131, 85–102.
Manna, M., Swarup, A., Wanjari, R., Ravankar, H., Mishra, B., Saha, M., Sarap, P., 2005. Long-term effect of fertilizer and manure application on soil organic carbon storage, soil quality and yield sustainability under sub-humid and semi-arid tropical India. Field Crop Res. 93 (2–3), 264–280.
Matson, P.A., Naylor, R., Ortiz-Monasterio, I., 1998. Integration of environmental, agronomic, and economic aspects of fertilizer management. Science 280 (5360), 112–115.
Matsushita, B., Yang, W., Chen, J., Onda, Y., Qiu, G., 2007. Sensitivity of the enhanced vegetation index (EVI) and normalized difference vegetation index (NDVI) to

topographic effects: a case study in high-density cypress forest. sensors 7 (11), 2636–2651.
Maxwell, K., Johnson, G.N., 2000. Chlorophyll fluorescence—a practical guide. J. Exp. Bot. 51 (345), 659–668.
Middleton, E.M., Huemmrich, K.F., Cheng, Y.-B., Margolis, H.A., 2016. 12 Spectral bioindicators of photosynthetic efficiency and vegetation stress. In: Hyperspectral Remote Sensing of Vegetation. CRC Press, pp. 265–288.
Mohammed, G.H., Binder, W., Gillies, S., 1995. Chlorophyll fluorescence: a review of its practical forestry applications and instrumentation. Scand. J. For. Res. 10 (1–4), 383–410.
Mohammed, G.H., Colombo, R., Middleton, E.M., Rascher, U., van der Tol, C., Nedbal, L., Meroni, M., 2019. Remote sensing of solar-induced chlorophyll fluorescence (SIF) in vegetation: 50 years of progress. Remote Sens. Environ. 231, 111177.
Murchie, E.H., Lawson, T., 2013. Chlorophyll fluorescence analysis: a guide to good practice and understanding some new applications. J. Exp. Bot. 64 (13), 3983–3998.
Nageswara Rao, R., Talwar, H., Wright, G., 2001. Rapid assessment of specific leaf area and leaf nitrogen in peanut (Arachis hypogaea L.) using a chlorophyll meter. J. Agron. Crop Sci. 186 (3), 175–182.
Nguy-Robertson, A., Gitelson, A., Peng, Y., Viña, A., Arkebauer, T., Rundquist, D., 2012. Green leaf area index estimation in maize and soybean: combining vegetation indices to achieve maximal sensitivity. Agron. J. 104 (5), 1336–1347.
Niblack, W., 1985. An Introduction to Digital Image Processing. Strandberg Publishing Company.
Nigon, T.J., Yang, C., Dias Paiao, G., Mulla, D.J., Knight, J.F., Fernández, F.G., 2020. Prediction of early season nitrogen uptake in maize using high-resolution aerial hyperspectral imagery. Remote Sens. 12 (8), 1234.
Niyogi, K.K., Björkman, O., Grossman, A.R., 1997. The roles of specific xanthophylls in photoprotection. Proc. Natl. Acad. Sci. 94 (25), 14162–14167.
O'brien, R.M., 2007. A caution regarding rules of thumb for variance inflation factors. Qual. Quant. 41 (5), 673–690.
Padilla, F.M., de Souza, R., Peña-Fleitas, M.T., Gallardo, M., Gimenez, C., Thompson, R. B., 2018. Different responses of various chlorophyll meters to increasing nitrogen supply in sweet pepper. Front. Plant Sci. 9, 1752.
Pancorbo, J., Camino, C., Alonso-Ayuso, M., Raya-Sereno, M., Gonzalez-Fernandez, I., Gabriel, J., Quemada, M., 2021. Simultaneous assessment of nitrogen and water status in winter wheat using hyperspectral and thermal sensors. Eur. J. Agron. 127, 126287.
Panhwar, Q.A., Ali, A., Naher, U.A., Memon, M.Y., 2019. Fertilizer management strategies for enhancing nutrient use efficiency and sustainable wheat production. In: Organic Farming. Elsevier, pp. 17–39.
Peñuelas, J., Baret, F., Filella, I., 1995. Semi-empirical indices to assess carotenoids/chlorophyll a ratio from leaf spectral reflectance. Photosynthetica 31 (2), 221–230.
Perry, E.M., Fitzgerald, G.J., Nuttall, J.G., O'Leary, G.J., Schulthess, U., Whitlock, A., 2012. Rapid estimation of canopy nitrogen of cereal crops at paddock scale using a canopy chlorophyll content index. Field Crop Res. 134, 158–164.
Phansalkar, N., More, S., Sabale, A., Joshi, M., 2011. Adaptive local thresholding for detection of nuclei in diversity stained cytology images. In: Paper Presented at the 2011 International Conference on Communications and Signal Processing.
Pinter Jr., P.J., Hatfield, J.L., Schepers, J.S., Barnes, E.M., Moran, M.S., Daughtry, C.S., Upchurch, D.R., 2003. Remote sensing for crop management. Photogramm. Eng. Remote. Sens. 69 (6), 647–664.
Plascyk, J.A., Gabriel, F.C., 1975. The Fraunhofer line discriminator MKII-an airborne instrument for precise and standardized ecological luminescence measurement. IEEE Trans. Instrum. Meas. 24 (4), 306–313.
Porcar-Castell, A., Tyystjärvi, E., Atherton, J., Van der Tol, C., Flexas, J., Pfündel, E.E., Berry, J.A., 2014. Linking chlorophyll a fluorescence to photosynthesis for remote sensing applications: mechanisms and challenges. J. Exp. Bot. 65 (15), 4065–4095.
Quemada, M., Gabriel, J.L., Zarco-Tejada, P., 2014. Airborne hyperspectral images and ground-level optical sensors as assessment tools for maize nitrogen fertilization. Remote Sens. 6 (4), 2940–2962.
Ramalho, J.C., Pons, T.L., Groeneveld, H.W., Azinheira, H.G., Nunes, M.A., 2000. Photosynthetic acclimation to high light conditions in mature leaves of Coffea arabica L.: role of xanthophylls, quenching mechanisms and nitrogen nutrition. Funct. Plant Biol. 27 (1), 43–51.
Raya-Sereno, M.D., Alonso-Ayuso, M., Pancorbo, J.L., Gabriel, J.L., Camino, C., Zarco-Tejada, P.J., Quemada, M., 2021. Residual effect and N fertilizer rate detection by high-resolution VNIR-SWIR hyperspectral imagery and solar-induced chlorophyll fluorescence in wheat. IEEE Trans. Geosci. Remote Sens. 60, 1–17.
Romina, D.S., Teresa, P.-F., Rodney, B.T., Marisa, G., Rafael, G., Francisco, M.P., 2019. The use of chlorophyll meters to assess crop N status and derivation of sufficiency values for sweet pepper. Sensors 19 (13), 2949.
Rondeaux, G., Steven, M., Baret, F., 1996. Optimization of soil-adjusted vegetation indices. Remote Sens. Environ. 55 (2), 95–107.
Roujean, J.-L., Breon, F.-M., 1995. Estimating PAR absorbed by vegetation from bidirectional reflectance measurements. Remote Sens. Environ. 51 (3), 375–384.
Rouse, J.W., Haas, R.H., Schell, J.A., Deering, D.W., 1974. Monitoring vegetation systems in the Great Plains with ERTS. NASA Spec. Publ. 351 (1974), 309.
Ruban, A.V., Lee, P.J., Wentworth, M., Young, A.J., Horton, P., 1999. Determination of the stoichiometry and strength of binding of xanthophylls to the photosystem II light harvesting complexes. J. Biol. Chem. 274 (15), 10458–10465.
Saibo, N.J., Lourenço, T., Oliveira, M.M., 2009. Transcription factors and regulation of photosynthetic and related metabolism under environmental stresses. Ann. Bot. 103 (4), 609–623.
Sayed, O., 2003. Chlorophyll fluorescence as a tool in cereal crop research. Photosynthetica 41 (3), 321–330.
Schächtl, J., Huber, G., Maidl, F.-X., Sticksel, E., Schulz, J., Haschberger, P., 2005. Laser-induced chlorophyll fluorescence measurements for detecting the nitrogen status of wheat (Triticum aestivum L.) canopies. Precis. Agric. 6 (2), 143–156.
Schepers, J., Francis, D., Vigil, M., Below, F., 1992. Comparison of corn leaf nitrogen concentration and chlorophyll meter readings. Commun. Soil Sci. Plant Anal. 23 (17–20), 2173–2187.
Schlemmer, M., Gitelson, A., Schepers, J., Ferguson, R., Peng, Y., Shanahan, J., Rundquist, D., 2013. Remote estimation of nitrogen and chlorophyll contents in maize at leaf and canopy levels. Int. J. Appl. Earth Obs. Geoinf. 25, 47–54.
Shcherbak, I., Millar, N., Robertson, G.P., 2014. Global metaanalysis of the nonlinear response of soil nitrous oxide (N2O) emissions to fertilizer nitrogen. Proc. Natl. Acad. Sci. 111 (25), 9199–9204.
Snyder, C.S., Bruulsema, T.W., Jensen, T.L., Fixen, P.E., 2009. Review of greenhouse gas emissions from crop production systems and fertilizer management effects. Agric. Ecosyst. Environ. 133 (3–4), 247–266.
Stagakis, S., González-Dugo, V., Cid, P., Guillén-Climent, M.L., Zarco-Tejada, P.J., 2012. Monitoring water stress and fruit quality in an orange orchard under regulated deficit irrigation using narrow-band structural and physiological remote sensing indices. ISPRS J. Photogramm. Remote Sens. 71, 47–61.
Stevenson, F.J., Cole, M.A., 1999. Cycles of Soils: Carbon, Nitrogen, Phosphorus, Sulfur, Micronutrients. John Wiley & Sons.
Syvertsen, J.P., 1984. Light acclimation in citrus leaves. I: changes in physical characteristics, chlorophyll, and nitrogen content. J. Am. Soc. Hortic. Sci. 109 (6), 807–812.
Syvertsen, J., Lloyd, J., McConchie, C., Kriedemann, P., Farquhar, G., 1995. On the relationship between leaf anatomy and CO2 diffusion through the mesophyll of hypostomatous leaves. Plant Cell Environ. 18 (2), 149–157.
Thorp, K., Wang, G., West, A., Moran, M., Bronson, K., White, J., Mon, J., 2012. Estimating crop biophysical properties from remote sensing data by inverting linked radiative transfer and ecophysiological models. Remote Sens. Environ. 124, 224–233.
Tóth, V.R., Mészáros, I., Veres, S., Nagy, J., 2002. Effects of the available nitrogen on the photosynthetic activity and xanthophyll cycle pool of maize in field. J. Plant Physiol. 159 (6), 627–634.
Verhoef, W., 1984. Light scattering by leaf layers with application to canopy reflectance modeling: the SAIL model. Remote Sens. Environ. 16 (2), 125–141.
Verhoeven, A.S., Adams III, W.W., Demmig-Adams, B., Croce, R., Bassi, R., 1999. Xanthophyll cycle pigment localization and dynamics during exposure to low temperatures and light stress in Vinca major. Plant Physiol. 120 (3), 727–738.
Vilfan, N., Van der Tol, C., Muller, O., Rascher, U., Verhoef, W., 2016. Fluspect-B: a model for leaf fluorescence, reflectance and transmittance spectra. Remote Sens. Environ. 186, 596–615.
Vilfan, N., Van der Tol, C., Yang, P., Wyber, R., Malenovský, Z., Robinson, S.A., Verhoef, W., 2018. Extending Fluspect to simulate xanthophyll driven leaf reflectance dynamics. Remote Sens. Environ. 211, 345–356.
Walker, A.P., Beckerman, A.P., Gu, L., Kattge, J., Cernusak, L.A., Domingues, T.F., Woodward, F.I., 2014. The relationship of leaf photosynthetic traits–Vcmax and Jmax–to leaf nitrogen, leaf phosphorus, and specific leaf area: a meta-analysis and modeling study. Ecol. Evol. 4 (16), 3218–3235.
Wang, Z., Skidmore, A.K., Darvishzadeh, R., Wang, T., 2018. Mapping forest canopy nitrogen content by inversion of coupled leaf-canopy radiative transfer models from airborne hyperspectral imagery. Agric. For. Meteorol. 253, 247–260.
Wang, Y., Suarez, L., Qian, X., Poblete, T., Gonzalez-Dugo, V., Ryu, D., Zarco-Tejada, P., 2021. Assessing the contribution of airborne-retrieved chlorophyll fluorescence for nitrogen assessment in almond orchards. In: Paper Presented at the 2021 IEEE International Geoscience and Remote Sensing Symposium. IGARSS.
Williams, C.K., Rasmussen, C.E., 1996. Gaussian Processes for Regression.
Williams, C.K., Rasmussen, C.E., 2006. Gaussian Processes for Machine Learning, Vol. 2. MIT press, Cambridge, MA.
Wood, C., Reeves, D., Duffield, R., Edmisten, K., 1992. Field chlorophyll measurements for evaluation of corn nitrogen status. J. Plant Nutr. 15 (4), 487–500.
Worton, B.J., 1989. Kernel methods for estimating the utilization distribution in home-range studies. Ecology 70 (1), 164–168.
Wu, C., Niu, Z., Tang, Q., Huang, W., 2008. Estimating chlorophyll content from hyperspectral vegetation indices: modeling and validation. Agric. For. Meteorol. 148 (8–9), 1230–1241.
Xiong, D., Chen, J., Yu, T., Gao, W., Ling, X., Li, Y., Huang, J., 2015. SPAD-based leaf nitrogen estimation is impacted by environmental factors and crop leaf characteristics. Sci. Rep. 5 (1), 1–12.
Yoder, B.J., Pettigrew-Crosby, R.E., 1995. Predicting nitrogen and chlorophyll content and concentrations from reflectance spectra (400–2500 nm) at leaf and canopy scales. Remote Sens. Environ. 53 (3), 199–211.
Zarco-Tejada, P.J., González-Dugo, V., Berni, J.A., 2012. Fluorescence, temperature and narrow-band indices acquired from a UAV platform for water stress detection using a micro-hyperspectral imager and a thermal camera. Remote Sens. Environ. 117, 322–337.
Zarco-Tejada, P.J., Morales, A., Testi, L., Villalobos, F.J., 2013. Spatio-temporal patterns of chlorophyll fluorescence and physiological and structural indices acquired from hyperspectral imagery as compared with carbon fluxes measured with eddy covariance. Remote Sens. Environ. 133, 102–115.
Zarco-Tejada, P.J., González-Dugo, M., Fereres, E., 2016. Seasonal stability of chlorophyll fluorescence quantified from airborne hyperspectral imagery as an indicator of net photosynthesis in the context of precision agriculture. Remote Sens. Environ. 179, 89–103.

Zarco-Tejada, P.J., Camino, C., Beck, P., Calderon, R., Hornero, A., Hernández-Clemente, R., Morelli, M., 2018. Previsual symptoms of Xylella fastidiosa infection revealed in spectral plant-trait alterations. Nat. Plants 4 (7), 432–439.

Zarco-Tejada, P.J., Poblete, T., Camino, C., Gonzalez-Dugo, V., Calderon, R., Hornero, A., Landa, B., 2021. Divergent abiotic spectral pathways unravel pathogen stress signals across species. Nat. Commun. 12 (1), 1–11.

Zebarth, B., Drury, C., Tremblay, N., Cambouris, A., 2009. Opportunities for improved fertilizer nitrogen management in production of arable crops in eastern Canada: a review. Can. J. Soil Sci. 89 (2), 113–132.

Appendix 2

Assessing the Contribution of Airborne-retrieved Chlorophyll Fluorescence for Nitrogen Assessment in Almond Orchards

This is the paper in its published format in IEEE IGARSS 2021 conference:

Wang, Y., Suarez, L., Qian, X., Poblete, T., Gonzalez-Dugo, V., Ryu, D., Zarco-Tejada, P.J., Assessing the contribution of airborne-retrieved chlorophyll fluorescence for nitrogen assessment in almond orchards, IEEE International Geoscience and Remote Sensing Symposium IGARSS, 2021, pp. 5853-5856, doi: 10.1109/IGARSS47720.2021.9554648.

IGARSS 2021 - 2021 IEEE International Geoscience and Remote Sensing Symposium | 978-1-6654-0369-6/21/$31.00 ©2021 IEEE | DOI: 10.1109/IGARSS47720.2021.9554648

ASSESSING THE CONTRIBUTION OF AIRBORNE-RETRIEVED CHLOROPHYLL FLUORESCENCE FOR NITROGEN ASSESSMENT IN ALMOND ORCHARDS

*Y. Wang [a, *], L. Suarez [a, b], X. Qian [c], T. Poblete [b], V. Gonzalez-Dugo [d], D. Ryu [a], P.J. Zarco-Tejada [a, b, d]*
** E-mail address: wang.y@unimelb.edu.au*

[a] Department of Infrastructure Engineering, Faculty of Engineering and Information Technology (FEIT), University of Melbourne, Melbourne, VIC 3010, Australia
[b] School of Agriculture and Food, Faculty of Veterinary and Agricultural Sciences (FVAS), University of Melbourne, Melbourne, VIC 3010, Australia
[c] Key Laboratory of Digital Earth Science, Aerospace Information Research Institute, Chinese Academy of Sciences, Beijing, 100094, China
[d] Instituto de Agricultura Sostenible (IAS), Consejo Superior de Investigaciones Cientificas (CSIC), Avenida Menendez Pidal s/n, 14004 Cordoba, Spain

ABSTRACT

Standard remote sensing methods for nitrogen (N) assessment in precision agriculture rely on empirical relationships built with chlorophyll *a+b* (C_{ab}) sensitive vegetation indices. Nevertheless, methods of N estimation based on the C_{ab} vs. N relationships are strongly affected by the saturation of these indices at high N levels, and by canopy structure, shadows and soil background variability. These effects are even more pronounced in heterogeneous orchards where the tree crown structural variability is a major factor that limits the transferability of the algorithms within- and across-tree crop species. Solar-induced fluorescence (SIF) has been proposed in precision agriculture as a plant functional trait related to N due to its link with photosynthesis. However, retrieving SIF from orchards is challenging due to the mixture of sunlit and shaded crown components. The present study explored the retrieval of airborne SIF in almond orchards from hyperspectral imagery, assessing its contribution to the estimation of N. Results show that the assessment of N improved when SIF was coupled to the model estimated C_{ab} (e.g., C_{ab}+SIF; r^2=0.95) as compared with using C_{ab} alone (r^2=0.87).

Index Terms - Chlorophyll Fluorescence, SIF, Nitrogen, Hyperspectral, Almond, FluSAIL RTM

1. INTRODUCTION

Nitrogen (N) is an important indicator of plant growth and productivity as it is the major limiting factor in photosynthetic capacity [1]. Monitoring N status timely can inform fertilizer management strategy in terms of balancing plant production against economic losses and environmental effects [2] for sustainable agriculture purposes. Monitoring the spatial and temporal variability of N status at large scales requires rapid and cost-effective remote sensing methods to overcome the limitations of traditional biochemical analyses of leaf tissues.

Traditional remote sensing methods for N assessment are commonly based on empirical models that use structural and chlorophyll-sensitive vegetation indices employing specific spectral bands [3]. Recent studies have proposed the use of plant traits estimated by radiative transfer models (RTMs) for assessing N in homogenous crops [4, 5]. However, the application of these methods to tree orchards is challenging due to the structural complexity of the canopies caused by clumping effects, crown heterogeneity, within-crown shadows, and soil background influence.

Solar-induced chlorophyll fluorescence (SIF) has been shown as a proxy for photosynthetic activities [6, 7] and therefore sensitive to the leaf nutrient levels [8]. A recent study [4] presented SIF as an indicator for N quantification in wheat phenotyping that improved the predictions when coupled to chlorophyll content (C_{ab}). However, the physiological dynamics of SIF vs. N may differ considerably between orchard trees and herbaceous crops due to the within-tree structural variability and background effects. In this study, we explored the retrieval of airborne-quantified SIF in almond orchards from hyperspectral imagery, assessing the contribution of SIF and spectral plant traits for N estimation.

2. MATERIAL AND METHODS

2.1. Study area

The study was conducted in a commercial almond orchard located in northwestern Victoria, Australia. The almond

orchard (Figure 1a) covers approximately 1200 hectares and was planted in 2006 (Northern blocks oriented N-S) and 2007 (Southern blocks with mixed N-S and E-W orientations). Three different varieties comprising Nonpareil (planted in every two rows), Price (planted in every six rows), and Carmel were planted in groups of 6 rows for cross-pollination purposes [9]. All blocks received the same amount of water and nutrient rates across the entire orchard.

2.2. Data collection

2.2.1. Field measurements and laboratory analyses

A total of 14 homogenous monitoring plots spread across the entire orchard were selected for leaf measurements and sampling purposes, comprising both Nonpareil and Carmel varieties. Leaf measurements were carried out before harvest on 20 fully exposed leaves per tree from each of the monitoring plots, comprising leaf C_{ab}, anthocyanins (A_{nth}), flavonol content and the nitrogen balance index (NBI) using a Dualex 4 Scientific instrument (FORCE-A, Orsay, France), leaf steady-state chlorophyll fluorescence (Ft) and leaf reflectance spectra within the visible and NIR region with FluorPen FP 110 and PolyPen RP 400 instruments (PSI, Brno, Czech Republic), respectively. Meanwhile, a total of 50 leaves per variety were collected from each plot for N determination in the laboratory using a LECO Nitrogen Analyzer (LECO Corporation, MI, USA).

2.2.2. Airborne hyperspectral imagery

Within a week of field data collection, an airborne campaign was carried out under clear sky conditions on 17th February 2020. A hyperspectral VNIR camera (micro-hyperspec model, Headwall Photonics, Fitchburg, MA, USA) and a thermal infrared camera (A655sc model, FLIR systems, Wilsonville, OR, USA) were installed in tandem on an aircraft (Cessna 172R) operated by the HyperSens Laboratory, the University of Melbourne's Airborne Remote Sensing Facility. The imagery was collected at midday flying in the solar plane at 550 m above ground level, yielding 45 cm and 60 cm pixel resolutions for the hyperspectral and thermal imagery, respectively. Raw images were then calibrated and pre-processed as described in Zarco-Tejada, et al. [10]. Reflectance spectra extracted from pure tree crowns (Figure 2a) and radiance extracted from sunlit vegetation pixels at the O_2-A absorption feature (Figure 2b) were used to quantify the spectral plant traits and SIF employed for the analysis, respectively.

2.3. Plant traits retrievals from hyperspectral imagery

Mean reflectance per plot was calculated from pure sunlit pixels (Figure 1b) for the 358 spectral bands acquired by the airborne hyperspectral camera. Reflectance spectra were used to calculate structural and chlorophyll indices, such as NDVI, EVI, MCARI2, CI and TCARI/OSAVI among

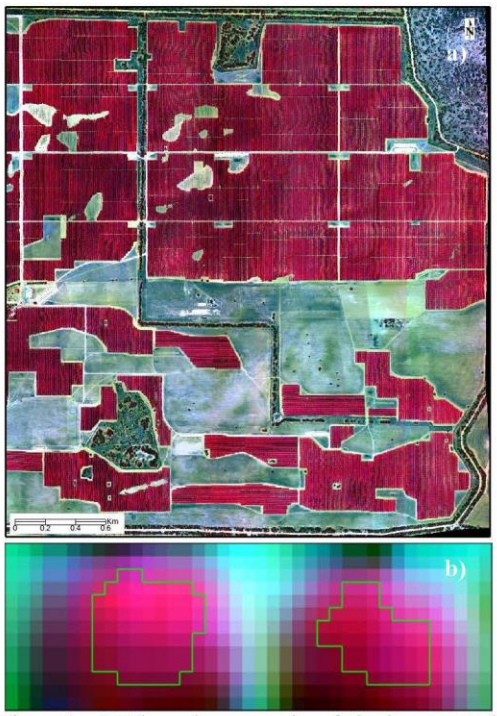

Figure 1. a) False color composite of the hyperspectral imagery acquired over a 1200 ha almond orchard in Victoria, Australia, b) image segmentation applied to individual tree crowns to extract tree crown reflectance and spectral radiance at the O_2-A spectral feature.

others (see Zarco-Tejada, et al. [10] for a complete list of indices). The spectral reflectance was also used as input for Fluspect-CX leaf [11] coupled with 4SAIL canopy RTM [12] as FluSAIL model to estimate C_{ab}, carotenoids (C_{ar}), A_{nth}, the de-epoxidation state of the xanthophyll-cycle pigments (C_x), dry matter (C_{dm}), mesophyll structure (N-struc), leaf area index (LAI), and the leaf inclination distribution ($LIDF_{a/b}$). A look-up table (LUT) containing 50,000 random simulations of FluSAIL was used to retrieve all plant traits for each tree crown at the same time using an artificial neural network model [13].

SIF was quantified from pure sunlit vegetation pixels through the Fraunhofer Line Depth (FLD) principle [14] using three bands (3FLD) [15] from the O_2-A oxygen absorption feature in the radiance spectra (Figure 2b). The method used the radiance at 762 nm (L_{762}) as L_{in}, L_{750} and L_{778} as L_{out} and the same spectral bands from the irradiance (E) spectra concurrently measured in the field at the time of flight.

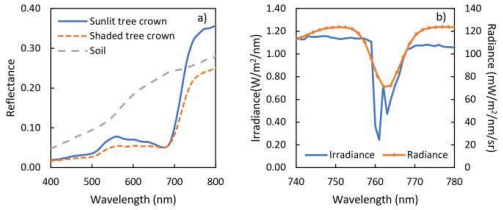

Figure 2. a) Spectra of different scene components extracted from the airborne hyperspectral image: reflectance of soil, sunlit and shaded tree crown pixels, b) radiance spectra extracted from sunlit tree crown pixels at the O_2-A feature, and field measured irradiance at the time of flight.

2.4. Statistical analysis for nitrogen estimation

Regression random forest machine learning algorithm [16], a computational method that can assess the relative variable importance, was employed to predict N by using the coefficient of determination (r^2) and RMSE as the first and second performance measure, respectively. The training and testing steps were performed using the leave-one-out-cross-validation (LOOCV) method for N prediction from a pool of representative parameters, including i) biochemical and structural plant traits retrieved from pure reflectance spectra by FluSAIL model inversion, ii) airborne quantified SIF from the radiance spectra, and iii) crop water stress index (CWSI) calculated from the thermal infrared imagery. For each set of inputs, the variance inflation factor (VIF) and out-of-bag (OOB) predictor importance with sensitivity analysis were employed to suppress the input collinearity and to evaluate the relative contribution of each input to the models, respectively. The final selection of variables for the N prediction model was obtained by filtering the most collinear and less contributing parameters.

3. RESULTS

The analysis of the field data illustrated the existing variability of leaf nitrogen and pigment content throughout the orchard (Figure 3), observing the ranges of variation for N, NBI, C_{ab} and A_{nth} based on leaf fluorescence quartiles.

Relationships between leaf N concentration vs. airborne NDVI (r^2=0.27, n.s., Figure 4a) showed that the crown structure was not a major driver in the N variability throughout the orchard. While TCARI/OSAVI chlorophyll index was better related to N (r^2=0.53, p<0.05, Figure 4b) than any other spectral index. Nevertheless, plant traits estimated by RTM inversion such as C_{ab} (r^2=0.70, p<0.001, Figure 4c) and airborne SIF (r^2=0.64, p<0.001, Figure 4d) yielded stronger relationships than standard indices against leaf N concentration. Airborne-quantified C_{ab} and SIF also showed statistically significant relationships with the equivalent field-measured leaf C_{ab} (r^2=0.64, p<0.001) and leaf Ft (r^2=0.61, p<0.001) (data not shown).

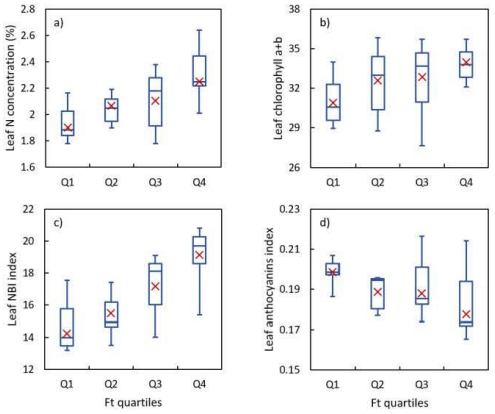

Figure 3. Ranges of variation for a) leaf nitrogen concentration, b) chlorophyll *a*+*b*, c) nitrogen balance index and d) anthocyanins content based on leaf fluorescence quartiles. Crossing line through the box and marker 'x' refer to the median and mean value, respectively. Box amplitude refers to the second and third quartiles' limits.

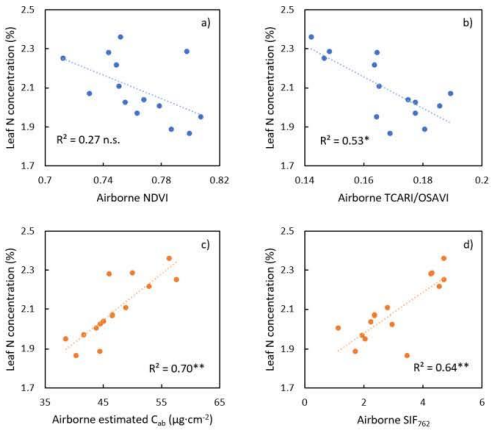

Figure 4. Relationships between nitrogen concentration and a) airborne NDVI, b) airborne TCARI/OSAVI, c) chlorophyll *a*+*b* estimated by RTM inversion, and d) SIF quantified at O_2-A using the 3FLD *in-filling* method from the airborne radiance spectra.
*p-value<0.05; **p-value<0.001; n.s.= not significant.

The relative contribution of each plant trait for estimating leaf nitrogen assessed by the OOB predictor importance analysis showed that the model estimated C_{ab} and airborne-quantified SIF were the spectra plant traits contributing the most (Figure 5), followed by C_{ar}, C_x and A_{nth} biochemical constituents. The structural trait LAI, and

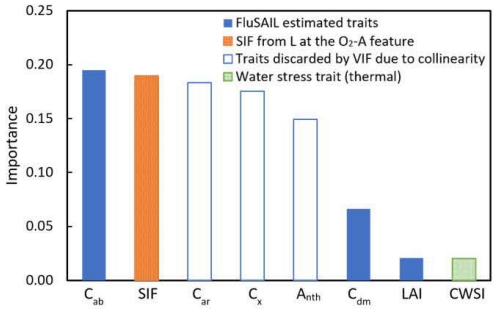

Figure 5. Relative contribution of each input to the model built to estimate N concentration from the pool of FluSAIL model inverted plant traits, airborne quantified SIF, and the water stress indicator CWSI.

the water stress indicator CWSI showed a weak contribution to N variability. However, the statistical analysis showed that C_{ab} and SIF were not strongly collinear, while C_{ar}, C_x and A_{nth} were discarded after presenting a VIF>10 with C_{ab}. Results also showed that the model performance for assessing N content was improved when coupling airborne SIF with any plant traits, particularly with C_{ab} derived from RTM inversion, increasing r^2 from 0.87 to 0.95 and reducing the RMSE from 0.064 to 0.044. As a result, the model consisting of C_{ab} and airborne SIF together explained 95% of the N variability in the almond orchard comprising different varieties, ages, and water status levels.

4. CONCLUSIONS

This study shows that airborne-retrieved chlorophyll fluorescence improves the prediction of leaf nitrogen content in almond orchards when coupled with plant traits. Notably, when airborne SIF is coupled to C_{ab} estimated by radiative transfer simulations, the model explained 95% of the variability of nitrogen in the almond orchard. The analysis showed that C_{ab} and SIF were non-collinear, while other biochemical constituents such as C_{ar}, C_x and A_{nth} estimated from RTM inversion were discarded by the VIF analysis as they presented strong collinearity with C_{ab}. This study demonstrates the interest of using SIF coupled to C_{ab} for the assessment of N in structurally complex canopies such as almond orchards for precision agriculture purposes.

5. ACKNOWLEDGMENTS

The authors gratefully acknowledge McPherson Family and Invergowrie Foundation for the financial support and the assistant from the Mallee Regional Innovation Centre (MRIC). Special thanks to Brian Slater for allowing this research to be carried out in the Aroona Farms and Rafael Romero, David Notario and Alberto Hornero from QuantaLab IAS-CSIC (Spain) for laboratory support.

6. REFERENCES

[1] J. R. Evans, "Photosynthesis and nitrogen relationships in leaves of C 3 plants," *Oecologia,* vol. 78, no. 1, pp. 9-19, 1989.

[2] F. J. Stevenson and M. A. Cole, *Cycles of soils: carbon, nitrogen, phosphorus, sulfur, micronutrients*. John Wiley & Sons, 1999.

[3] P. Hansen and J. Schjoerring, "Reflectance measurement of canopy biomass and nitrogen status in wheat crops using normalized difference vegetation indices and partial least squares regression," *Remote sensing of environment,* vol. 86, no. 4, pp. 542-553, 2003.

[4] C. Camino, V. González-Dugo, P. Hernández, J. Sillero, and P. J. Zarco-Tejada, "Improved nitrogen retrievals with airborne-derived fluorescence and plant traits quantified from VNIR-SWIR hyperspectral imagery in the context of precision agriculture," *International journal of applied earth observation and geoinformation,* vol. 70, pp. 105-117, 2018.

[5] F. Baret, V. Houlès, and M. Guerif, "Quantification of plant stress using remote sensing observations and crop models: the case of nitrogen management," *Journal of Experimental Botany,* vol. 58, no. 4, pp. 869-880, 2007.

[6] P. J. Zarco-Tejada, A. Catalina, M. González, and P. Martín, "Relationships between net photosynthesis and steady-state chlorophyll fluorescence retrieved from airborne hyperspectral imagery," *Remote Sensing of Environment,* vol. 136, pp. 247-258, 2013.

[7] G. Krause and E. Weis, "Chlorophyll fluorescence and photosynthesis: the basics," *Annual review of plant biology,* vol. 42, no. 1, pp. 313-349, 1991.

[8] N. Tremblay, Z. Wang, and Z. G. Cerovic, "Sensing crop nitrogen status with fluorescence indicators. A review," *Agronomy for sustainable development,* vol. 32, no. 2, pp. 451-464, 2012.

[9] W. Asai, W. Micke, D. Kester, and D. Rough, "The evaluation and selection of current varieties," *Almond production manual,* pp. 52-60, 1996.

[10] P. Zarco-Tejada *et al.*, "Previsual symptoms of Xylella fastidiosa infection revealed in spectral plant-trait alterations," *Nature Plants,* vol. 4, no. 7, pp. 432-439, 2018.

[11] N. Vilfan *et al.*, "Extending Fluspect to simulate xanthophyll driven leaf reflectance dynamics," *Remote sensing of environment,* vol. 211, pp. 345-356, 2018.

[12] W. Verhoef, L. Jia, Q. Xiao, and Z. Su, "Unified optical-thermal four-stream radiative transfer theory for homogeneous vegetation canopies," *IEEE Transactions on geoscience and remote sensing,* vol. 45, no. 6, pp. 1808-1822, 2007.

[13] M. H. Hassoun, *Fundamentals of artificial neural networks*. MIT press, 1995.

[14] J. A. Plascyk and F. C. Gabriel, "The Fraunhofer line discriminator MKII-an airborne instrument for precise and standardized ecological luminescence measurement," *IEEE Transactions on Instrumentation and measurement,* vol. 24, no. 4, pp. 306-313, 1975.

[15] S. W. Maier, K. P. Günther, and M. Stellmes, "Sun-induced fluorescence: A new tool for precision farming," *Digital imaging and spectral techniques: Applications to precision agriculture and crop physiology,* vol. 66, pp. 207-222, 2004.

[16] L. Breiman, "Random forests," *Machine learning,* vol. 45, no. 1, pp. 5-32, 2001.

Appendix 3

Leaf Nitrogen Assessment with ISS DESIS Imaging Spectrometer as Compared to High-Resolution Airborne Hyperspectral Imagery

This is the paper in its published format in IEEE IGARSS 2022 conference:

Wang, Y., Suarez, L., Gonzalez-Dugo, V., Ryu, D., Moar, P., Zarco-Tejada, P.J., Leaf Nitrogen Assessment with ISS DESIS Imaging Spectrometer as Compared to High-Resolution Airborne Hyperspectral Imagery, IGARSS 2022 - 2022 IEEE International Geoscience and Remote Sensing Symposium, 2022, pp. 5444-5447, doi: 10.1109/IGARSS46834.2022.9884759.

LEAF NITROGEN ASSESSMENT WITH ISS DESIS IMAGING SPECTROMETER AS COMPARED TO HIGH-RESOLUTION AIRBORNE HYPERSPECTRAL IMAGERY

*Y. Wang [1, *], L. Suarez [1, 2], V. Gonzalez-Dugo [3], D. Ryu [1], P. Moar [4], P.J. Zarco-Tejada [1, 2, 3]*
** E-mail address: wang.y@unimelb.edu.au*

[1] Department of Infrastructure Engineering, Faculty of Engineering and Information Technology (FEIT), University of Melbourne, Melbourne, VIC 3010, Australia
[2] School of Agriculture and Food, Faculty of Veterinary and Agricultural Sciences (FVAS), University of Melbourne, Melbourne, VIC 3010, Australia
[3] Instituto de Agricultura Sostenible (IAS), Consejo Superior de Investigaciones Cientificas (CSIC), Avenida Menendez Pidal s/n, 14004 Cordoba, Spain
[4] College of Science, Health and Engineering, School of Engineering and Mathematical Sciences, La Trobe University, Victoria 3086, Australia

IGARSS 2022 - 2022 IEEE International Geoscience and Remote Sensing Symposium | 978-1-6654-2792-0/22/$31.00 ©2022 IEEE | DOI: 10.1109/IGARSS46834.2022.9884759

ABSTRACT

Traditional methods to estimate leaf nitrogen (N) from satellite imagery rely on structural and chlorophyll *a*+*b* (C_{ab}) vegetation indices. Recent progress with airborne hyperspectral imagery identified C_{ab} and SIF as critical indicators for evaluating leaf N variability, yielding superior performance than standard vegetation indices. In tree orchards, accurate physiological assessments require high-spatial-resolution hyperspectral imagery to minimize canopy architecture and soil background effects. Understanding the potential of coarse-spatial-resolution spaceborne hyperspectral imagery for leaf N estimation is critical. In this study, DESIS hyperspectral imagery collected on board the International Space Station was used to assess the quantification of leaf N, evaluating the relative contributions of physiological plant traits and SIF. High-resolution airborne hyperspectral imagery and ground N data were used for validation. Results show that C_{ab} and SIF were the most critical parameters explaining leaf N both from DESIS and from airborne hyperspectral imagery, yielding strong correlations against ground truth N data (r^2=0.90, p<0.0001) and with airborne-predicted N (r^2=0.75, p<0.0001).

Index Terms – DESIS, Nitrogen, Hyperspectral, Spaceborne, Almond, Chlorophyll, SIF, Plant traits

1. INTRODUCTION

Accurate leaf nitrogen (N) assessment is crucial for ensuring adequate nutrient levels and determining fertilizer requirements over the course of the growing season. Monitoring leaf N status at large scales requires remote sensing technologies to achieve affordable quantifications compared with traditional biochemical analyses of leaf tissues. Standard remote sensing methods for N assessment typically use structural and chlorophyll-sensitive vegetation indices derived from multispectral sensors, but relationships saturate at high N levels [1]. Spaceborne hyperspectral sensors can measure detailed spectral features over large areas. The German Aerospace Center (DLR) Earth Sensing Imaging Spectrometer (DESIS) onboard the International Space Station (ISS) is capable of collecting hyperspectral imagery from space. However, leaf N assessment in row-structured orchards is affected by the canopy architecture and background. Thus, the implications of using coarser spatial resolution hyperspectral imagery on the accuracy of N estimation in heterogeneous orchards are crucial.

Previous work [2, 3] on the assessment of leaf N from airborne hyperspectral imagery demonstrated that Solar-Induced Fluorescence (SIF) and physiological plant traits (i.e., C_{ab} and other leaf biochemicals) retrieved from radiative transfer models (RTM) yielded superior N estimates than standard vegetation indices. These methods showed that C_{ab} and SIF predicted 95% of the N variability in almond orchards. However, the importance of specific plant traits may differ considerably at coarser spatial resolution due to the structural and background effects. This study investigates the contribution of SIF and the leaf biochemistry quantified by RTM inversions from ISS DESIS hyperspectral imagery for large-scale N assessment in almond orchards, with comparison against high-resolution airborne hyperspectral imagery and ground truth data used as validation.

2. MATERIALS AND METHODS

2.1. Study area

The study site is a commercial almond orchard covering about 1,200 hectares, located in northwestern Victoria,

Australia. Three different almond varieties were alternately planted in groups of 6 rows for cross-pollination [4] in 2006 and 2007, comprising Nonpareil (50%), Carmel (33%), and Price (17%). Plant varieties are spaced apart by 7 m and trees by 4.4 m, respectively. Nutrients were supplied to plants via drip fertigation and separated by one-hour intervals between varieties. During the 2020-2021 growing season, the fertigation rate for Nonpareil was 10% lower than that of Carmel and Price throughout the orchard.

2.2. Datasets

2.2.1. Field measurements

The field measurements and leaf sampling were conducted at the pre-harvest stage on February 1, 2021 in 13 homogeneous study plots throughout the orchard. A total of eighty fully exposed leaves of Nonpareil and Carmel were collected and measured from each study plot by different handheld instruments, including leaf C_{ab}, anthocyanins (Anth), flavonol content and the nitrogen balance index (NBI) using a Dualex-4 Scientific instrument (FORCE-A, Orsay, France), steady-state leaf chlorophyll fluorescence (Ft) with a FluorPen FP 110 (PSI, Brno, Czech Republic), and leaf reflectance spectra over the visible and NIR regions with a PolyPen RP 400 instrument (PSI, Brno, Czech Republic). Moreover, ten additional leaves per variety (a total of 100 leaf samples per plot) were collected for N determination in the biochemical laboratory using the Dumas Combustion method [5] with a LECO Nitrogen Analyzer (LECO Corporation, MI, USA).

2.2.2. Airborne hyperspectral imagery

An airborne campaign was carried out at solar noon under clear sky conditions on January 31, 2021. A hyperspectral line-scanning sensor (Micro-Hyperspec VNIR model, Headwall Photonics, Fitchburg, MA, USA), covering 371 bands from the visible and the near-infrared regions with an FWHM of 5.8nm and a spectral sampling interval of 1.6 nm, was flown onboard the Cessna 172R aircraft operated by the HyperSens Laboratory, the Airborne Remote Sensing facility of The University of Melbourne. The imagery was collected at 550 m above ground level with a spatial resolution of 40 cm. Pre-processing and calibration steps of the raw images were performed as described in Zarco-Tejada et al. [6]. The high-spatial resolution of the airborne hyperspectral imagery enabled the extraction of sunlit vegetation pixels to quantify leaf biochemistry and SIF [2]. In a two-year validation study conducted for the entire orchard, leaf N (r^2=0.95, p<0.001, Figure 1) was estimated with C_{ab} and SIF being the most critical plant traits [3].

2.2.3. DESIS hyperspectral imagery acquired from the ISS

A 30-meter spacebore hyperspectral scene was captured by the DESIS imaging spectrometer onboard the ISS on January 23, 2021. The imagery covers 235 spectral bands, ranging from the visible to the near-infrared regions with a 3.5 nm

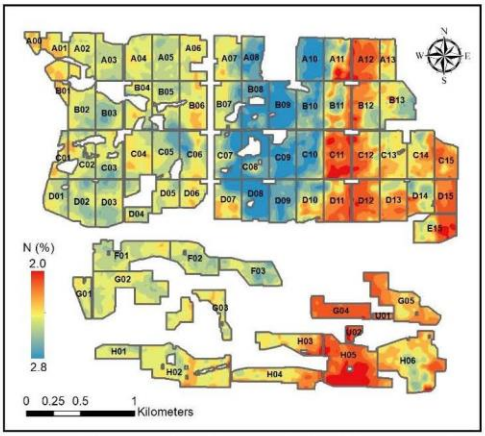

Figure 1. Airborne predicted N map derived from C_{ab} and SIF at a 1,200-ha almond orchard study site in Victoria, Australia.

FWHM and a 2.55 nm sampling interval [7]. As a result of the signal noise in the blue and green spectral regions, additional cross-calibration was performed for DESIS L2A imagery using vegetation, soil and water features from airborne hyperspectral imagery by 3×3 DESIS pixel windows (Figure 2).

2.3. Plant traits retrievals and SIF quantification

The reflectance spectra of individual vegetation pixels were extracted for the calculation of structural and chlorophyll indices (e.g., NDVI, EVI, TCARI/OSAVI), as well as plant traits (e.g., C_{ab}, carotenoids (C_{car}), Anth, the de-epoxidation state of the xanthophyll-cycle pigments (C_x), dry matter (C_{dm}) and leaf area index (LAI)) retrieval from FluSAIL RTM [8, 9]. An artificial neural network model [10] based on a look-up-table (LUT) with random 50,000 simulations was used to retrieve the physiological plant traits.

The Fraunhofer Line Depth (FLD) principle [11] was used to calculate SIF using the O_2-A oxygen absorption feature from the DESIS L1C radiance imagery. Irradiance data were derived from auxiliary data collected at the nearest station on the day of DESIS overpass. The same method was applied to the airborne hyperspectral imagery to retrieve SIF and the plant traits by RTM inversions.

2.4. Statistical analysis for nitrogen estimation

The statistical methods used to assess N from airborne imagery [2, 3] were applied in this study to DESIS data. The variance inflation factor (VIF) collinearity assessment and the out-of-bag (OOB) predictor importance were also determined for DESIS. We compared the relative contributions of physiological plant traits (i.e., C_{ab}, C_{car}, Anth,

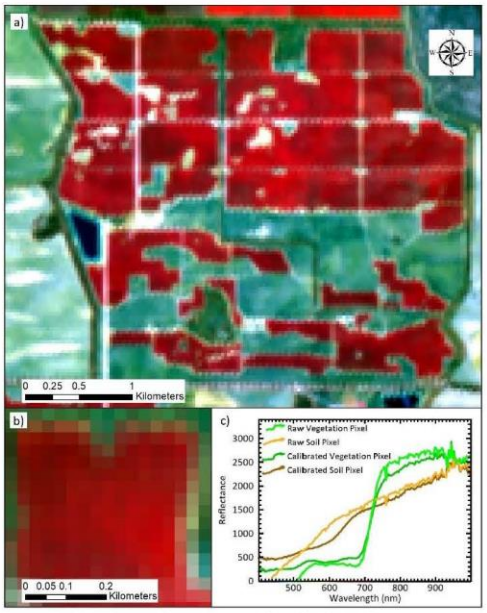

Figure 2. a) False colour composite of DESIS hyperspectral imagery over a 1,200-ha almond orchard, b) DESIS zoom-in view over the planting blocks, and c) reflectance spectra from raw L2A image and cross-calibrated DESIS imagery.

C_x, C_{dm}, LAI) and SIF to estimate leaf N between spaceborne DESIS hyperspectral and airborne hyperspectral imagery throughout the almond orchard. The leaf N estimates obtained from random forest regression models using DESIS were validated with field measured leaf N and the high-resolution airborne hyperspectral-based retrievals.

3. RESULTS

The traditional structural indices (e.g., NDVI, MCARI1) calculated from DESIS hyperspectral imagery were strongly related to C_{ab}, but yielded a weak relationship with N (Table 1). NDVI yielded r^2=0.35 (p<0.05) with leaf measured C_{ab}, but was unable to explain N when compared either against laboratory N measurements (r^2=0.08, n.s.) or the airborne-based N validation map (r^2=0, n.s.). These results suggest that the variability of the canopy architecture captured at the spaceborne scale did not explain leaf N orchard variability. Other traditional chlorophyll indices (e.g., TCARI/OSAVI) used for N assessment did not correlate with leaf C_{ab} nor N from DESIS data, likely due to the mixture of soil and shaded canopy components captured at such spatial resolution. Nevertheless, CTRI1 [12] exhibited a significant correlation with leaf N (r^2=0.45, p<0.05) and with the airborne-predicted N (r^2=0.74, p<0.01), outperforming other vegetation indices. SIF quantified from DESIS showed statistically significant relationships with field measured Ft (r^2=0.52, p<0.01) (data not shown), leaf C_{ab} (r^2=0.62, p<0.01) and with leaf N (r^2=0.56, p<0.01).

Table 1. Coefficients of determination (r^2) for the DESIS vegetation indices against field measurements and N derived from the airborne hyperspectral imagery.

Vegetation index	Leaf C_{ab}	Leaf PRI	Leaf N (%)	Airborne predicted N (%)
NDVI	0.35**	0.06	0.08	0
EVI	0.65***	0.24*	0.31**	0.20
MCARI1	0.69***	0.29*	0.35**	0.27*
SRPI	0.01	0.26	0.18	0.33**
TCARI/OSAVI	0.06	0.19	0.20	0.03
CTRI1	0.20	0.47***	0.45**	0.74***
SIF	0.62***	0.62***	0.56***	0.67***

*p < 0.1, **p < 0.05, ***p < 0.01

As illustrated in Table 2, C_{ab} retrieved by RTM showed greater correlations with leaf C_{ab} (r^2=0.31, p<0.1), leaf N (r^2=0.63, p<0.01) and airborne-predicted N (r^2=0.80, p<0.01) than chlorophyll indices. In addition to C_{ab}, other plant traits such as C_x (r^2=0.71, p<0.01) were also strongly correlated with leaf N. Significant relationships were also observed between retrieved leaf pigments (i.e., C_{ab}, C_{car}, C_x) and SIF (e.g., C_{ab}, r^2=0.59, p<0.01). In contrast to biochemical plant traits, the structural trait LAI did not yield a significant relationship with leaf C_{ab} nor N at DESIS scale.

Table 2. Coefficients of determination (r^2) among RTM-derived plant traits from DESIS and field measurements, canopy SIF and N derived from the airborne hyperspectral imagery.

Estimated parameter	Leaf C_{ab}	SIF	Leaf N (%)	Airborne predicted N (%)
C_{ab} (µg/cm²)	0.31*	0.59***	0.63***	0.80***
C_{car} (µg/cm²)	0.07	0.32**	0.17	0.14
Anth (µg/cm²)	0.10	0.01	0.03	0.16
C_x	0.26*	0.41**	0.71***	0.38**
C_{dm} (g/cm²)	0.07	0.12	0.37**	0.27*
LAI	0.14	0.22	0.07	0.01

*p < 0.1, **p < 0.05, ***p < 0.01

The relative contribution of each plant trait to leaf N estimation from spaceborne DESIS and airborne scales appeared to be highly consistent (Figure 3). These results identified C_{ab}, SIF, and C_x as the most critical spectral traits when explaining N variability, followed by the rest of the retrieved biochemical constituents and biophysical traits. Furthermore, the statistical analysis revealed that C_{ab} and SIF were non-collinear (VIF<5) but other biochemical constituents (i.e., C_x, C_{car} and C_{dm}) showed higher collinearity with C_{ab}. These collinear traits were dropped from the final model to reduce redundancy. Consequently, a

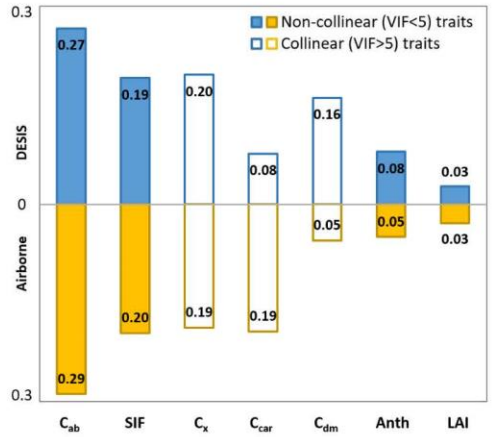

Figure 3. Relative contribution of FluSAIL RTM-inverted plant traits and SIF on the N prediction models from DESIS and airborne hyperspectral imagery.

model consisting of C_{ab} and SIF together yielded r^2=0.90 (p<0.0001) against leaf N, and r^2=0.75 (p<0.0001) against airborne-predicted N in the almond orchard comprising different varieties, ages, and planting structures.

4. CONCLUSIONS

Results shown in this study demonstrate that RTM-derived plant traits and SIF retrieved from DESIS hyperspectral imager onboard the International Space Station yielded strong relationships with ground leaf N and with estimatd N carried out from high-resolution airborne hyperspectral imagery. The most critical parameters explaining N from DESIS in this study agreed with those derived from the airborne hyperspectral imagery. Accordingly, the estimated C_{ab} retrieved by RTM inversion and SIF made a greater contribution to explaining leaf N than the rest of the biochemical constituents and biophysical traits, both from DESIS and airborne hyperspectral imagery. C_{ab} and SIF predicted 90% of the leaf N variability found in the almond orchard, obtaining a 75% agreement with the high-resolution airborne N estimates. The present study confirms the importance of the coupled C_{ab} and SIF for leaf N assessment in tree orchards at the spaceborne scale, demonstrating the feasibility of large-scale leaf N quantification for precision agriculture purposes.

5. ACKNOWLEDGMENTS

We are grateful to McPherson Family and Invergowrie Foundation for the financial support and the assistant from the Mallee Regional Innovation Centre (MRIC). Special thanks to Xiaojin Qian and Tomas Poblete from HyperSens Remote Sensing Laboratory for their support during the field and airborne campaigns. We acknowledge German Aerospace Center (DLR) for accessing DESIS data and Brian Slater for allowing this research to be carried out in Aroona Farms. We also thank Rafael Romero, David Notario and Alberto Hornero from QuantaLab IAS-CSIC (Spain) for laboratory support.

6. REFERENCES

[1] M. Schlemmer *et al.*, "Remote estimation of nitrogen and chlorophyll contents in maize at leaf and canopy levels," *International Journal of Applied Earth Observation and Geoinformation,* vol. 25, pp. 47-54, 2013.

[2] Y. Wang *et al.*, "Assessing the Contribution of Airborne-Retrieved Chlorophyll Fluorescence for Nitrogen Assessment in Almond Orchards," in *2021 IEEE International Geoscience and Remote Sensing Symposium IGARSS*, 2021: IEEE, pp. 5853-5856.

[3] Y. Wang, L. Suarez, T. Poblete, V. Gonzalez-Dugo, D. Ryu, and P. Zarco-Tejada, "Evaluating the role of solar-induced fluorescence (SIF) and plant physiological traits for leaf nitrogen assessment in almond using airborne hyperspectral imagery," *Remote Sensing of Environment,* In Review.

[4] W. Asai, W. Micke, D. Kester, and D. Rough, "The evaluation and selection of current varieties," *Almond production manual,* pp. 52-60, 1996.

[5] J. B. A. Dumas, "Procedes de l'analyse Organic," *Annales de Chimie et de Physique (Annals of Chemistry and of Physics),* vol. 247, pp. 198-213, 1831.

[6] P. Zarco-Tejada *et al.*, "Previsual symptoms of Xylella fastidiosa infection revealed in spectral plant-trait alterations," *Nature Plants,* vol. 4, no. 7, pp. 432-439, 2018.

[7] A. Eckardt *et al.*, "Desis (dlr earth sensing imaging spectrometer for the iss-muses platform)," in *2015 IEEE international geoscience and remote sensing symposium (IGARSS)*, 2015: IEEE, pp. 1457-1459.

[8] N. Vilfan *et al.*, "Extending Fluspect to simulate xanthophyll driven leaf reflectance dynamics," *Remote sensing of environment,* vol. 211, pp. 345-356, 2018.

[9] W. Verhoef, L. Jia, Q. Xiao, and Z. Su, "Unified optical-thermal four-stream radiative transfer theory for homogeneous vegetation canopies," *IEEE Transactions on geoscience and remote sensing,* vol. 45, no. 6, pp. 1808-1822, 2007.

[10] M. H. Hassoun, *Fundamentals of artificial neural networks.* MIT press, 1995.

[11] J. A. Plascyk and F. C. Gabriel, "The Fraunhofer line discriminator MKII-an airborne instrument for precise and standardized ecological luminescence measurement," *IEEE Transactions on Instrumentation and measurement,* vol. 24, no. 4, pp. 306-313, 1975.

[12] G. A. Carter, "Ratios of leaf reflectances in narrow wavebands as indicators of plant stress," *Remote sensing,* vol. 15, no. 3, pp. 697-703, 1994.

Appendix 4

Evaluating the Contribution of Cx to Leaf Nitrogen Quantification using Fluspect and Airborne Imaging Spectroscopy in Almond Orchards

This is the paper in its accepted format in IEEE IGARSS 2023 conference.

EVALUATING THE CONTRIBUTION OF C_X TO LEAF NITROGEN QUANTIFICATION USING FLUSPECT AND AIRBORNE IMAGING SPECTROSCOPY IN ALMOND ORCHARDS

*Y. Wang [1, *], L. Suarez [1, 2], D. Ryu [1], P.J. Zarco-Tejada [2, 1, 3]*
** E-mail address: wang.y@unimelb.edu.au*

[1] Department of Infrastructure Engineering, Faculty of Engineering and Information Technology (FEIT), University of Melbourne, Melbourne, VIC 3010, Australia
[2] School of Agriculture, Food and Ecosystem Sciences (SAFES), Faculty of Sciences (FoS), University of Melbourne, Melbourne, VIC 3010, Australia
[3] Instituto de Agricultura Sostenible (IAS), Consejo Superior de Investigaciones Cientificas (CSIC), Avenida Menendez Pidal s/n, 14004 Cordoba, Spain

ABSTRACT

Among all essential nutrients, nitrogen (N) is required by plants in large quantities throughout the entire developmental process. This is due to its importance for plant growth and development and as a primary source of energy for photosynthesis. Previous research has demonstrated that solar-induced chlorophyll fluorescence (SIF) coupled with chlorophyll *a*+*b* content (C_{ab}) improved the estimation of leaf N, outperforming standard vegetation indices. The present study investigates the contribution of leaf C_x, a measure of the de-epoxidation state of the xanthophyll cycle, for explaining leaf N variability, concluding that it ranks third after C_{ab} and SIF consistently over two growing seasons. Among the rest of the biochemical constituents estimated by model inversion, C_x contributed more than anthocyanins (Anth), the total carotenoid content (C_{car}), and crown-level structural traits.

Index Terms — C_x, airborne hyperspectral, nitrogen, xanthophyll cycle, de-epoxidation, PRI

1. INTRODUCTION

Nitrogen (N) is one of the major nutrients taken up during active plant growth and plays a significant role in preserving high fruit quality and yield [1, 2]. Consequently, a precise and sustainable agricultural management strategy in almond orchards requires an accurate leaf N status assessment in order to fine-tune fertilizer applications.

Conventional remote sensing (RS) methods to assess leaf N rely on empirical algorithms involving chlorophyll-sensitive vegetation indices (VIs) calculated from spectral bands in the visible, red-edge, and near-infrared regions, such as $CI_{red\text{-}edge}$ [3], TCARI/OSAVI [4], NDRE [5], and CCCI [6] among others. Additionally, the PRI family of indices, which involves 2-3 spectral bands in the green region, is sensitive to changes in xanthophyll pigments composition and has been proposed as a proxy for photosynthesis rate through light-use efficiency [7-9], therefore being suggested as N-induced stress indicators [10, 11].

As alternatives to VI-based methods, a number of studies have focused on the estimation of leaf N using models based on plant traits, such as chlorophyll [12] content derived through radiative transfer model (RTM) inversion [13, 14]. The C_x parameter in the Fluspect-Cx RTM [15] tracks the dynamics of the de-epoxidation state of the xanthophyll cycle, thus receiving considerable attention in recent years. The model assessment of the xanthophyll epoxidation is based on in vivo absorption coefficients for two extreme states of the carotenoid [16] pool, corresponding to the two states of xanthophyll de-epoxidation and describes the intermediate states as a lineal mixture of these two extreme states.

Recent advances have proposed models with leaf biochemistry and dynamic spectral traits linked to photosynthesis, such as solar-induced fluorescence (SIF), to explain the leaf N variability. SIF has been demonstrated as a plant stress indicator and proxy for leaf N content in various crop species. In a recent study, SIF was found to improve the leaf N estimation in almonds [17], concluding that C_{ab} and SIF were the two most important predictors for leaf N content. As a step forward, we investigate the potential contribution of several plant traits linked to photosynthesis to

assess leaf N variability in almond orchards, particularly the xanthophyll pigments.

2 MATERIALS AND METHODS

2.1. Study area and field data collection

The study site consists of a 1,200-hectare commercial almond orchard (see Fig. 1a for an overview of the orchard in a false-color composite image) in Robinvale, northwest Victoria, Australia, with a Mediterranean climate. An almond tree planting program was undertaken in 2006 (northern blocks oriented N-S) and 2007 (southern blocks with mixed N-S and E-W orientations. Fig. 1b), including varieties of Nonpareil, Price, and Carmel. A drip fertigation system is used to supply nutrients, with one-hour intervals between rows of trees. Fertigation is adjusted based on previous year observations, resulting in different application rates between varieties.

The field collection of leaf samples and ground data measurements were conducted at the pre-harvest stage for two growing seasons, 2019-2020 (March 2020) and 2020-2021 (February 2021). Fifteen monitoring plots were sampled throughout the orchard, averaging two Nonpareil trees and two Carmel trees per plot. As part of the measurement process, 20 fully exposed mature leaves per tree were measured for leaf C_{ab}, anthocyanins (Anth), flavonol content, and the nitrogen balance index (NBI) using a Dualex 4 Scientific instrument (FORCE-A, Orsay, France). We also determined leaf steady-state chlorophyll fluorescence (Ft) and leaf reflectance spectra within the visible and near-infrared (VNIR) region with FluorPen FP 110 and PolyPen RP 400 instruments (PSI, Brno, Czech Republic), respectively. Moreover, 20 additional leaves were sampled per plot for laboratory nutrient analysis using a LECO Nitrogen analyzer (LECP Corporation, MI, USA).

2.2. Acquisition of airborne hyperspectral imagery

Airborne campaigns were carried out within a week of each field campaign. The piloted aircraft, operated by the HyperSens Laboratory at The University of Melbourne, was equipped with a hyperspectral line-scanning sensor (Micro-Hyprspec VNIR model, Headwall Photonics, Fitchburg, MA, USA) with 5.8 nm FWHM covering 371 spectral bands over the VNIR region. The flights' height at 550 m above ground level yielded a spatial resolution of 40 cm, enabling the identification of each tree crown and shaded features. Image pre-processing and calibration were performed following the method in [18]. Consequently, image mosaics of reflectance and radiance were derived over the orchard.

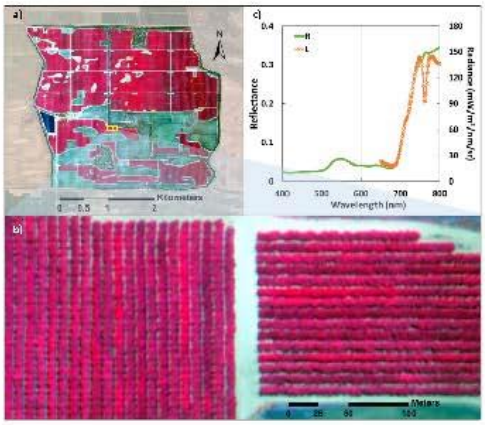

Fig. 1. (a) Colour-infrared overview of the airborne hyperspectral image acquired over a study area of 1,200 hectares at a 40-cm spatial resolution using 371 visible and near-infrared spectral bands. (b) Zoomed view of the planting blocks for almond rows that are oriented east-west and north-south. (c) Sample reflectance (R, green colour) and radiance (L for SIF calculation, orange colour) spectrum extracted from the airborne hyperspectral image.

2.3. SIF quantification and plant traits estimation

Based on pure sunlit vegetation pixels extracted from radiance image, SIF was quantified by the Fraunhofer Line Depth (FLD) method [19] from O_2-A oxygen absorption features at 762 nm. The reflectance mosaic was used to extract spectra from tree crowns used for the calculation of vegetation indices and the inversion of plant traits from RTM. C_x, along with other biochemical constituents (e.g., C_{ab}, C_{car}, and Anth), and structural traits (e.g., LAI) were retrieved simultaneously by constructing a 10-hidden layer artificial neural network (ANN) based on 500,000 simulations using the coupled Fluspect-Cx and 4SAIL model [20].

2.4. Nitrogen prediction model assessment

As part of a previous two-year validation study performed in the orchard, C_{ab} and SIF were identified as the most critical plant traits for leaf N estimation [17]. With the retrieved plant traits, Gaussian process regression models were constructed for each year incorporating single plant traits (i.e., C_{car}, C_x, Anth, LAI) in addition to C_{ab} and SIF. The training and testing steps were performed using leave-one-out cross-validation. Furthermore, the variance inflation factor (VIF) and out-of-bag predictor importance were employed to assess the input collinearity and relative contribution of the inputs, respectively.

3. RESULTS

The xanthophyll pigment-related indices extracted from tree crowns were highly correlated with leaf N, in particular, PRI ($r^2 = 0.48$, p-value < 0.005 in 2020, and $r^2 = 0.27$, p-value < 0.05 in 2021), and PRI_{m4} ($r^2 = 0.34$, p-value < 0.05 in 2020, and $r^2 = 0.50$, p-value < 0.005 in 2021). The RTM-derived parameter C_x, however, exhibited a superior and consistently significant relationship with leaf N for both years ($r^2 = 0.61$ in 2020 and $r^2 = 0.62$ in 2021; p-values < 0.005). Relationships were obtained between C_x vs. leaf-measured PRI_{m4} ($r^2 = 0.48$ in 2020 and $r^2 = 0.46$ in 2021; p-values < 0.005) and airborne-derived PRI_{m4} ($r^2 = 0.50$ in 2020 and $r^2 = 0.42$ in 2021; p-values < 0.01, Fig. 2).

Based on the relative contribution of each input to leaf N estimation, C_x was demonstrated as the best non-collinear (VIF<10) predictor after C_{ab} and SIF. Moreover, the model incorporating C_x along with C_{ab} and SIF (e.g., RMSE = 0.079% in 2020+2021) outperformed the model built with C_{ab} and SIF alone (e.g., RMSE = 0.092% in 2020+2021). With a model consisting of C_{ab}, C_x, and SIF ($N = f(C_{ab}, C_x, SIF)$: $r^2 = 0.86$ in 2020, $r^2 = 0.65$ in 2021, and $r^2 = 0.87$ in 2020+2021, Fig. 3), leaf N variability was better explained than any other model combinations for each individual year and when combining the two years together. These results suggest that the RTM-derived C_x estimated from airborne hyperspectral imagery is an important predictor for leaf N assessment in almond orchards, improving the model performance when coupled to C_{ab} and SIF.

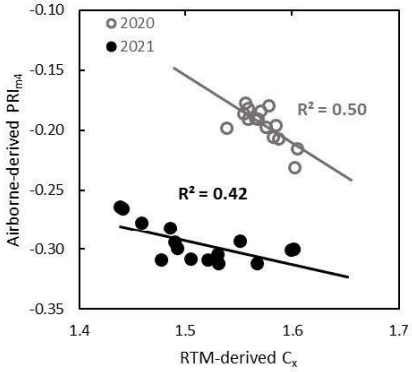

Fig. 2. Relationships between RTM-derived C_x and airborne-derived PRI_{m4} in 2020 (hollow grey circle) and 2021 (solid black circle). All p-values < 0.01.

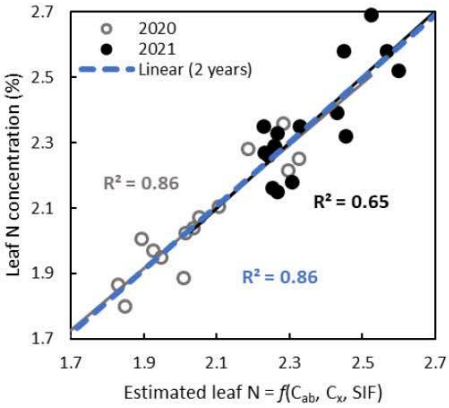

Fig. 3. Relationships between leaf N concentration (%) and predicted leaf N using models based on chlorophyll content, C_x, and SIF. The blue dashed line represents correlation when combining data from 2 years. All p-values < 0.005.

4. CONCLUSIONS

This study demonstrates that the RTM-derived C_x parameter, an indicator of the xanthophyll pigments cycle, ranked third behind C_{ab} and SIF when explaining the observed variability of leaf N in almond orchards. The leaf N prediction model that incorporated C_x in addition to C_{ab} and SIF was found to outperform any other combinations of plant traits over the course of two years. Other leaf biochemical constituents such as anthocyanins (Anth), the total carotenoid content (C_{car}), dry matter (C_{dm}), and structural traits yielded lower contributions when explaining the leaf N variability in almond orchards.

5. ACKNOWLEDGMENTS

The authors would like to thank the McPherson Family and Invergowrie Foundation for their financial support and assistance from the Mallee Regional Innovation Centre (MRIC). Our gratitude goes out to Xiaojin Qian and Tomas Poblete from HyperSens Remote Sensing Laboratory for their support provided during the field and airborne campaigns. In acknowledgment of Brian Slater's permission to conduct this research at Aroona Farms. Rafael Romero, David Notario, and Alberto Hornero from QuantaLab IAS-CSIC (Spain) are also acknowledged for their laboratory support.

6. REFERENCES

[1] S. Saa and P. H. Brown, "Fruit presence negatively affects photosynthesis by reducing leaf nitrogen in almond," *Functional Plant Biology,* vol. 41, no. 8, pp. 884-891, 2014.

[2] S. Muhammad *et al.*, "Seasonal changes in nutrient content and concentrations in a mature deciduous tree species: Studies in almond (Prunus dulcis (Mill.) DA Webb)," *European Journal of Agronomy,* vol. 65, pp. 52-68, 2015.

[3] A. A. Gitelson, A. Viña, T. J. Arkebauer, D. C. Rundquist, G. Keydan, and B. Leavitt, "Remote estimation of leaf area index and green leaf biomass in maize canopies," *Geophysical research letters,* vol. 30, no. 5, 2003.

[4] D. Haboudane, J. R. Miller, N. Tremblay, P. J. Zarco-Tejada, and L. Dextraze, "Integrated narrow-band vegetation indices for prediction of crop chlorophyll content for application to precision agriculture," *Remote sensing of environment,* vol. 81, no. 2-3, pp. 416-426, 2002.

[5] G. Fitzgerald, D. Rodriguez, L. Christensen, R. Belford, V. Sadras, and T. Clarke, "Spectral and thermal sensing for nitrogen and water status in rainfed and irrigated wheat environments," *Precision Agriculture,* vol. 7, no. 4, pp. 233-248, 2006.

[6] G. Fitzgerald, D. Rodriguez, and G. O'Leary, "Measuring and predicting canopy nitrogen nutrition in wheat using a spectral index—The canopy chlorophyll content index (CCCI)," *Field Crops Research,* vol. 116, no. 3, pp. 318-324, 2010.

[7] J. Gamon, J. Penuelas, and C. Field, "A narrow-waveband spectral index that tracks diurnal changes in photosynthetic efficiency," *Remote Sensing of environment,* vol. 41, no. 1, pp. 35-44, 1992.

[8] G. G. Drolet *et al.*, "A MODIS-derived photochemical reflectance index to detect inter-annual variations in the photosynthetic light-use efficiency of a boreal deciduous forest," *Remote Sensing of Environment,* vol. 98, no. 2-3, pp. 212-224, 2005.

[9] C. J. Nichol *et al.*, "Remote sensing of photosynthetic-light-use efficiency of boreal forest," *Agricultural and Forest Meteorology,* vol. 101, no. 2-3, pp. 131-142, 2000.

[10] J. A. Moran, A. K. Mitchell, G. Goodmanson, and K. A. Stockburger, "Differentiation among effects of nitrogen fertilization treatments on conifer seedlings by foliar reflectance: a comparison of methods," *Tree physiology,* vol. 20, no. 16, pp. 1113-1120, 2000.

[11] D. Whitehead *et al.*, "Photosynthesis and reflectance indices for rainforest species in ecosystems undergoing progression and retrogression along a soil fertility chronosequence in New Zealand," *Oecologia,* vol. 144, no. 2, pp. 233-244, 2005.

[12] C. M. Lee *et al.*, "An introduction to the NASA Hyperspectral InfraRed Imager (HyspIRI) mission and preparatory activities," *Remote Sensing of Environment,* vol. 167, pp. 6-19, 2015.

[13] S. Jay, F. Maupas, R. Bendoula, and N. Gorretta, "Retrieving LAI, chlorophyll and nitrogen contents in sugar beet crops from multi-angular optical remote sensing: Comparison of vegetation indices and PROSAIL inversion for field phenotyping," *Field Crops Research,* vol. 210, pp. 33-46, 2017.

[14] F. Baret, V. Houlès, and M. Guerif, "Quantification of plant stress using remote sensing observations and crop models: the case of nitrogen management," *Journal of experimental botany,* vol. 58, no. 4, pp. 869-880, 2007.

[15] N. Vilfan *et al.*, "Extending Fluspect to simulate xanthophyll driven leaf reflectance dynamics," *Remote sensing of environment,* vol. 211, pp. 345-356, 2018.

[16] J. A. Gamon *et al.*, "Relationships between NDVI, canopy structure, and photosynthesis in three Californian vegetation types," *Ecological Applications,* vol. 5, no. 1, pp. 28-41, 1995.

[17] Y. Wang, L. Suarez, T. Poblete, V. Gonzalez-Dugo, D. Ryu, and P. Zarco-Tejada, "Evaluating the role of solar-induced fluorescence (SIF) and plant physiological traits for leaf nitrogen assessment in almond using airborne hyperspectral imagery," *Remote Sensing of Environment,* vol. 279, p. 113141, 2022.

[18] P. Zarco-Tejada *et al.*, "Previsual symptoms of Xylella fastidiosa infection revealed in spectral plant-trait alterations," *Nature Plants,* vol. 4, no. 7, pp. 432-439, 2018.

[19] J. A. Plascyk and F. C. Gabriel, "The Fraunhofer line discriminator MKII-an airborne instrument for precise and standardized ecological luminescence measurement," *IEEE Transactions on Instrumentation and measurement,* vol. 24, no. 4, pp. 306-313, 1975.

[20] W. Verhoef, L. Jia, Q. Xiao, and Z. Su, "Unified optical-thermal four-stream radiative transfer theory for homogeneous vegetation canopies," *IEEE Transactions on geoscience and remote sensing,* vol. 45, no. 6, pp. 1808-1822, 2007.

Appendix 5

Nitrogen Estimation in Almond Orchards from DESIS Imaging Spectrometer Onboard the International Space Station

This is the paper in its accepted format in 1st DESIS User Workshop.

NITROGEN ESTIMATION IN ALMOND ORCHARDS FROM DESIS IMAGING SPECTROMETER ONBOARD THE INTERNATIONAL SPACE STATION

Y. Wang [1] *, L. Suarez [1, 2], D. Ryu [1], P. Moar [3], P. J. Zarco-Tejada [1, 2, 4]

[1] Department of Infrastructure Engineering, Faculty of Engineering and Information Technology (FEIT), University of Melbourne, Melbourne, Victoria 3010, Australia - (wang.y, l.suarez, dryu, pablo.zarco)@unimelb.edu.au
[2] School of Agriculture and Food, Faculty of Veterinary and Agricultural Sciences (FVAS), University of Melbourne, Melbourne, Victoria 3010, Australia
[3] College of Science, Health and Engineering, School of Engineering and Mathematical Sciences, La Trobe University, Victoria 3086, Australia - P.Moar@latrobe.edu.au
[4] Instituto de Agricultura Sostenible (IAS), Consejo Superior de Investigaciones Cientificas (CSIC), Avenida Menendez Pidal s/n, 14004 Cordoba, Spain

KEY WORDS: DESIS, Nitrogen, Airborne, Hyperspectral, Almond, Validation, Plant traits.

ABSTRACT

Accurate nitrogen (N) assessment is crucial for precise and sustainable agricultural management. Understanding crop nutrient status in a timely manner is essential to improve the efficiency of fertilizer application throughout the growing season across the entire farm. Standard remote sensing methods for N assessment are built upon empirical relationships with structural and chlorophyll-sensitive vegetation indices derived from multispectral sensors. In contrast, hyperspectral imagers can collect detailed spectral signatures resulting from the combination of all biochemical constituents and canopy structure, which provides more physiological links for improved crop N quantification. In addition to the high spectral and temporal resolutions, hyperspectral sensors onboard satellite and airborne platforms can collect imagery over large areas allowing for the monitoring of nitrogen levels across entire farms. Nevertheless, unlike homogenous crops, the detailed assessment of tree orchards requires higher spatial resolutions to reduce the extensive effects of canopy structure and soil background. Therefore, it is important to understand the applicability of coarser-resolution satellite imagery with hyperspectral capabilities for the accurate prediction of N in heterogeneous orchards.

This study explores the feasibility and performance of N status assessment from the German Aerospace Center (DLR) Earth Sensing Imaging Spectrometer (DESIS) over a 1,200-hectare almond orchard, as compared to high-spatial resolution airborne hyperspectral imagery. The experiment was conducted throughout the almond growing season from Nov 2020 to Jan 2021 in Victoria, Australia. Two airborne campaigns were conducted at almond kernel-filling and pre-harvest stages. A hyperspectral VNIR camera (Headwall Photonics, Fitchburg, MA, USA) was installed on board an aircraft, collecting imagery at a 40 cm spatial resolution and 358 bands in the 400-1000 nm spectral range. DESIS hyperspectral sensor on board the International Space Station (ISS) was used to collect imagery with 235 spectral bands in the 400-1000 nm at 2.55 nm spectral resolution (FWHM) and 30 m spatial resolution. Work was carried out to cross-validate the DESIS reflectance spectra from the airborne imagery using field targets comprising dense canopy, soil, water body and mixed features. Results of the analysis carried out using the NIR and different spectral bands in the visible part of the spectrum will be discussed.

Previous work for N assessment at the orchard level enabled the generation of a nitrogen map using the airborne hyperspectral imagery from advanced spectral-based plant traits comprising Solar-Induced Fluorescence (SIF) and chlorophyll $a+b$ content estimated from FluSAIL radiative transfer model, validated against ground truth measurements (r^2=0.95; p<0.001). The methodology was applied to every tree in the entire orchard using the airborne hyperspectral mosaic, obtaining a high-resolution map of N distribution. Assessment of N estimates from DESIS hyperspectral imagery will be discussed, assessing the structural effects of non-homogeneous orchard canopies on the accuracy of parameter retrievals. This research will contribute to the evaluation of DESIS for precision agriculture applications, in particular for large-scale mapping of N in tree crops.

* Corresponding author